Nonlinear Model and Control of Electro Hydraulic Servo-Systems

Shirin Valilou

Department of Engineering and Applied Science
(Information Engineering and Mechatronics)

University of Bergamo

Supervisor: Prof. Paolo Righettini
Co-Adviser: Prof. Roberto Strada

A thesis submitted for the degree of

Doctor of Philosophy

Oct 2017

UNIVERSITY OF BERGAMO
School of Doctoral Studies
Doctoral Degree in: Engineering and Applied Science
XXX Cycle
SSD: Meccanica Applicata alle Macchine (ING-IND/13)

TITLE:
Nonlinear Model and Control of Electro Hydraulic Servo-Systems

Supervisor: Prof. Paolo Righettini
Co-Adviser: Prof. Roberto Strada

Doctoral Thesis

Shirin Valilou
Student ID: 1036208

Academic year 2017/18

Dedication

There are a number of people without whom this thesis might not have been written, and to whom I am greatly indebted.

To my parents,
The reason of what I become today, they instilled me in the virtues of perseverance and commitment and relentlessly encouraged me to strive for excellent, thanks for their great support and continued care.

To my beloved husband, Ehsan Khademolama,
I am speechless! I can barely find words to express all the wisdom, love and support he has given me, I am eternally grateful for his endurance, encouragement and enthusiastic support in all these years.

I would like to express my sincere gratitude to professor ***Paolo Righettini*** *and professor* ***Roberto Strada*** *for their guidance, supervision and help through this project.*

Also, I would like to express my gratitude to all my teachers and all of them who directly and indirectly help me in completion of this study.

Shirin Valilou

Abstract

In many applications, the use of hydraulic drives is still preferable to other driving powers. For instance, in shaking table systems for simulating earthquake signal, hydraulic actuators are still widely applied, because the technology of electrical actuators does not (yet) provide the superior performance of hydraulic actuators in generating high power to weight ratio. However, with increasing demands on the performance of complex motion systems, the limits of performance of hydraulic servo-systems, due to the nonlinear and dynamic characteristics of these systems, come into the picture. Most nonlinearities of these systems arise from compressibility of the hydraulic fluid, the complex flow properties of the servo-valve, valve overlap and friction in the hydraulic cylinder. Aside from the nonlinear nature of the hydraulic dynamics, there are many considerable model uncertainties, such as internal and external leakages and external disturbances, which cannot be modeled exactly. Therefore, in order to design a high performance controller for simulating the earthquake signal, which is the goal of a servo-hydraulic shaking table, a suitable dynamical model of the system needs to be formulated.

In this thesis beside a specific application of hydraulic actuator which is a shaking table system, an integrated approach to model and control of a hydraulic servo-system is presented. The application of servo-hydraulic shaking table shows the dynamics and nonlinearities of the servo-valve and the compressibility of hydraulic oil, which constitute the limits of the servo-system performances. Especially, in case of the acceleration model and control of a hydraulic servo-system. In the shaking table application, for modeling and identification of the system, in contrary to the previous works, which in them the position and pressure sensors are used, only the position and acceleration sensors are available and then for control purpose only position sensor is accessible.

In order to obtain structural insight in the way that the performance is limited by the properties of (the subsystems of) the hydraulic servo-system, the modeling

procedure has been treated thoroughly in this thesis. At the one hand, this has opened the way to model-based control design, so that unavoidable limits of performance can be narrowly approached. At the other hand, the obtained insight appears to be useful in the system design stage, such that potential control problems may be avoided by proper system design.

Because of the twofold purpose of the modeling, with control design requiring quantitatively accurate models and simulating the behavior of the system precisely which requiring qualitative insight in the system behavior, the so-called white-box and gray-box modeling approaches have been applied. These approaches comprise physical modeling including model analysis by means of simulation, and subsequent identification and validation of the obtained physical models, using experimental data.

In the physical modeling stage, a consistent integration of the nonlinear dynamic of the different hydraulic actuator subsystems, namely servo-valve and cylinder have been presented. In this model, the most nonlinearities of the system, which arise from compressibility of the hydraulic fluid, the complex flow properties of the servo-valve, valve overlap and friction in the hydraulic cylinder, are simulated. Four different kinds of friction model are considered and the accuracy of these models for simulating the behavior of the system have been compared experimentally. However, it has been shown that for simulating the behavior of the system, nonlinear modeling of the friction is not enough. Then, by gathering some position and acceleration information of the real system, the sensitivity of the model to different nonlinearities of the system have been investigated. This led to the insight, that only some of the model nonlinear effects are really relevant, such as the nonlinear flow characteristic of the servo-valve spool due to non-ideal port geometries and the compressibility of hydraulic oil, and the position dependence of the actuator's dynamics. Therefore, based on the experimental results, two new nonlinear dynamic models for simulating the behavior of position, velocity and acceleration outputs of the servo-hydraulic shaking table have been proposed. First in the gray-box method, with defining six main parameters of the model and identifying them for different sinusoidal inputs, a neural network model is proposed. Second in the white-box method, a new empirical nonlinear model for effective bulk modulus of hydraulic oil has been proposed which increases the accuracy of the model to predict the behavior of the position, velocity

and acceleration output of the system with respect to different kind of inputs such as pulse and sinusoidal inputs and wide range of frequencies. The achievements of this model would be helpful for following reasons:

1. Since the proposed model can predict precisely the behavior of the system, the designed controller based on this model can enhance the performances of the model based force controller which is the goal of the shaking table for tracking acceleration reference signal.

2. It reduces the cost of the hydraulic servo-systems with eliminating the acceleration and internal pressure sensors. In all the previous works, using the pressure or force sensors for controlling the force or acceleration of the servo-hydraulic actuators are necessary. While, with considering this new model the pressure and force output of the system can be estimated with high accuracy.

3. It is not always possible to measure the full state of the servo-hydraulic system due to the hardware limitations. Therefore, it is suitable for constructed old industrial systems (such as the shaking table) which inserting pressure sensor inside them without changing the structure of the system is impossible.

4. The computational simulation developed by model could serve as a powerful result-interpretation tool and parameter optimization of the designed controller with respect to any parameter identification.

In addition, not every physical system can be controlled by having the full state feedback measurements from sensors. Since, in reality all the acceleration sensors have various kinds of gravity biases, velocity sensors do not give directly the velocity in fact they are force or position sensors which the velocity comes from filtering then integration combination which has so many bias or differentiation then filtering combinations which has so many delays and pressure sensor measurement which involve noise. In this approach, the link between the physical and the system theoretic interpretation of the properties of the hydraulic servo-system are strongly emphasized. This makes, that the presented models are not only useful for shaking table design, but also for the design of the hydraulic servo-system.

Finally, based on the task specification of the shaking table, which is tracking the position and velocity reference signals with considering uncertain load conditions, different kinds of robust controllers have been designed. For this purpose, the full order dynamic model of the system is simplified in a new approach and then due to the availability of only the position sensor on the experimental setup, a robust sliding mode observer has been designed which can estimate robustly the velocity and acceleration states of the system from the position sensor with high accuracy. Experiments with a hydraulic actuator in a single degree-of-freedom setup have shown the validity of the approach for control design. The experimental results of the closed loop system by considering three different designed controllers, feed forward PI controller, sliding mode and super twisting controller for uncertain load condition have been presented. An analysis of the control strategies for this setup shows that the position and velocity output of the system with considering the sliding mode and super twisting controller and different load conditions can robustly and accurately track the reference signals. In addition, the comparison between the responses of these three controllers demonstrates that the super twisting sliding mode controller has smaller error and smother input controller and response than the sliding mode and feedforward PI controller.

Contents

List of Figures

Chapter 1

Introduction

Hydraulic fluid power is one of the oldest forms of power transmission, which despite the period of rapid growth of electric power generation and its desirability because of high-performance motion control, became accepted for a wide variety of applications. In recent years, it has been widely used in many industrial applications such as aerospace, machining plants, robotics, motion simulators, fatigue testing systems, metal-processing plants, mining, special purpose machines and so on. With increased possibilities in applying advanced control methods, among others due to increased computer power and ongoing developments in control theory, higher demands are made on the modeling of the nonlinear dynamic behavior of hydraulic servo-systems. More detailed descriptions of dominant nonlinear characteristics and relevant dynamics over wide frequency ranges have to be taken into account.

The main nonlinearities in hydraulic systems arise from the compressibility of the hydraulic fluid, the complex flow properties of the servo-valve, valve overlap and the friction in the hydraulic actuators. They depend on factors, which are difficult to measure or estimate online, such as oil bulk modulus, viscosity and temperature. Aside from the nonlinear nature of the hydraulic dynamics, there are many considerable model uncertainties, such as internal and external leakages and external disturbances, which cannot be modeled exactly. Therefore, conventional feedback control, which is easily tuned by hand, is only sufficient for some cases. Advanced (model-based) control methods are necessary if high performance motion control is required.

In this thesis, in addition to a specific application of hydraulic actuator, a shaking table servo-system, an integrated approach to the modeling of a hydraulic servo-system is presented. First, a consistent integration of the nonlinear dynamic modeling of the different subsystems of the hydraulic servo-system, namely servo-valve and actuator are presented. In this model, the most nonlinear characteristics of the hydraulic actuator consist of compressibility of the hydraulic fluid, the complex flow properties of the servo-valve, valve overlap and friction in the hydraulic cylinder are simulated. Then, based on the experimental results a new nonlinear model for simulating the behavior of the system is proposed. This model comprises a systematic approach of theoretical modeling, model simplification and identification, and experimental validation. In this approach, the link between the physical and the system theoretic interpretation of the properties of the hydraulic servo-system are strongly emphasized. This makes, that the presented models are not only useful for shaking table control design, but also for the design of the hydraulic servo-system. Then, a 3^{rd} order nonlinear simplified model is derived based on the hydraulic servo-system model. This model is used for designing observer and different kind of controllers.

After an introduction into the hydraulic servo-technique in Section 1.1, the role of hydraulic servo-technique in shaking table control is highlighted in Section 1.2. This discussion motivates the research on the modeling of hydraulic servo-systems, leading to the problem statement of Section 1.3. After that, the approach for research is given in Section 1.4, while an outline of the thesis in Section 1.5 completes this Chapter.

1.1 Hydraulic servo-technique

1.1.1 History and motivation for hydraulic drives

A brief but very interesting history of hydraulic mechanisms has been compiled in [138, 18, 169]. In the following, we summarize the latter work and refer the reader to both references for more complete treatment.

The performance of mechanical work using pressurized and moving fluids dates back for nearly six millennials. The Egyptians and Chinese used to move water and wind to do work and records show that the advanced civilization in China in 4000

B.C. constructed and utilized wooden valves to control water flow through pipes made of bamboo.

The above applications did of course use dynamic properties of fluids and kinetic energy was employed to perform useful work. Whereas, the scientific progress was made in the Middle Ages in connection with fluid power and it was not until 1648 that a Frenchman, Blaise Pascal, formulated the law that states the pressure in a fluid is transmitted equally in all directions. Then the first industrial application of the hydraulic press (using water as the working fluid) was performed by Josef Bramah (1749-1814), in 1795, in London.

Following the invention of the steam engine by James Watt (1736-1819), hydrostatic machines were widely used in England for energy exchange in the form of pressurized water networks. Pumps driven by steam engines were employed to generate pressurized water, which was in turn used to actuate pistons driving the processing machines (e.g., mills).

In the second half of the 19th century, W.G. Armstrong (1810–1900) developed many hydrostatic machines and devices, primarily for use in shipbuilding (e.g., capstans, lifting jacks). Some of these control devices still resemble those used today.

Interest returned to fluid power at the end of 20th century due to an increase in the use of servo control techniques, which allow accurate closed loop motion control. The development of hydraulic servo-techniques was pushed further by the contributions of Blackburn in [26]. Then governments and industries supported research at several universities has accelerated hydraulic control technology which increased the usage of hydraulic systems in many applications. Nowadays, hydraulic servo-systems are used [141]:

- where relatively large forces or torques are required (industrial presses, mobile lifting, digging, material handling equipment, etc.),
- where fast, stiff response of resisting loads is needed (machine tool drives, flight simulators, rolling mills, etc.),
- where accurate control of response is necessary (control surfaces of aircraft, machine tool slides, industrial robots, etc.),

- where manual control of motion involving substantial forces is essential (heavy machinery, aircraft controls, automotive power steering, etc.), and
- as the final actuator subsystem in complex automatically controlled situations (electro-hydraulic flight simulators, industrial robots, fatigue and other programmable test rigs, theater stage control, etc.).

Hydraulic control systems provide many advantages over other types of control (e.g., electrical motors), some of which are [141]:

- Hydraulic systems can produce larger forces/torques, and have higher load stiffness.
- The hydraulic fluid acts as a superb lubricant and avoids wear.
- Hydraulic actuators have higher speed of response with fast starts, stops, and speed reversals.
- Hydraulic systems may be operated under different conditions (continuous, intermittent, reversing, stalled).
- Both linear and rotary actuators are available and add to the great flexibility of hydraulic power elements.
- Overloading protection is easy.
- Smaller and lighter compact systems with long component life are available.

Besides the advantages of fluid power, there are obviously some disadvantages, some of which are [141]:

- There is always a need for hydraulic power generation; electrical power is generally more readily available.
- Components of hydraulic systems are relatively expensive because of the small allowable tolerances.
- A hydraulic system is relatively difficult to maintain; it should be free from leaks, the fluid should be free of dirt and contamination, and breaks with complete loss of fluid should be prevented as much as possible.

- Hydraulics are not so flexible, linear, accurate, and inexpensive as electronic and/or electromechanical devices in the manipulation of low power signals for purposes of mathematical computation, error detection, amplification, instrumentation, and compensation. Therefore, hydraulic devices are generally not desirable in the low power portions of control systems.

Despite these disadvantages, there are various applications, where their advantages make hydraulic drives the best alternative. In most of these present applications, accurate motion control is required. This means, that hydraulic systems generally operate in closed loop, i.e. as a servo-system. A characterization of such hydraulic servo-systems is given in the next Section.

1.1.2 Characterization of hydraulic servo-systems

Hydraulic servo-system is an arrangement of individual components, interconnected to provide a desired form of hydraulic transfer. The basic structure of hydraulic systems is shown in figure 1.1 and consist of: the supply unit providing pressurized fluid, the valves for controlling the direction of pump flow, the level of power produced, and the amount of fluid and pressure to the actuator, the actuator itself, and the measurement and control devices.

1.1.2.1 Supply unit

Although there is a lot of technology involved in modern power units for the oil supply of a hydraulic servo-system, the functionality of this subsystem is simple, at least from the point of view of hydraulic servo control. The supply unit should provide fluid power to the servo-system, in the form of a constant supply pressure, independent of the demanded flow as much as possible. Generally, this fluid power is generated by an electrical motor, driving a hydraulic pump. By means of a pressure control mechanism, for instance a pressure relief valve, a constant supply pressure level is maintained. Short-term pressure variations due to pump flow pulsations and peak flow demands are mostly equalized by a hydraulic accumulator, which should be mounted at a short distance from the servo-valve. A cooling system

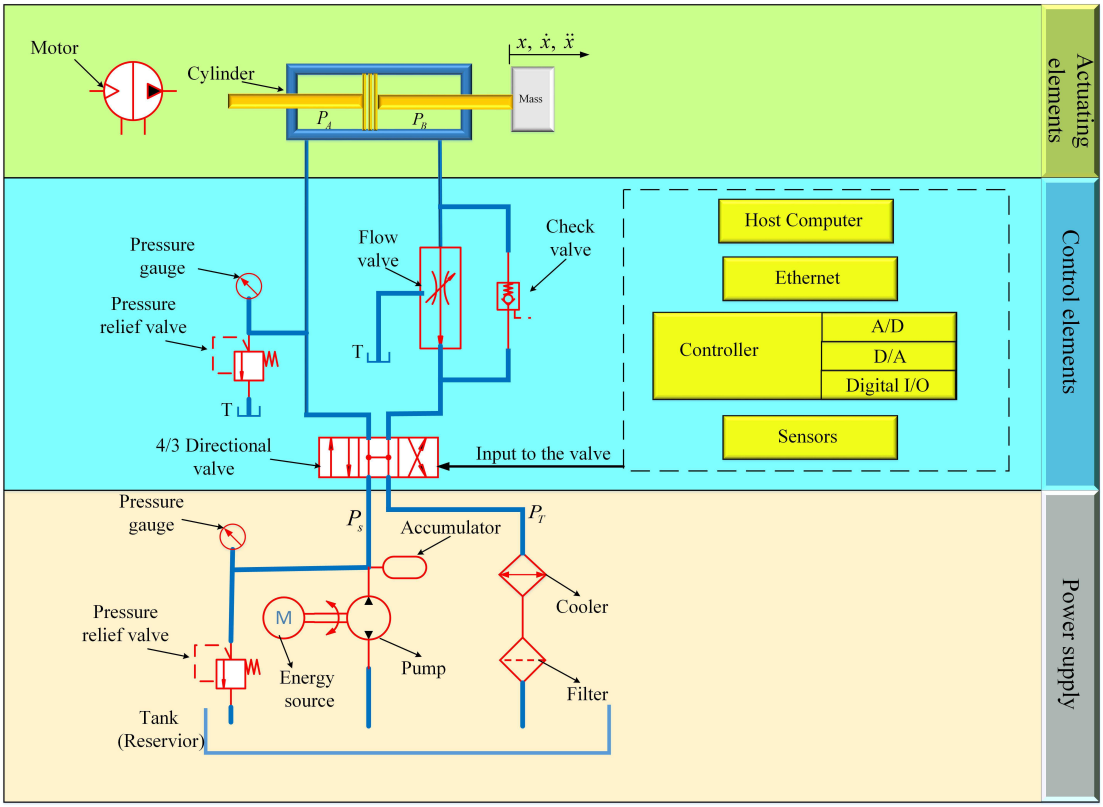

Figure 1.1: Basic structure of hydraulic systems.

with a temperature control loop maintains an operational temperature, generally in between 30 and 40^0C.

The basic configurations of hydraulic power supplies that provide constant supply pressure are shown in figure 1.2. The two classical pressure sources (a) and (d) are simple and safe (especially in conjunction with the use of an accumulator). Concept (c) is becoming more and more popular due to further development of electrical drive control. Switch-off pumps are not so common, since they can lead to persistent pressure fluctuations.

In the cases where the hydraulic system is subject to wide fluctuations in load (i.e., pressure and/or flow), load-sensing systems are predestined to save substantial energy. These systems have found wide application in mobile hydraulics and, of late, also in industrial hydraulics.

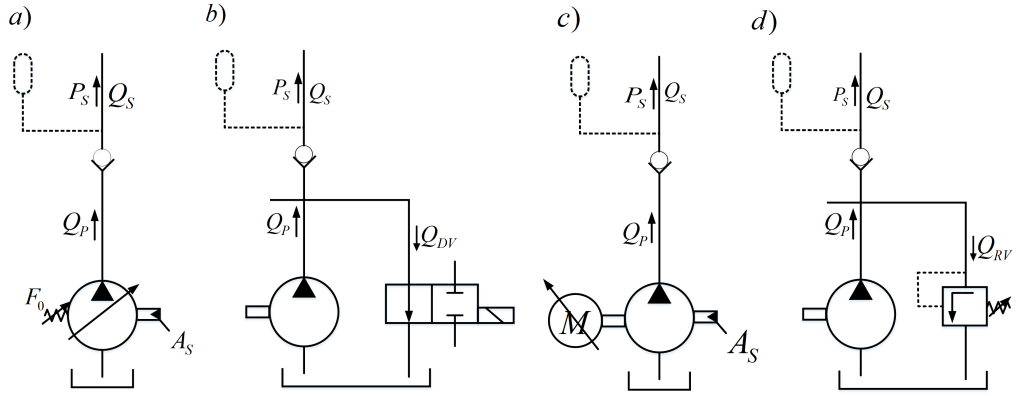

Figure 1.2: Basic configuration of pressure sources.

Other hydraulic control structures use power supplies in the form of flow sources, known as hydrostatic transmissions or pump/motor circuits (typically applied in ship steering systems, antenna drives or vehicle drive systems), as shown in figure 1.3.

The **open circuit** (figure 1.3a) uses a pump to produce flow, which is utilized by a simple or complex system, with the return flow exhausting to the tank. The inlet section of the pump draws the fluid from the tank to complete the circuit.

The **closed circuit** (figure 1.3b) is a continuous circuit between pump and motor, i. e., the pump output flow is sent directly to the hydraulic motor and then returned in a continuous motion to the pump. The tank and heat exchanger take up leakage and auxiliary function flow. Closed circuits are typically used to maintain a given output speed proportional to a pump input command, and offer continuously variable output speed in all four quadrants.

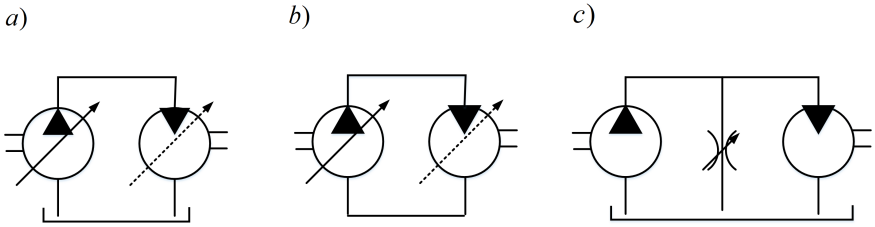

Figure 1.3: Power supplies as flow sources (a) open circuit, (b) closed circuit, (c) principle of bypass control

The **principle of bypass control** (figure 1.3c) is to return the overproduced flow from the constant-delivery pump to the tank by means of an adjustable throttle valve.

A detailed description and properties of all power supply configurations mentioned in this section can be found in [208].

1.1.2.2 Valves

Valves are the most important mechanical (or electrical) link to the fluid interface in hydraulic systems. Different types of flow control valves have been developed for hydraulic control systems, as described in [141, 90]. Basically, they can be divided into three classifications: sliding, seating and flow dividing. examples of these are spool, flapper and jet pipe valves respectively.

The most widely used valve is the sliding valve employing spool type construction. Spool valves are classified by: (a) the number of ways flow can enter and leave the valve, (b) the number of loads and (c) the type of center when the valve spool is in neutral position (figure 1.4) . **Closed center or overderlap valves**

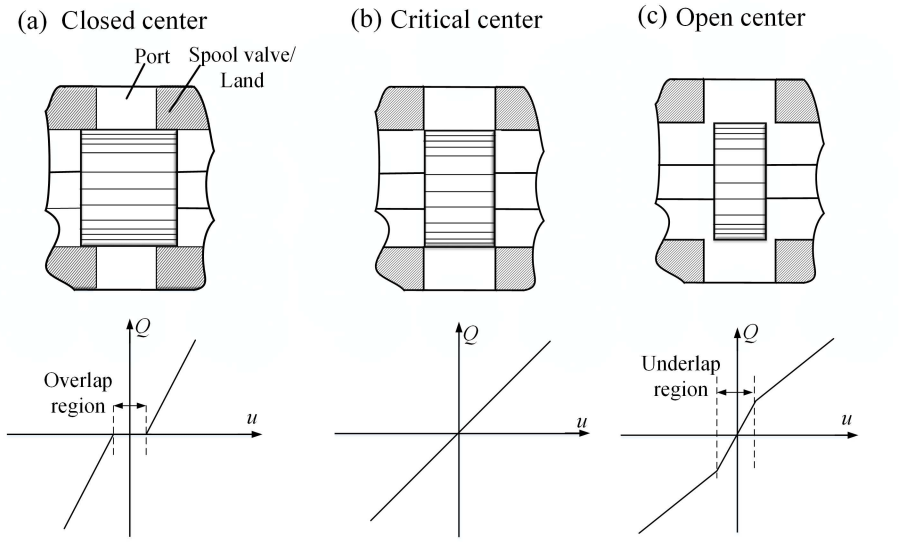

Figure 1.4: (a) Definition of closed center valve and its flow-signal graphs, (b) Definition of critical center valve and its flow-signal graphs, (c) Definition of open center valve and its flow-signal graphs.

have a land width greater than the port width when the spool is at neutral and for a short period all valve ports are sealed against each other(figure 1.4a). **Critical center or zero lapped valves** have a land width identical to the port width and is a condition approached by practical machining (figure 1.4b). **Open center or underlap valves** have a land width smaller than the port in the valve sleeve and for a short period all valve ports are connected to each other (figure 1.4c). The most important characteristic of different center type of valves is the flow gain which has the shape shown in figure 1.4.

The vast majority of valves are manufactured with critical center because of the emphasis on the linear flow gain. Closed center valves are not desirable because of the dead-band characteristic in the flow gain. Dead-band results in steady state error and in some cases can cause backlash which may lead to stability problems. Open center valves are used in applications which require a continuous flow to maintain reasonable fluid temperatures and also in constant flow systems. However, the large power loss at neutral position, the decrease in flow gain outside the underlap region and the decrease pressure sensitivity of open center valves restrict their use to special applications. The gain of systems using open center valves must be adjusted with the valve at neutral because of the increased flow gain near null. Therefore the system error and bandwidth are adversely affected when the valve is away from neutral because of the decreased flow gain. This aspect of open center valves is most undesirable.

Spool valve manufacture requires that close and matching tolerances be held so that such valves are relatively expensive and sensitive to fluid contamination. Tolerances required for flapper valves are not as stringent, which makes them attractive with regard to these two aspects. However, the relatively large leakage flows limit their application to low power levels. Flapper valves are used extensively as the first stage valve in two-stage electro-hydraulic and hydro-mechanical servo-valves. Poppet-type valves are basically two way valves and therefore are restricted to applications such as check and relief valves, in which reversal in flow direction is not required. The jet pipe valve is not as widely used as the flapper valve because of large null flow, characteristics not easily predicted, and slower response. The main advantage of jet pipe valves is their insensitivity to dirty fluids. However, the

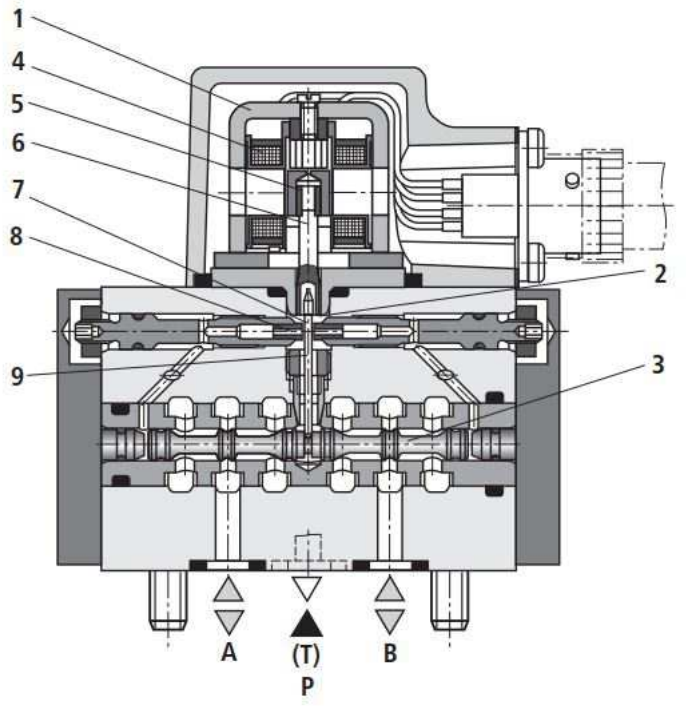

Figure 1.5: Drawings of a two-stage flapper-nozzle servo-valve (Bosch Rexroth, RE29564) [1: hydraulic amplifier (principle: nozzle flapper plate) 2: control spool 3: main spool 4: solenoid, 5: armature, 6: flexure tube, 7: flapper, 8: control nozzles, 9: spring (mechanical feedback).]

more predictable flapper valve has similar performance characteristics and is usually preferred.

In this thesis, based on the application, a servo-hydraulic shaking table, a double-acting hydraulic actuator is used. For this kind of actuators the four-way spool valve of the flapper-nozzle type as shown in figure 1.5, is most widely applied. So, the attention in this thesis will be restricted to this type of servo-valves. The working principle of this type of servo-valve is described in more detail in next section; the functionality is, that an electrical control signal is converted into a high-power oil flow, driving the actuator. Thereby, the relation between control input and delivered flow is achieved by applying an open center valve [141, 197], allowing proper closed loop servo control of the actuator.

1.1.2.3 Actuator

In the complete range of hydraulic actuators, a major classification can be given by distinguishing actuators with a limited and with a continuous travel. The latter ones are always of the rotary type, and can generally be used either as pump or as motor. Although these motors are mostly servo controlled and show resemblance with other servo-actuators, they are left out of consideration here.

The limited travel actuators can be classified as either rotary actuators of the vane type or as linear actuators of the piston type. From servo control point of view, vane actuators are completely equivalent to piston actuators, with the restriction that vane actuators are by definition symmetric, i.e. the displacement flow during motion is equal for both actuator chambers. So, without loss of generality at this point, the attention can be restricted to linear hydraulic actuators.

In the class of linear actuators, there are different basic configurations, suitable for different applications. Most well-known are the symmetric (double-rod in figure 1.6a) and the asymmetric (single-rod in figure 1.6b) actuator. In this figure, some part of a single rode cylinder have shown. The main advantage of the symmetric actuator is its stiffness and its symmetric load capability, which makes the actuator useful for high-performance applications with dynamic loads. The asymmetric actuator to the contrary, is less stiff, but is well-suited to counteract large asymmetric

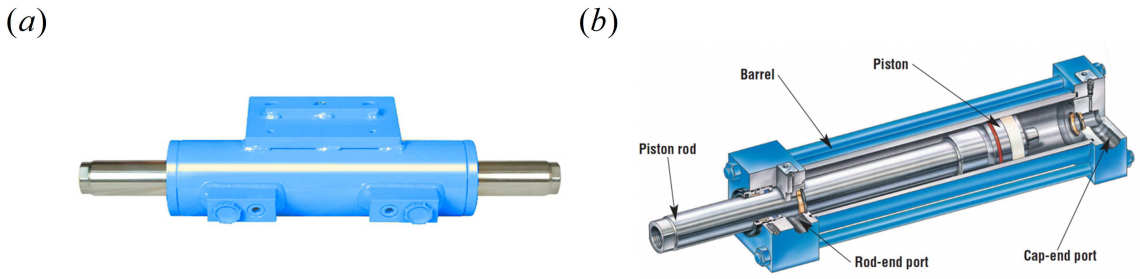

Figure 1.6: Different configurations of linear hydraulic actuators of the piston type; (a) double-rod and (b) single-rod.

(static) loads, e.g. gravity forces. So, it is clear that the type of actuator to be used is highly dependent on the application, where aspects as sort of load, available construction space, required performance and allowed costs play a role in the choice. Therefore, based on the application in the shaking table, the attention in this thesis will be restricted to a double-rod symmetric actuator.

From the viewpoint of servo control, it may be emphasized here, that a good system design should be seen as a prerequisite to achieve a good performance by means of closed loop control. In other words, closed loop control should not be used to compensate for the shortcomings in the system design, but to obtain an optimal performance given a well-designed system. Actually, the measurement and control hardware, necessary to close the loop of the servo-system, form an important part of this system design.

1.1.2.4 Measurement and control hardware

In early days of hydraulic position servo control, the actuator position was fed back mechanically to the valve spool, for instance in power steering systems. Nowadays, the actuator is provided with one or more transducers and an electronic control device.

The basic feedback in a hydraulic servo-system is generally obtained from a position transducer, measuring the piston displacement, and allowing the control of it. Besides that, a pressure difference transducer is widely applied, to obtain damping of the natural oscillation of the hydraulic system, or even to allow the control of exerted forces. In applications where explicit force control is the primary goal, such as fatigue testing machines, it is usual to mount a force transducer instead of a pressure difference transducer. In cases, where high-bandwidth position control is required, a velocity transducer may be added, although this is a rather expensive solution.

So, for feedback control purposes, transducers for position, pressure difference and possibly the exerted force, are most usual. Additionally, absolute pressure transducers and accelerometers are sometimes used for testing purposes, for instance in experimental setups and prototype systems.

In the past decades the control hardware generally consisted of an analog device, in which the (linear) control algorithm was implemented. Nowadays, most hydraulic servo-systems are controlled by more powerful digital control systems. For instance, the combination of high-resolution A/D and D/A-conversion with a Digital Signal Processor (DSP) is a powerful means to achieve a high closed loop performance, by implementing complex dynamic and possibly nonlinear control algorithms. Therewith, the hydraulic servo-technique has evolved to a high level of technology, where new limits on system requirements and control performance can now be reached.

1.2 Shaking table

As illustrative example, a new servo-hydraulic shaking table with one degree of freedom (DOF), is developed at the university of Bergamo. Shaking table is an important experimental device for simulating dynamic response of complex mechanical systems to high natural dynamic forces. It has been widely used in many industrial applications such as aerospace [93, 227], automotive [103] and civil engineering [122, 62, 230, 156, 166, 167]. In recent years, its usage stands out in civil engineering for analyzing and simulating dynamic response of high rise buildings and structures to earthquakes and wind storms.

This system consist of high-performance mechanical and electrical equipment which must be design to work smoothly and effectively together. To this end, every component of the shaking table system was designed based on the requirement of the entire system and the cost. The major components of the system are divided into five categories:

- Program data acquisition
- Control
- Hydraulic power system
- Servo-valve and actuator
- Slip table and foundation.

A diagram of the various components of the system is shown in figure 1.7. For simulating a desired signal, an electrical command signal is sent by the personal

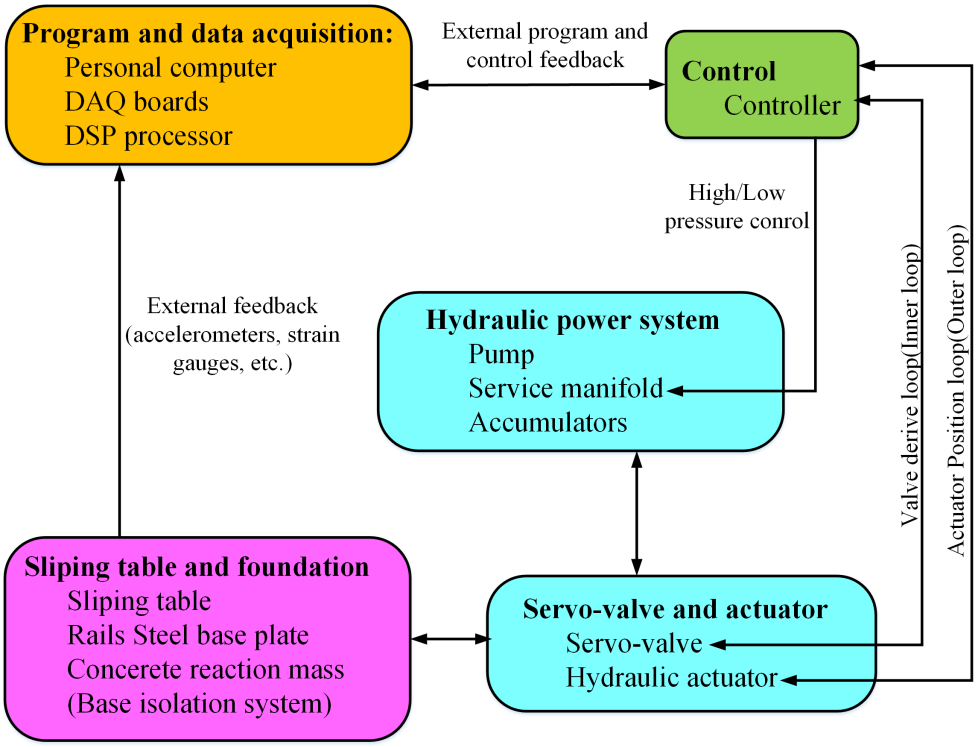

Figure 1.7: Diagram of the shaking table components.

computer to the controller. Then controller produces the suitable control input for sending to the servo-valve which opens or closes the valve appropriately to port a portion of the constant slow of hydraulic fluid that is being provided by the pump into the actuator. This fluid forces an actuator arm, which is connected to the slip table, to move in the desired direction. Test specimens, such as scaled models of structures, are fixed to the slip table. Feedback from the various components can be fed back to the personal computer for the purposes of control or data acquisition. A full hardware description of the experimental shaking table will be presented at the experimental section.

1.3 Problem statement

Due to requirement of large force and displacement in the shaking tables, they are mostly driven by servo-hydraulic actuators. Unfortunately, the dynamic char-

acteristics of these systems are highly nonlinear and relatively difficult to control. Therefore, in order to design a high performance controller for simulating the acceleration behavior which is the goal of a servo-hydraulic shaking table, a suitable dynamical model of the system needs to be formulated. Therefore, the problem statement for this thesis is formulated as follows:

Improve the quality of the models of hydraulic servo-system with respect to their intended use:

- To obtain insight in the system behavior,
- To eliminate the acceleration and pressure sensors and reduce the cost of the system,
- To perform model based control design.

Because of the three-fold intended use of the models, a rather general approach to the modeling of hydraulic servo-systems is required, covering the whole range of theoretical modeling (for insight), identification and validation (for reliable use in control design), and the application of the model-knowledge in control design and system design. Therefore as described in the previous sections, for increasing the performance of modeling, it seems to be important to include the complex flow properties of the servo-valve, valve overlap, the compressibility of the hydraulic oil and friction in the hydraulic cylinder in the investigations. Against this background, the general problem statement is worked out in four main topics for the research:

Each of these topics will be worked out below, as a motivation for the approach

1. Modeling of the hydraulic actuator includes modeling of the compressibility of the hydraulic oil or Effective bulk modulus of hydraulic oil and friction of the hydraulic cylinder,
2. Modeling of the servo-valve,
3. Identification and validation of the model,
4. Control design for hydraulic servo-system.

for research. A detailed description and a literature review summery for all these topics have been presented in the following.

1.3.1 Modeling of the hydraulic actuator

The theoretical modeling of hydraulic servo-systems is well-developed in the past decades. Standard text-books on hydraulic servo-systems, as for instance those by [141, 197, 200, 3, 90], provide a thorough analysis of the basics of the hydraulic servo-technique. Among others, this analysis comprises the theoretical modeling of the dynamical and nonlinear effects in various hydraulic components, among which hydraulic actuators. Besides these basic contributions, there are numerous other contributions [134, 136, 42, 229, 219, 92, 221, 225], in which the dynamic modeling of hydraulic actuators is reported.

Many researchers use the three basic mathematical relationships: the pressure-flow equation of the valve, the continuity equation of the fluid and the pressure-load equation. In this method, as stated before, in order to improve the simulation results, the model of the nonlinear characteristics of the system such as compressibility of the hydraulic fluid, the complex flow properties of the servo-valve, valve overlap and friction in the hydraulic cylinder are needed (see, for instance, [134, 136, 42]). The results in these papers show that even with considering different nonlinear friction models, the simulated velocity for a small range of velocity and frequencies is fairly correct and so is the simulated acceleration. Additionally, in [141, 229, 219] have been shown that the acceleration output of the system to the sinusoidal inputs, is distorted and it contains harmonics with the fundamental frequency and its integer multiplications. In [92, 221, 225], for simulating the acceleration response, have been considered a sinusoidal function with known frequencies. Then, the amplitude and phase of each function are calculated based on the least mean square method [92], the Kalman filter [221] and the unscented Kalman filter [225]. However, the input frequency of the system in all these methods is assumed to be known and the acceleration sensor data are always needed for updating the identification parameters. Furthermore, as stated in these papers, it takes 0.5[s] for the parameters to converge to the actual amplitude and phase of harmonics which is suitable for the control process up to 1[Hz]. Therefore, these methods are not suitable for the shaking table which has nominal frequency 10[Hz]. As another method in [168], the acceleration of the system has been simulated based on feed-forward neural network method. This method needs high computation resources and it has 2[s] convergence

window at the first run which in some cases it causes instability in control feedback loop. Thus, in order to model the acceleration behavior of hydraulic actuators to any kind of inputs, it is needed to model the nonlinear features of the system such as effective bulk modulus and friction in the hydraulic cylinder as accurately as possible.

1.3.1.1 Modeling of the friction in the hydraulic cylinder

Friction forces between two surfaces in contact arise as a result of the microscopic irregularities and asperities. The effects of friction depend on many factors, such as displacement and relative velocity of the bodies, properties of the surface materials, presence of lubrication, temperature, etc. Different models have been derived based on the experimental observation of friction phenomena which captured the friction components in a more or less accurate way. Interesting reviews of the main friction characteristics and classical models can be found in [10, 155, 9, 99], starting from the basic concept of friction as a force that opposes motion, captured by the pure Coulomb model, up to complex static and dynamic models. Complex models are mostly built upon the simple model elements with additional characteristics, which can handle dynamic behavior. Yet the science of tribology is still far from having a complete picture on how friction works in all extent, therefore these models are mostly based on experimental experiences, rather than deep scientific background.

A complete history of tribology science has been compiled in [50]. In the following, we present a brief history and the latter work of friction.

The classic laws of sliding friction were discovered by Leonardo da Vinci in 1493, a pioneer in tribology. He claimed that the frictional resistance was the same for two different objects of the same weight but making contacts over different widths and lengths. He also found that the force needed to overcome friction is doubled when the weight is doubled. Then, Guillaume Amontons in (1663-1705) rediscovered the tow original laws of friction that had been discovered by Da Vinci. By using the classical dynamics, Leonard Euler (1707-1783), expressed the value of the coefficient of friction by parameters which could be easily measured.

The understanding of friction was further developed by Charles-Augustin de Coulomb(1736-1806). Coulomb investigated the influence of four main factors on

friction: the nature of the materials in contact and their surface coatings; the extent of the surface area; the normal pressure (or load); and the length of time that the surfaces remained in contact (time of repose). Coulomb further considered the influence of sliding velocity, temperature and humidity, in order to decide between the different explanations on the nature of friction that had been proposed. The distinction between static and dynamic friction is made in Coulomb's friction law, although this distinction was already drawn by Johann Andreas von Segner in 1758.

Arthur Jules Morin (1833) developed the concept of sliding versus rolling friction. Osborne Reynolds (1866) derived the equation of viscous flow. This completed the classic empirical model of friction (static, kinetic, and fluid) commonly used today in engineering. In 1877, Fleeming Jenkin and J. A. Ewing investigated the continuity between static and kinetic friction.

The focus of research during the 20th century has been to understand the physical mechanisms behind friction. Frank Philip Bowden and David Tabor (1950) showed that, at a microscopic level, the actual area of contact between surfaces is a very small fraction of the apparent area.

Nowadays, several mathematical models, which are used to describe the friction behaviors observed in mechanical systems, have been proposed in literature [10, 83, 49, 185, 114, 51, 5, 9]. Some of these models have been commonly used to express the friction of hydraulic cylinder [9, 49, 215, 216, 190]. The simple friction [9] which is used to simulate many mechanical systems, is the combination of Coulomb friction, viscous friction and static friction. However, this model cannot predict the dynamic friction behaviors in the sliding regime of a hydraulic cylinder when the system operates under oscillating velocity conditions [215].

In [215], has been studied the dynamic friction characteristics of a hydraulic cylinder under oscillating velocity conditions in the negative resistance regime, i.e., in the velocity range where the friction force decreases with increasing velocity. They have shown that when the piston velocity varies sinusoidally with velocity reversals, the dynamic friction force–velocity characteristic exhibits a hysteric behavior (frictional lag) around the steady-state friction characteristic. In addition, they have shown a decrease of the maximum friction force observed after one cycle of the velocity variation. In order to simulate those dynamic friction behaviors of the hydraulic cylinder, they have modified the LuGre model in [49] by incorporating lubricant

film dynamics into the model and have shown that the proposed model, called the modified LuGre model, can simulate the dynamic friction behaviors observed experimentally in the sliding regime of the hydraulic cylinder with a relatively good accuracy. However, in [191], has been shown that based on the experimental results, the simulated velocity with considering modified LuGre model is fairly correct. In addition, in [167, 190] have been pointed out that these models are valid with the assumption of the frequency up to 2[Hz] and the velocity under 0.15[m/s], that is a limit in real practical shaking tables. Aside from these problems, obtaining real value for some parameters in LuGre model is very difficult and some experiments and sensors are needed which can be expensive and time consuming [190].

In the chapter 3, we will discuss about the theories and experimental results of these frictions.

1.3.1.2 Modeling of the Effective Bulk Modulus for hydraulic oil

Interaction of the spring effect of liquid and the mass of mechanical parts gives a resonance in nearly all hydraulic components. In most cases this resonance is the chief limitation to dynamic performance. The fluid spring is characterized by the value for the bulk modulus. Mathematically, it expresses the change in density of the liquid as external pressure is applied to the liquid. It shows both the "stiffness" of the system and the speed of transmission of pressure waves. Therefore, stability of servo-hydraulic systems and efficiency of hydraulic systems is affected by the value of compressibility.

Despite the frequent assumption that hydraulic fluid is incompressible, the fact remains: All fluids have some degree of compressibility. Granted, fluid compressibility may be neglected in systems that do not require tight control of response and where operating pressure and fluid volume are moderate. However, when applying high pressure to a large volume of fluid, a significant amount of energy can be expended to compress the fluid, essentially squeezing the fluid's molecules closer together. The result can be delayed response, a loaded actuator may not move until upstream fluid has been compressed, and the energy stored in the fluid may cause the actuator to continue moving after its control valve has closed. With many of today's hydraulic systems operating at pressures 5000 [psi] and higher, ignoring

bulk modulus can compromise response time of a system. Applied pressure should directly affect the action of the system rather than compress the fluid. This is why it is so important to design systems with as little fluid as possible between the control valve and the actuator.

There have been many studies and publications on the topic of the bulk modulus without considering the effect of entrained air [209, 54, 179]. However, the real bulk modulus with considering the effect of entrained air, temperature and mechanical compliance in the hydraulic systems is presented by the value for the effective bulk modulus. Unfortunately, it is one of the most ambiguous parameters because it is always influenced by the entrapped air, working pressure, and temperature variation [135, 40, 87]. In addition, it is a difficult task to measure and estimate the effective bulk modulus in real systems [102]. Therefore, system performances with respect to positioning, power loss, response time and stability of servo-hydraulic systems is affected by the value of bulk modulus.

In recent years, several theoretical models have been proposed to simulate the dependence of the effective bulk modulus upon pressure and entrained air content [213, 154, 146, 65, 170]. In [104, 87], based on the experimental verification of these models, have been shown that the IFAS model in [146] can simulate most accurately the behavior of the effective bulk modulus. However, as shown in these papers, the minimum time for maximizing the input pressure are 2.5[s], which in our study is almost the steady state case.

1.3.2 Modeling of the servo-valve

In the field of servo-valve modeling, extensive theoretical modeling work has been presented with emphasis on different subjects. Basic work has been performed again in [141], where he mainly takes the viewpoint of system design, and comes up with very useful design rules for spool valves, flapper-nozzle elements, etc. Furthermore, the effect of turbulent flow through small orifices has been extensively studied in literature [63, 159, 31], as well as flow forces on a flapper element [141, 26, 125, 202, 140, 126, 123, 13, 100] and leakage flows along a valve spool [141, 7, 68, 90]. There are also studies considering the complete nonlinear dynamic behavior of a flapper-nozzle valve among others in [126, 124, 33, 201]. Although these references

are quite valuable from a theoretical point of view, especially because they often include an experimental validation of the studied phenomena, they do not provide the link to the practice of hydraulic servo-control design, because it is generally not clear, how the model parameters have been chosen. A serious complication is here, that manufacturers are not willing to provide the necessary information on geometrical parameters, and even may not be able to provide some of the model parameters because they are not (easily) measurable. This implies that the model parameters have to be identified from input-output behavior. Generally, this identification issue is not addressed in literature on servo-valve modeling. Another problem with available literature is that the discussions mainly remain restricted to the servo-valve behavior on its own, without considering the implications for closed loop servo control.

Contrary to the theoretical modeling approach for hydraulic servo-valves found in literature, there is a tendency in contributions on hydraulic servo control design, to approximate servo-valve dynamics by simple linear low-order models [59, 88, 150, 204, 206, 101, 43]. Also in these cases, the identification issue is mostly not addressed, while moreover the adopted models do not properly reflect the underlying physical behavior of the valve.

In short, in this thesis, the modeling of the servo-valve as a research topic are presented, according to the following considerations:

- In order to obtain insight in the dynamics and nonlinearities of the servo-valve, extensive theoretical modeling is to be performed. The desired insight not only concerns the character of the dynamics of the servo-valve, but also the relevance of different nonlinearities, related to certain physical effects, that may be present in the servo-valve. Thus, the obtained insight can be used in system design, i.e. to determine the requirements on the servo-valve.

- For control design purposes, experimentally validated dynamic models of the servo-valve are required. Thereby, the relevant nonlinearities are to be included, in order to use the models for robustness analysis and possibly for nonlinear control design. So, nonlinear identification of the servo-valve models

is to be performed, such that the obtained insight from the theoretical modeling is preserved. This requires special attention for the experiment design and the identification method.

- Although the experimental part of the servo-valve modeling is necessarily applied to a certain type of servo-valve (related to the hydraulic servo-system for the shaking table application), the approach to the modeling of the servo-valve should be general, so that it also applies to other valves of the flapper-nozzle type.

With this discussion, a line of thinking is developed for the modeling of a servo-hydraulic system and its parameters estimation and control, as explained next.

1.3.3 Identification and validation of the model

Models of real systems are of fundamental importance in virtually all disciplines. It can be useful for system analysis, i.e., for gaining a better understanding of the system. Models make it possible to predict or simulate a system's behavior. As mentioned before, due to the nonlinearities and uncertainties of the servo-hydraulic systems, designing a high performance controller for them needs to formulate a suitable dynamical model of the system and identify its parameters as precisely as possible.

In the construction of a model, physical laws can be used such as Newton's Law that requires specialized knowledge in the system. The model which is derived directly from some first principles by taking into account the connection between the components of the system is called white box model. A grey box model or semi-physical modeling are obtained when white box model contains some parameter that have unknown or uncertain numerical values. In the context of nonlinear model identification, many researchers have described grey box modeling as assuming a model structure based on first principle in hydraulic system and used recursive method for estimating the model parameters [90, 96, 19, 167]. Eventually, Black box models approach can be used which allow sufficient input-output measurements in developing a mathematical model that represent the system dynamics. Researchers in [110, 112, 98], have applied nonlinear system identification by using Hammerstein

model for modeling the nonlinear system. In [236, 237], has been discussed some practical issues concerning the identification of electro-hydraulic actuator using discrete linear as a black box model. In [16, 131], have been applied recurrent neural networks for identification and control in electro-hydraulic actuator.

In this thesis, after the model has been formulated, the parameters of the model can be identified from experimental data by applying suitable methods in an appropriate way. Experimental validation of the identified dynamic model is performed by comparing the results with corresponding measurements. Thus, black-box identification is left out of consideration in this research, as it can not handle the physical structure of the model. On the other hand, white-box modeling is not possible either, because there is insufficient a-prior knowledge on the theoretical model parameters. For these reasons, a Grey-box model for the system will be derived.

1.3.4 Control design for hydraulic servo-system

As mentioned earlier, high-performance motion control asks for model-based control. As far as position control for hydraulic actuators is concerned, basic principles have been discussed thoroughly in [141, 90, 197]. Besides that, applications of more modern control techniques to hydraulic servo-systems have been reported extensively in literature. Examples are state feedback control [75, 199, 228, 55, 111], robust control [142, 152, 193], sliding mode control [129, 30, 38, 20, 72, 105, 231], adaptive techniques [29, 36] and intelligent control [173, 160, 233], to mention only some. Another interesting development in hydraulic servo control is the so-called cascade ΔP control strategy, presented in [172] and worked out and formalized in [81]. This method actually emphasizes high-frequency pressure difference control by high-gain pressure difference feedback, rather than position control.

Although the different applications reported in literature are quite valuable, in the sense that they prove the validity of a certain control design approach for a certain application, a general relation between the application dependent control requirements and the applied control strategy can hardly be recognized. What is desirable in fact, is a general approach for model-based control design for hydraulic servo-systems, based on task specifications of the application and on available model

knowledge of the system at hand. This actually constitutes the fourth research topic of this thesis, including the following aspects to be considered:

- Based on the shaking table application and its different mass, it is to be taken account to design a robust control for servo-hydraulic systems.
- Given the task specification for the control loop of the hydraulic servo-system, a survey of basic actuator control strategies will be given, where the design is obviously model-based. This will have to include a discussion of the benefits of certain control strategies with respect to the given task specification, possibly in relation to the type of application.
- Highly important is the explicit inclusion of the implications of the properties of the servo-valve and friction in the cylinder on the closed loop performance, when discussing the control design for hydraulic servo-systems. In fact, this is the point, where the benefits of model-based control design should really become clear.
- For the shaking table application, which only position sensor is available, velocity and acceleration estimation require attention.
- At last but not least important aspect concerns the experimental evaluation of model-based control design. This means, that only control design and testing at simulation level is not sufficient, but that experimental implementation by means of digital controllers is required. Therewith, it is not only possible to evaluate the model-based control design strategy, but also to validate the obtained models of the system in view of control design.

1.4 Approach for research

In the description of the approach for research in this Section, the four main research topics are (to some extent) taken together. Actually, it is a functional description of the approach for research, rather than a detailed overview of the research program.

In order to obtain structural insight in the behavior of the hydraulic servo-system, with respect to relevant dynamics as well as relevant nonlinearities, the

starting point is the theoretical, physical modeling of the complete servo-system. That means, a theoretical model is constructed from basic physical laws, using and combining available contributions on theoretical modeling of hydraulic systems in literature. The result is a nonlinear dynamic (simulation) model of the hydraulic servo-system, including actuator and servo-valve. This model is used to perform various simulations, with realistic physical parameters for the given shaking table application, so that structural insight in the relevant dynamics and nonlinearities of the system can be obtained.

The obtained insight can be used to simplify and reduce the model where possible, and to neglect irrelevant nonlinearities. In this phase, linearization of the model plays an important role, as it provides much insight in the dynamic characteristics of the system. For instance, it allows a judgment, whether dynamics due to the servo-valve and the actuator nonlinearities may be expected to play an important role or not.

An important issue in the linearization and simplification step is the physical structure of the dynamic model. This structure is always preserved in the chosen approach, in order to allow the inclusion of the relevant physical nonlinearities in the model. The judgment whether nonlinearities are relevant or not is primarily based on nonlinear simulation results.

After the model has been linearized, reduced and relevant nonlinearities have been included again, the model parameters are identified from experimental data. Thereby, the dominant nonlinearities of the system are explicitly taken into account by proper experiment design and by applying the well-known Describing Function Method in an appropriate way. Experimental validation of the identified nonlinear dynamic models of the servo-system is performed by comparing nonlinear simulations with corresponding measurements.

As a final part of the research, with an experimentally validated model of the complete hydraulic servo-system available, a survey of basic (model-based) control strategies can be given. First, a robust observer will be designed to estimate the state of velocity and acceleration from position sensor of the system. Then, aspects like application dependent task specifications, implications of servo-valve dynamics and the actuator nonlinearities, only with position measurement, and experimental conditions are considered.

1.5 Outline of the thesis

After a sketch of the general approach for research in the previous Section, an overview of the contents of the thesis follows in this section.

Chapter 2: Physical Fundamentals of Hydraulics
This chapter will discuss some general physical properties of the working fluid and cover equations of fluid motion, types of flow and flow through various passages (pipelines, orifices, and valves), which are needed in the subsequent sections.
Chapter 3: Physical modeling
This chapter gives the theoretical model relations that constitute the nonlinear dynamic model of the complete hydraulic servo-system using first principles. This involves Comprehensive models for servo-valve, the actuator and its nonlinearities such as internal and external leakage, friction and effective bulk modulus and the motor.
Chapter 4: Identification and experimental validation
Accurate models or model parameters can be constructed from experimental input-output data. Different identification procedures are described and illustrated in this chapter that lead to:

- Linear-in-parameters models whose parameters can be estimated using classical least-squares analysis.
- Conventional non-linear models to be identified by the prediction error method and its subclasses.
- Neural-network-based models. The most popular types of neural networks, multi-layer perceptrons and radial basis functions, are considered.

As stated before, all these approaches lead to grey-box models.
Chapter 5: Control design
The purpose of this Chapter is to give a detailed survey of strategies in (model-based) control design for hydraulic servo-systems, including theoretical background. The algorithms covered encompass:

- Conventional controllers. Linear controllers (e.g., PI, state space, etc.)that are widely used in hydraulic systems are reviewed.
- Compensation of static nonlinearities. Conventional linear control structures are extended by compensating typical nonlinearities.
- Sliding mode control. Due to uncertainties in the hydraulic actuator and different masses which will be used for testing different structures, it is necessary to design a robust control for this kind of system.
- The very important practical aspect of state estimation, especially velocity and acceleration of hydraulic servo-systems is also addressed at the end of this chapter.

chapter 6: Case study and Experimental Results
In this chapter, the main contribution of the thesis are listed as:

- Analyzing the acceleration response of the hydraulic servo-system to a sinusoidal input signal.
- Identification of the system parameters with considering three different kinds of friction model.
- Analyzing the sensitivity of the system nonlinear model to variation different nonlinear parameters and find out the effects of the modeled nonlinearities.
- A new gray-box modeling of the shaking table with neural network is proposed.
- A new empirical nonlinear model for effective bulk modulus of the system is proposed which the whole model of the system with considering this nonlinearity can predict the behavior of the system as precisely as possible.
- The nonlinear model of the system with considering a new simplification method are simplified and its parameters are identified for using in control designing.
- Three different kinds of controller are designed base on only the position sensor.

In this chapter, the experimental evaluation of different strategies in system identification and model-based control discussed in previous chapters have been completed by applying on the uni-axial servo-hydraulic shaking table.

For identification purpose, the behavior of the experimental setup to different sinusoidal input is studied. The time and frequency response of the system shows that the acceleration output of the hydraulic servo-system to sinusoidal inputs is seriously distorted and it contains the harmonics which is multiplication of the fundamental harmonic. Then, the parameters of a typical nonlinear model of hydraulic system with considering three different kinds of friction mode are identified. However, the comparison between the simulated and experimental result shows that the identified model can not simulate the behavior of the system in wide band frequency and different input signals. Therefor, two nonlinear dynamic model for simulating the behavior of the system are proposed. First, with defining 6 main parameters of the typical model and identifying them for different sinusoidal inputs, a neural network model is proposed. Second, a new empirical nonlinear model for simulating the acceleration behavior of a servo-hydraulic shaking table in dynamic and steady state flow situations is proposed. Based on the experimental observations, this model is attained by modifying the IFAS model for simulating the effective bulk Modulus of the hydraulic oil.

Finally, based on the task specification of the shaking table which is tracking the position and velocity reference signals with considering uncertain load conditions, different kinds of robust controller design are presented. For control designing purpose, the full order dynamic model of the system is simplified in a new approach and then due to the availability of only the position sensor on the experimental setup, a robust sliding mode observer is designed which can estimate the velocity and acceleration states of the system from the position sensor. Experiments with a hydraulic actuator in a single degree-of- freedom setup have shown the validity of the approach for control design. The experimental results of the closed loop system controlling by three different controllers (feed forward PI controller, sliding mode and super twisting controller) with considering different load condition and reference signals are presented. An analysis of different control strategies for this setup led to the conclusion, that super twisting sliding mode controller shows a smaller error and smother response for position and velocity trajectory tracking with respect to

sliding mode and feedforward PI controller.

Chapter 7: Conclusions and recommendations

The final Chapter of this thesis gives the conclusions that can be drawn on the presented results, as well as a number of recommendations for future work.

Chapter 2

Properties of fluid

A fluid is defined as a substance that cannot sustain a shearing stress. A fluid can be liquid or gaseous. Liquids and gases may be distinguished by their relative incompressibility and the fact that a liquid may have a free surface while a gas expand to fill its confining container. The science of fluid power is concerned with the utilization of pressurized liquid or gas to transmit power, but we will be dealing exclusively with hydraulic fluids (i.e., liquids).

The purpose of this chapter is to define some physical properties of hydraulic fluids, and to discuss the fundamental laws and equations of fluid motion, types of flow, and the flow through orifices and valves. The writing of this chapter was largely influenced by the extensive discussions on flow through orifices and valves in the standard textbooks by [106, 141, 207, 32, 2] and more recently the fine work by [76, 90, 37].

2.1 Physical properties of fluid

The normal tension on the surface element of a fluid is called pressure. It is, at a given point, identical in all directions. Pressure can be calculated as

$$P = \frac{Force}{Area} = \frac{F}{A} \tag{2.1}$$

and thus has the dimensions of force per unit area $[N/m^2]$.

2.2 Viscosity and related quantities

All fluids, including oil and air have fundamental properties and follow basic fluid mechanics laws. The viscosity of a fluid is its resistance to flow. Some fluids, like water, are thin and have low viscosity while others like honey are thick and have high viscosity. The fluids for hydraulic systems are a compromise. If the viscosity is too low, fluid will leak by internal seals causing a volumetric loss of efficiency. If the viscosity is too high, the fluid is difficult to push through hoses, fittings and valves causing a loss of mechanical efficiency. Viscosity is of such significance that it is common practice to designate the fluid by its viscosity at a certain temperature.

The coefficient of dynamic viscosity, η, is the parameter that represents the existence of tangential forces in liquids in movement. Suppose two plates (or fluid layers) are moving at a distance apart of dy, and at a relative velocity dv_x (see Figure 2.1), then the shear stress

$$\tau = \frac{Shear force}{Area} = \eta \frac{dv_x}{dy} \tag{2.2}$$

arises. Thereby, η is a proportionality factor and is called dynamic viscosity.

The coefficient of kinematic viscosity, η, is the ratio of the coefficient of dynamic viscosity to the fluid density, i.e.,

$$\mu = \frac{Dynamic\ viscosity}{Density} = \frac{\eta}{\rho} \tag{2.3}$$

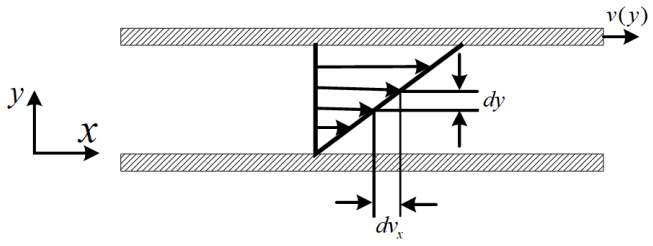

Figure 2.1: Couette flow; definition of shear stress.

The dynamic viscosity of liquids varies considerably with the temperature:

$$\eta_T = \eta_0 e^{-\lambda_1 (T - T_0)} \tag{2.4}$$

where η_0 is the dynamic viscosity at reference temperature T_0. The viscosity-temperature coefficient λ_1 should be determined by experiments for the fluid considered. For mineral oils, it lies between 0.036 and 0.057 $[K^{-1}]$.

The influence of pressure is given by

$$\eta = \eta_0 e^{\alpha p} \tag{2.5}$$

where α is the viscosity-pressure coefficient that depends on the temperature; see table 2.1 for the mineral oil HLP 32. For HFC fluids and HFD fluids the values of $\alpha = 0.35\ [Pa^{-1}]$ and $\alpha = 2.2\ [Pa^{-1}]$ can be used respectively. The effect of pressure on viscosity is not so important in practice.

Table 2.1: Viscosity-pressure coefficient for the mineral oil HLP 32.

$T\ [^\circ C]$	$\alpha\ [10^{-2} Pa^{-1}]$
0	3.268
10	2.9
20	2.595
30	2.339
40	2.121
50	1.933
60	1.77
70	1.626
80	1.499
90	1.385
100	1.283

2.3 Mass density, Bulk modulus and related quantities

Mass density is defined as mass per unit of volume:

$$\rho = \frac{Mass}{Volume} = \lim_{\Delta v \to 0} \frac{\Delta m}{\Delta V} = \frac{dm}{dv} \tag{2.6}$$

For petroleum based hydraulic fluids the approximate value is $\rho = 850\ [kg/m^3]$. Indeed, the density of hydraulic fluids is a function of both pressure and temperature, i.e., $\rho = \rho(P, T)$. However because changes in density as a function of pressure and temperature are small for a liquid, the first three terms of a Taylor's series for two variables may be used as an approximation [141]:

$$\begin{aligned} \rho &\approx \rho_{op} + \left(\tfrac{\partial \rho}{\partial p}\right)_T (P - P_{op}) + \left(\tfrac{\partial \rho}{\partial T}\right)_p (T - T_{op}) \\ &= \rho_{op}\left[1 + \tfrac{1}{E}(P - P_{op}) - \alpha(T - T_{op})\right] \end{aligned} \tag{2.7}$$

where

$$E = \rho_{op}\left(\frac{\partial P}{\partial \rho}\right)_T, \qquad \alpha = -\frac{1}{\rho_{op}}\left(\frac{\partial \rho}{\partial T}\right)_P \tag{2.8}$$

where ρ, P and T are respectively the mass density, pressure, and temperature of the fluid and ρ_{op}, P_{op} and T_{op} are the mass density, pressure, and temperature of the fluid at an operating point. Equation (2.7) is the linearized equation of state for fluids. The mass density increases as pressure is increased and decreases with temperature increase. In hydraulic phenomena, the usual assumption of constant temperatures reduces the linearized state equation (2.7) of fluids to the simple form [141]

$$\rho = \rho_0 + \frac{\rho_0}{E} P \tag{2.9}$$

where ρ_0 is the mass density at zero pressure. In the equation (2.8), because mass density is mass divided by volume, equivalent expression is:

$$E = -V_0\left(\frac{\partial P}{\partial V}\right)_T \tag{2.10}$$

$$\alpha = \frac{1}{V_0}\left(\frac{\partial V}{\partial T}\right)_P \tag{2.11}$$

where V is the total volume and V_0 is the initial total volume of the liquid. The quantity E is the change in pressure divided by the fractional change in volume at a constant temperature and is known as the isothermal tangent bulk modulus. It is called isothermal because the temperature is assumed constant and tangent because $\frac{\partial P}{\partial V}$ is the slope at some operating point.

Misinterpretation of the published data for fluid bulk modulus can be a real problem because how the measurement is made can influence the actual bulk modulus value. It is important to realize that since liquids in compression do not follow Hook's law, the relationship between pressure and volume change is not linear; consequently, at a given pressure P the bulk modulus can be defined either based on the slope of the tangent to the curve at P (called tangent bulk modulus) or is based on the slope of a line connecting P to the origin which can be regarded as an average value of bulk modulus over the range from 0 to P (called secant bulk modulus). From a "thermodynamic point of view", tangent bulk modulus $\rho\frac{\partial P}{\partial T}$ is more correct (see equation (2.8)) since it was derived from the approximate equation of state for a liquid.

Tangent bulk modulus is always greater than the secant bulk modulus, except at atmospheric pressure where they are equal. Tangent bulk modulus at pressure P is approximately equal to the secant bulk modulus at pressure $2P$ [107].

What makes the definition of bulk modulus more complex is that at any given temperature and pressure, there are four different values of bulk modulus with large differences between them. With reference to figure 2.2, these four different bulk moduli (which relates to the thermodynamic condition as well as the mathematical condition) are:

- Isothermal secant bulk modulus

$$\bar{E}_T = -V_0\left(\frac{P - P_0}{V - V_0}\right)_T \tag{2.12}$$

- Isothermal tangent bulk modulus

$$E_T = -V\left(\frac{\partial P}{\partial V}\right)_T \tag{2.13}$$

- Isentropic (adiabatic) secant bulk modulus

$$\bar{E}_S = -V_0\left(\frac{P - P_0}{V - V_0}\right)_S \tag{2.14}$$

- Isentropic (adiabatic) tangent bulk modulus

$$E_S = -V\left(\frac{\partial P}{\partial V}\right)_S \tag{2.15}$$

Subscripts S and T in equation (2.12) to (2.15) denote the conditions of constant entropy and temperature respectively. At conditions of constant entropy and absence of heat transfer, the bulk modulus is defined as the isentropic bulk modulus. As can be seen from figure 2.2, the value of isentropic bulk modulus is larger than isothermal bulk modulus [79]. The reason is that by compressing the fluid isentropically, the

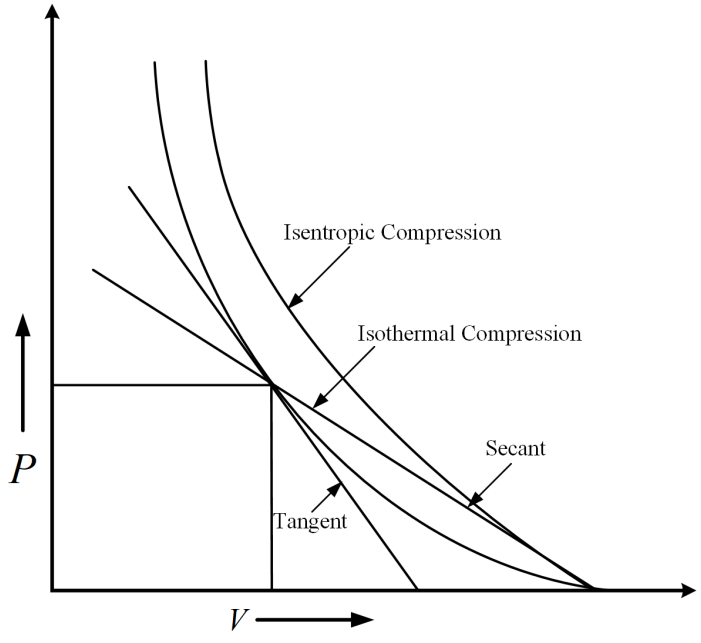

Figure 2.2: Comparison of different bulk modulus definitions

fluid temperature increases and the resulting thermal expansion of the fluid will compensate for the volume decrease due to pressure. Accordingly the smaller volume change results in larger bulk modulus value.

In reality, it is only in reversible processes that constant entropy happens and as such, processes are always irreversible. This implies that the entropy is not constant in real applications. Because of this, many sources refer to the isentropic bulk modulus as the "adiabatic bulk modulus" which means that the entropy during the compression process is not necessarily constant but no heat transfer occurs during the process. For the remaining of this thesis, the term adiabatic will be used rather than isentropic.

Another form of bulk modulus that is referred to in the literature is called "sonic bulk modulus" [181]. However its value is the same as the adiabatic bulk modulus, and will not be considered as a separate form of bulk modulus. Rather it can be considered as a different method of measuring the adiabatic bulk modulus of the fluid.

It should be noted that in the definition of secant bulk modulus, the volume appearing in the numerator is V_0, while that in the tangent bulk modulus is V. Sometimes incorrect substitution of V_0 for V in the bulk modulus equation can affect the numerical value especially at high pressures or when calculating the bulk modulus of liquids containing air/gas. Therefore, it is very important in reporting the values for bulk modulus that the condition of the test and the exact definitions used should always be followed [177]. Unfortunately, this is often not done in much of the literature.

Table 2.2 shows different bulk modulus values for different definitions for a typical hydraulic mineral oil of viscosity 100 $[cSt]$ at $20°C$ and 50 $[MPa]$ in the absence of air/gas bubbles [80]. Differences are observed and therefore it is very important to choose the appropriate bulk modulus definition according to the conditions of operation. Hayward (1970) [80] has suggested using the adiabatic secant modulus for sudden changes of pressure, the isothermal secant modulus for slow changes of pressure, and the adiabatic tangent modulus for the pressure changes due to the propagation of a sound wave.

As already mentioned, from a thermodynamic point of view, equations involving the tangent bulk modulus are those that should be used. However, these equations

Table 2.2: Bulk modulus values for a typical hydraulic oil (no entrained air/gas) at $20°C$ and 50 $[MPa]$

Adiabatic secant bulk modulus	2.15 $[GPa]$
Adiabatic tangent bulk modulus	2.41 $[GPa]$
Isothermal secant bulk modulus	1.88 $[GPa]$
Isothermal tangent bulk modulus	2.15 $[GPa]$

involve a differential coefficient $\frac{\partial P}{\partial \rho}$ (slope at an operating condition) which may not be easily evaluated from experimental readings. Therefore, usually secant (isothermal or adiabatic) bulk modulus is used in engineering applications which involve algebraic equations and can be easily evaluated. In addition, secant bulk modulus can be used to derive tangent bulk modulus at any pressure. This relationship in which it is assumed that secant bulk modulus increases linearly with pressure was given by Hayward (1967) [80]:

$$E = \frac{\bar{E}(\bar{E} - P)}{\bar{E} - P\frac{d\bar{E}}{dP}} \tag{2.16}$$

Often it is easier to measure the adiabatic tangent bulk modulus than the isothermal one; for example using ultrasonic measurement techniques. Using thermodynamic relationships, it is then possible to convert the measured adiabatic tangent bulk modulus values to the isothermal ones [80]. This relationship is given by:

$$\frac{C_P}{C_v} = \frac{E_S}{E_T} \tag{2.17}$$

In the literature, there are many formula for the calculation of the density of hydraulic fluids as a function of temperature and pressure. For example, the density at atmospheric pressure (1 $[bar] = 10^5$ $[N/m^2]$) and variable temperature T is given

by

$$\rho_T = \frac{\rho_0}{1 + \beta_T(T - T_0)} \tag{2.18}$$

where ρ_0 is the density at reference temperature T_0 (say $15°C$), and β_T denotes the heat expansion factor, e.g., 0.65×10^{-3} $[K^{-1}]$ for mineral oils, 0.7×10^{-3} $[k^{-1}]$ for HFC-fluids, and 0.75×10^{-3} $[K^{-1}]$ for HFD-fluids [90]. The density of hydraulic fluids following a change in pressure can be expressed as

$$\rho_P = \frac{\rho_0}{1 - \kappa_P(P - P_0)} \tag{2.19}$$

where κ_P is the compressibility factor

$$\kappa_P = \frac{1}{V_0}\left(\frac{\partial V}{\partial P}\right)_T \tag{2.20}$$

For variable temperature and variable pressure the density can be calculated by

$$\rho = \rho_T(1 + \kappa_P \Delta P) \tag{2.21}$$

Typical values for κ_P are: 0.7×10^{-4} $[bar^{-1}]$ for mineral oils, 0.3×10^{-4} $[bar^{-1}]$ for HFC-fluids, and 0.35×10^{-4} $[bar^{-1}]$ for HFD-fluids [90]. From these values, it can be concluded that the effect of pressure on the fluid density is minor, and thus negligible in practice.

2.3.1 The oil spring

Another effect of bulk modulus is that any constrained oil volume behaves like a spring. Figure 2.3 shows a double acting cylinder [3].

There is oil on both sides of the piston. For generality, the two sides of the cylinder are not matched for piston area. Consider the situation where the oil flow to or from the cylinder is blocked so volumes V_1 and V_2 are trapped. The effective bulk modulus of the trapped oil accounting for entrapped air and hose and cylinder compliance is E. Suppose a incremental force ΔF is applied to the piston and the rod moves Δx relative to the cylinder. The pressure in V_1 will fall by ΔP_1 and the pressure in V_2 will rise by ΔP_2. If this were a conventional metallic spring, we would

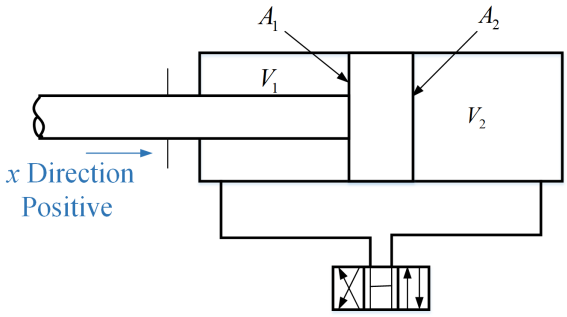

Figure 2.3: Trapped oil in a cylinder treated as a spring.

write the expression for stiffness as:

$$k = \frac{\Delta F}{\Delta x} \tag{2.22}$$

Using the characteristics of the cylinder, this expression can be written:

$$k = \frac{-\Delta P_1.A_1}{\Delta V_1/A_1} + \frac{\Delta P_2.A_2}{\Delta V_2/A_2} \tag{2.23}$$

The sign convention implies that an increase in pressure is positive and that an increase in fluid volume is likewise positive. Now recast equation (2.15) in the form:

$$-\frac{\Delta P}{\Delta V} = \frac{E}{V} \tag{2.24}$$

Hence the spring rate expression can be written:

$$k = \frac{E.A_1^2}{V_1} + \frac{E.A_2^2}{V_2} = E(\frac{A_1^2}{V_1} + \frac{A_2^2}{V_2}) \tag{2.25}$$

We now need to investigate the variation of stiffness as the relative values of V_1 and V_2 change. This is most easily done by introducing a total oil volume V_T that does not change as the piston moves. The stiffness expression will then have the form:

$$k = E(\frac{A_1^2}{V_1} + \frac{A_2^2}{V_T - V_1}) \tag{2.26}$$

This expression may be plotted or the rules of calculus applied to show that the

stiffness has a minimum value when:

$$\frac{A_1^2}{V_1} = \frac{A_2^2}{V_T - V_1} = \frac{A_2^2}{V_2} \tag{2.27}$$

Now most cylinders that will be used for precise positioning of loads will use a double, symmetrical rod configuration. In the usual situation where the pipe connections from the valve have equal volumes, the minimum stiffness condition occurs when the piston is in the center of its travel.

2.3.2 Relationship of bulk modulus to pressure and temperature

As pressure increases, bulk modulus of all liquids at first increases rapidly because of a decrease in the intermolecular gaps; as the pressure becomes higher, molecules become in contact with their neighbors and the rate of increase in bulk modulus value is reduced [188, 210]. From experimental results, it can be shown that over moderate pressure ranges (up to about 80 $[MPa]$ (800 $[bar]$) with mineral oil), the secant bulk modulus (isothermal or adiabatic) can be expressed as a linear function of pressure.

$$\bar{E} = E_0 + mP \tag{2.28}$$

where E_0 is the bulk modulus at zero gauge pressure and m is a constant which for a particular fluid is temperature independent [80].

With increase in temperature, the bulk modulus of most liquids will decrease [188]. As temperature increases, molecules will move faster which results in the expansion of hydraulic fluid and a corresponding reduction in the density of the fluid. Reduction in the density means increase in the intermolecular gaps in the fluid which results in the reduction of the fluid bulk modulus.

2.4 Effective bulk modulus

The bulk modulus of a liquid is substantially lowered by entrained gas and mechanical compliance. According to Merritt (1967) [141], estimates of entrapped air in

hydraulic systems run as high as 20% when the fluid is at atmospheric pressure. As the pressure is increased, much of this air dissolves into the liquid and does not affect the bulk modulus. The major source of mechanical compliance may be the hydraulic lines connecting valves and pumps to actuators.Therefore, the real bulk modulus with considering the effect of entrained air, temperature and mechanical compliance in the hydraulic systems is presented by the value for the effective bulk modulus.

2.4.1 Effect of entrained air

Air/gas is known to have a substantial effect on the compressibility of a liquid. Thus it would be expected that the bulk modulus value would vary as well. Air/gas is known to exist in hydraulic systems in three forms [133]:

- **Free air/gas:** air/gas pockets trapped in part of the system and can be removed from the hydraulic system by proper bleeding of the system.
- **Entrained air/gas:** air/gas bubbles (typically 0.127 to 0.635 [mm] in diameter) which are dispersed in the oil. Existence of free or entrained air/gas in a hydraulic system significantly reduces the effective bulk modulus of the system. The term "bubbly oil" is used by Hayward (1965) [79] for oil which contains discrete bubbles of entrained air/gas in which relatively thick films of oil separate these bubbles from each other.
- **Dissolved air/gas:** invisible bubbles stored in the empty space between the fluid molecules and uniformly spread throughout the fluid. Test data indicates that as long as the air/gas is in solution, it does not affect the liquid bulk modulus [132].

The process of air/gas dissolving into the liquid is usually described by Henry's law, which states that at a constant temperature, the weight of a given gas dissolved in a given type and volume of liquid, will increase as the pressure of the gas increases. The amount of gas that can be dissolved in oil is referred to its solubility [189].

Magorien (1993) [133] suggested that the term adsorption instead of absorption can be used to better describe the process of dissolving bubbles into the liquid.

Adsorption is defined as a process in which the extremely thin film of the air/gas is accumulated on the surface of the liquid in contact with the air/gas. Absorption indicates a process in which the air/gas diffuses into the bulk of the liquid. The adsorption rate is a function of pressure and inverse function of the diameter of the air/gas bubble [133]. Hayward (1965) [79] showed that when a column of bubbly oil is compressed, at first the rate of solution is very rapid, and then slows down because of saturation of the skin of oil around each bubble with dissolved air/gas (Adsorption). Thereafter, the rate of solution will depend upon the air/gas diffusion rate from this surface layer into the body of the oil (Absorption). He also studied the compressibility of bubbly oil under sudden compression and showed that the true law of compression that air/gas bubbles follow is much closer to isothermal than adiabatic. In hydraulic applications, the rate of solution of air/gas when the bubbly oil is suddenly compressed (for example, from the inlet to the outlet of a pump) is of interest. Experiments show that using higher pressure or a less viscous oil will increase the rate of solution [79].

By increasing the temperature or lowering the external pressure, air/gas will leave the free intermolecular spaces and will come out of solution. Therefore, depending on the operating conditions in which the fluid is subjected, it is possible for the dissolved air/gas to become entrained (and vice versa). By increasing the pressure, the entrained air/gas can be redissolved into the fluid, but it is possible that not all of the released gas redissolves again even by increasing the pressure. The reason for this behavior is explained by the fact that some air/gas bubbles are not always close to an empty intermolecular space; as a result they cannot dissolve and consequently stay in entrained form [132].

In practice, hydraulic fluids typically become aerated in use and as stated before, it has a significant effect on bulk modulus. Some work has been done on determining the bulk modulus of liquid-air mixtures which four equations have commonly been used to express the effective bulk modulus of hydraulic oil with entrained air. The four equations are Wylie in [213], Nykänen in [154], Backé and Murrenhoff in [15] and the model used at IFAS so far [147] ("IFAS model"). The Wylie , Backé and Murrenhoff and Nykañen models were derived with a constant bulk modulus of oil, and the IFAS model is based on the bulk modulus of oil which changes with pressure as shown in equation (2.32). The Wylie and Backé and Murrenhoff models use the

equation for an isothermal process, while the Nykaïen and IFAS models express a polytropic process. Kajaste in [97] modified the Wylie model for the polytropic process as shown in equation (2.29). The equations of these four formula are as follow:

- Wylie model (modified by Kajaste): ($\bar{E} = E_0$)

$$E = \frac{\bar{E}}{1 + \alpha\left(\frac{P_0}{P}\right)^{\frac{1}{\kappa}}\left(\frac{\bar{E}}{\kappa P} - 1\right)} \tag{2.29}$$

- Nykänen model: ($\bar{E} = E_0$)

$$E = \frac{\left(\alpha\left(\frac{P_0}{P}\right)^{\frac{1}{\kappa}} + \frac{1-\alpha}{1+\frac{1}{\bar{E}}(P-P_0)}\right)^2}{\frac{\alpha\left(\frac{P_0}{P}\right)^{\frac{1}{\kappa}}}{\kappa P} + \frac{1-\alpha}{\left(1+\frac{1}{\bar{E}}(P-P_0)\right)^2\bar{E}}} \tag{2.30}$$

- Backé and Murrenhoff model: ($\bar{E} = E_0$)

$$E = \bar{E}\frac{1+\alpha}{1 + \left(\frac{P_0}{P}\right)^{1/\kappa}\alpha\frac{\bar{E}}{\kappa P}} \tag{2.31}$$

- IFAS model: ($\bar{E} = E_0 + m.P$)

$$E = \frac{(1-\alpha)\left(1 + \frac{m(P-P_0)}{E_0}\right)^{-\frac{1}{m}} + \alpha\left(\frac{P_0}{P}\right)^{\frac{1}{\kappa}}}{\frac{1}{E_0}(1-\alpha)\left(1 + \frac{m(P-P_0)}{E_0}\right)^{-\frac{m+1}{m}} + \frac{\alpha}{\kappa P_0}\left(\frac{P_0}{P}\right)^{\frac{\kappa+1}{\kappa}}} \tag{2.32}$$

with

Note that the expressions given above require the accurate determination of many quantities (for example, of the volume of gas entrained in the liquid), and thus may be difficult to use in practice.

Figure 2.4 shows the differences of the effective bulk modulus with various entrained air content calculated using the four equations presented in the preceding text. Because of the different assumptions in the derivation process, the effective bulk modulus have different values depending on entrained air content and pressure.

E the effective bulk modulus of oil with entrained air,
$\bar{E}$ isentropic bulk modulus of the liquid (without entrained air),
E_0 a constant term,
m the pressure related term in the bulk modulus of oil,
α volumetric content air at initial pressure (entrained air content),
P_0 the initial pressure,
P liquid pressure, and
κ the polytropic constant of air.

Especially in low-pressure regions (say, $p \leq 100$ $[bar]$), the influence of entrained gas on the bulk modulus is substantial. At a pressure of about 0.6 $[bar]$, entrained air can explode (so-called Diesel effect). This effect cause highly undesired erosion defects, power losses, pressure peaks, and noise. This phenomenon is better known as cavitation (sudden implosion of gas bubbles, when fluid pressure decreases under vapor pressure). In the study presented in this thesis, the IFAS model was chosen to be compared with measurements because experimental results in [109, 104] show that the bulk modulus of oil depends on pressure ($\bar{E} = E_0 + mP$). The IFAS model also corresponds well with the experimental results.

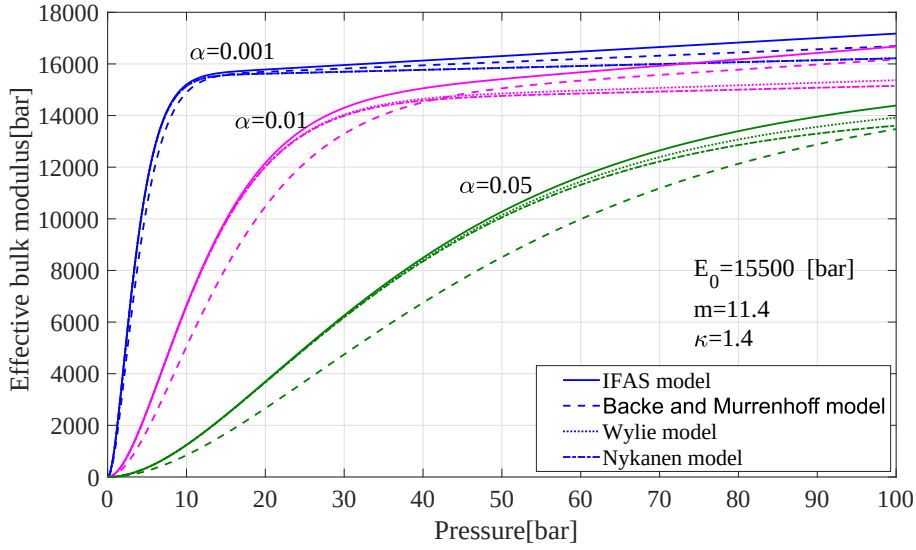

Figure 2.4: Influence of entrained air volume on the isentropic bulk modulus

2.4.2 Influence of mechanical compliance

The bulk modulus of cylindrical pipelines can be calculated as

$$E = \bar{E}\frac{1}{1 + \frac{\bar{E}}{E_p}w} \tag{2.33}$$

where E_P is the bulk modulus of the (steel) pipeline. For thick-walled pipelines the coefficient w is given by

$$w = \frac{2\left(\frac{d_0}{d_i}\right)^2(1+v) + 3(1-2v)}{\left(\frac{d_0}{d_i}\right)^2 - 1} \tag{2.34}$$

with

d_0 outer diameter,
d_i inner diameter, and
v Poisson's number, $v = 0.3$ for steel.

For thin-walled pipelines with the wall thickness s, $(s/d_0 < 0.1)$, Equation 2.34 approximates to

$$w = \frac{d_i}{s}. \tag{2.35}$$

2.4.3 Resonance of hydraulic systems

The natural frequency of a spring mass combination is:

$$f = \frac{1}{2\pi}\frac{\sqrt{kg}}{W} \tag{2.36}$$

where f = frequency, Hz
W = weight, kg
k = spring rate, kg/m, and
g = acceleration due to gravity, m/sec^2.
To equate this to a hydraulic system, we only need to substitute bulk modulus for spring rate. Thus, a low modulus also lowers the natural frequency of a system. For

example, if 1% air content changes the bulk modulus by 50%, its natural frequency decreases by 30%. This greatly reduces the stability of the system.

2.4.4 Empirical effective bulk modulus

Other researchers have derived empirical formula for the calculation of the effective bulk modulus E, including the effects of entrained air and mechanical compliance, based on direct measurements. The commonly used equation for calculation of the bulk modulus E for hydraulic cylinders in German literature is that of Lee in [116]:

$$E = a_1 E_{\max} \log(a_2 \frac{P}{P_{\max}} + a_3) \tag{2.37}$$

with the parameters $a_1 = 0.5$, $a_2 = 90$, $a_3 = 3$, $E_{max} = 18000$ bar, and $P_{max} = 280$ bar.

Hoffmann in [84] proposed the formula

$$E = E_{\max}[1 - \exp(-0.4 - 2 \times 10^{-7} p)] \tag{2.38}$$

with the pressure p in pascals.

According to Eggerth in [54], the effective bulk modulus can be expressed as

$$E = \frac{1}{k_1 + k_2 \left(\frac{p}{p_0}\right)^{-\lambda}} \tag{2.39}$$

with the parameters k_1 and k_2 in table 2.3; P_0 is assumed to be 10 $[bar]$.

Table 2.3: Parameters of Eggerth's formula

Temperature $[^\circ C]$	$k_1[10^{-10} m^2/N]$	$k_2[10^{-10} m^2/N]$	λ
20	4.943	1.9540	1.480
50	5.469	3.2785	1.258
90	5.762	4.775	1.1

The relations for effective bulk modulus E are plotted in figure 2.5. Although these formula are approximate, they are sufficient for design purposes. However, experimental data are always preferable.

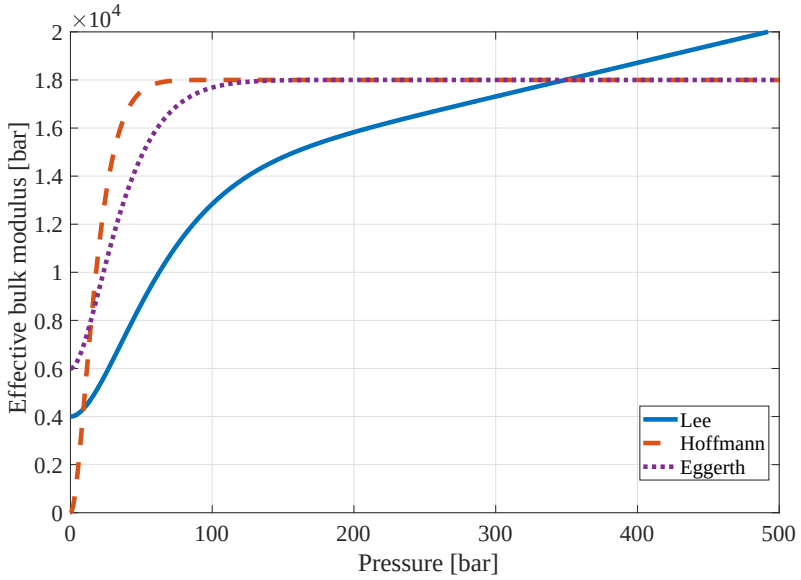

Figure 2.5: Comparison of different formula for the calculation of E

2.5 Fluid flow fundamentals

Knowledge of the fundamental laws and equations which govern the flow of fluids is essential for the rational design of hydraulic control components and systems. This section will discuss the general equations of fluid motion, type of flow and flow through orifices. More detailed derivations can be found in a number of standard textbooks on fluid mechanics [176, 180, 145, 56, 35].

Fluids are made up of discrete particles-molecules. An accurate analysis would have to consider the motion of each particle, and this would be hopeless analytically. For example, the density at any geometrical point would depend on whether there exists a molecule at that point. Therefore, we must rely on "continuous" theory and consider the statistical properties of a fluid. This concept is in conflict with molecular theory, but it is sufficiently accurate for engineering purposes. However, at low pressures where there are large distances between molecules or when the distances between molecules are comparable in magnitude to the significant dimensions of the problem, the kinetic theory would be required.

2.5.1 Navier-Strokes equation

The momentum conservation equation which is the result of Newton's second law is known as the Navier-Stokes equation:

$$\rho\frac{dv}{dt} = \rho.g - grad(P) + \eta\left[div(grad(v)) + \frac{1}{3}grad(div(v))\right] \tag{2.40}$$

where

- $\rho.g$ represents the body forces.
- $\rho\frac{dv}{dt}$ the inertial forces.
- $grad(P)$ is the vector of components $\partial p/\partial x_i$. It corresponds to the derivative or inclination of the pressure in the direction of the flow.
- The term $\eta.div(grad(v))$ represents diffusion of the vector v within the flow. It represents the action of one particle on the others owing to the effect of viscosity.
- The term $\frac{1}{3}\eta.grad(divv)$ represents the influence of compressibility and vanishes in the case of incompressible liquids.

Letting the fluid be incompressible and dividing equation (2.40) throughout by ρ leads to

$$\frac{dv}{dt} = g - \frac{1}{\rho}grad(P) + \mu.div(grad(v)) \tag{2.41}$$

Given the hypothesis of the external forces being derived from a potential ξ, then $g = grad(\xi)$. Thus, in the case of incompressible liquids, equation (2.41) becomes

$$-grad(\xi) + \frac{1}{\rho}grad(P) = -\frac{dv}{dt} + \mu.div(grad(v)) \tag{2.42}$$

If the potential is that of gravity, $\xi = -g.z$ then dividing throughout by g gives:

$$-grad(z + \frac{P}{\gamma}) = -\frac{1}{g}\frac{dv}{dt} + \frac{\eta}{\gamma}.div(grad(v)) \tag{2.43}$$

with $\gamma = pg$. In the case of a perfect or ideal liquid, $\eta = 0$, which does not exist in reality, equation (2.43) becomes

$$grad(z + \frac{P}{\gamma}) = -\frac{1}{g}\frac{dv}{dt} \tag{2.44}$$

For a fluid element along the path line, equation (2.43) can be rearranged, taking into account $\eta = \rho.\mu$ and $\gamma = \rho.g$, to give Euler's equation

$$\frac{\partial}{\partial s}\left(z + \frac{P}{\gamma}\right) = -\frac{1}{g}\frac{dv}{dt} + \frac{\mu}{g}div(gradv) \qquad\qquad v = v_s. \tag{2.45}$$

2.5.2 Bernoulli's Theorem

Considering equation 2.45, and bearing in mind that

$$\frac{dv}{dt} = \frac{\partial v}{\partial t} + v\frac{\partial v}{\partial s} \tag{2.46}$$

$$v\frac{\partial v}{\partial s} = \frac{\partial(v^2/2)}{\partial s} \tag{2.47}$$

it follows that

$$\frac{\partial}{\partial s}\left(z + \frac{P}{\gamma} + \frac{v^2}{2g}\right) = -\frac{1}{g}\frac{dv}{dt} + \frac{\mu}{g}div(gradv) \tag{2.48}$$

The first element of the equation has an essentially global energy significance. It represents the variation in the total energy discharged per unit weight of a particle along its trajectory.

If the viscosity terms are removed from the equation, i.e., the flow may resemble a perfect fluid, we have

$$\frac{\partial}{\partial s}\left(gz + \frac{gP}{\gamma} + \frac{v^2}{2}\right) = -\frac{1}{g}\frac{dv}{dt} \tag{2.49}$$

In the case of steady flow, $\frac{\partial v}{\partial t} = 0$, energy conservation holds:

$$E = z + \frac{P}{\gamma} + \frac{v^2}{2g} = const. \tag{2.50}$$

this being the expression that represents Bernoulli's theorem for one-dimensional

steady flows. In the case of an incompressible liquid in steady flow, in which the friction forces and, consequently, energy losses can be disregarded, the total energy of a particle is maintained along its trajectory.

2.5.3 continuity equation and pressure transients

Consider a control tube as depicted in Figure 2.6. The integral form of the mass conservation (continuity) equation can be formulated as

$$\int_{(1)}^{(2)} \frac{\partial(\rho A)}{\partial t} ds + \rho_2 v_2 A_2 - \rho_1 v_1 A_1 = 0 \tag{2.51}$$

where the density $\rho = \rho(t, s)$ is, in general, not constant.

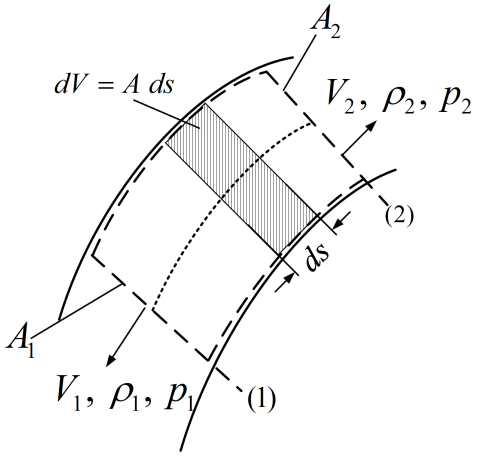

Figure 2.6: Definition of control tube.

For incompressible fluids, i.e., $\rho = const.$ (which is a standard assumption in hydraulics), Equation (2.51) can be reduced to

$$v_1(t)A_1 = v_2(t)A_2 \qquad (\rho = const.) \tag{2.52}$$

or more generally

$$Q = v(t)A = const \qquad (volume flow) \tag{2.53}$$

For steady flow the continuity equation can be expressed as

$$\rho_1 v_1(t) A_1 = \rho_2 v_2(t) A_2 \qquad (\rho \neq const.) \tag{2.54}$$

or in the general form

$$\dot{m} = \rho v A = const \qquad (mass\ flow\ rate) \tag{2.55}$$

Next, the mass conservation equation is written in the differential coordinate-free form (for a control tube element of length ds; see Figure 2.6)

$$\frac{\partial \rho}{\partial t} + div(\rho v) = 0 \tag{2.56}$$

Again, two special cases can be given:

$$\begin{array}{ll} div(v) = 0 & (\rho = const) \\ div(\rho v) = 0 & (steady\ flow) \end{array} \tag{2.57}$$

Given a coordinate system (Cartesian, cylindrical or spherical), Equation (2.55) can take a specific form by providing the expression for the divergence (div) operator in that coordinate system. The expression of the continuity equation in a cylindrical coordinate system (r, φ, x) is given by:

$$\frac{\partial \rho}{\partial t} + \frac{1}{r}\left(\frac{\partial(\rho r v_r)}{\partial r} + \frac{\partial(\rho v_\varphi)}{\partial \varphi}\right) + \frac{\partial(\rho v_x)}{\partial x} = 0 \tag{2.58}$$

Consider again the mass conservation equation for a control volume V and let the accumulated or stored mass of fluid inside be m with a mass density of ρ. Since all fluid must be accounted for, as the medium is assumed continuous, the rate at which mass is stored must equal the incoming mass flow rate minus the outgoing mass flow rate. Therefore, we can write

$$\sum \dot{m}_{in} - \sum \dot{m}_{out} = \frac{d(\rho V)}{dt} = \rho \dot{V} + V \dot{\rho} \tag{2.59}$$

Taking into account equation (2.9) and dividing equation (2.59) by ρ leads to

$$\sum Q_{in} - \sum Q_{out} = \dot{V} + \frac{V}{E}\dot{p} \tag{2.60}$$

if the volume is fixed ($V = V_0$) equation (2.59) becomes

$$\dot{p} = \frac{E}{V_0}\left(\sum Q_{in} - \sum Q_{out}\right) \tag{2.61}$$

This equation is fundamental for the description of the pressure dynamics in hydraulic compartments.

2.6 Flow through passage

Two distinct types of fluid flow through passages can occur:

- Laminar or viscous flow, in which each fluid particle describes a well-defined trajectory, with a velocity only in the direction of the flow.
- Turbulent or hydraulic flow (this being the most usual in hydraulic phenomena), in which each particle, apart from the velocity in the direction of the flow, is animated by fluctuating cross-current velocities.

The Reynolds number, Re, defined by

$$\mathrm{Re} = \frac{\rho v d_h}{\eta} = \frac{v d_h}{\mu} \tag{2.62}$$

is the characteristic parameter: for lower values of Re, the flow is laminar; for higher values the flow is turbulent. Thereby, v is the average velocity of flow. d_h represents the hydraulic diameter, which is defined by

$$d_h = \frac{4A}{S} \tag{2.63}$$

where A is the flow section area and S is the flow section perimeter. For each flow case, the characteristic length is agreed upon and empirical values are obtained

for the Reynolds number which describes transition from that viscosity to inertia-dominated flows.

Transition from laminar to turbulent flow has been experimentally observed to occur in the range $2000 < R < 4000$. Below $R = 2000$ the flow is always laminar, above $R = 4000$ the flow is usually, but not always turbulent. It is possible to have laminar flow at Reynolds number considerably above 4000 if extreme care is taken to avoid disturbances which would lead to turbulence. However, these instances are exceptional, and the high limit of 4000 is a good rule.

2.6.1 Laminar flow in pipes

Let us first consider steady laminar flow in pipes. such pipes are often termed capillary tubes because the small diameters usually result in laminar flow. However, it should be recognized that low velocities or large viscosity can also result in laminar flow in pipes of larger diameter. As fluid enters a pipe (see figure 2.7) the velocity profile is constant at a value v if there is rounding of the inlet. The fluid velocity at pipe wall is zero, and this layer of fluid exerts considerable shear force on the inner layers whose velocities must exceed v to satisfy the law of continuity. The boundary layer thus formed increase in thickness until the center of the pipe is reached. The velocity profile then becomes parabolic and remains parabolic throughout the length of pipe. Let v_0 denotes the peak velocity of the entrance velocity profiles. For a parabolic profile, the peak velocity is $2\bar{v}$ which $\bar{v}$ is the average velocity. The ratio $v_0/\bar{v}$ then varies from unity at the entrance to two at the length of pipe where a parabolic velocity profile is established.

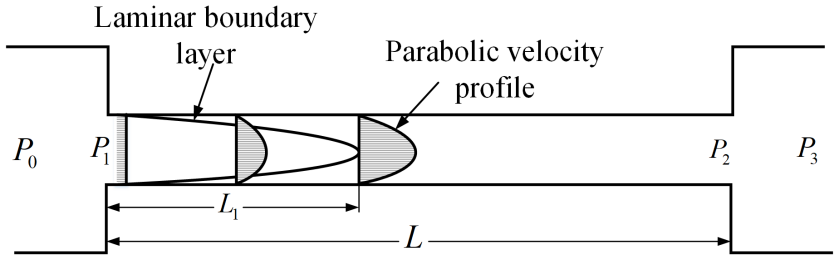

Figure 2.7: Laminar flow in a pipe

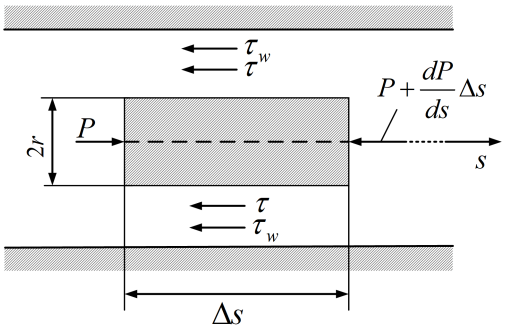

Figure 2.8: Force equilibrium of fluid elements in cylindrical pipelines

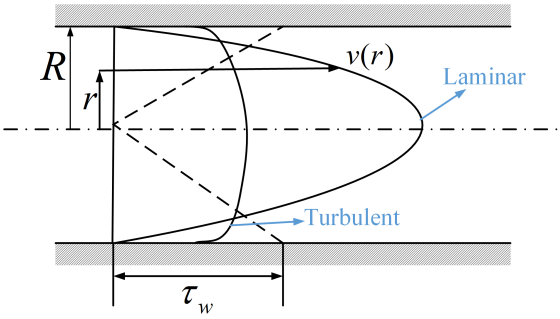

Figure 2.9: Velocity profiles for laminar and turbulent flows in a cylindrical pipeline

By considering a cylindrical pipeline of radius $r \leq R$ the Shear stress at the pipeline wall (see figure 2.8)is given by

$$\begin{cases} \tau = -\frac{r}{2}\frac{dp}{dx} \\ \tau_w = -\frac{R}{2}\frac{dp}{dx} \end{cases} \Rightarrow \frac{\tau}{\tau_w} = \frac{r}{R} \tag{2.64}$$

Now based on equation (2.2)

$$\tau = -\eta\frac{dv}{dr} = -\frac{r}{2}\frac{dp}{dx} \tag{2.65}$$

Equations (2.64) and (2.65) can then be combined to obtain

$$\frac{dv}{dr} = \frac{r}{2\eta}\frac{dp}{dx} \tag{2.66}$$

the relationship for calculating the velocity profile for laminar flows in cylindrical pipelines. In fact, the integration of equation (2.66) (with $dp/dx = const.$, and $v(R) = 0$) yields the velocity profile (Figure 2.9)

$$v(r) = -\frac{1}{4\eta}(R^2 - r^2)\frac{dp}{dx} \tag{2.67}$$

and leads to the maximum velocity and the mean velocity

$$v_{\max} = v(0) = -\frac{R^2}{4\eta}\frac{dp}{dx} \qquad \bar{v} = -\frac{R^2}{8\eta}\frac{dp}{dx} \tag{2.68}$$

respectively.

Finally, the continuity equation (2.51) and equation (2.68) are combined to give the so called Hagen-Poiseuil equation

$$Q = A\bar{v} = -\frac{\pi R^4}{8\eta}\frac{dp}{dx} \tag{2.69}$$

2.6.2 Turbulent flow in pipes

Flow patterns and equations for turbulent flow in pipes are based largely on experimental observation. As flow enters the pipe (see figure 2.10), the initial boundary layer is laminar but becomes turbulent(except for a very thin laminar sublayer) after a very short distance. This turbulent boundary layer increases in thickness to the center of the pipe in a transition length of about 25 to 40 pipe diameters. A rather blunt velocity profile, with a peak velocity of about $1.2[v]$, is then established and remains throughout the pipe length.

The empirical equation giving the pressure drop for fully developed turbulent flow is:

$$P_1 - P_2 = f\frac{L}{d_h}\frac{\rho v^2}{2} \tag{2.70}$$

where f is the friction factor which depends on Reynolds number and pipe roughness. The additional pressure drop due to the transition length is about $0.09\rho v^2/2$ and is negligible in most computation. Pressure drops due to entrance and exit losses are also usually negligible.

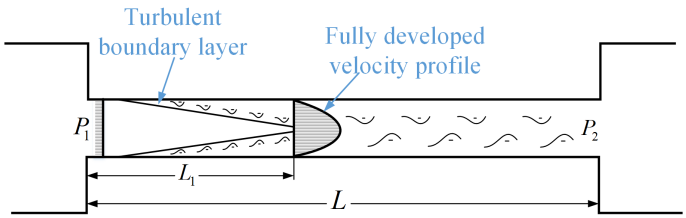

Figure 2.10: Turbulent flow in a pipe.

Equation 2.70 to the Hagen-Poiseuille law, the friction for laminar flow is

$$f = \frac{64}{R} \tag{2.71}$$

In the turbulent flow range Blasius experimentally determined the friction factor to be

$$f = \frac{0.3164}{R^{0.25}} \tag{2.72}$$

for smooth pipes and Reynols numbers less than $100,000$.

2.6.3 Orifice Equations for Turbulent Flow

Since most orifice flows occur at high Reynolds numbers, this region is of major importance. Such flows are often referred to as "turbulent" (figure 2.11b), but the term does not have quite the same meaning as in pipeline flow. Referring to Figure 2.11a, the fluid particles are accelerated up to the jet velocity between sections 1 and 2. The flow between these sections is streamline or potential flow, and experience justifies the use of Bernoulli's theorem in this region.

According to Bernoulli's theorem, the total energy losses of the hydraulic flow are derived from the energy degraded into heat by friction of the particles against one another and by friction of the particles against the walls of the conduit. The energy dissipated due to friction between sections 1 and 2 will be equal to

$$\Delta p_{1s} = (p_1 + \frac{\rho v_1^2}{2} + \rho g z_1) - (p_2 + \frac{\rho v_2^2}{2} + \rho g z_2) \tag{2.73}$$

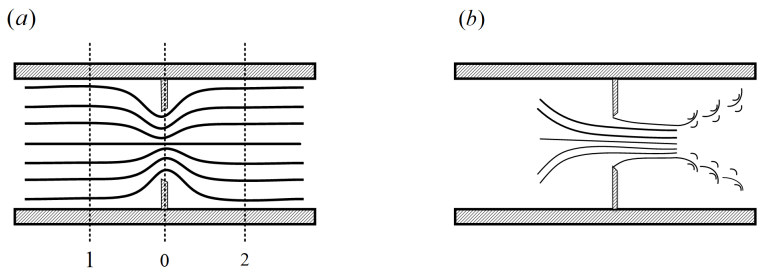

Figure 2.11: Flow through an orifice: (a) laminar flow; (b) turbulent flow

It is common to use the dimensionless pressure loss factor ξ;, which is defined as

$$\xi = \frac{\Delta p_{1s}}{\rho v_1^2/2} \qquad or \qquad \Delta p_{1s} = \frac{\xi \rho v_1^2}{2} \tag{2.74}$$

The factor ξ depends on the geometry of the conduit and on the Reynolds number which can be approximated by

$$\xi(\mathrm{Re}) = \frac{k_1}{\mathrm{Re}} + k_2 \tag{2.75}$$

Taking into account that at a point far from the orifice

$$v_1 = v_2 = v \quad and \qquad A_1 = A_2 = A = \frac{\pi}{4} d^2 = const \tag{2.76}$$

we get the flow as the product of conduit area and the speed, i. e.,

$$Q = Av = A\sqrt{\frac{2}{\rho\xi}(p_1 - p_2)} \tag{2.77}$$

Instead of equation (2.77), it is common in the field of hydraulics to use the modified orifice equation

$$Q = \alpha_d A \sqrt{\frac{2}{\rho}\Delta p} \tag{2.78}$$

where α_d is the discharge coefficient. Theoretically, $\alpha_d = \frac{\pi}{\pi+2} = 0.611$. This can be used for all sharp-edged orifices regardless of the particular geometry, if the flow is turbulent and $A_0 << A$.

Chapter 3

Physical modeling of hydraulic servo-system

This chapter is devoted to the derivation of physical models for hydraulic servo-systems and contains the most relevant dynamic and nonlinear effects that are involved in hydraulic servo-systems. The model derivation is based on the physical fundamentals described in previous chapter and on first principles. Although the presented model has to be identified and validated experimentally, as discussed in the next chapter, it forms a good basis both for control design and for system design.

3.1 Introduction

This Chapter started with a short-term description of the system model, the hydraulic servo-system, and the system boundary, in section 3.1. After that, the modeling method is discussed in some detail in section 3.2, while section 3.3 provides the theoretical model of the hydraulic servo-system.

3.1.1 System description

Even though a general description of hydraulic servo-systems has already been given in Chapter 2, a more precise description in our specific shaking table, in view of the mathematical model of this system, is given in this chapter.

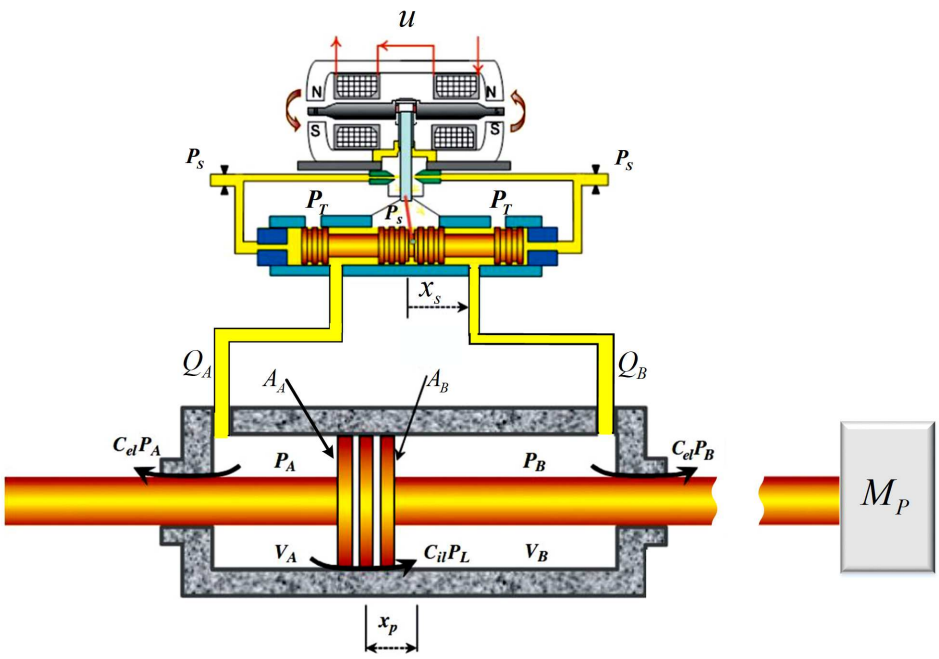

Figure 3.1: Schematic drawing of hydraulic servo-system.

From modeling point of view, almost any flow-controlled hydraulic servo-system can be reduced to the basic structure shown in figure 3.1. The control input u of the servo-valve is used to control the oil flow through the ports of the solenoid. Oil is provided by a power supply unit under presumably constant supply pressure P_s, while the return flow is fed to a tank under the (low) return pressure P_T.

The actuator (cylinder) consists of two oil chambers, separated by the piston. The resulting oil flows Q_A and Q_B moving into and out of the chambers drive the piston, thereby generating the required pressures P_A and P_B respectively, to move the load of the actuator. In this way, the piston motion (expressed in terms of piston velocity) depends on the load of the actuator. Actually, for motion systems with free moving bodies, this load can be seen as an inertia M_P plus some external load or force F_{ext} which might include gravity forces for example.

The valve opening and the pressure drop over the valve result in the oil flow, will generate a movement (translation) of actuator. This explains the basic integrating behavior of a hydraulic actuator between the input x_s and the output x_p (piston

position). Because the oil in the two chambers is compressible, the two oil columns act as two springs. The load is clamped between these "springs" via the piston. This causes the second-order behavior, which is always found in series with the integrating character of a hydraulic actuator.

Drawing the system boundary around the hydraulic servo-system, described above, there are a number of interfaces with the environment of the system, where energy exchange may take place. Mainly, these interfaces can be seen as bilateral couplings, with energy exchange by means of a flow variable and a potential variable. This bilateral coupling is easily taken into account in the model by appropriate definition of impedance and admittance relations, both for the system and the environment. However, in many cases, simplifying assumptions are quite realistic, for instance, when the interface is meant for information exchange rather than energy exchange. This particularly holds for the first two of the five interfaces of the system with the environment:

1. **Control input**- For the control input u, generally a voltage, it is quite realistic to consider it as an ideal input signal; the input impedance for the electrical signal is infinitely large.

2. **Measured output**- Depending on the application or the experimental setup, a number of system states can be measured by means of sensors (transducers). The sensors are designed to be ideal in the sense that their output impedance is zero, while they do not affect the measured states.

3. **Actuator load**- This is the most important interface, because there is a significant energy exchange. The type of energy exchange depends on the load characteristics, i.e. the load impedance $F_{ext}/\dot{x_p}$, and determines the total dynamic behavior of the servo-system.

4. **Actuator base**- The actuator base should always be designed to be as stiff as possible, with an impedance (say: inertia) which is large enough to avoid parasitic energy exchange. In other words, no parasitic motions of the base should occur. Whenever (unexpected) parasitic motions occur in an application, one should be aware of the fact, that the impedance of the base affects

the system dynamics. In that case, the actuator cannot be assumed to be rigidly connected to a base with infinite impedance.

5. **Power supply**- In most hydraulic servo applications, the power supply unit is designed in such a way, that the system maintains a constant supply pressure for a certain range of operation, i.e. oil flow demand. An effective way to do this, is the application of hydraulic accumulators [197], in combination with a pressure controlled flow pump. Especially for high performance demands on the hydraulic servo-system with respect to piston-velocity, one should be aware that the limits of the range of operation may be reached, resulting in pressure drops. This may be taken into account in the model, by modeling the supply pressure P_s, as well as the return pressure P_T, to be dependent on the delivered flow Q_A and Q_B. For ideal oil supply, the pressures P_s, and P_T are constant.

In order to reduce the complexity of the modeling of the system inside the defined system boundary, it is useful to distinguish a number of fundamental subsystems.

First, there is the servo-valve, which transfers the control input into the oil flows, depending on the actuator pressures. Although this device is designed to be fast and to show linear input-output behavior, its real behavior is generally not ideal. Because the valve flow drives the actuator, any non-ideal behavior of the valve propagates through the complete servo-system, for which reason the valve is explicitly considered in the modeling as a separate subsystem.

Second, there is the hydraulic actuator including load mass, with the driving oil flows Q_A and Q_B as inputs, and correspondingly the actuator pressures P_A and P_B, and position x_p or velocity $\dot{x_p}$ as outputs. The hydraulic actuator as subsystem forms the kernel of the complete hydraulic servo-system. As stated before, in order to avoid parasitic energy exchange, the actuator base should always be designed to be as stiff as possible.

The set of pipelines between the valve and the actuator is to be considered as a third subsystem, which is important, for instance, when the actuator has a long stroke. Because of the compressibility and the inertia of the oil, the relatively long pipelines cannot be seen as static devices; pressure waves travel with a finite velocity through the line and are almost ideally reflected at the end of the line. Owing to the

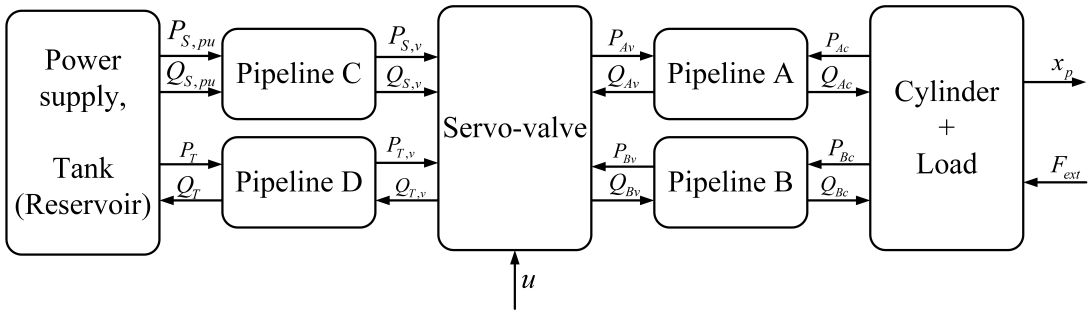

Figure 3.2: Subsystems of hydraulic servo-systems with interconnections.

pipeline dynamics, pressures and flows at the cylinder side have to be distinguished from those at the valve side. This is indicated in figure 3.2, where the pressures and the flows have been given indices, depending on whether the valve-side variables or the cylinder-side variables are concerned; the index Av denotes the valve-side of pipeline A, and the index Ac denotes the cylinder-side; the indices Bv and Bc denote the valve and cylinder side of pipeline B respectively.

Next, the set of pipelines between the power supply system and the valve, as well as between the tank and the valve, is considered as a fourth subsystem. This is especially important when the distance between main line and accumulator/valve is large. In many hydraulic servo-control applications, where the valve is placed very close to the cylinder, the dynamics of the return line (or case drain line for motors) may be important for the function and especially for the durability of the hydraulic system. Finally, the power supply unit, which in most hydraulic servo-applications, is designed in such a way that the system maintains a constant supply pressure for a certain range of operation, i.e., oil flow demand.

Thus, taking pipeline dynamics into account, the complete hydraulic servo-system can be represented by its five subsystems, with interconnections as shown in figure 3.1. However, for low-frequency behavior, where pipeline effects do not plays role in the input-output behavior, and for an ideal oil supply, the model of a hydraulic servo-system reduces to one with only two subsystems (valve + cylinder), see figure 3.2.

3.1.2 Approach to modeling

For the approach to modeling, the intended use of the models is of importance. On the one hand, the resulting models should provide physical insight in the system behavior and in the different physical phenomena that play a role in this behavior, in order to allow their use for system design. On the other hand, model-based control design requires an accurate mathematical description of the real system, both with respect to dynamics and with respect to relevant nonlinearities.

In order to obtain insight in the different physical phenomena, that play a role in the behavior of the hydraulic servo-system, the modeling approach starts with general theoretical modeling of the complete system. Thereby, the models are based on basic fluid-mechanical expressions such as the pressure-flow equation of the valve, the continuity equation of the fluid and the pressure-load equation and so on. In the theoretical modeling, all effects are included that are expected to play a role in the dynamic behavior of the system, based on earlier work in the area of hydraulic servo technique.

The actual insight in the system behavior is obtained by performing many simulations with the nonlinear theoretical model. These simulation results are used to evaluate whether certain physical effects deliver a relevant contribution to the overall system behavior or not. This may be in the sense of dynamics, or in the sense of nonlinearity. It should be noted here, that this insight is mainly of qualitative value; because it is difficult to find a realistic set of physical parameters for the theoretical model, this model does not have a high predictive value in the quantitative sense.

Whereas the model of the hydraulic servo-system is also to be used for control design, the model should not only be qualitatively correct, but should also have predictive value in a quantitative sense. This means, that the model should accurately represent the dynamic and nonlinear behavior of a real system. This is possible, if there is a clear relation between the input-output behavior of the model and the parameters of the model. However, in the experimental chapter will be shown that the existed model in the literature cannot simulate the dynamic behavior of the hydraulic servo system accurately. Therefore, by modifying the existing model of the nonlinear features of the system based on the experimental results, a new empirical model will be suggested for simulating the behavior of the hydraulic servo-system.

Then, the parameters of the system can be chosen or adjusted such that the model fits the behavior of some real servo-system. In other words, it should be possible to identify the model from experimental input/output data.

For this purpose, it is at least required, that the model is of the same order as the relevant dynamics of the real system, and that only the dominant nonlinearities of the real system are included in the model. So, the model should not include irrelevant dynamics and/or nonlinearities. Actually, the theoretical model, including 'all' physical phenomena that possibly play a role in the system behavior, does not fulfill these requirements on the model; it is too complex to be used directly for control design purposes. It should therefore be simplified.

However, in order not to disregard the advantages of the theoretical model, the simplification should be such, that:

- the (dominant) dynamic behavior described by the theoretical model is preserved, and
- the physical structure of the model is preserved, so that (dominant) nonlinear effects related to certain physical phenomena can be taken into account. Related to these requirements, a simplified model of the hydraulic servo-system is obtained in two stages.

In the first stage, the dynamic behavior of the system is abstracted from the theoretical model by means of linearization. Based on physical insight, partially obtained from the simulations with the theoretical model, the linearized model can be reduced (while preserving the physical structure of the model) such as to obtain minimal order models, describing the dominant dynamic behavior of the system.

In the second stage, the obtained models are extended with the nonlinearities of the theoretical model that seem to be relevant, again based on the results of the simulations with the theoretical model. Thereby, the nonlinear effects described by nonlinear equations in the theoretical model are rewritten in a simplified form, with a minimum number of parameters, like proposed by Handroos and Vilenius [77]. In this way, there is a clear relation between the model parameters and the resulting nonlinearity in the system, while physical interpretation is still possible. So, the effects of nonlinearities, related to certain physical phenomena, on the system

behavior, can be analyzed easily, in a quantitative sense, by means of simulations with the simplified nonlinear dynamic model.

With this two-stage approach to the simplification of the theoretical model, a physically structured nonlinear dynamic model of the hydraulic servo-system is obtained, which forms the basis for experimental identification and validation, as discussed in experimental Chapter.

In the next section, the modeling and simulation of the hydraulic system with different subsystems is discussed.

3.2 Modeling of an electro-hydraulic servo-valve

Because the flapper-nozzle servo-valve is a rather complex device, the theoretical modeling is rather complicated. In line with other research on this topic, reported in the literature [141, 126, 127, 198, 200, 157, 46], a lot of dynamic and nonlinear effects are included, resulting in a rather complex nonlinear model, just for the servo-valve.

A problem with this model is that it is difficult to choose the large number of physical parameters in the model such that quantitatively valid simulation results are obtained. Although many parameters may be known rather exactly a prior, many parameters are only known within some (wide) range, and some are even completely unknown. This may be due to manufacturing tolerances, or due to the fact that manufacturers do not provide parameter values, because they consider it as proprietary information [201].

The consequence of this problem is that the theoretical model is not useful for quantitative analysis of the servo-valve behavior. Nevertheless, a lot of qualitative insight can be obtained from simulations, which can be utilized to reduce the (linearized) servo-valve model such that only relevant dynamics are taken into account. Furthermore, the simulation results provide the necessary insight to decide, which nonlinearities of the servo-valve are (possibly) relevant. Thus, a relatively simple model for the servo-valve can be derived, which includes relevant nonlinearities and dynamics which forms a good basis for experimental identification of the servo-valve properties, as explained in next Chapter.

The purpose of the modeling and simulation of the electro-hydraulic servo-valve is to obtain insight in its dynamic and nonlinear behavior. This modeling helps to know which physical phenomena cause severe nonlinearity in the (dynamic) behavior of the servo-valve, and how they affect the performance of the complete hydraulic servo-system, in order to be able to come up with proper specifications for the servo-valve. For instance, manufacturers provide frequency responses in their catalogs, which show considerable amplitude dependence. By means of extensive theoretical modeling and simulation, the backgrounds of the nonlinear servo-valve behavior may be understood, and implications on the servo-system performance may be investigated.

In this section, after a description of the servo-valve, an explanation of the model structure is given, including a discussion of the nonlinear effects to be taken into account.

Description of the servo valve

The basic function of an electro-hydraulic servo-valve is to control a high power output, the oil flow, with a low-power input, the electrical control signal. Thereby, the input-output relation should be linear over some defined input range, independent of the power demand at the output. As already depicted in figure 3.1, the control of the oil flow takes place by the control of a number of port openings via the positioning of a spool in its bushing. Because the spool position may be affected by the delivered oil flow due to flow forces, especially if a large power amplification (large flow) is required, flow-control valves are often of the servo-valve type with multiple stages.

One of the most common servo-valve types is the two-stage flapper-nozzle valve, as depicted in figure 3.3. Actually, there are two stages of power amplification. First, the flapper-nozzle system converts the flapper motion, driven by a low-power electrical torque motor, into a hydraulically powered motion of the spool. Second, the small spool motions control relatively large oil flows through the spool ports, which is the second power amplification.

Referring to figure 3.3, the principle of operation of this type of servo-valves can be explained as follows. The electro-magnetic torque motor drives the flapper, which is connected to the housing by a spring-like element, the flexure tube; viscous

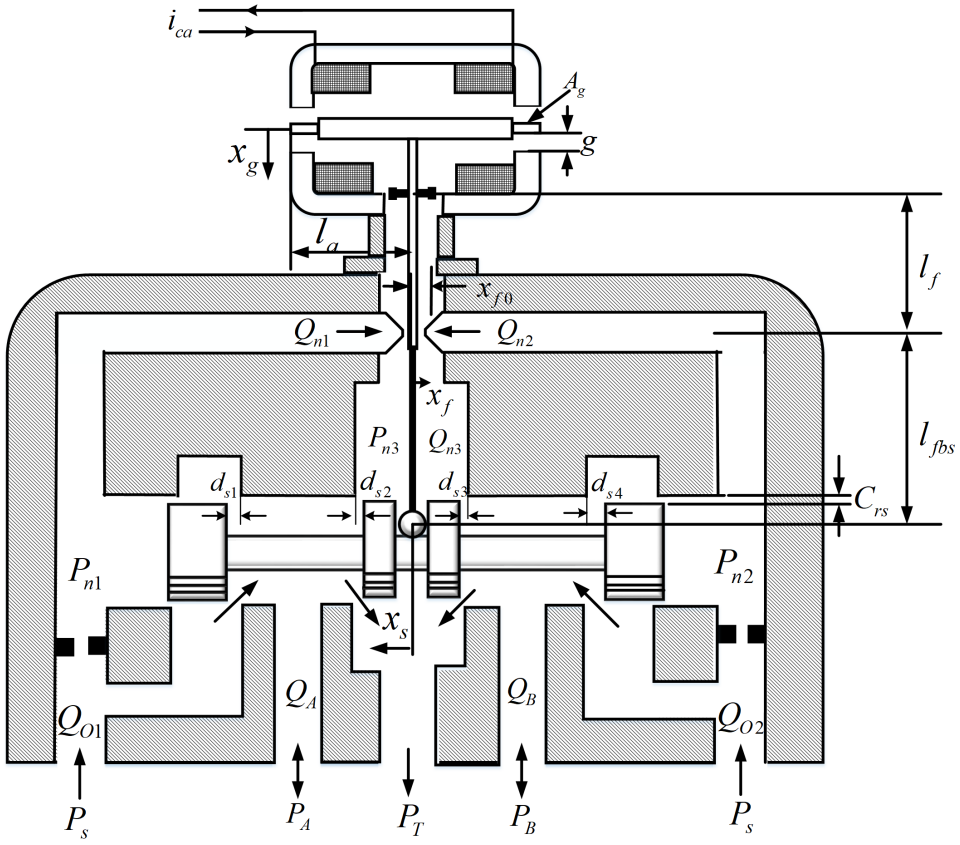

Figure 3.3: Schematic drawing of two-stage flapper-nozzle valve; overview with valve in null position.

damping is provided because the flapper is surrounded by oil. The generated flapper deflection x_f (see figure 3.3) controls the oil flows through the nozzles; the flow through the right nozzle reduces, while the flow through the left nozzle increases. Thus, the pressures at both sides of the spool are controlled, while the spool moves leftward. The resulting deformation of the feedback spring provides a force feedback: in the steady state situation, the torque from the torque motor is in equilibrium with the feedback spring deformation, which is proportional to the spool position.

Structure of the flapper-nozzle valve model

Many researchers have presented different contributions in nonlinear dynamic model of a flapper-nozzle valve [141, 126, 127, 198, 200, 157, 46]. Based on these theoretical

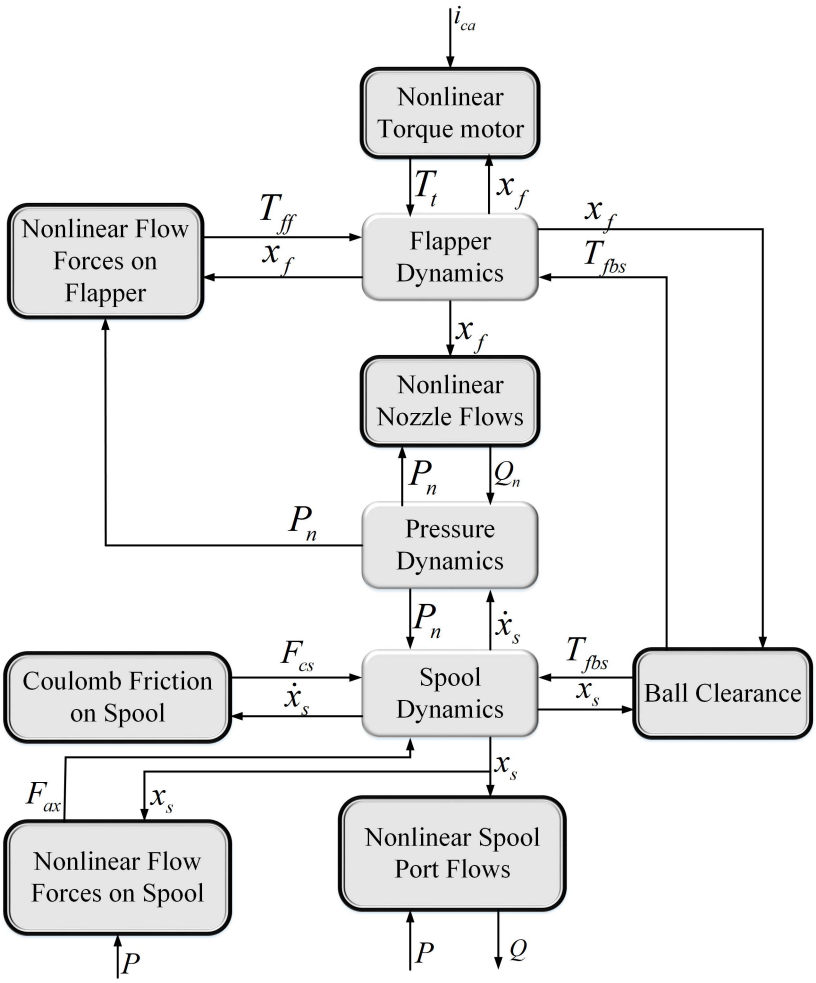

Figure 3.4: Block scheme representation of nonlinear flapper-nozzle valve model

models, the presented model in this section reflects the physical structure of the system. Thereby, a large number of nonlinear effects are included, leading to a model structure as depicted in figure 3.4. The structure of the valve and the motivation to include the indicated nonlinear effects is as follows:

- **Nonlinear torque motor** Although for small flapper deflections the torque motor behaves linear [141] the underlying physics involve a nonlinearity, which may affect the static and even the dynamic input-output behavior [141, 201].

- **Flapper dynamics** Due to the significant inertia of the flapper, together with

the spring like behavior of the flexure tube, flapper dynamics are involved. The model of these dynamics is constituted by an equation of motion, including interaction forces due to the nozzle flows and the feedback spring.

- **Nonlinear nozzle flows** The flapper position x_f controls the nozzle flows Φ_n , depending on the nozzle pressures P_n. The nonlinear model for these nozzle flows forms a basis of the flapper-nozzle valve model; in fact, the principle of operation of this type of valve is based on this flapper-nozzle element.

- **Nonlinear flow forces on flapper** Directly related to the nozzle flows, and therefore dependent on the flapper position x_f and the nozzle pressures P_n, are the flow forces on the flapper. These forces effectively result in a nonlinear torque T_{ff} on the flapper, which may affect the dynamic performance of the valve [141].

- **Pressure dynamics** As the model structure of figure 3.4 clearly indicates, the motion of the spool is actually driven by the pressure dynamics, for which the nozzle flows form a direct input. Therefore, these pressure dynamics, a result of the compressibility of the oil, also form an important link in the model.

- **Spool dynamics** The inertia of the spool introduces spool dynamics, to be described by an equation of motion. Different nonlinear effects contribute to this motion, as explained next.

- **Ball clearance** There may be some clearance of the ball at the end of the feedback spring in the slot of the spool. The result is a nonlinearity in the feedback spring torque T_{fbs} as a result of the flapper position x_f and the spool position x_s, which may have serious implications for the input-output behavior of the valve.

- **Coulomb friction on spool** The motion of the spool may be disturbed by the effect of Coulomb friction on the spool; this effect is also to be considered in the model.

- **Nonlinear spool port flows** The actual flow to be controlled by the servo-valve is determined by the spool port configuration, and depends not only on

the spool position x_s, but also on the pressures P at the spool ports. Considerable nonlinearity may be involved here [141], requiring special attention in the modeling and simulation of the servo-valve model.

- **Nonlinear flow forces on spool** Comparable to the flow forces on the flapper, the flows through the spool ports induce nonlinear forces on the spool, which may have some effect on the input-output behavior of the valve [139, 140, 8, 26].

3.2.1 Modeling of the flapper-nozzle system

Torque motor

The electro-magnetic torque motor, which drives the flapper, is controlled by an electrical current i_{ca}. This current is generated by a current amplifier, which converts the valve control input u (a voltage) into a current, with

$$\frac{L_{tm}}{R_{tm}}\dot{i}_{ca} + i_{ca} = K_{ca}u \tag{3.1}$$

where L_{tm} is the inductance of the torque motor, R_{tm} the resistance of the torque motor, and K_{ca} the current amplifier gain. In this equation, it is quite realistic to consider the input impedance for the electrical signal is infinitely large. Therefore, the equation (3.1) is expressed as:

$$i_{ca} = K_{ca}u \tag{3.2}$$

because the dynamics of the electric circuitry of the current amplifier and of the electro-magnetic circuitry of the torque motor are relatively fast, they are neglected. Often the torque T_t generated by the torque motor is assumed to be linearly dependent of the input current for the small rotations of the armature occurring in the servo-valve [141]. However, theoretically the following nonlinear relation describes the input-output behavior of the torque motor [141, 201]:

$$T_t = \frac{\mu_0 A_g l_a}{4}\left[\left(\frac{M_0 + i_{ca}N}{g - x_g}\right)^2 - \left(\frac{M_0 - i_{ca}N}{g + x_g}\right)^2\right] \tag{3.3}$$

with μ_0 the magnetic permeability of air, A_g the area of the gap normal to the magnetic flux direction, l_a the length of the armature, M_0 the magnetomotive force of the permanent magnets, N the number of coil windings and g the gap distance at neutral position of the armature.

The variation of the gap distance due to armature rotations is expressed in the displacement of the armature tip x_g, which is related to the deflection of the flapper between the nozzles, x_f, by the armature rotation and the flapper length l_f, as follows:

$$x_g = \frac{l_a}{l_f} x_f \tag{3.4}$$

Actually both displacements are described by the equation of motion of the flapper-armature combination, which constitutes the flapper dynamics.

Flapper dynamics

The equation of motion of the flapper has the torque T_t as driving torque. As the flapper rotates only over small angles (≈ 0.01 $[rad]$), the equation of motion can be expressed in terms of the flapper deflection:

$$\frac{J_a}{l_f}\ddot{x}_f = T_t - B_a\dot{x}_f - K_a x_f + T_{ff} - T_{fbs} \tag{3.5}$$

with J_a the inertia of the flapper-armature, B_a the viscous friction coefficient of the flapper, and K_a the spring constant of the flexure tube that connects the flapper to the housing. T_{ff} represents the nonlinear contribution due to flow forces on the flapper and the last term T_{fbs} is the feedback spring torque which only applies in case of mechanical spool position feedback.

Nozzle flows

The flow forces on the flapper are determined by the pressures in the nozzles and the actual flow through the nozzles. With the nozzle pressures $P_{ni},\ i = 1, 2$ being determined by the second stage, the nozzle flows $Q_{ni},\ i = 1, 2$ are modeled as turbulent flows through small restrictions [141, 140]. Because the ratio of the flapper-nozzle distance $x_{f0} \pm x_f$ (with x_{f0} the flapper-nozzle distance in neutral position, and x_f the flapper displacement) with respect to the nozzle diameter D_n is small (< 0.1), it

is assumed that the nozzle flows are determined by the curtain area between nozzle and flapper [141]. This results in:

$$\begin{aligned} Q_{n1} &= C_d \pi D_n (x_{f0} + x_f) \sqrt{2 \tfrac{P_{n1} - P_{n3}}{\rho}} \\ Q_{n2} &= C_d \pi D_n (x_{f0} + x_f) \sqrt{2 \tfrac{P_{n2} - P_{n3}}{\rho}} \end{aligned} \tag{3.6}$$

Hereby, C_d is the discharge coefficient for turbulent flows, and ρ is the density of the fluid (oil). The pressure P_{n3} is the common nozzle outlet pressure.

The value of the pressure P_{n3} is determined by a leakage restriction, which is present in most flapper-nozzle valves. The collective nozzle flows return to tank through this outlet restriction, so that the common nozzle output pressure P_{n3} is considerably higher than the small return pressure P_T. This not only reduces the sum of the (leakage) flows through the nozzles equation (3.6), but also avoids cavitation effects in the flapper-nozzle system.

The outlet restriction introduces a dynamic equation for the common nozzle output pressure in the theoretical model. This equation is obtained by writing the mass balance for the volume between the nozzles and the outlet orifice as follows, assuming turbulent flow through the outlet orifice:

$$\dot{P}_{n3} = \frac{E}{V_{n3}} \left(Q_{n1} + Q_{n2} - C_d A_{n3} \sqrt{2 \frac{P_{n3} - P_T}{\rho}} \right) \tag{3.7}$$

with E the bulk modulus of oil, V_{n3} the volume of oil between the nozzles and the outlet orifice, and A_{n3} the orifice area.

Flow forces on flapper

With the nozzle pressures determined by the second stage, and the flows by equation (3.6) and (3.7), it is possible to describe the flow forces on the flapper in (3.5) in more detail. Several researchers have been investigating these flow forces and reported their results in literature [125, 141, 95, 14, 45, 58]. In general form, the force $F_{fi},\ i = 1, 2$ due to a nozzle flow on the flapper can be expressed as [125]:

$$F_{fi} = \frac{\pi}{4} D_n^2 F R_i(x_f)(P_{ni} - P_T) \tag{3.8}$$

where $FR_i(x_f),\ i = 1, 2$ is the so-called Force Ratio, depending on the flapper position. A Force Ratio $FR = 1$ corresponds to the situation, that the flapper-nozzle distance is zero: the flow force then equals the static nozzle-pressure times the nozzle area.

An expression for the Force Ratio, which is mostly used to model flow forces in literature [127, 140, 141], can be obtained by a simple momentum analysis [125], and reads as follows:

$$\begin{aligned} FR_1(x_f) &= 1 + \left[\frac{4C_d(x_{f0}+x_f)}{D_n}\right]^2 \\ FR_2(x_f) &= 1 + \left[\frac{4C_d(x_{f0}-x_f)}{D_n}\right]^2 \end{aligned} \tag{3.9}$$

With this expression, and l_f the length of the flapper, the resulting torque in equation (3.5) due to flow forces on the flapper becomes:

$$\begin{aligned} T_{ff} &= l_f\left[F_{f1} - F_{f2}\right] \\ &= \tfrac{\pi}{4}D_n^2 l_f\left(\left[1 + \left(\tfrac{4C_d(x_{f0}+x_f)}{D_n}\right)^2\right](P_{n1} - P_{n3})\right) - \\ &\quad \tfrac{\pi}{4}D_n^2 l_f\left(\left[1 + \left(\tfrac{4C_d(x_{f0}-x_f)}{D_n}\right)^2\right](P_{n2} - P_{n3})\right) \\ &= \tfrac{\pi}{4}D_n^2 l_f\left(\left[1 + \left(\tfrac{4C_d}{D_n}\right)^2(x_{f0}^2 + x_f^2)\right](P_{n1} - P_{n2})\right) + \\ &\quad \left(\left[\left(\tfrac{4C_d}{D_n}\right)^2 2x_{f0}x_f\right](P_{n1} + P_{n2} - 2P_{n3})\right) \end{aligned} \tag{3.10}$$

It might be noted from equation (3.10), that there is a major contribution to the torque due to flow-forces from the difference of the two nozzle pressures, which only slightly depends on the flapper position x_f in a quadratic way. On the other hand, there is a contribution which is linear in x_f, in which the average of pressure difference between the nozzle pressures and the outlet pressure is involved.

Note hereby, that the torque T_{ff}; depends on the flapper position x_f with a positive sign, as the nozzle pressures P_{n1} and P_{n2} are always larger than the outlet pressure P_{n3}. Physically, this positive sign corresponds to a negative 'stiffness': the flow forces tend to destabilize the flapper position, contrary to what is reported by Wang et al. [202].

Anyhow, given the theoretical expression for the torque due to flow forces on the flapper (3.10), it can be stated that the contribution of these forces, modeled

this way, is almost linear. However, depending on the geometry of the flapper-nozzle system, the Force Ratio occurring in practice may be completely different from (3.9).

3.2.2 Modeling of two-stage flapper-nozzle valve

Pressure and spool dynamics

In the two-stage flapper-nozzle valve, the flapper-nozzle system may be seen as a flow controller, according to equation (3.6). Together with the flows through the inlet restrictions:

$$\begin{aligned} Q_{O1} &= C_d A_0 \sqrt{2\tfrac{P_s - P_{n1}}{\rho}} \\ Q_{O2} &= C_d A_0 \sqrt{2\tfrac{P_s - P_{n2}}{\rho}} \end{aligned} \tag{3.11}$$

where A_0 is the orifice area of the inlet restrictions, the nozzle flows determine the nozzle pressures, as the following mass balances for the valve chambers must hold [141]:

$$\begin{aligned} \dot{P}_{n1} &= \tfrac{E}{V_{n1}}(Q_{O1} - Q_{n1} + A_s \dot{x}_s) \\ \dot{P}_{n2} &= \tfrac{E}{V_{n2}}(Q_{O2} - Q_{n2} + A_s \dot{x}_s) \end{aligned} \tag{3.12}$$

Herein, $V_{ni},\ i = 1, 2$ are the valve chamber volumes, and A_s and $\dot{x}_s$ the spool side area and the spool velocity respectively. Although theoretically the valve chamber volumes change with spool position, this effect is not taken into account, because this variation is relatively small ($< 5\%$) in general.

The spool velocity, and also the spool position, is described by the equation of motion of the spool:

$$M_s \ddot{x}_s = A_s(P_{n2} - P_{n1}) - w_s \dot{x}_s - \frac{T_{fbs}}{(l_f - l_{fbs})} - F_{cs} - F_{ax} \tag{3.13}$$

where M_s is the mass of the spool, w_s the viscous friction coefficient, l_{fbs} the length of the feedback spring (if present), and F_{cs} and F_{ax} the Coulomb friction force and the axial flow force on the spool respectively. The axial flow force on the spool will be described in more detail later in this Section.

Concerning the Coulomb friction force on the spool, it can be modeled in many different ways [10]. In this case, a model is adopted where the friction force F_{cs} is constant during movement (acting in opposite direction of the velocity), and varying

during standstill (representing 'stiction'), similar as described in [178].

If a mechanical feedback of the spool position to the flapper position is present, the corresponding feedback spring torque acting on the flapper can be related to virtual deformations at the end of the spring, using the feedback spring constant K_{fbs}, as follows (see also figure 3.4(b)):

$$T_{fbs} = K_{fbs}\left[\frac{l_f + l_{fbs}}{l_f}x_f + x_s\right] \tag{3.14}$$

In case there is some clearance of the ball fitting in the slot in the spool, to be denoted by c_b the above equation is modified such that the feedback spring torque equals zero for:

$$-c_b \leq (\frac{l_f + l_{fbs}}{l_f})x_f + x_s \leq c_b \tag{3.15}$$

Outside these bounds the spool displacement x_s in equation (3.14) is replaced by $x'_s = x_s + c_b$ if the bound in equation (3.15) is exceeded on the right hand side, and by $x'_s = x_s - c_b$ if the bound in equation (3.15) is exceeded on the left hand side.

Obviously, the feedback spring torque T_{fbs} introduces a reaction force on the spool in equation (3.13). Therewith, the feedback spring constitutes a strong coupling between the dynamics of the flapper motion (3.5) and those of the spool motion (3.13). In case the spool position feedback is not mechanical, but electrical, this coupling is not present, and the contributions of the feedback spring torque T_{fbs} in (3.5) and (3.13) have to be set to zero. In the same time, the equation for the torque motor input (3.2) has to be modified to:

$$i_{ca} = K_{ca}(u - K_{sp}x_s) \tag{3.16}$$

with K_{sp} the feedback gain, including the spool position transducer gain.

With the equations so far, the closed loop dynamics of the flapper-nozzle system and the spool have been modeled. The actual model of the two-stage valve is now completed by describing the resulting flows through the spool ports.

Spool port flow and corresponding forces

A lot of fundamental research has been performed on flows through small restrictions

[57, 31, 85]. A more practical treatment for the case of flow through the ports of a servo-valve spool is given by Merrit and Viersma [141, 197]. They state, that the flows can in general be assumed to be turbulent, possibly with constant discharge coefficient C_d. In that case, for given spool position x_s and pressures at the spool ports P_A and P_B, the valve flows are determined by a static relation, which reflects the geometry of the ports. For the configuration, shown in figure 3.3, the equations for the servo-valve flows Φ_{m1} and Φ_{m2} (with neglecting leakage flow) are determined by the following equations:

$$\begin{aligned} Q_A &= C_v A_{s1} sign(P_s - P_A)\sqrt{|P_s - P_A|} - C_v A_{s2} sign(P_A - P_T)\sqrt{|P_A - P_T|} \\ Q_B &= C_v A_{s3} sign(P_B - P_T)\sqrt{|P_B - P_T|} - C_v A_{s4} sign(P_s - P_B)\sqrt{|P_s - P_B|} \end{aligned} \tag{3.17}$$

where $C_v = C_d h_s \sqrt{\frac{2}{\rho}}$ with h_s the width of the spool port openings. By assuming sharp edges, the spool port opening areas $A_{si}, \quad i = 1, 2$ can be written as:

$$\begin{aligned} A_{si} &= \begin{cases} \sqrt{(x_s + d_{si})^2 + c_{rs}^2} & x_s \geq -d_{si} \\ 0 & x_s < -d_{si} \end{cases} \qquad i = 1, 3 \\ A_{si} &= \begin{cases} \sqrt{(d_{si} - x_s)^2 + c_{rs}^2} & x_s \leq d_{si} \\ 0 & x_s > d_{si} \end{cases} \qquad i = 2, 4 \end{aligned} \tag{3.18}$$

where c_{rs} the radial clearance between the spool and its bushing, and d_{si} the underlap of port i in the neutral spool position.

3.2.3 Simplified dynamic characteristics of servo-valves

As discussed in the previous chapter, an accurate analytical description of valves would be extremely difficult and involve a large number of parameters. Furthermore, it is problematic to find a reasonable set of physical parameters for the theoretical servo-valve model (see [141, 90, 197] for details).

Nowadays, manufacturers catalog information usually provides the well-known step responses and/or frequency responses for various sizes and types of valve. Therefore, it is useful to use this information to develop simple model approximations of valve which forms the basis for experimental identification and validation

in chapter 5.

In the literature [141, 116, 90], with neglecting the irrelevant nonlinear effects, have been suggested an approximation of the servo-valve by a second-order model of the form

$$\frac{1}{w_v^2}\ddot{x}_s^* + \frac{2D_v}{w_v}\dot{x}_s^* + x_s^* + f_{hs}sign(\dot{x}_s^*) = k_v u \tag{3.19}$$

with the normalized valve position, velocity, acceleration, and the valve input signal with respect to the maximum stroke and maximum valve voltage:

$$x_s^* = \frac{x_s}{x_{s,\max}} \qquad -1 \leq x_s^* \leq 1 \tag{3.20}$$

$$\dot{x}_s^* = \frac{\dot{x}_s}{x_{s,\max}} \qquad -\dot{x}_{s,\lim} \leq \dot{x}_s \leq \dot{x}_{s,\lim} \tag{3.21}$$

$$\ddot{x}_s^* = \frac{\ddot{x}_s}{x_{s,\max}} \tag{3.22}$$

The parameters valve gain K_v, natural frequency w_v and damping coefficient D_v in equation (3.19) can be gained from identification or normally extracted from the manufacturer catalog information. The parameter f_{hs} takes into account the valve hysteresis and response sensitivity.

The dynamic model according to equation (3.19) with its five parameters and the flow equations (3.17) are usually possible to use as typical dynamic model of servo-valve. The parameters of this model are determined from the manufacturer's catalog and/or by means of identification (using the manufacturer's parameters as initial guesses), regardless of the complexity of the servo-valve. However, the parameters of the simplified model no longer have a direct physical interpretation, i.e., they cannot be used to reconstruct any physical parameters of the servo-valve. It might be noted here that, for control design purposes, an accurate (and often real-time capable) characterization of the dynamics is required, which makes the simplified model, once validated, useful. On the other hand, the complicated model provides insight that can be used for system design, i.e., in the component design stage, where exact knowledge of the model parameters is not necessary.

3.3 Modeling of a hydraulic actuator

Whereas the servo-valve is used to control a high power oil flow, the hydraulic actuator transforms this hydraulic energy in terms of flow and pressure into mechanical energy in terms of velocity and force. In many cases, this results in large motions of an inertial load; in other cases it results in large exerted forces to a stiff environment under small actuator displacements. Thus, the hydraulic actuator is the basic functional element of the hydraulic servo-system, and so is the model of the actuator the basic element of the complete servo-system model. In this Section, the theoretical model of the actuator is presented, and an analysis of the dynamics and nonlinearities of the actuator is given.

As outlined in Chapter 1, the configuration of the actuator will depend on the application. Nevertheless, it is possible to cover most hydraulic servo actuators in a theoretical model by representing them by two actuator chambers, separated by a moving piston, like depicted in figure 3.5.

The theoretical modeling of the hydraulic actuator is less involved than that of the servo-valve. Basically, the principal model relations have been given earlier, among others, by Merritt [141] and by Viersma [197]. In the basic actuator model, internal leakage and friction of the actuator have to be taken into account. Many hydraulic actuators in servo applications are provided with hydrostatic bearings, and for this type of bearings theoretical relations for the leakage and friction are available, which will be presented in this section.

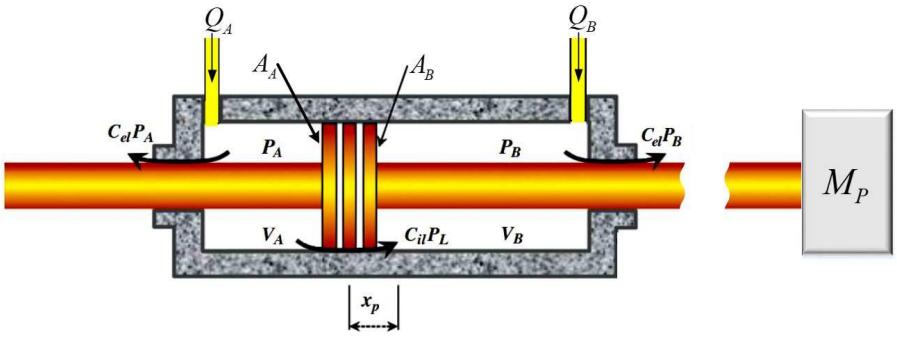

Figure 3.5: Schematic drawing of hydraulic servo-system.

3.3.1 Pressure Dynamics in Cylinder Chambers

The physical modeling of a hydraulic actuator is well-known [141, 197, 90] and is very often described in literature [1, 6, 232, 128, 71, 174, 165, 167, 200]. The actuator model consists of mass balances for each actuator chamber, and an equation of motion for the piston.

With the sign definitions of the actuator variables given in figure 3.5, the mass balances of the respective actuator chambers give state equations for the actuator pressures at both sides of the piston, by taking into account the oil compressibility with bulk modulus E (different model of bulk modulus have been presented in the chapter 2):

$$\begin{aligned} \dot{P}_A &= \tfrac{E}{V_A}(Q_A - Q_{el,A} - Q_{il} - A_A\dot{x}_p) \\ \dot{P}_B &= \tfrac{E}{V_B}(-Q_B + Q_{el,B} - Q_{il} + A_B\dot{x}_p) \end{aligned} \tag{3.23}$$

where A_A and A_B are the respective piston areas, which are not necessarily equal in the general case. Q_{il} and Q_{el} denote the internal leakage flow and the external leakage flow respectively. V_A and V_B are the volume of the respective actuator chambers, both including the valve connecting and chamber volume which can be written as:

$$\begin{aligned} V_A &= V_{pl,A} + (x_{p,\max} + x_p)\, A_A = V_{A0} + x_p A_A \\ V_B &= V_{pl,B} + (x_{p,\max} - x_p)\, A_B = V_{B0} - x_p A_B \end{aligned} \tag{3.24}$$

Hereby, $x_{p,\max}$ is half the actuator stroke and $V_{pl,A}$ and $V_{pl,B}$ are the pipeline volumes at the A-side and B-side respectively. The initial chamber volumes V_{A0} and V_{B0} consist of an "efficient" part (i.e., the volume required to fill only the chambers) and an "inefficient" part (i.e., mainly the volume of pipelines between the valve and the actuator).

For the leakage flows across the piston Q_{il} and the leakage flows Q_{el} out of the respective actuator chambers, it is often assumed that they can be described as small laminar flows through a narrow gap. Defining some laminar leakage coefficients C_{il} and C_{el} the respective leakage flows in figure 3.5 can be described by:

$$\begin{aligned} Q_{il} &= C_{il}(P_B - P_A) \\ Q_{el,A} &= C_{el}P_A \\ Q_{el,B} &= C_{el}P_B \end{aligned} \tag{3.25}$$

3.3.2 Equation of piston motion

The piston position x_p and velocity $\dot{x}_p$ in (3.23) are obtained from the equation of motion of the piston:

$$M_p\ddot{x}_p = A_B P_B - A_A P_A - F_{fric} + F_{ext} \tag{3.26}$$

where M_p is the inertia of the piston including the inertia of the load. F_{fric} is the friction force on the piston which in the next subsection different models of the friction in the literature have been discussed. The external force F_{ext} is the sum of the forces acting on the piston, that are not algebraically related to the actuator pressures or the velocity or the acceleration of the piston.

With the differential equations (3.23) and (3.26) the basic actuator dynamics are modeled, including leakage and friction effects. A more detailed description of these latter phenomena in the case that the actuator has hydrostatic bearings, is given in the next Subsections.

3.4 Friction model

In servo hydraulic systems, friction has an impact on the system dynamics in all regimes of operation. It serves to provide damping at all frequencies, notably those above the bandwidth of control. At the upper limits of performance, friction will affect the design of time optimal control and determine the limits of speed and power. Across the performance spectrum friction contributes to the dynamics. Furthermore, hard nonlinearities and possibly destabilizing friction effects at low velocity compound the problems of control. Therefore, to accurately design compensation, friction must be modeled.

Several mathematical models to describe the steady-state friction characteristics have been proposed (see [49, 215, 216, 9, 41, 190, 227, 185, 114, 51, 5, 155, 191],) and are widely used in mechanical systems including a hydraulic system. For control of high precision machines, the physics of solid-to-solid contact and the transition from solid-to-solid contact to fluid lubrication pose serious challenges. When parts are in static friction and before motion begins, the displacement allowed by elastic

surface deformation can be significant, giving a dynamic for small motions that bears little resemblance to the dynamics of large motions. Friction reversal during velocity reversal is a hard nonlinearity. Friction as a function of velocity may be, practically speaking, non-Lipschitz. And the transition from solid-to-solid contact to full fluid lubrication may bring a destabilizing drop in friction. This may occur at velocities that are small but important for tiny motions. However, yet the science of tribology is still far from having a complete picture on how friction works in all extent, therefore most of these models are mostly based on experimental experiences, rather than deep scientific background.

In the first part of this section, the nature of friction is investigated by considering the phenomena documented in earlier studies of friction. Then, some of the common friction models and assumptions are described in brief.

3.4.1 Friction characteristics

The total friction in a given situation can be divided up in different types of friction which are characterized by the velocity state at which they act and their dependence of this state. Furthermore, certain phenomenons exist which characterize the nature of friction. These frictions (see figure 3.6) and effects according to Armstrong [9] are:

Static friction (Sticktion) The force necessary to initiate motion from rest. It is often greater than the kinetic friction.

Kinetic friction (Coulomb friction, Dynamic friction) A friction component that is independent of the magnitude of the velocity.

Viscous friction A friction component that is proportional to velocity and, in particular, goes to zero at zero velocity.

Stribeck friction A friction phenomenon that arises from the use of fluid lubrication and gives rise to decreasing friction with increasing velocity at low velocity.

Break-away force The transition from rest (static friction) to motion (kinetic friction).

Dahl effect A friction phenomenon that arises from the elastic deformation of bonding sites between two surfaces which are locked in static friction. The Dahl effect causes a sliding junction to behave as a linear spring for small displacements.

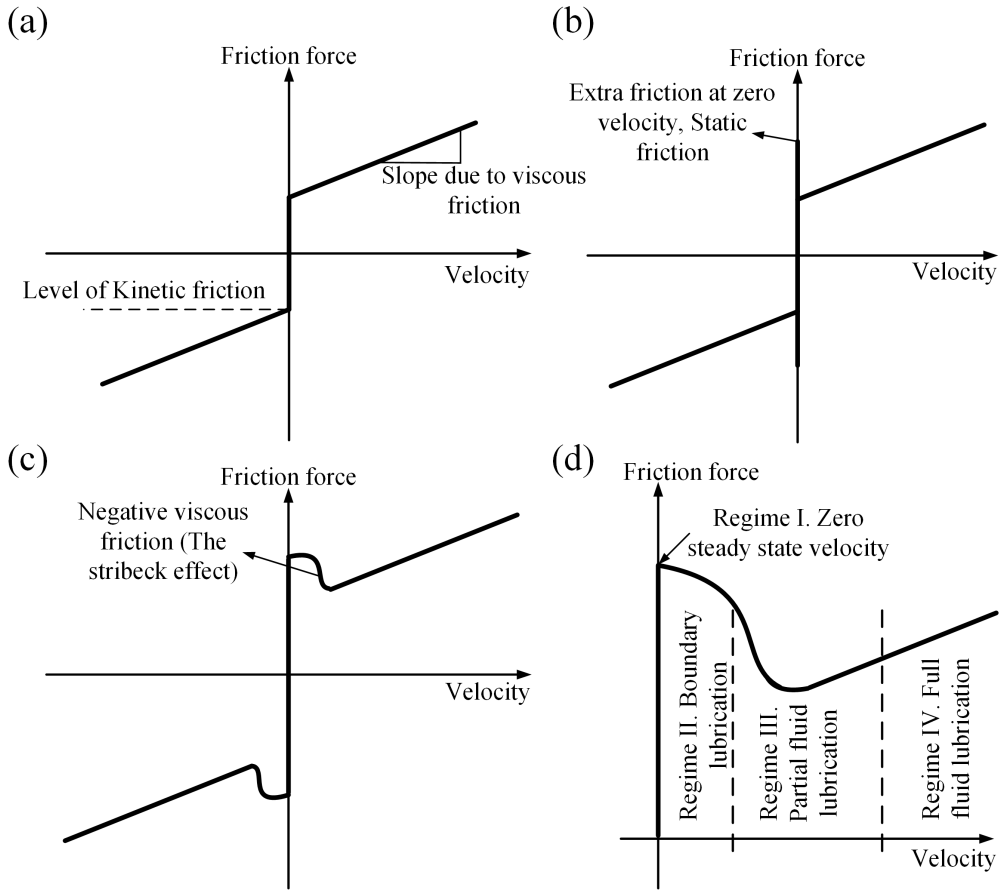

Figure 3.6: Friction models. (a) Kinetic plus Viscous Friction Model; (b) Static plus Kinetic plus Viscous Friction Model; (c) Negative Viscous plus Kinetic plus Viscous Friction Model; (d) The Generalized Stribeck Curve, showing friction as a function of velocity for low velocities.

As seen in figure 3.6, friction is considered a function of velocity. As mentioned earlier the kinetic friction is independent of velocity and always present. On the contrary, the viscous friction is proportional to the velocity and it occurs in fluid lubricated interfaces (figure 3.6(a)). Figure 3.6(b) illustrates, in some cases the break-away force, which is the force necessary to initiate motion, is larger than the force needed to sustain motion because of the static friction. The static friction and the Dahl effect are closely correlated as the Dahl effect is a consequence of the static friction and the asperities of the surfaces in the interface. Static friction is the

greatest cause to stick-slip motion which is explained later. Another consequence of correlation between the Dahl effect and the static friction is position dependence of the static friction. An in depth explanation of the Dahl effect and static friction can be found in [9]. The Stribeck effect is illustrated in figure 3.6(c) which suggests that the drop from the static friction does not happen instantaneously whereby the friction decreases with increasing velocity for low velocities. The Stribeck curve in figure 3.6(d) gives a closer look at friction at low velocity and show the three moving regimes, of the four in total, which contribute to the dynamics a controller confronts as the system accelerates away from zero velocity [9].

The Stribeck curve is a representation of the friction in a system which is lubricated with grease or oil, as is the case in most mechanical systems. The curve illustrates how the different regimes of lubrication change according to velocity and how this affects the friction. The lubrication regimes provides a physical explanation for the friction phenomenons, but this will not be covered in depth here. For more information see [10, 9].

From figure 3.6, it is apparent that all the different kinds of friction, except viscous, are discontinuous when the velocity is zero. This property along with the Stribeck effect causes nonlinearity and the consequences of this, with respect to servo systems, will be discussed in the following subsection.

3.4.2 Friction in servo system

Upper and lower bounds

Friction brings both positive and negative traits into a servo system. Friction can bring damping into a system which otherwise would be unstable. This damping is provided at all frequencies both under and over the bandwidth of the control. Besides playing a role in the dynamics of the system, friction affects the speed and power and thereby limiting the overall performance. Most often systems are assessed at their upper performance bounds with regards to maximum speed, maximum force and so on. Just as much as friction affects the upper bounds of performance, it affects the lower bounds, as very small displacements and corresponding low velocities can be unobtainable because of friction and its nonlinear nature at low velocity. The

nonlinearity causes a periodic process of sticking and slipping motion called stick-slip which limits the lower bounds with regards to minimum achievable displacement and minimum sustainable velocity [9].

Hunting

Stick-slip may arise during low speed motion with any control design and another consequence of the nonlinearity of friction, when using integral control, is a phenomenon called Hunting. Hunting is a integral-induced periodic oscillation around the reference position. According to [211], the static and coulomb friction form a dead zone in the system because of the earlier mentioned break-away force, which is the force necessary to create motion. Integral control eliminates the steady state error caused by the dead zone, but it might lead to hunting as the friction becomes larger at low velocities, as illustrated by the Stribeck curve (figure 3.6(d)). The increased friction at low velocity might cause the mechanism to stop before reaching the desired point. As the error accumulates in the feedback control system the mechanism will start moving when the break away force is exceeded. This motion reduces the friction from the maximum static friction to a sliding level and the over-driven control input results in overshoot whereby the desired point is passed and the system has to reverse. This repeats and the stick and slide motions results in oscillations around the desired position.

Friction lag

So far, friction have been assumed to have a steady dependence of velocity as shown by the Stribeck curve. It has been assumed that if the velocity changes then the friction will change simultaneously. Though, experiments by [82] have shown that there is a lag in the change of the friction, which is designated as frictional lag. Frictional lag is illustrated in figure 3.7.

As can be observed in figure 3.7 a lag in the friction force is present when a change in the velocity occurs. This is assumed to be because of the time needed for the new height of film thickness to be established, this phenomenon is also known as the squeeze effect. The film thickness develops slowly and decreases rapidly while accelerating and decelerating respectively, hence the frictional force will have a different time lag depending on whether an acceleration or deceleration has occurred [4].

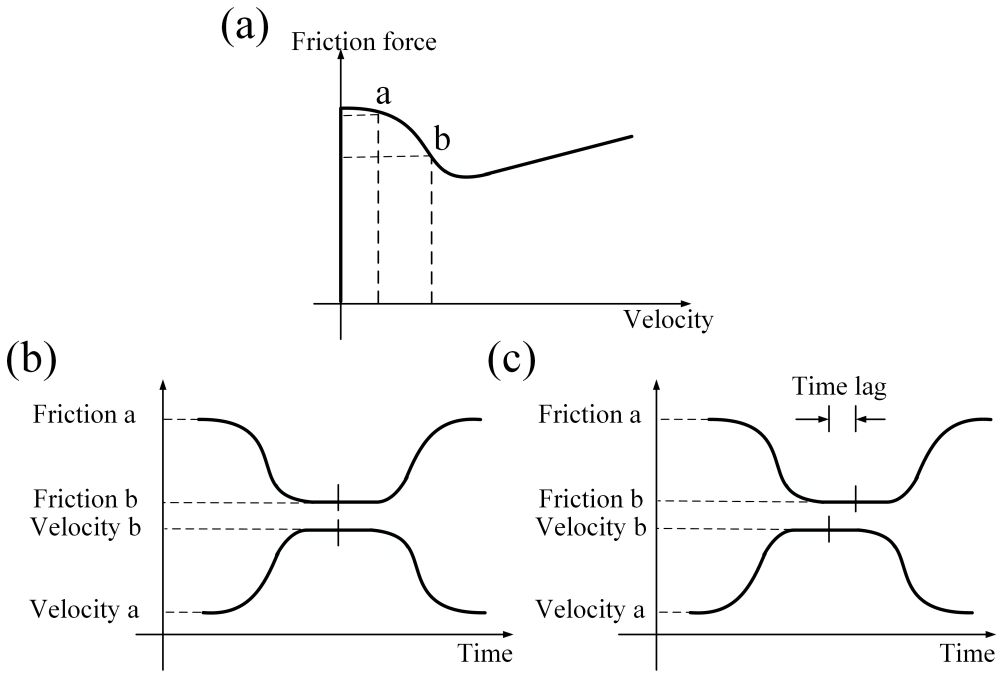

Figure 3.7: Time Relation between a Change in Velocity and the Corresponding Change in Friction.

Friction hysteresis

Hysteresis refers to a system that may exhibit path rate dependent memory. Friction hysteresis is caused by friction lag and the fact that boundary film layer develops and decreases at different rates depending on the velocity and applied force, amongst other factors.

Friction hysteresis is apparent, when the friction force is plotted as a function of the position or velocity of the system, in form of hysteresis loops. A such loop can be seen in figure 3.8.

It should be noted that the development of a such loop, is not only dependent on given inputs, but also on previous inputs and states. The shape of hysteresis loops can thus differ depending on the properties of the system.

The distinction between local and non-local memory is made when considering the modeling of the loops, and is the difference whether or not it is able to model hysteresis loops within a larger loop, respectively [113]. A position dependent hys-

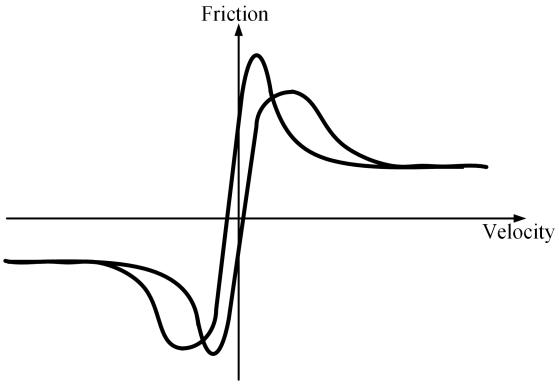

Figure 3.8: A typical rate dependent hysteresis loop

teresis loop with the non-local memory aspect is presented in figure 3.9. This figure illustrates measurements of the hysteresis force plotted as as a function of the measured position performed by [113]. At every new point from A to F the sign on the velocity reference is changed. As seen, this creates hysteresis loops within the bigger loop. These loops illustrate the hysteresis non-local memory aspect: When an internal loop is closed the system behaves as if the closed loop never occurred.

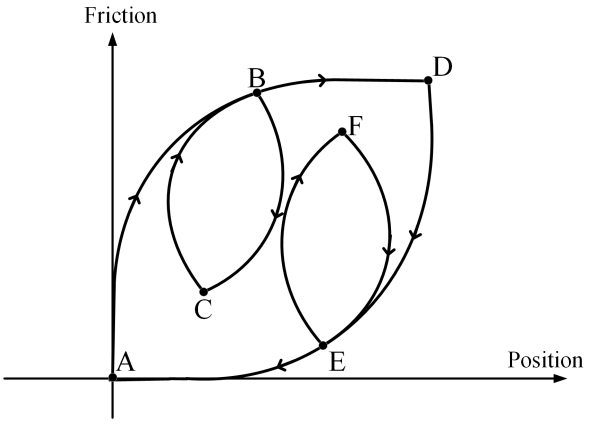

Figure 3.9: The relation between the position and hysteresis force depicting the hysteresis memory aspect.

Stick-Slip motion

Stick-slip motion occurs at close to zero velocity and is apparent in the form of

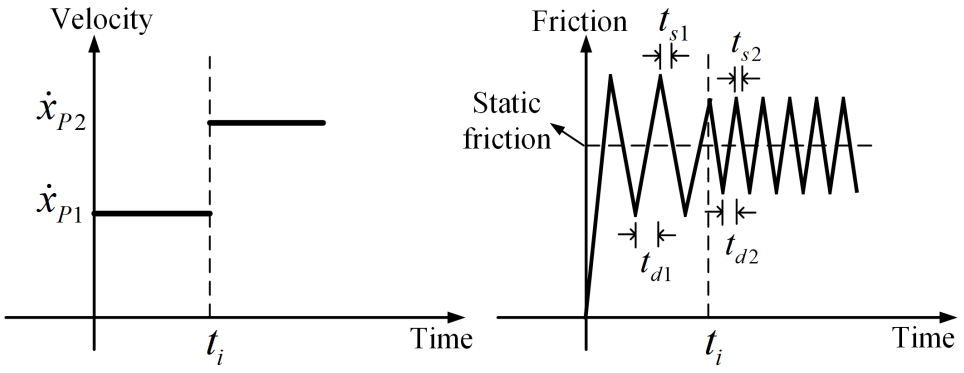

Figure 3.10: Stick-Slip.

sudden jerking motion. Considering an object at rest on which an external load is applied and increased until the stiction level is reached. As the object starts to move relatively to a surface in contact, the friction transcends from static to dynamic friction level which is, for limited boundary lubrication, a lower value. The external force applied is then decreased until the force is insufficient to sustain the motion and the object is brought to a hold at which point the cycle is repeated. This is also illustrated in figure 3.10.

As illustrated, a low average velocity, depicted by $\dot{x}_{P1}$, results in a high difference in friction force and this leads to a more apparent stick slip motion. The time the object is at rest is referred to as the dwell time an is denoted by t_d, likewise is the time when slipping occurs called the slip time denoted by t_s.

3.4.3 Mathematical model of friction

This section will give a review of both classic and modern friction models which are common in modeling of servo-hydraulic systems. The purpose of the mathematical friction models is to capture and describe the effects of friction with the necessary degree of detail, for it to be a valid and useful representation. Many different friction models exist. There are the steady state models which are characterized by being simple but with a minor degree of detail. Then there are the more advanced static and dynamic models which give more detailed descriptions by including the Stribeck effect and other phenomena. This section will present the classic models for

the static friction, Coulomb friction and Viscous friction, and the advanced static models of Armstrong's seven parameter model [10], the exponential model [28] and the dynamic LuGre model [49].

3.4.3.1 Steady state models

The steady sate models of friction deal with describing the Coulomb friction, viscous friction and the static friction. A combination of these three are the most commonly used friction models in controls as they are described by simple expressions. Especially the Coulomb friction has often been used for friction compensation. The general notion for the classical friction models is that friction opposes motion. Furthermore, the Coulomb frictions magnitude is independent both the velocity, $\dot{x}_p$, and surface area. The Coulomb friction is described by

$$F_C = \mu F_N sign(\dot{x}_p) \tag{3.27}$$

where F_C is the Coulomb friction, F_N is the normal force and μ is the coefficient of friction. The model of (3.27) does not specify Coulomb friction for zero velocity where the friction force can be anything in the interval between $-F_C$ and F_C. Therefore the complete model for the Coulomb friction is:

$$F_C = \begin{cases} -F_C & if \dot{x}_p > 0 \\ [-F_C, F_C] & if \dot{x}_p = 0 \\ F_C & if \dot{x}_p < 0 \end{cases} \tag{3.28}$$

The viscous friction is dependent of the velocity both in magnitude and direction. The expression is derived from theory of hydrodynamics and is:

$$F_v = f_v \dot{x}_p \tag{3.29}$$

Where F_v is the viscous friction force, f_v is the viscous friction parameter and $\dot{x}_p$ is the velocity. A better fit to experimental data is sometimes found when using the following expression:

$$F_v = f_v |\dot{x}_p|^{\delta_v} sign(\dot{x}_p) \tag{3.30}$$

Where δ_v depends on the geometry of the application.

The static friction occurs when the system is at rest. This friction is clearly not a function of velocity. Instead, it is a modeled using the external force as:

$$F_s = \begin{cases} F_{ex} & if \quad \dot{x}_p = 0 \quad and \quad |F_{ex}| < F_s \\ F_s sign(F_{ex}) & if \quad \dot{x}_p = 0 \quad and \quad |F_{ex}| \geq F_s \end{cases} \tag{3.31}$$

F_S is the static friction while F_{ex} is the external force. The expressions in (3.27), (3.29) and (3.31) are the classical friction components and they are combined in different ways to establish an overall model. Any combination of these components are referred to as a classical model and the combination of all three is illustrated in figure 3.6(b).

Stribeck curve

The model below was employed by [82]

$$F_{fric} = F_C + \frac{F_s - F_C}{1 + \left(\frac{\dot{x}_p}{v_s}\right)^2} + F_v \dot{x}_p \tag{3.32}$$

where the Coulomb, viscous and static friction is denoted by F_C, F_v and F_s respectively. v_s is the characteristic velocity $\dot{x}_p$ of the Stribeck curve. Hess and Soom reported systematic dependence of F_v and v_s on lubricant and loading parameters.

Another proposal for modeling the Stribeck effect is a linearized exponential equation of Bo and Pavelescu [28]. The viscous friction term was added by Armstrong-Hélouvry [10]. This model appears often in friction literature and is mentioned by [9, 28, 155, 44] among others. It is given by a function of velocity as follows:

$$F_{fric} = F_C + (F_s - F_C) e^{-(\frac{\dot{x}_p}{v_s})^n} + F_v \dot{x}_p \tag{3.33}$$

where n is an additional empirical parameter. In the literature surveyed by Bo and Pavelescu [28], they find the range of n from 0.5 to 1. Armstrong-Hélouvry [10] employs $n = 2$ and Fuller [60] suggest $n = very\ large$ for systems with effective boundary lubricants.

The Márton and Lantos model

Another simple representation of the Stribeck curve is the Márton and Lantos [137] friction model originates from the Tustin. The model captures the basic frictional phenomenon and simply superposes them on one another. The three features are the Coulomb friction F_C, the static friction F_s with the negative viscous effect determined by $\dot{x}_{st}$ and the viscous friction F_v.

$$F_{fric} = \left(F_C + (F_s - F_C) e^{-\frac{|\dot{x}_p|}{\dot{x}_{st}}} \right) sign(\dot{x}_p) + F_v \dot{x}_p \tag{3.34}$$

The parameters used in the Tustin model can be found both for the positive and negative friction regime, but will only be covered for the positive in the following. The discussed model makes use of the linear tendency of the Tustin exponential model as the velocity evolves towards infinity. In figure 3.11 a linear function F_{d1} is given covering the high velocity regime of the friction, and thereby the fourth Stribeck curve regime.

It is obvious that the linear approximation F_{d2} diverges significantly at low velocities. To model the friction at low velocities a second linear function F_{d1} is derived, decreasing from the stiction level. F_{d1} and F_{d2} can approximately describe the friction force progress from the low velocity regime influenced by stiction to the high velocity regime approximating the simple viscous friction. Introducing the switching

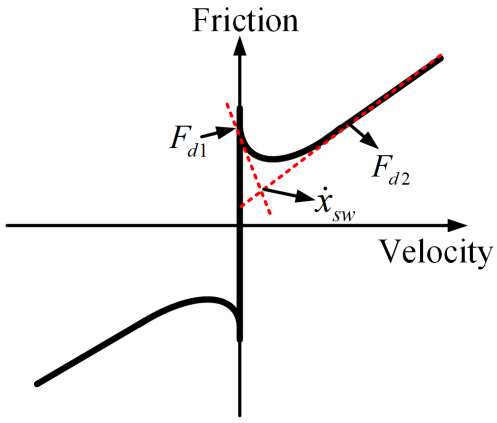

Figure 3.11: Two linear functions approximating the friction force.

velocity $\dot{x}_{sw}$, where the two linear functions intersect, constitutes the friction model presented as [137].

$$F_{fric} = \begin{cases} F_{d1} & if \quad 0 \leq \dot{x} \leq \dot{x}_{sw} \\ F_{d2} & if \quad \dot{x}_{sw} < \dot{x} \end{cases} \tag{3.35}$$

By linearization of the Tustin model, the parameters for the two linear functions can be obtained.

$$F_{d1} = F_s + \left.\frac{\partial F_{Tustin}(\dot{x}_p)}{\partial \dot{x}_p}\right|_{\dot{x}_p=0} \dot{x}_p = \overbrace{F_s}^{a_1} + \overbrace{\left(\frac{F_C - F_s}{\dot{x}_{st}} + F_v\right)}^{b_1} \dot{x}_p \tag{3.36}$$

$$\begin{aligned} F_{d2} &= F_{fric}(\dot{x}_{p,\max}) + \left.\frac{\partial F_{Tustin}(\dot{x}_p)}{\partial \dot{x}_p}\right|_{\dot{x}_p=\dot{x}_{p,\max}} (\dot{x}_p - \dot{x}_{p,\max}) \\ &= \overbrace{F_{fric}(\dot{x}_{p,\max})}^{a_2} + \overbrace{\left(\frac{F_C - F_s}{\dot{x}_{st}} e^{-\frac{|\dot{x}_{p,\max}|}{\dot{x}_{st}}} + F_v\right)}^{b_2} (\dot{x}_p - \dot{x}_{p,\max}) \end{aligned} \tag{3.37}$$

where $\dot{x}_{p,max}$ is the maximum velocity present in the data generating the Stribeck curve. The switch velocity deciding which linear function to use is given as:

$$\dot{x}_{sw} = \frac{a_1 - a_2}{b_2 - b_1} \tag{3.38}$$

Having two options when calculating the friction leads to a switching in the control strategy. In the same manner as for the positive regime two linear functions can also be derived for the negative velocity.

The classical models are simple, but not very detailed in their description as effects like the Stribeck friction, frictional lag and hysteresis, is not captured at all. This limits the models applicability at zero and low velocity where friction is recognized to be most destabilizing [49]. In order to capture the Stribeck effect, and provide a general description, more advanced static friction models are needed. Attempts at this are presented hereafter along with the LuGre model, which is a dynamic friction model that includes rate dependent friction phenomena like frictional lag, hysteresis and varying break-away forces[155].

3.4.3.2 Dynamic models

Armsrong's seven parameter model

Armstrong's model [10] is made up of two expressions, one for when in the state of sticktion, and one describing the sliding regime. The model consists of seven parameters represented in the expressions (3.39) and (3.40).

Not sliding (Pre-sliding displacement):

$$F_f(x) = -k_t x \tag{3.39}$$

Sliding (Coulomb + viscous + Stribeck curve friction with frictional memory):

$$F_f(\dot{x}_p, t) = -\left(F_C + F_v \left|\dot{x}_p\right| + \frac{F_s(\gamma + t_d)}{1 + \left(\frac{\dot{x}_p(t-\tau_L)}{\dot{x}_{st}}\right)} \right) sign(\dot{x}_p) \tag{3.40}$$

Rising static friction (friction level at breakaway):

$$F_s(\gamma, t_d) = F_{s,a} + (F_{s,\infty} - F_{s,a}) \frac{t_d}{t_d + \gamma} \tag{3.41}$$

where

$F_f(.)$: the instantaneous friction force

F_C : the Coulomb friction force

F_v : the viscous friction force

F_s : magnitude of the Stribeck friction (frictional force at breakaway is $F_C + F_s$)

$F_{s,a}$: magnitude of the Stribeck friction at the end of the previous sliding period

$F_{s,\infty}$: magnitude of the Stribeck friction after a long time at rest (with a slow application of force)

k_t : tangential stiffness of the static contact

$\dot{x}_{st}$: characteristic velocity of the Stribeck friction

τ_L : time constant of frictional memory

γ : temporal parameter of the rising static friction

t_d : dwell time, time at zero velocity

As the model consists of two expressions, a logical element requiring another eighth parameter is presumably necessary, if the model is to be implemented. Compared to the classical models, this models captures the Stribeck effect but in contrast has a lot of parameters which must be determined or estimated. For approximate ranges for the parameters of the model see [10].

LuGre model

The LuGre model by [49] is a dynamic model of friction which includes the Stribeck effect and the rate dependent effects such as frictional lag, hysteresis and varying break-away forces. The LuGre model is established by assuming the contact between the surfaces of two rigid bodies to be like elastic bristles in figure 3.12.

The average bristle deflection is denoted by z and modeled as:

$$\frac{dz}{dt} = \dot{x}_p - \frac{|\dot{x}_p|}{g(\dot{x}_p)} z \tag{3.42}$$

where

$$g(\dot{x}_p) = F_c + (F_s - F_c) e^{-\left(\frac{\dot{x}_p}{v_s}\right)^n} \tag{3.43}$$

is an arbitrary positive function which express the Stribeck effect. This function is not necessarily symmetric and depends on factors such as material properties, lubrication and temperature. The final LuGre model by adding the viscous friction

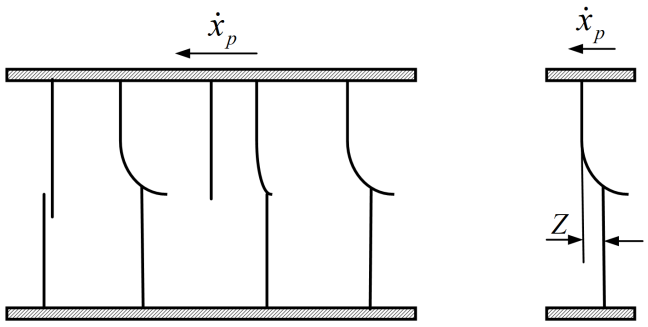

Figure 3.12: Bristle model.

is described by:

$$F_{fric} = \sigma_0 z + \sigma_1 \frac{dz}{dt} + \sigma_2 \dot{x}_p \tag{3.44}$$

where σ_0 is stiffness of bristles, σ_1 is micro-viscous friction coefficient for bristles and σ_2 is viscous friction coefficient. The advantage of this model, is that besides it is valid in both rotational and linear coordinates, it describes the phenomena for normally flat surfaces as well as for rolling bearings element.

Modified LuGre model

The LuGre model presented by [49] have been modified in [215] with considering a dimensionless lubricant film thickness parameter h into the Stribeck function $g(\dot{x}_p)$. In this model, a first order lag element is considered for the lubricant film dynamics, in which the time constant is varied among the acceleration, deceleration and dwell periods. The mean deflection of the elastic bristles is denoted by z and the rate of deflection is modeled by:

$$\frac{dz}{dt} = \dot{x}_p - \frac{|\dot{x}_p|}{g(\dot{x}_p, h)} z \tag{3.45}$$

where

$$g(\dot{x}_p, h) = F_c + ((1-h)F_s - F_c) e^{-\left(\frac{\dot{x}_p}{v_s}\right)^n} \tag{3.46}$$

describing the Stribeck effect by incorporating the lubricant film thickness parameter h. The dynamic model of lubricant film with a varying time constant is given by:

$$\frac{dh}{dt} = \frac{1}{\tau_h}(h_{ss} - h) \tag{3.47}$$

$$\tau_h = \begin{cases} \tau_{hp} & \dot{x} \neq 0, h \leq h_{ss} \\ \tau_{hn} & \dot{x} \neq 0, h > h_{ss} \\ \tau_{h0} & \dot{x} = 0 \end{cases} \tag{3.48}$$

$$h_{ss} = \begin{cases} k_f |\dot{x}|^{\frac{2}{3}} & |\dot{x}| \leq |v_b| \\ k_f |v_b|^{\frac{2}{3}} & |\dot{x}| > |v_b| \end{cases} \tag{3.49}$$

$$k_f = (1 - \frac{F_c}{F_s}) |v_b|^{-\frac{2}{3}} \tag{3.50}$$

where the steady-state lubricant film thickness h_{ss} is assumed to vary only in the negative resistance regime and kept constant outside the regime, k_f is the proportional constant for lubricant film thickness, v_b is the velocity at maximum film thickness and τ_h, τ_{hp}, τ_{hn} and τ_{h0} are time constant for lubricant film dynamics, acceleration period, deceleration period and dwell period separately. The final friction force is given by:

$$F_{fric} = \sigma_0 z + \sigma_1 \frac{dz}{dt} + \sigma_2 \dot{x}_p \tag{3.51}$$

Finally, in [190], by replacing the usual fluid friction term has been replaced with a first-order lead dynamics, a new extended LuGre model has been presented. This model is as following:

$$F_{fric} = \sigma_0 z + \sigma_1 \frac{dz}{dt} + \sigma_2 (\dot{x}_p + T\ddot{x}_p) \tag{3.52}$$

where T is time constant for fluid friction dynamics. In this paper [190], has been shown that the friction model in equation (3.52) can simulate the real hysteric behaviors of the friction force–velocity curve in the fluid lubrication regime.

Chapter 4

Identification and validation methods for hydraulic servo-system

In the previous Chapter, the theoretical model of the hydraulic servo-system with different model of nonlinearities has been presented. This finally led to a relatively non-linear dynamic model, describing the relevant dynamics and nonlinearities of the system, which forms the basis for experimental identification and validation. The identification of the model parameters from experiments and the validation of the resulting simulation model for a real hydraulic servo-system is the topic of this Chapter.

4.1 Introduction

The aim of the identification and validation is to use experimental data from the different subsystem to determine the model parameters vector $\bar{\theta}$ with n component such that the model prediction differ as little as possible from measured values according to a specified criterion; see figure 4.1. The most common choice for a

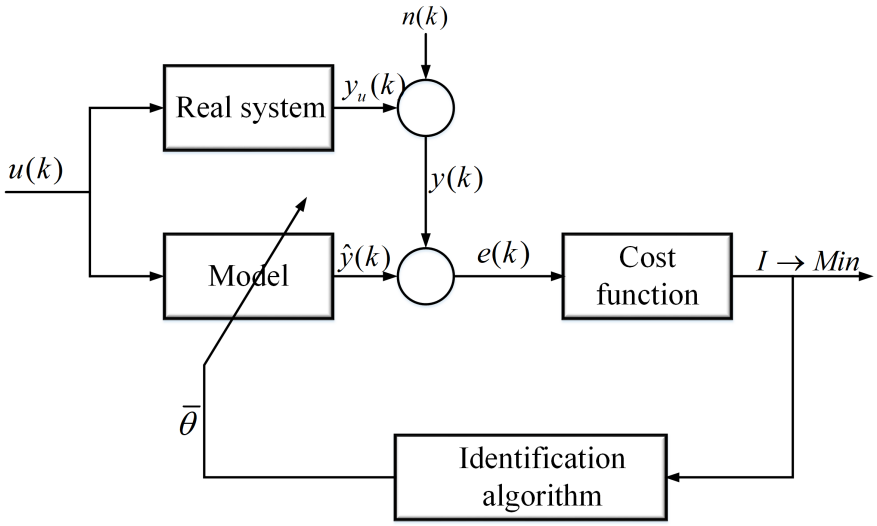

Figure 4.1: Identification task: determine model such that residual e minimized.

criterion is the sum of squared errors or its square root,

$$I(\bar{\theta}) = \frac{1}{2N} \sum_{k=1}^{N} e^2(k) \qquad with \quad e(k) = y(k) - \hat{y}(k) \tag{4.1}$$

Since the objective is to find the minimum of this function $I(\bar{\theta})$, it is called a "loss function" or "performance criterion". In this equation,k denotes discrete time samples ($k = \frac{t}{T_0}$, T_0: sampling period), $\hat{y}$ is the estimated output, and N is the number of data points. The measured system output y is usually corrupted with the noise $n(k)$. So the actually desired output y_u is unknown.

An identification algorithm reduces the cost I regarding the identification data. Linear and nonlinear optimization problems applying this special kind of loss function are called least square and nonlinear least squares problems.

In the following, a brief survey of the identification and validation process of the hydraulic servo-system is given.

4.1.1 Identification procedure

Each identification session consists of a series of basic steps. Some of them may be hidden or selected without the user being aware of his choice. Clearly, this can result in poor or suboptimal results. In each session the following action should taken:

- Collect information about the system
- Select a model structure to represent the system
- Choose the model parameters to fit the model as well as possible to the measurements: selection of a goodness of fit criterion
- Validate the selected model

Each of these points is discussed in more detail next.

4.1.1.1 Collect information about the system

If we want to build a model for a system, we should get information about it. This can be done by just watching the natural fluctuation, but design and perform the experiments which actively excite the system are more efficient. For this purpose, the user has to select an excitation that optimize his own goal (for example minimum cost, minimum time or minimum power consumption for a given measurement accuracy) within the operator constraints. Thereby, the type of signals to be used during experiments plays an important role and the quality of the final result is depended on the choices that are made. Therefore, the excitation of nonlinear system dynamics is the subject of the next subsection.

Excitation of nonlinear system dynamics

In the field of nonlinear system identification, the use of Pseudo Random Binary Signals (PRBS) is widespread [187, 203, 117, 236, 130, 118]. However, Leontaritis and Billings show [118], that for nonlinear systems identifiably can be lost with this type of excitation signal. Therefore, they recommend other types of random excitation signals, such as an independent sequence with a Gaussian distribution for a system with power constraints, and an independent sequence with a uniform distribution

for a system with an amplitude constraint on the input. In [25], has been shown that for proper identification of the general model, separable (random) processes are essential as inputs. Without giving this property in detail here, it can be stated that Gaussian processes (so with normal distribution) and sine-wave processes belong to this class [25]. This is also shown by Atherton [12], who uses this property to show that the Describing Function leads to the best linear approximation of the system for that class of input signals. It is therefore not surprising, that Atherton treats two types of Describing Function's , namely the Sinusoidal Input Describing Function and the Random Input Describing Function.

So, when applying Describing Function theory to characterize the dynamics of a nonlinear system, a choice has to be made between sinusoidal input signals and normally distributed random signals. In this work, a sinusoidal input signal with amplitude A_u and frequency f, i.e. $u(t) = A_u sin(2\pi ft)$ has been used for two reasons [196]:

- Sinusoidal signals have a deterministic and periodic character, so that they excite the nonlinearities of a system in a deterministic and reproducible way. Given the periodic character of the input signal, time averaging may be used to get rid of noise effects, without affecting the deterministic nonlinear input-output behavior [48]. This does not hold for input signals with a random character; they excite the nonlinearities of the system in a random way, and time averaging will also reduce the effects of the nonlinearity on the input-output behavior. Thus, the random signal causes the input-output behavior to be 'linearized'.

  In case a linear characteristic of the system is required, while no structural information on the nonlinearity of the system is available, this linearized effect of random excitation signals may be utilized. However, when structural insight in the nonlinear character of the system is available, which is the case here, this information should be utilized to distinguish between linear dynamics and nonlinearity, meaning that random excitation signals are not appropriate.

- An important reason to apply sinusoidal signals is to avoid the effect of intra-kernel interference [162]. Because the Describing Function method might be

interpreted as that input frequencies pass independently through the system, it is important to obtain experimental Describing Function's under conditions that avoid intra-kernel interference. This is possible by applying a sinusoidal input of a single input frequency, which guarantees that the output at that frequency component is just the result of the applied input signal at that frequency, and not related to other spectral components of the input.

With the arguments given, the sinusoidal function has been chosen as the input to the identification of the nonlinear models of the hydraulic servo-system. Then, the same arguments and other inputs such as PRBS play a role in the validation of the identified models, as is discussed next.

4.1.1.2 Selection of an appropriate model structure

A choice should be made within all the possible mathematical models that can be used to represent the system. Again a wide variety of possibilities exist as:

- Parametric versus nonparametric models
  In a parametric model, the system is described using a limited number of characteristic quantities called the parameters of the model whereas in the nonparametric model the system is characterized by measurements of a system function of a filter described by its poles and zeros and the motion equations of a piston. An example of a nonparametric model is the description of a filter by its impulse response at a large number of points.

  Usually, create a nonparametric model is easier than a parametric one, because the modeler needs less knowledge about the physical model of the system. However, physical insight and concentration of information are essential for parametric models. In this thesis, we will concentrate on parametric models.

- White box models, black box and Grey box models
  In the construction of a model, physical laws whose availability and applicability depend on the insight and skills of the experimenter can be used (Newton's law, Pascal law, etc.). Specialized knowledge related to different scientific fields may be brought into this phase of the identification process. Therefore, all equations and parameters can be determined by theoretical modeling. Such

a model is called a white box model. Typically, models whose structure is completely derived from first principles are also subsumed under the category white box models even if some parameters are estimated from data.

Another approach is to extract a black box model from the data. Instead of making a detailed study and developing a model based upon physical insight and knowledge, a mathematical model is proposed that allows sufficient description of any observed input and output measurements. That reduces the modeling effort significantly. For example, instead of modeling the shaking table using physical laws, an input output relation, taking the form of a high-order transfer function, could be proposed.

Finally, grey box models represent a compromise or combination between white and black box models. Almost arbitrary nuances are possible. Besides the knowledge from first principles and the information contained in the measured in rules may also be utilize in grey box models. These models are characterized by an integration of various kinds of information that are easily available. Typically, the determination of the model structure relies on prior knowledge while the model parameters are mainly determined by measurement data.

- Linear models versus nonlinear models
  In real life, almost every system is nonlinear. Because the theory of nonlinear system is very involved, these are mostly approximated by linear models, assuming that in operation region the behavior can be linearized. This kind of approximation makes it possible to use simple models. This choice depends strongly on the intended use of the model and the performance of the linearized model.

  In this thesis, in chapter 6, an attempt has been made to describe different models that have actually been successfully applied on servo-hydraulic shaking table. As stated before, nonlinear model is used for simulating the behavior of the system for designing control laws and further tests. However, for designing a controller using a simplified model is more applicable.

  Besides classical identification techniques, artificial neural networks methods can be used to describe nonlinear dynamic systems of hydraulic servo- systems

and are therefore addressed in this chapter. The sections on neural networks are mostly focused on a selected few concepts out of the many proposed and briefly described the aspects of practical applications of the method.

- Online versus offline identification
  Online estimation algorithms estimate the parameters of a model when new data is available during the operation of the model. In offline estimation, you first collect all the input/output data and then estimate the model parameters . Parameter values estimated using online estimation can vary with time, but parameters estimated using offline estimation do not.

  Since most parameters in hydraulic servo-systems do not change during operation, in literature the offline identification is mostly performed and used for adjusting the servo-control before the operation accordingly. This approach is frequently taken and has the merit that one can avoid many of the problems of identifiably of the parameters: a series of experiments can be carefully designed, such that single properties are clearly observable in each experiment, until all interesting parameters can be accurately inferred from accumulated information. Furthermore, it is possible to estimate model delays with offline estimation which is not possible in online estimation. Therefore, it is recommended to avoid online identification algorithms when other solutions are available and sufficient.

  However, adaptive control is an example of online estimation application where it is useful to identify the model online, simultaneously with the acquisition of measurements [218, 70, 235, 143, 226]. In spite of the good performance of this controller, the usage of this controller is limited because of the huge computational process. In this thesis, mostly focused on the offline identification process.

4.1.1.3 Match the selected model structure to the measurements

Once a model structure is chosen, it should be matched as well as possible with the available information about the system. Mostly this is done by minimizing a criterion that measures a goodness of the fit. The choice of this criterion is extremely

important because it determines the stochastic properties of the final estimator. Usually, the cost function defines the error between the experimental data and the model. There are many choices and each of them can leads different estimator with its own properties. It can be chosen using intuitive insight of the system with simple test on its existence.

4.1.1.4 Validate the selected model

Finally, the validity of the selected model should be tested to find out the identified model can describe the available data properly or there are still indication that some of the data are not well modeled. In practice, the best model is not always preferred. Often a simpler model that describes the system within user specified error bounds is preferred. Tools will be provided that guide the user through this process by separating the remaining errors into different classes, for example, unmodeled linear dynamics and nonlinear disturbances. From this information, further improvements of the model can be proposed, if necessary.Thereby, two types of model validation can be distinguished:

- Validation of the identified model with respect to the data that were used for the identification.
- Validation of the model with respect to 'fresh' data, which were not used for the identification step. This is called cross-validation. The fresh data may be just another measurement, i.e. obtained with another realization of the stochastic input and/or noise processes. However, it is also possible to validate the model with data, obtained from other types of input signals.

During the validation tests, it is always important to keep the application and performance in mind. The model should be tested under the same condition as it will be used later. Exploration should be avoided as much as possible. The application also determines what properties are critical.

In the following, a more extensive elaboration of the identification approach, with describing the nonlinear least square method for optimization and the artificial neural network method is given.

4.2 Nonlinear least square problems

As discussed in the previous section, the quadratic loss function in equation (4.1) is introduced as the most common in practice. If the parameters of the system are linear, a least squares problem arises. For nonlinear parameters, the optimization of the loss function

$$I(\bar{\theta}) = \sum_{k=1}^{N} f^2(k, \bar{\theta}) \tag{4.2}$$

is known as a nonlinear least squares problem. Note that (4.1) is a special case of (4.2). In this section, effective methods are introduced that exploit this information on the loss function's structure. In vector form (4.2) becomes:

$$I(\bar{\theta}) = \bar{f}^T \bar{f} \qquad with \quad \bar{f} = [f(1, \bar{\theta})\ f(2, \bar{\theta})\ \dots f(3, \bar{\theta})]^T \tag{4.3}$$

where here and in the following the argument $\bar{\theta}$ is dropped for brevity.

In the following, the gradient and the Hessian of this loss function will be derived. The jth component of the gradient is:

$$g_i = 2\frac{\partial I(\bar{\theta})}{\partial \theta_j} = 2\sum_{k=1}^{N} f(k)\frac{\partial f(k)}{\partial \theta_j} \tag{4.4}$$

Therefore, with the Jacobian matrix:

$$\bar{J} = \begin{bmatrix} \frac{\partial f(1)}{\partial \theta_1} & \dots & \frac{\partial f(1)}{\partial \theta_n} \\ \vdots & & \vdots \\ \frac{\partial f(N)}{\partial \theta_1} & \dots & \frac{\partial f(N)}{\partial \theta_n} \end{bmatrix} \tag{4.5}$$

the gradient can be written as

$$\bar{g} = 2\bar{J}^T \bar{f} \tag{4.6}$$

The entries of the Hessian of the loss function are obtained by calculation of the derivative of the gradient (4.4) with respect to parameter θ_l:

$$H_{ij} = \frac{\partial^2 I(\bar{\theta})}{\partial \theta_j \partial \theta_l} = 2\sum_{k=1}^{N} \left(\frac{\partial f(k)}{\partial \theta_l}\frac{\partial f(k)}{\partial \theta_j} + f(k)\frac{\partial^2 f(k)}{\partial \theta_l \partial \theta_j} \right) \tag{4.7}$$

The first term in the sum of (4.7) is the squared Jacobian of f, and the second term is $\bar{f}(k)$ multiplied by the Hessian of $f(k)$. Denoting the entries of the Hessian of $f(k)$ as $T_{lj}(k) = \frac{\partial^2 f(k)}{\partial\theta_l \partial\theta_j}$, the Hessian of the loss function in (4.7) becomes

$$\bar{H} = 2\bar{J}^T\bar{J} + 2\sum_{k=1}^{N} f(k)\bar{T}(k) \tag{4.8}$$

If the second term in (4.8) is denoted as $\bar{S}$, the Hessian of the loss function can be written as:

$$\bar{H} = 2\bar{J}^T\bar{J} + 2\bar{S} \tag{4.9}$$

The nonlinear least squares methods introduced below exploit this structure of the Hessian to drive an algorithm that is a general and efficient approach. The nonlinear least squares algorithms can be divided two categories.

Methods of the first category neglected $\bar{S}$ in equation (4.9). In this equation, if $\bar{S} \approx 0$, the approximation of the hessian will be defined by $\bar{H} \approx 2\bar{J}^T\bar{J}$. This condition is met for small $f(k)$ in (4.8). Since the $f(k)$ usually represent residual (errors) these methods are called small residual algorithms. The advantage of this approach is that the Hessian can be obtained by the evaluation of first order derivatives (Jacobian) only. Since for most problems the gradients of the residuals are available analytically, the approximate Hessian can be computed with low computational cost. The two popular algorithms are Gauss-Newton and Levenberg-Marquardt methods described below.

The approaches of the second category are called Large residual algorithms. They do not neglect the $\bar{S}$ term but spend extra computation on either approximating $\bar{S}$ or switching between a universal Newton and nonlinear least squares Gauss-Newton method. Note that, in principle, it is possible to compute $\bar{S}$ exactly. However, this would require the evaluation of many second order derivative terms. As for the general Newton method this would be practical only if the second order of the optimization problem was low. Therefore, such an approach would lead directly to the general Newton method, annihilating the advantages of the nonlinear least squares structure. Because of the extra effort involved the large residual algorithms are recommended only if $\bar{S}$ is significantly. For a more detailed treatment see [149].

4.2.1 Gauss-Newton Method

The Gauss-Newton method is the nonlinear least squares version of the general Newton method. Since the gradient can be expressed as $\bar{g} = \bar{J}^T \bar{f}$ and the Hessian is approximated by $\bar{H} \approx J^T J$, the Gauss-Newton algorithm becomes:

$$\bar{\theta}_k = \bar{\theta}_{k-1} - \eta_{k-1}(\bar{J}_{k-1}^T \bar{J}_{k-1})^{-1} \bar{J}_{k-1}^T \bar{f}_{k-1} \tag{4.10}$$

It approximately (as $\bar{S} \to \bar{0}$) shares the properties of the general Newton algorithm, but no second order derivatives are required. As with the classical Newton algorithm, in its original form, no line search is performed and η_{k-1} is set to 1. However, aline search makes the algorithm more robust and consequently Gauss-Newton with line search, the so-called damped Gauss-Newton, is widely applied.

In practice, the matrix inversion in (4.10) is not usually performed explicitly. Instead the following n-dimensional linear equation system is solved to obtain the search direction $\bar{Y}_{k-1}$:

$$(\bar{J}_{k-1}^T \bar{J}_{k-1})\bar{Y}_{k-1} = \bar{J}_{k-1}^T \bar{f}_{k-1} \tag{4.11}$$

This system can either be solved via Cholesky factorization or it can formulated as the linear least squares problem $\left\| \bar{J}_{k-1}\bar{Y}_{k-1} + \bar{f}_{k-1} \right\| \to \min$ and then be solved via orthogonal factorization of $\bar{J}_{k-1}$. However, no matter how the search direction is evaluated, problems occur if the matrix $\bar{J}_{k-1}^T \bar{J}_{k-1}$ is poorly conditioned or even singular. The smaller the least eigenvalue of $\bar{J}_{k-1}^T \bar{J}_{k-1}$ is, the slower is the rate of convergence of the Gauss-Newton method. The Levenberg-Marquardt algorithm discussed next deals with these problems.

4.2.2 Levenberg-Marquardt method

The Levenberg-Marquardt algorithm is an extension of the Gauss-Newton algorithm. The idea is to modify (4.10) to

$$\bar{\theta}_k = \bar{\theta}_{k-1} - \eta_{k-1}(\bar{J}_{k-1}^T \bar{J}_{k-1} + \alpha_{k-1}\bar{I})^{-1} \bar{J}_{k-1}^T \bar{f}_{k-1} \tag{4.12}$$

where again the matrix inversion is not performed explicitly but by solving:

$$(\bar{J}_{k-1}^T \bar{J}_{k-1} + \alpha_{k-1}\bar{I})\bar{Y}_{k-1} = \bar{J}_{k-1}^T \bar{f}_{k-1} \tag{4.13}$$

The addition of $\alpha_{k-1}\bar{I}$ in (4.12) to the approximation of the Hessian $\bar{J}_{k-1}^T \bar{J}_{k-1}$ is equivalent to the regularization in rigid regression for linear least squares problems. It solves the problems of a poorly conditioned $\bar{J}_{k-1}^T \bar{J}_{k-1}$ matrix.

The Levenberg-Marquardt algorithm can be interpreted as follows. For small values of α_{k-1} it approaches the Gauss-Newton algorithm, while for large values of α_{k-1} it approaches the steepest decent method. Close to the optimum the second order approximation of the loss function performed by the Gauss-Newton method is very good, and a small α_{k-1} should be chosen far away from the optimum the Gauss-Newton method may diverge, and a large α_{k-1} should be chosen. For sufficiently large values of α_{k-1} the matrix $\bar{J}_{k-1}^T \bar{J}_{k-1} + \alpha_{k-1}\bar{I}$ is positive definite, and a decent direction is guaranteed. Therefore, a good strategy for determination of α_{k-1} is as follows. Initially, some positive value for α_{k-1} is chosen. Then at each iteration α_{k-1} is decreased by some factor, since the parameters are assumed to approach their optimal values where the Gauss-Newton method is powerful. If the decrease of α_{k-1} leads to a bad search direction (i.e. loss function values increases) then α_{k-1} is again increased by some factor until a downhill direction results.

4.3 Neural Networks

Neural networks, as the name implies, try loosely to imitate the network of neurons in the brain where computation takes place through a large number of simple processing elements. Neural networks build up complexity out of simple blocks. A typical neural network consists of a number of simple processing units interconnected to form a complex network. Layers of such units are arranged so that data is entered at the input layer and passes though either one or several intermediate layers before reaching the output layer. In supervised learning the network is trained by operating on the difference between the actual output and the desired output of the network, the prediction error, to change the connection strengths between the nodes. By iterating, the weights are modified until the output error reaches an acceptable level.

This process is called machine learning because the network adjusts the weights so that the output pattern is reproduced.

There are two main problem types that can be studied using neural networks static problems, and dynamic problems. Static problems include pattern recognition, classification, and approximation. Dynamic problems involve lagged variables and are more appropriate for system identification and related applications. Depending on the architecture of the network the training problem can be either nonlinear in the parameters, which involves optimization or linear in the parameters, which can be solved using classical least squares type approaches. The training algorithms can be categorized into supervised, unsupervised, or reinforcement learning. Neural networks have excellent approximation properties but these are usually based on standard function approximation results using, for example, the Weierstrass theorem which applies equally well to polynomials, rational functions, and other well-known models. Neural networks use a terminology that is slightly different from that used in system identification, although the meanings or descriptions are almost identical. For example, in neural networks the typical terminology includes weights and training or learning, whereas the equivalent in system identification would be parameter estimates and estimation.

In this thesis the emphasis will be on the use of neural networks in system identification problems which involve nonlinear and dynamic relationships [22, 21, 39]. However, classical neural networks are purely gross static approximating machines. There is no dynamics within the network. Hence, when fitting dynamic models, all the dynamics arise by allocating lagged inputs and outputs to the input layer of the network. The training procedure then produces the best static approximation that relates the lagged variables assigned to the input nodes to the output. There are more complex network architectures, including recurrent networks [78, 149], which produce dynamics by introducing increasing orders of lagged variables to the input nodes. But in both cases it is very easy to over-specify the lags and this can lead to over-fitting and poor generalization properties. For example, if lags $u(t-2)$, $u(t-7)$, and $u(t-28)$ were the important lags in a problem, a typical neural network model would simply include all lags up to 28. However, this produces a grossly over-complicated approximation, causes long training times, and typically leads to

models that induce ghost nonlinear effects. This is a key problem in system identification and one solution is to use a forward orthogonal least squares algorithm to select the lags and then assign these lags as input nodes to the neural network.

All the problems that are relevant to linear and nonlinear system identification are also relevant to neural networks which are used for dynamic modeling. It is often incorrectly claimed that neural networks are robust and are not affected by noise. This is both true and false, and has to be qualified. In pattern recognition, for example, a neural network can be trained on static features recorded from a series of faces. Even when presented with noisy images of faces, the network should still be able to find the best fit to classify the faces. In this example it can be said that the network does accommodate noise. However, in dynamic applications all the results on the effects of noise and bias on estimation or training of the network weights still applies to neural network models. So, if there is colored noise on the output measurements then in general, unless noise models are fitted as part of the neural network training, all the weights in the network will be biased. This is especially true for neural networks which are trained with an emphasis on reducing the mean squared error of the residuals. Such an approach can produce very misleading results, even with estimation and training data sets, and the best solution is to use the model validity tests [27, 23] to determine if there is anything predictable left in the residuals after network training. Simply driving the mean squared error in the residuals to a small value can lead to grossly incorrect results [61, 234].

Neural networks have several advantages which the most important of them are:

- large number of simple units
- highly parallel units
- strongly connected units
- robustness against the failure of signal units
- easy to train and use.

The biggest criticism of the classical neural network models is that the models produced are completely opaque and usually cannot be written down or analyzed.

It is therefore very difficult to know what is causing what, to analyze the model, or to compute dynamic characteristics from the model. Neural networks have simplified the modeling but complicated the model. There are applications where this is not important, for example, where a gross approximation is all that is required. But this is normally not the case in system identification, where the user wants to understand what dynamic effects and model terms are contained in the models, wants to analyze the stability and study the frequency domain behavior [61]. These disadvantages can be illustrated using a simple example. Consider the case of two simple systems that can both be described by a linear second-order dynamic model, but where the dynamics are different in each case because while the form of the system model is the same, the parameter values are different. For example, two coupled cylindrical tanks where a pump supplies liquid to the first tank and the problem is to control the level in the second coupled tank. Data is collected from both these systems where the noise on the output measurements is sufficient so that it is not obvious from inspection of the time records that the systems are second order. If the classical multi-layered perceptrons or radial basis networks are applied, first the user will have to decide how many lags to assign as input nodes and then typically a nonlinear neural network model will be fitted to both data sets. Because the models are opaque, it will not be at all obvious that the underlying model in both cases is a simple linear second-order system with different parameter values. This means ghost nonlinear effects have been introduced to model very simple linear systems, and the models are likely to be biased if the noise is correlated and has not been properly accommodated within the modeling or training of the networks. Neural networks are highly parallel and information is distributed through the many weights and connections within the network. In other words, the network by its very nature destroys or at least hides the specific rule that it has learn; the rule is distributed over all the network weights and is not explicit. This is an example where the modeling has been simplified at the expense of complicating the model. Some of these points will not be relevant to all applications, but they are for dynamic modeling.

In this section, one of the most common neural network architecture, the multi-layer perceptrons (MLP) which in chapter 6 is used for parameter estimation of the shaking table is described briefly (for more details see [149, 66, 24]).

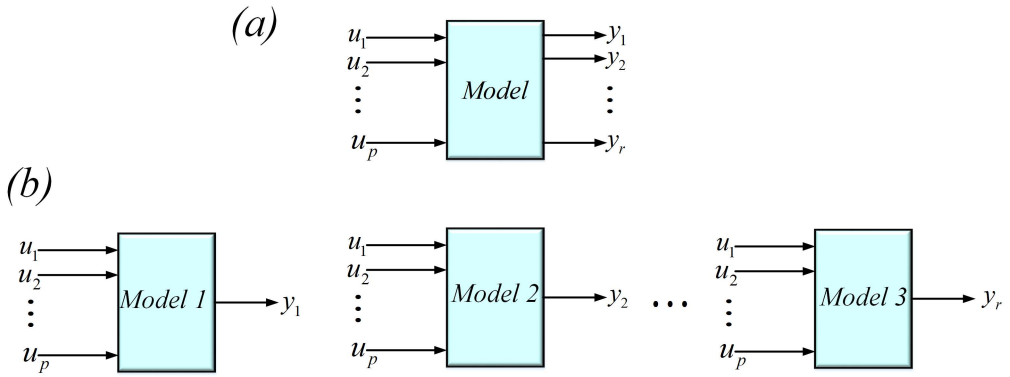

Figure 4.2: System model: (a) a general MIMO model, (b) decomposition of a MIMO model into MISO models.

4.3.1 Basic function formulation

Nonlinear static models perform a mapping from p inputs u_i gathered in a $p$dimensional input vector $\bar{u} = [u_1\ u_2\ ...\ u_p]^p$ to r outputs y_j gathered in an r-dimensional output vector $\bar{y} = [y_1\ y_2\ ...\ y_r]^T$. Such a general model is called a Multi Input Multi Output (MIMO) models, see figure 4.2(a). Typically, such a MIMO model is decomposed into r different Multi Input Single Output (MISI) models, see figure 4.2(b) for the following reasons:

- Each MISO model is simpler than an overall MIMO and thus easier understand, to validate, and to apply in practice.
- The required accuracy of each of the r model outputs can be adjusted separately. There is no need for a single loss function that weights the r output errors and thus performs an accuracy tradeoff between the different model outputs.
- Different model architectures, structures and optimization techniques can be applied to each MISO sub-problem, which makes the modeling and identification approaches more appropriate, flexible and powerful.

In opposition to these advantages, a MIMO model usually offers faster evaluation speed, i.e, the time required to calculate to model outputs for given model inputs.

Even though the MIMO models can be expected to be significantly more complex than each of the MISO models, its complexity is usually less that r times higher. Several parts of the structure and parameters of the MIMO model ate typically useful for modeling of more than one output. These common structures and parameters cannot be exploited by the separate MISO models. Nevertheless, the advantages of a MIMO model decomposition according to figure 4.2(b) are significant in most real world situations. Thus in all that follows only MISO models and Single Input Single Output (SISO) models are addressed. So a static MISO model can be described by the following mapping from the p-dimensional input to the one-dimensional output:

$$\widehat{y} = f(\bar{u}) \tag{4.14}$$

From all possible realization of this function $f(.)$ almost all alternatives of practical interest can be written in following basis function formulation:

$$\widehat{y} = \sum_{i=1}^{M} \theta_i^{(l)} \phi_i(\bar{u}, \bar{\theta}_i^{(nl)}) \tag{4.15}$$

The output $\widehat{y}$ is modeled as a weighted sum of M basis function $\phi_i(\cdot)$. The basis function are weighted with the linear parameters $\theta_i^{(l)}$ and they depend on the inputs $\bar{u}$ and a set of nonlinear parameters gathered in $\theta_i^{(nl)}$. In order to realize a nonlinear mapping, the basis function have to be nonlinear. Thus, the parameters $\theta_i^{(nl)}$ on which the basis function depend are necessarily nonlinear.

Often models incorporate an offset parameter (sometimes called "bias") that adjusts the operating point. Such an offset can be included in the basis function formulation by the introduction of a "dummy" basis function $\phi_i(\cdot)$, which is always equal to 1. Its corresponding linear parameter $\theta_i^{(l)}$ implements the offset,

$$\widehat{y} = \sum_{i=0}^{M} \theta_i^{l} \phi_i(\bar{u}, \bar{\theta}_i^{nl}) \qquad with \quad \phi_0(\cdot) = 1. \tag{4.16}$$

The basis function formulations (4.15) and (4.16) can be illustrated as the network shown in figure 4.3. Generally, the basis function $\phi_0(\cdot)$ can be of different type for each node. If all basis functions are of the same type and differ only in their

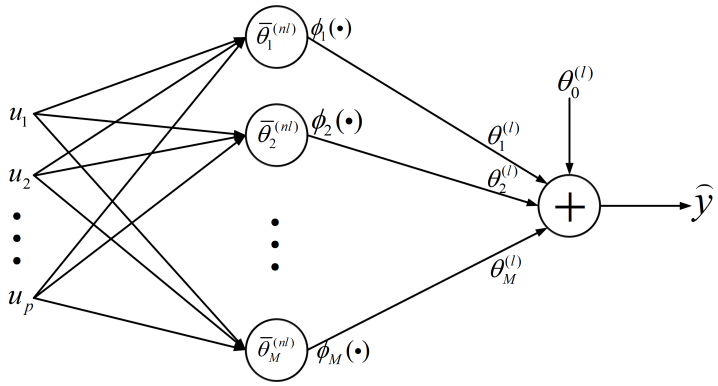

Figure 4.3: A network of basis functions. Each nods represents one basis function that depends on its nonlinear parameter vector $\theta_i^{(nl)}$. Depending on the specific model, the offset $\theta_0^{(l)}$ may exist or not.

parameters the network is called an artificial neural network. Then the nodes of the network in figure 4.3 are called neurons. The node at the output is called the output neuron, and all output neurons together are called the output layer. Each of the M nodes in the center that realizes a bias function is called the hidden layer neuron, and these neurons together are called the hidden layer. Finally, the inputs are sometimes denoted as input neurons, and all of them together are called the input layer. However, these neurons only fan out the inputs to all hidden layer neurons, and do not carry out any real calculation.

For a neural network, the linear parameters associated with the output neurons are called output weights:

$$\theta_i^{(l)} = w_i \tag{4.17}$$

Therefore, the equation (4.16) becomes:

$$\widehat{y} = \sum_{i=0}^{M} w_i \phi_i(\bar{u}). \tag{4.18}$$

The output neurons is usually a linear combination of the hidden layer neurons $\phi_i(\cdot)$ with an additional offset w_0 which is sometimes called "bias" or "threshold".

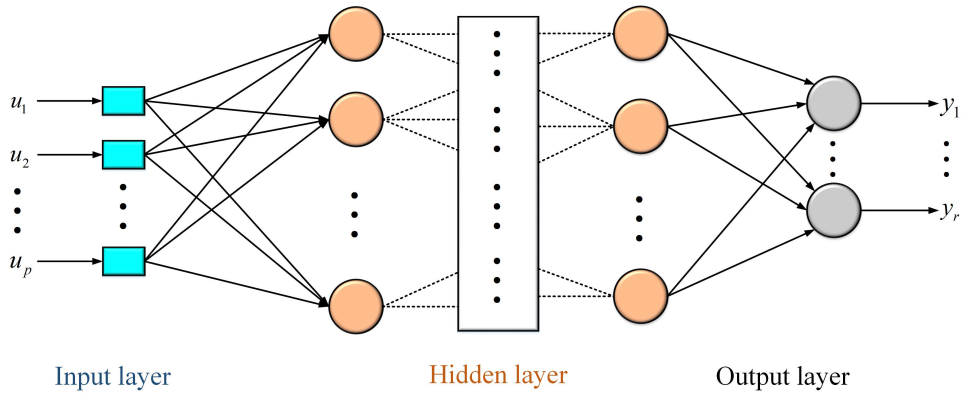

Figure 4.4: A multi-layered perceptrons with p input variables and r output variables.

4.3.2 The Multi layered Perceptrons

The typical structure of an multi layered perceptrons with one input layer, a number of hidden layers, and one output layer is illustrated in figure 4.4. The input layer consists of p measurable source neurons or input variables which distribute the inputs to the first layer. The outputs from the first layer nodes then become inputs to the second layer, and so on. There is no connection between the nodes within the same layer. The last layer acts as the network output layer and all the layers between the input and output are usually referred to as hidden layers. In figure 4.4, the output layer consists of r observable computational neurons, or output variables. Each layer in the network is made up of basic computing elements or neurons, which in the multi layered perceptrons typically consist of an activation function defined as a nonlinear static function of the weighted sum of the inputs plus a threshold parameter (see equation (4.18)). The output of each neuron is the output of the activation function. A typical choice for the nonlinear activation function is the sigmoid function as

$$f(x) = \frac{1}{1 + e^{-x}} \tag{4.19}$$

which gives a smooth model with the advantage that gradient-based parameter estimation methods can be used (see figure 4.5). The output nodes usually do not contain a threshold parameter and the activation functions are just a linear

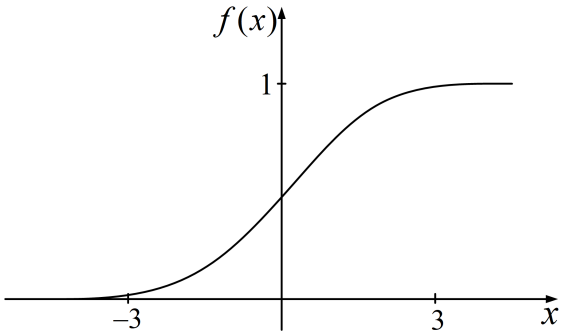

Figure 4.5: Common choices for global basis functions: a sigmoid function.

weighted sum. Network training consists of determining the linear weights and threshold parameters in every neuron in the network by minimizing the difference between the network output and the measured output, or the prediction errors. The classical training algorithm is based on back-propagation, which is simply a steepest descent algorithm. However, steepest decent is known to be slow to converge and because the network is a nonlinear in the parameter model, local minimum can be a problem.

4.3.3 Feedforward neural networks with Marquardt algorithm

In this section, the Marquardt algorithm for nonlinear least squares is presented and is incorporated into the backpropagation algorithm for training feedforward neural networks [74]. This algorithm is good balance between the complexity and simplicity of networks which is used for shaking table parameters estimation [168].

The backpropagation learning is a popular algorithm which there has been considerable research on methods to accelerate the convergence of the algorithm. The most popular approaches have used conjugate gradient or Gauss-Newton (secant) methods. The Gauss-Newton methods are considered to be more efficient, but their storage and computational requirements go up as the square of the size of the network. There have been some limited memory Gauss-Newton (one step secant) algorithms that speed up convergence while limiting memory requirements. If exact

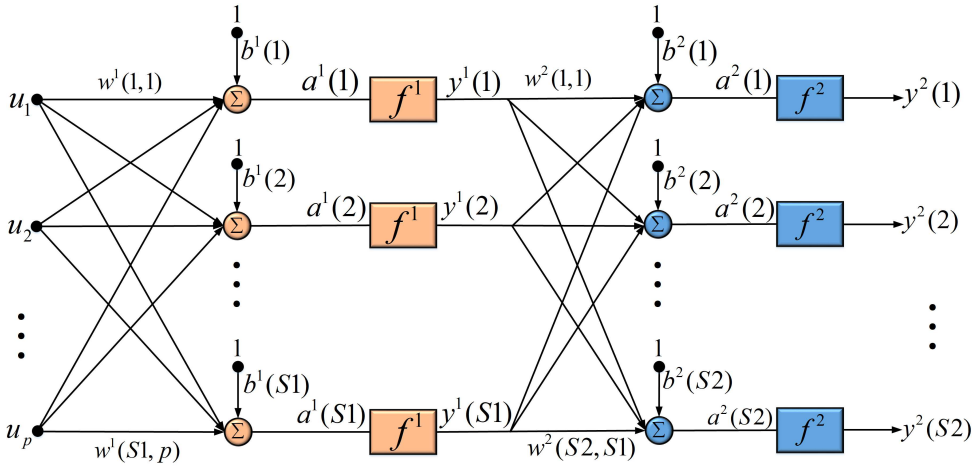

Figure 4.6: Common choices for global basis functions: a sigmoid function.

line searches are used, the one step secant methods produce conjugate directions. Another area of numerical optimization that has been applied to neural networks is nonlinear least squares.

The more general optimization methods were designed to work effectively on all sufficiently smooth objective functions. However, when the form of the objective function is known it is often possible to design more efficient algorithms. One particular form of objective function that is of interest for neural networks is a sum of squares of other nonlinear functions. The minimization of objective functions of this type is called nonlinear least squares.

Most of the applications of nonlinear least squares to neural networks have concentrated on sequential implementations, where the weights are updated after each presentation of an input/output pair. This technique is useful when online adaptation is needed, but it requires that several approximations be made to the standard algorithms. The standard algorithms are performed in batch mode, where the weights are only updated after a complete sweep through the training set. In the following, the application of a nonlinear least squares algorithm to the batch training of multi-layer perceptrons is presented.

4.3.3.1 Backpropagation algorithm

Consider a multilayer feedforward network, such as the two-layer network of figure 4.6 The net input to unit i in layer $k+1$ is

$$a^{k+1}(i) = \sum_{j=1}^{Sk} w^{k+1}(i,j) y^k(j) + b^{k+1}(i) \tag{4.20}$$

The output of unit i will be

$$y^{k+1}(i) = f^{k+1}(a^{k+1}(i)) \tag{4.21}$$

For an M layer network the system equations in matrix form are given by

$$\bar{y}^{k+1}(i) = \bar{f}^{k+1}(W^{k+1}\bar{y}^k + \bar{b}^{k+1}) \qquad with \quad \bar{y}^0 = \bar{u}, \qquad k = 0, 1, ..., M-1 \tag{4.22}$$

The task of the network is to learn associations between a specified set of input-output pairs $\{(\bar{u}_1, \bar{t}_1), (\bar{u}_2, \bar{t}_2), ..., (\bar{u}_Q, \bar{t}_Q)\}$.

The performance index for the network is

$$V = \frac{1}{2}\sum_{q=1}^{Q} (\bar{t}_q - \bar{y}_q^M)^T (\bar{t}_q - \bar{y}_q^M) = \frac{1}{2}\sum_{q=1}^{Q} \bar{e}_q^T \bar{e}_q \tag{4.23}$$

where $\bar{y}_q^M$ is the output of the network when the qth input, $\bar{u}_q$, is presented, and $\bar{e}_q = \bar{t}_q - \bar{y}_q^M$ is the error for the qth input. For the standard backpropagation algorithm we use an approximate steepest descent rule. The performance index is approximated by

$$\widehat{V} = \frac{1}{2}\bar{e}_q^T \bar{e}_q \tag{4.24}$$

where the total sum of squares is replaced by the squared errors for a single input/output pair. The approximate steepest (gradient) descent algorithm is then

$$\Delta w^k(i,j) = -\mu \frac{\partial \widehat{V}}{\partial w^k(i,j)} \tag{4.25}$$

$$\Delta b^k(i) = -\alpha \frac{\partial \widehat{V}}{\partial b^k(i)} \tag{4.26}$$

where α is the learning rate. Define

$$\delta^k(i) \equiv \frac{\partial \widehat{V}}{\partial a^k(i)} \tag{4.27}$$

as the sensitivity of the performance index to changes in the net input of unit i in layer k. Now it can be shown, using (4.20), (4.24), and (4.27), that

$$\frac{\partial \widehat{V}}{\partial w^k(i,j)} = \frac{\partial \widehat{V}}{\partial a^k(i)} \frac{\partial a^k(i)}{\partial w^k(i,j)} = \delta^k(i) y^{k-1}(j) \tag{4.28}$$

$$\frac{\partial \widehat{V}}{\partial b^k(i)} = \frac{\partial \widehat{V}}{\partial a^k(i)} \frac{\partial a^k(i)}{\partial b^k(i)} = \delta^k(i) \tag{4.29}$$

It can also be shown that the sensitivities satisfy the following recurrence relation

$$\bar{\delta}^k = \dot{F}^k(\bar{a}^k) W^{k+1} \bar{\delta}^{k+1} \tag{4.30}$$

where

$$\dot{F}^k(\bar{a}^k) = \begin{bmatrix} \dot{f}^k(a^k(1)) & 0 & \dots & 0 \\ 0 & \dot{f}^k(a^k(2)) & \dots & 0 \\ \vdots & \vdots & \ddots & \vdots \\ 0 & 0 & \cdots & \dot{f}^k(a^k(SK)) \end{bmatrix} \tag{4.31}$$

and

$$\dot{f}^k(a) = \frac{df^k(a)}{da} \tag{4.32}$$

This recurrence relation is initialized at the final layer

$$\bar{\delta}^M = -\dot{F}^M(\bar{a}^M)(\bar{t}_q - \bar{y}_q) \tag{4.33}$$

Finally, for minimizing the performance index in the equation (4.23), the Marquardt-Levenberg algorithm which is defined in subsection 4.2.2, is used.

In summary, the algorithm which described above is as follows:

1. Present all inputs to the network and compute the corresponding network outputs (using (4.22)), and errors ($\bar{t}_q - \bar{y}_q^M$). Compute the sum of squares of errors over all inputs ($V(\bar{\theta})$).

2. Compute the Jacobian matrix (using (4.5), (4.28), (4.29), (4.30), and (4.33)).

3. Solve (4.13) to obtain $\bar{Y}_{k-1}$ (For the results shown in the next section Cholesky factorization was used to solve this equation.)

4. Recompute the sum of squares of errors using $\bar{\theta}+\bar{Y}$. If this new sum of squares is smaller than that computed in step 1, then reduce α in equation (4.13), let $\bar{\theta} = \bar{\theta} + \bar{Y}$, and go back to step 1. If the sum of squares is not reduced, then increase α and go back to step 3.

5. The algorithm is assumed to have converged when the norm of the gradient (4.6) is less than some predetermined value, or when the sum of squares has been reduced to some error goal.

4.4 model validation and comparison of model structures

The problem of model validation is to determine whether the identified model does agree sufficiently well with the behavior of the real system, as it is described by available data [196, 90]. Thereby, two types of model validation can be distinguished:

- Validation of the identified model with respect to the data that were used for the identification.

- Validation of the model with respect to 'fresh' data, which were not used for the identification step. This is called cross-validation [90]. The fresh data may be just another measurement, i.e. obtained with another realization of the stochastic input and/or noise processes. However, it is also possible to validate the model with data, obtained from other types of input signals.

In the field of system identification, different techniques of (non-linear) model validation are found [90, 24, 149], such as statistical tests on residuals (correlation tests), evaluation of the loss function as a function of the model order, and simulation of the identified model. Because the identification is used a grey box model, the effect of the model order on the loss function are not directly applicable. this model is useful for black-box identification, where the required model order is completely unknown a prior. Furthermore, the correlation tests is sensitive to all the system lags (as described in the previous chapter, hydraulic actuators due to the friction have lag which fined the exact parameters is almost impossible), it is not quite useful. So, what remains as most practical method of model validation, is simulation of the identified nonlinear model. Besides that , physical insight in the system behavior will be used interpret and evaluate the outcomes of the identification.

In this chapter, some techniques for the identification and validation of nonlinear systems have been discussed. In fact, the discussion already contains some choices in the approach to the identification and validation of the hydraulic servo-system models, given the approach for the servo hydraulic shaking table identification and validation in the chapter 6.

Chapter 5

Control methods for hydraulic servo-system

The aim of this chapter is to give a theoretical background to the control design methods which is applied on the real shaking table in chapter 6. The benefits and limitation associated with the existed control methods, by presenting a brief review of the literature on previous control strategies of hydraulic shaking tables are presented. Then, as the main discussion in this chapter, the theoretical information related to linear and nonlinear control design methods will be presented.

Each of the design methods -linear and nonlinear alike- has advantages and disadvantages, strengths and limitations. It is depend on the application and the limitation of the system which based on it the designer needs to understand all of these to be in the best possible position to develop a satisfactory design with minimal effort.

5.1 Introduction

In most applications the control problem for the hydraulic servo-system can be described as the problem of controlling the piston motion, where the hydraulic actuator should exert the forces desired for this motion. In the case of the shaking table, the purpose of the control systems is to reproduce reference signals with low distortion. Accurate control of actuators is vital to the effectiveness of such apparatus. How-

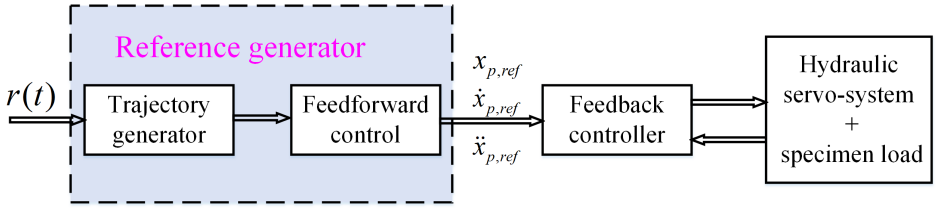

Figure 5.1: General motion control structure for single DOF a servo-hydraulic motion system.

ever, the system dynamics of a shaking table and the specimens to be tested on the shaking table are usually very complex and nonlinear. Achieving the control goal can prove to be challenging.

Taking the problem of controlling a single Degree Of Freedom (DOF) hydraulically driven motion system, there are some options for the setup of the motion control strategy, which may all be generalized to the control structure, shown in figure 5.1. In this structure, three parts are recognized:

- Trajectory generation. This part, possibly fed by some external drive signal, generates the desired trajectory for the motion system. In many (industrial) applications, the trajectory generator generates just a desired position trajectory, which is to be followed by the system. More advanced trajectory generators also provide desired velocities and accelerations, which can be used in the feedforward part. For instance, in shaking table applications, the program of the system provides the full desired trajectory of the position, velocity and acceleration of the system.

- Feedforward control. With the desired trajectory available, feedforward control can be used to generate signals to be supplied to the (feedback) control system, such that the controlled motion system realizes the desired trajectory as good as possible. Actually, the optimal feedforward control uses an ideal inverse model of the system, to generate just those control signals, that realize the desired trajectory. Although in that case no feedback would be necessary, the feedback part is essential, because it is impossible to implement an exact inverse model of the motion system.

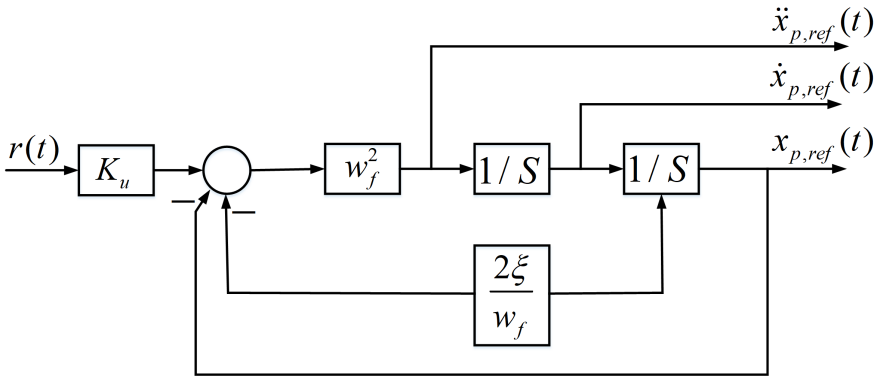

Figure 5.2: Reference generator for actuator feedback control.

- Feedback control. The feedback control can be seen as a corrective control, in order to cope with (modeling) errors in the feedforward path and with unknown disturbances. It combines the feedforward signals with the feedback of measured output signals of the system.

The reference generator for the actuator feedback control, that will be used in chapter 6, is shown in figure 5.2. It has the general functionality of the reference generator sketched above, with a trajectory generator and a feedforward part.

The trajectory generator is just a second order low-pass filter, driven by the external input signal $r(t)$, with adjustable cut-off frequency w_f:

$$\frac{1}{w_f^2}\ddot{x}_{p,ref}(t) + \frac{2\xi_f}{w_f}\dot{x}_{p,ref}(t) + x_{p,ref} = k_u r(t) \tag{5.1}$$

By means of this frequency w_f, the frequency contents of the desired position-velocity-acceleration trajectory can be adjusted. Note hereby, that in the high-frequency range, the desired accelerations are proportional to ${w^2}_f$. So, in terms of physics, a high cut-off frequency w_f implies high demands on the system. In this thesis, due to use of the jerk (the rate of change of acceleration) control, the feedforward control is equal to 1.

5.1.1 Task specification for single DOF hydraulic actuator control

In a hydraulic actuator, the control signal activates the spool valve that controls the flow of hydraulic fluid into and out of the actuator. This flow in turn causes a pressure differential buildup that is proportional to the actuator force. Even if the spool valve dynamics are ignored, the control signal fundamentally controls the derivative of the actuator force and not the force itself. Furthermore, hydraulic systems are highly nonlinear and subject to parameter uncertainty; parameters change with time as a result of variations in operating conditions and component degradation. For example, the supply pressure is subject to variation that may be generated by the operation of other actuators in a multi-user environment [158]. The flow and pressure coefficients, characterizing fluid flow into and out of the valve, are functions of load and supply pressure and can vary under different operating conditions [205]. Also, the effective bulk modulus in hydraulic systems can significantly change under various load conditions, oil temperature, and air content in the oil [94]. Furthermore, based on the application of the hydraulic actuator, the load and the external forces of the system may be varying. In the case of the shaking table due to test of the different specimen, the load of the system can be highly varying. Design of a controller in the face of such a range of parameter variations and disturbances is challenging. Therefore, when focusing on the feedback control of the hydraulic servo-system, as is done in this Chapter, it is important to incorporate different load conditions in the investigations. For that purpose, in the chapter 6, with the use of the removable loads, different load conditions for the hydraulic actuator can be created. Within this setting, different actuator feedback control strategies are to be evaluated, including the effect of the use of (possibly available) feedforward signals. In these investigations, the reference generator of the previous Subsection is used. Under these conditions, the aim of the hydraulic actuator control design is, to obtain a feedback controller, that meets the following specifications:

- The controlled hydraulic actuator tracks the desired position-velocity-acceleration trajectory $x_{p,ref}(t)$, $\dot{x}_{p,ref}(t)$ and $\ddot{x}_{p,ref}(t)$ from the reference generator as close as possible.

- Different load conditions have minimum effect on the performance of the actuator feedback control loop, while the controller structure and parameters are independent of the load condition.

Actually these specifications are quite general, and it depends on the application, how these specifications look like in more detail. For instance, in machine-tool applications, hard requirements can be expected concerning steady state positioning accuracy and overshoot properties during transients, while tracking of the acceleration profile may be of less importance. However, taking the example of shaking table motion control, high-bandwidth tracking of the position, velocity and acceleration trajectory under different load conditions is extremely important, as well as minimization of acceleration noise.

Considering the feedback control of hydraulic motion systems, the remainder of this Chapter is used to discuss different hydraulic actuator control design techniques with respect to the general task specification of this Section.

5.1.2 literature survey

In the field of hydraulic actuator control, a wide variety of applications is found, with different control design techniques applied to obtain the desired results. Investigating literature in this area, it is hard to find a clear relation between the task specification for the specific application, and the applied control strategy. Therefore in this section, with the focus placed on the control schemes for hydraulic shaking tables, the algorithms that are currently used in the testing industry, as well as those which are the subject of academic and industrial research, have been presented [222].

Proportional-Integral-Differential controller

The proportional-Integral-Differential (PID) controller is the most widely and successfully applied controller. The PID controller uses a combination of proportional, integral and derivative action on the control error to produce the output of the controller to minimize the error. A typical PID controller can be expressed by

$$u = K_p e + K_I \int_0^t e dt + K_D \frac{de}{dt} \tag{5.2}$$

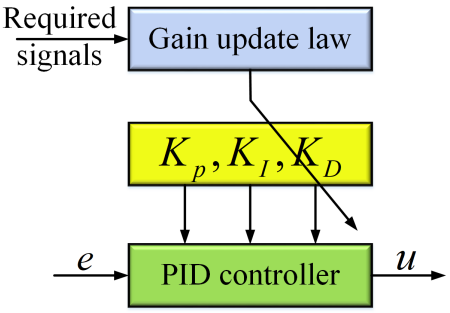

Figure 5.3: Block diagram of gain update for PID controller.

where e is the difference between the reference variable and the measured variable, u the output of the controller. K_P , K_I and K_D are the proportional, the integral and derivative gains, which have different functions for the PID controller. To decrease the system response time, the proportional gain can be increased, but this will decrease the system stability margin and increase the frequency of oscillation. The integral function increases system accuracy by reducing to zero any residual error after the command has expired. A non-zero value for error causes the residual error to be integrated over time until it is large enough to drive the actuator to its final position. The derivative function is used to improve the control loop dynamic stability by reducing the overshoot at higher proportional gain settings [224]. Suitable values for the three parameters have to be tuned optimally to achieve a good control performance of the controller. The classical PID tuning approach can be Ziegler-Nichols and Cohen-Coon [89].

The PID controller has been widely used in hydraulic systems, including hydraulic shaking tables, in which P controller is mostly used. Null shifts always occur in servo valves, degrading the system precision. To cancel this phenomenon, the integral action is added when the system is not in motion. Many hydraulic control systems still use a PID controller and many operators are looking for solutions to improve their PID control systems. Consequently, there are many new developed PID controllers combined with modern control methods [64].

Generally, the three gains of a traditional PID controller are constant, so one way to upgrade a PID controller is to obtain time-varying gains for the PID controller. Its basic control scheme is shown in figure 5.3, where e is the error, u the output

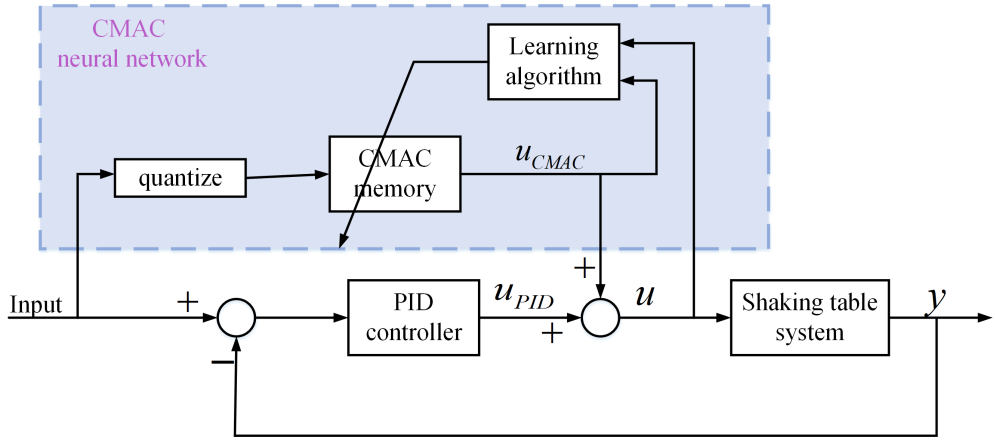

Figure 5.4: CMAC based PID controller.

of the PID controller. The required signal may include e and its time derivative, reference input and system response. Wu et al. in [212] used fuzzy control theory to tune the PID gains to achieve better disturbance rejection. It is crucial to choose suitable fuzzy rules for K_p, K_i and K_d, and define appropriate membership functions for the control error and its derivative. Guo et al. in [73] used back propagation (BP) neural network to adjust PID gains. The classical PID controller was initially directly used to control the system. When the control error was relatively small, the controller was then switched to a BP-based PID controller. The disadvantages of this method are slow training rate, unstable learning and memory, and local minimization. Elbayomy et al. in [55] applied genetic algorithm (GA) to tune the PID gains, resulting in improved control performance, but the gains were offline calculated by GA, and the initial population of GA can influence the iteration. If the system operating environment changes, the PID gains will have to be re-calculated by GA. Another way is to add a control loop using modern control methods. Yao et al. in [224] utilized a cerebellar model articulation controller (CMAC) neural network as a feedforward compensator connected in parallel with a PID controller, as shown in figure 5.4. The total control input was generated by adding the PID output and the output of the CMAC. With the action of CMAC, the control signal will be mainly formed by the CMAC. The operation of CMAC can be viewed as lookup table. This can lead to much memory being occupied.

Many PID controllers are improved by combining neural networks as described previously, but their performance is closely related to the structure of the neural network, its generalization, parameter selection, and initial states. This depends very much on the experience and ability of the user.

For hydraulic shaking tables, the PID controller cannot meet its requirements, such as wide frequency bandwidth, high tracking performance and high power spectral density (PSD) replication precision. A PID controller is just a part of the whole control system of a shaking table, which usually needs other control methods. Users tend to improve their testing equipment gradually based on existing control schemes.

Three-variable controller

The three-variable controller has been successfully adopted in hydraulic shaking tables in Japan [186], China [219] and other countries. MTS Systems Corporation is a global seismic earthquake simulator provider that adopts three-variable controllers [153]. The three-variable controller can extend the system frequency bandwidth and improve the system stability and is usually used for acceleration control. However, since the hydraulic control system is a displacement control system, the acceleration command is required to be converted to the corresponding displacement signal. The task is completed by an input filter as shown in figure 5.2.

The three variables include displacement, velocity and acceleration. For the three-variable controller, it needs the input three variables and the feedback three variables. The input filter, which is mainly comprised of two integral loops, generates the input three variables for the three-variable controller. The reference displacement ($x_{p,ref}$) to the hydraulic actuator is calculated from the double integration of the reference acceleration. This reference actuator displacement provides better prediction of the actuator displacement for the reference acceleration ($\ddot{x}_{p,ref}$). The feedback displacement can be measured from the displacement sensor usually integrated in the hydraulic actuator. The feedback acceleration is from the accelerometer. Using the feedback displacement and the feedback acceleration, the feedback velocity can be synthesized by a circuit.

The three-variable controller can be considered as two parts, the feed-forward and the feedback. The former is used to extend the frequency bandwidth, while the feedback is used to guarantee the system stability. The input filter can be expressed

by equation (5.1). The two parts of the three-variable controller can also be written as transfer functions

$$T(s) = K_{dr} + K_{vr}s + K_{ar}s^2 \tag{5.3}$$

and

$$S(s) = K_{df} + K_{vf}s + K_{af}s^2 \tag{5.4}$$

Figure 5.5 shows the block diagram of this type of controller by using the equations (5.1), (5.3) and (5.4) [220]. The gains of the input filter, K_u , w_f and ξ_f can be determined by system requirements, and the gains of the three-variable controller can be manually tuned according to the system frequency bandwidth and system stability. They can be a basic controller for a hydraulic shaking table. Practical applications have proved its feasibility and effectiveness [91]. The control scheme is based on linear control theory, and does not take the system nonlinearities and the specimen dynamics into consideration. Though it can extend the system acceleration frequency bandwidth, this is restricted by hydraulic natural frequency and the natural frequency of the servo valve.

Minimal control synthesis

The minimal control synthesis (MCS) algorithm was originally formulated by Stoten et al. [183]. It is a form of adaptive control, derived from a standard model reference adaptive control algorithm [115, 223]. Minimal control synthesis does not require any knowledge of plant dynamic parameters other than the degree of freedom and system dimension. It can cope with internal variations and external disturbances, and yield quick response to disturbances [183]. For a plant modeled by the state

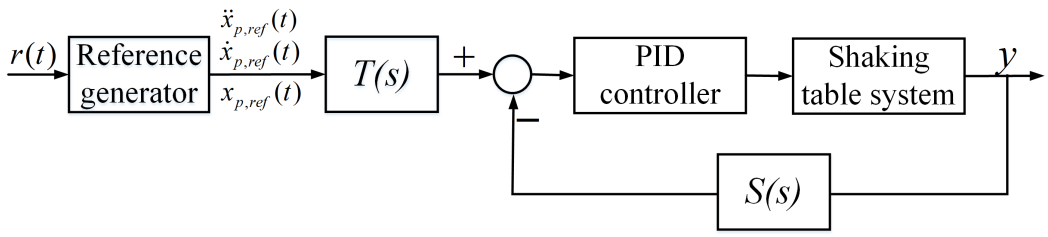

Figure 5.5: The block diagram of the three-variable controller.

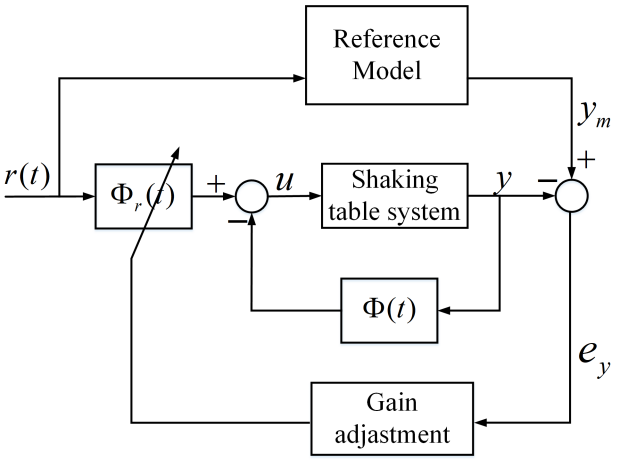

Figure 5.6: Minimal control synthesis control scheme.

space equation

$$\dot{x}(t) = Ax(t) + Bu(t) + d(t) \tag{5.5}$$

where x is the state vector, u the control input, d the disturbance. A and B are the plant parameter matrices. The block diagram of MCS is shown in figure 5.6. The input is modified by a reference model that is used to produce the desired closed-loop response, which is compared with the plant output. The gains are adaptively adjusted in order to achieve a good tracking performance.

The control input is given by

$$u(t) = \Phi(t)y(t) + \Phi_r(t)r(t) \tag{5.6}$$

where $r(t)$ is the system input, $y(t)$ the plant response. $K(t)$ and $K_r(t)$ are the gains. They are adjusted by the adaptive law

$$\Phi(t) = \int_0^t \alpha e_{yy}(\tau)x^T(\tau) + \beta e_{yy}(t)x^T(t) \tag{5.7}$$

$$\Phi_r(t) = \int_0^t \alpha e_{yy}(\tau)r^T(\tau) + \beta e_{yy}(t)r^T(t) \tag{5.8}$$

where α and β are the adaptive weights, which can be tuned empirically. $e_{yy}(t)$ is

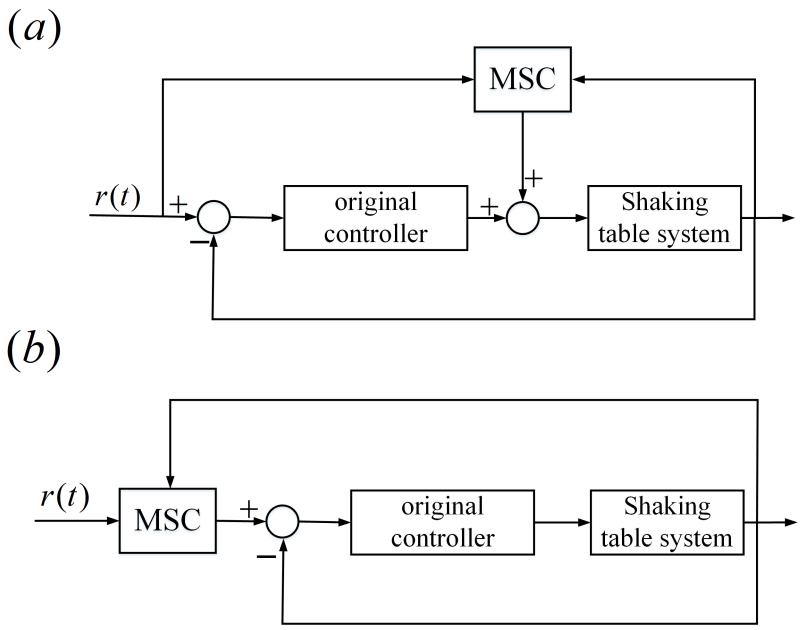

Figure 5.7: Application minimal control synthesis to hydraulic shaking table. (a) Inner-loop strategy; (b) Outer-loop strategy.

given by

$$e_{yy} = C_e e_y = C_e[y_m(t) - y(t)] \tag{5.9}$$

where C_e is a constant linear matrix. There are two configurations of MCS application to a control system: the inner-loop strategy and the outer-loop strategy [183]. For a unidirectional hydraulic shaking table, the two strategies are shown in figure 5.7.

The MCS can be implemented in parallel with the original control system, resulting in the inner-loop control strategy, while the outer-loop strategy modifies the system input, and the modified input is sent to the original controller. The outer-loop scheme is easier to be implemented on an existing control system.

Minimal control synthesis can also be applied to a multi-channel hydraulic shaking table by adding inverse kinematics and direct kinematics. Minimal control synthesis has been applied to several multi-channel hydraulic shaking tables, such as shaking tables at the University of Bristol and at Athens Technical University [183]. From the experimental results, it can be seen that MCS can achieve improvement

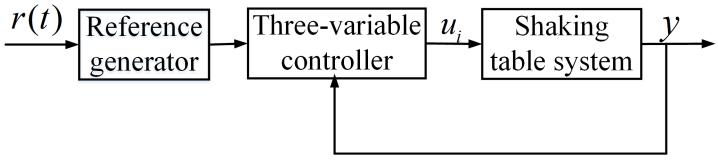

Figure 5.8: The feed-forward minimal control synthesis combined with the three-variable controller.

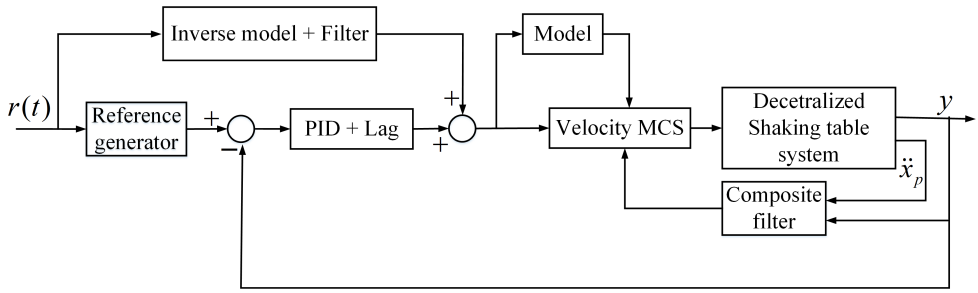

Figure 5.9: Inverse model velocity minimal control synthesis.

in tracking demand amplitude, especially for PSD, but for sinusoidal waves, it still cannot solve the phase delay.

Stoten and Shimizu [184] extended the original MCS algorithm by omitting the feedback term $\Phi(t)x(t)$ and keeping an explicitly feedforward adaptive control, $\Phi_r(t)r(t)$, resulting in the feedforward MCS, which was used in combination with the three-variable controller for the shaking table at the Nishimatsu Company in Japan. The control configuration is shown in figure 5.8. The three-variable controller acts as an inner-loop component. This proposed control scheme can improve the low-frequency tracking performance of the shaking table.

The MCS algorithm has been implemented in a decentralized form, which treats the whole plant as a set of single-input, single-output (SISO) systems.

Gizatullin and Edge [67] reported an adaptive control scheme (shown in figure 5.9) based on a velocity cascade with an inverse model feedforward for the multi-axis shaking table at the University of Bath to reduce the interaction between hydraulic actuators and to ensure good tracking performance. The shaking table has six hydraulic cylinders: three in vertical and the other three in horizon. It used decentral-

ized position control for each hydraulic cylinder, which was linearized as a cascade transfer function of a second-order transfer function and an integrator. The control strategy extended the standard MCS by adding an integral action and the velocity for the MCS. The filter has a form of $\frac{w^2}{(s+w)^2}$. The reference model is a second-order transfer function, whose parameters were selected to ensure faster and better adaptation. The part of the inverse model and filter is used as the feed-forward. The feedback velocity was obtained by the composite filter, whose function is to estimate the velocity from the measured position and acceleration of the cylinder. To reduce the effect from the mount motion, it used two accelerometers attached at the end of the piston rod and to the cylinder mount, respectively. The difference between the two accelerometers generates the relative rod acceleration, which was fed to the composite filter. A lag term, which is a first-order transfer function, was additionally added to the classical PID to increase the amplitude margin of the open- loop frequency response. The control performance was compared with three other fixed-gain control schemes. This control method needs a nominal inverse plant transfer function in the feed-forward path, so it relies on the assumption that the plant is linear and the trans- fer function of the plant is known.

For the MCS-based control schemes for hydraulic shaking tables, the adaptive weights of MCS are empirically set. They are usually constants or determined by simple iteration. Its final values can influence the control performance. If the values are too big, it will increase the system's closed-loop noise. Furthermore, this control method can be efficient for slow time- varying systems, but for fast time-varying systems, for example, specimen collapse resulting in substantial modification of the system transfer function, the adaptive gains will be unable to be adaptively adjusted. In this case, making the adaptation effective in a very short time can lead the control system to be unstable.

Feed-forward-based control scheme

Kuehn et al. in [108] investigated a feedback/feedforward control strategy based on the receding horizon control (RHC). In their control structure, $r(t)$ is the reference trajectory, y the output, n the measurement noise and d the disturbance input. K_{FF} and K_{FB} are the feedback and feed-forward gain matrices, respectively. u_{FB} is the feedback control, and is given by $u_{FB} = K_{FB}x$, the feedback control, u_{FF} is

determined by $u_{FF} = K_{FF}r$. K_{FF} and K_{FB} are offline computed by using RHC. The estimator was designed using the pole placement method. The experimental results show that the amplitude response of the feedback/feedforward controller is flat through $40[Hz]$. Moreover, it had better phase characteristics in the acceleration transfer function than a feedback control using the linear quadratic regulator. Since K_{FF} and K_{FB} are offline computed, if the plant is highly nonlinear, or the system has fast time-varying parameters, they cannot track parameter variations, thus satisfied control performance cannot be achieved.

Nakata [148] studied the acceleration trajectory tracking control (ATTC) to improve the acceleration control performance of earthquake simulators. The structure is shown in figure 5.10. In the figure, $\ddot{x}_{p,ref}$ is the reference table acceleration, at the table acceleration response, x_p the actuator displacement, $\bar{x}_p$ the estimated actuator displacement, $\hat{x}_{p,ref}$ the reference actuator displacement. It can be seen that the control algorithm can be divided into two parts: acceleration control and displacement feedback. The acceleration feed-forward controller can be computed offline, and its output is

$$u_{FF} = G_{FF}\hat{H}_T^{-1}\ddot{x}_{p,ref} \tag{5.10}$$

where G_{FF} is a low-pass filter of the feed-forward controller, and $\hat{H}_T^{-1}$ is the inverse of the approximated table acceleration transfer function. Instead of using double integration to generate the reference actuator displacement, the strategy used a system dynamics command compensator to compute the reference displacement for

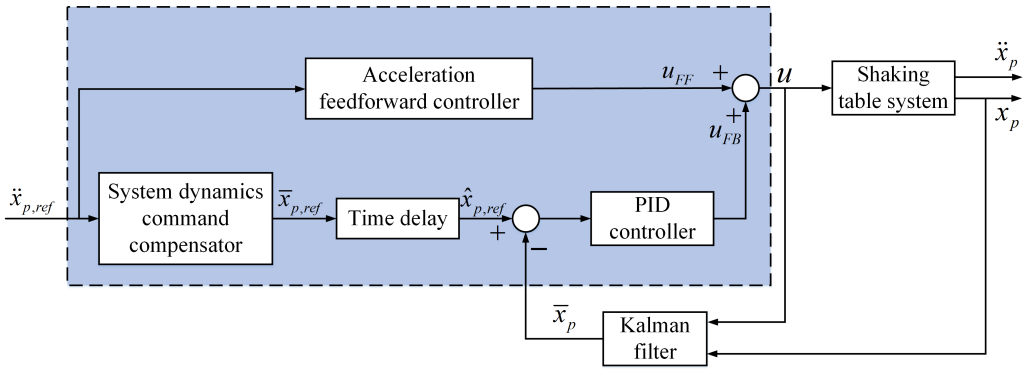

Figure 5.10: Acceleration trajectory tracking control.

actuator from the reference table acceleration. The reference displacement is given as

$$x_p = \hat{H}_{TO}\hat{H}_T^{-1}x_{p,ref} \tag{5.11}$$

where $\hat{H}_{TO}$ is the approximated open-loop transfer function from the valve command to the actuator displacement. A Kalman filter was adopted to reduce noise in the feedback displacement. In the whole control scheme, the feed-forward controller is the driving source, while the displacement feedback loop is used to stabilize the table. The time delay was used to avoid synchronous actions from the feed-forward and the feedback. The ATTC method has been implemented on the earthquake simulator at the Johns Hopkins University. Experimental results showed good performance and repeatability of the acceleration trajectory tracking control over the conventional displacement control.

The advantage of the ATTC method is that it can change the controller parameters to achieve flexible setting, ranging from an open-loop feedforward acceleration control to a conventional closed-loop feedback displacement control, but it highly depends on the accuracy of modeling of transfer functions, for example, $\hat{H}_T^{-1}$. When the system dynamics change, all models have to be re-calculated.

Shen et al. [62] proposed an acceleration time waveform replication using hybrid control combined with feedforward compensation and adaptive inverse control. It introduced the inverse transfer function (ITF) of the acceleration closed-loop system as the feed-forward compensator, which mainly consists of the inverse model $\hat{G}_a^{-1}(z)$ and the modeling error ΔG. $\hat{G}_a^{-1}(z)$, which converts the reference acceleration into the reference displacement, was identified by the recursive extended least square algorithm and was offline designed by a zero phase error tracking controller. The modeling error ΔG is the difference between the estimated system model $\hat{G}_a(z)$ and the actual plant model. The whole control system is complex, and it can suffer computation burden.

Phillips et al. [163] developed a control scheme for a uniaxial shaking table, as shown in figure 5.11. The whole control strategy can be separated into two parts shown in dashed boxes. The left dashed box was computed offline, while the right dashed box was calculated online. $G_{au}^{-1}(s)$, the inverse model of shaking table transfer function from the input voltage to its measured acceleration $\ddot{x}_p$, is the

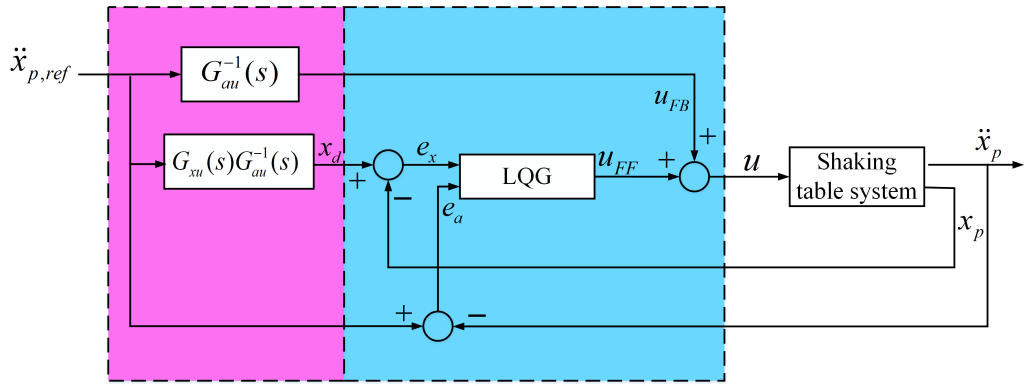

Figure 5.11: Model-based feedback control.

feedforward controller designed to compensate the shaking table dynamics. $G_{xu}(s)$ is the transfer function from the command to the measured displacement x_p. The term $G_{xu}(s)G_{xu}^{-1}(s)$ was used to generate the desired displacement $x_{p,ref}$. The authors assumed that the desired acceleration ad can be known prior to testing, so the feed-forward part of the control system can be completely calculated offline. The feedback controller was designed by linear-quadratic regulator (LQR) weighting the displacement and acceleration feedback. The authors also used transfer function iteration for comparison. The error between the desired and the feedback acceleration was further applied to iteratively improve the feed-forward command. The outputs of the feed-forward controller and the feedback controller, u_{FF} and u_{FB}, are added to form the control input u. The left dashed box highly relies on transfer function modeling, and this part is offline calculated, so this will limit its use in strong nonlinear systems or systems with fast time-varying parameters.

Other control schemes

Newell et al. [151] developed a controller based on the Kalman filter for the seismic simulator at the University of Rotterdam. The controller utilized an optimal reference trajectory obtained by minimizing an acceleration tracking error. The optimization incorporated a nonlinear realization of the simulator dynamics. The nonlinear system model was linearized about the reference trajectory and the resulting system was used to develop time-varying feedback gains, which produced the

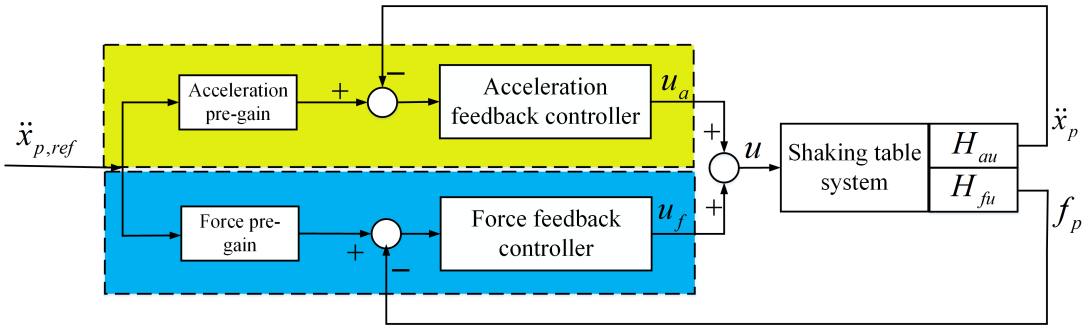

Figure 5.12: Direct acceleration feedback control with force feedback.

correction to the reference control.

Stehman and Nakata [182] proposed a direct acceleration feedback control with force stabilization. It is shown in figure 5.12. There are two feedback control loops: an acceleration control loop and a force feedback control loop. The former controller was designed for acceleration tracking, while the latter controller was applied to stabilize the table to prevent table drift. The two pre-gains were used to modify the reference acceleration $\ddot{x}_{p,ref}$. H_{au} and H_{fu} represent the transfer functions from the valve command to the table acceleration response and to the measured force, respectively, and they were determined by using experimental system identification methods. The loop shaping design approach was adopted to design the controller of the acceleration feedback loop. The force feedback controller was designed to ensure stability for table drift. The control scheme was validated by experiments on the hydraulic shaking table at the Johns Hopkins University. At the same time, it should minimize its impact on the acceleration feedback loop. But there are some hardware requirements. It needs restoring springs to provide forces proportional to the stable position. A load cell is also needed to measure the force.

Yang and Schellenberg in [217] utilized the sliding mode control method to regulate the movement of a single DOF hydraulic shaking table. The SMC was designed by a Lyapunov-like stability function. The nonlinearity of the specimen, the saturation of the actuator control force and an additional external disturbance were taken into consideration to model the system dynamics properly. It needs the actual displacement and velocity of the table, as well as its desired displacement and velocity. Simulations only compare with the open-loop and the traditional PID control

algorithms.

Structure-table interaction is the coupling of the dynamics between the shaking table and the dynamics of the test structure, resulting in lower control accuracy. This interaction can be more difficult to solve when specimens change dynamics because of damage or other nonlinearities as the nature of the interaction will change. Horiuchi et al. [86] proposed a reaction force compensation (RFC) in real time for reaction force of the specimen on the table. The RFC used the inverse dynamics with measured reaction force to calculate the compensation signal for cancellation of the reaction force. The measurement and the inverse dynamics require low-pass filters, resulting in the restriction of disturbance suppression characteristics in the feedback system. Seki et al. [171] designed a control method to suppress the reaction force generated by a specimen on the shaking table. The reaction force was measured by sensors. The control scheme needs measured pressure, piston displacement, table velocity and acceleration for the feedback controller. Up to now, the dynamic coupling problem is still an unsolved problem, since the specimen dynamics can vary greatly and suddenly, resulting in uncertainty of the coupling dynamics. This poses great difficulty in modeling the dynamics between the shaking table and the tested specimen.

Conclusion

Considering some basic control strategies for hydraulic actuators, it can be concluded that the solution to the control problem is related to the application, i.e. the setting of the control problem. If only a position reference is available, which is to be tracked, the control strategy necessarily focuses on position servo control. Besides a pressure difference feedback loop to provide damping, a velocity feedback loop can be added, resulting in full state feedback with improved performance.

In case additional reference signals are available, they should be used as feedforward signals for the different (state) feedback loops. Especially the use of a proper pressure difference reference, obtained from a feedforward model for the inertial and external forces acting on the piston, can improve the performance considerably. As indicated in figure 5.13, when a pressure difference reference $P_{L,ref}$ is available, it can be fed forward to the pressure difference feedback loop. This pressure difference reference can be used as a feedforward compensation, while it does not affect the

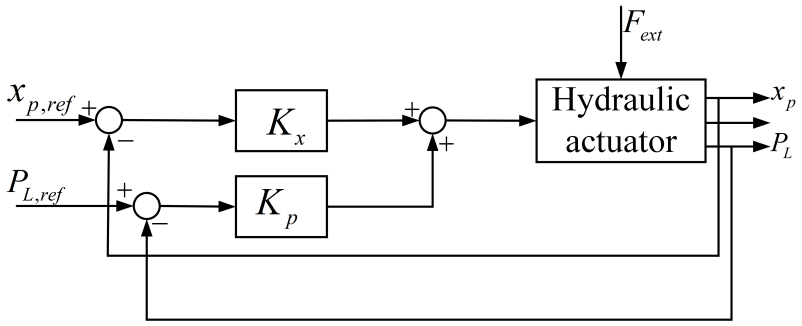

Figure 5.13: Direct acceleration feedback control with force feedback.

closed loop dynamics of the system, but in case of a precise feedforward model, i.e. an exact estimated load weight, it contributes to a better input-output performance. In the situation of the simultaneous supply of a position reference and a pressure difference reference, the feedback control design gets the character of a trade-off between position control and pressure control. Although, this method leads to over-damped closed loop dynamics by increasing the pressure feedback gain, at the cost of a smaller position feedback gain, the input-output behavior can be considerably improved, especially in the high-frequency region, where acceleration forces play an important role. Furthermore, the pressure difference feedforward allows compensation for external forces by providing an estimation of the external forces on the table. This method can be utilized to compensate the interaction forces in the two-level control of multi DOF motion systems. Thereby, the feedback design has to be directed towards pressure difference control, while position (and velocity) feedback is used to obtain tracking of the desired trajectory.

Whenever a reference for the velocity is available in the control setting, it should be fed forward to the servo-valve, to compensate for inherent velocity errors of the servo- system without feedforward. This velocity feedforward improves the low-frequency tracking behavior considerably. The possible availability of a model of the input nonlinearity of the hydraulic actuator should be utilized to linearize the controlled system. This concerns both the load sensitivity of the flow and the static nonlinearity of the flow due to geometrical servo-valve properties. The nonlinearity related to position dependence of the actuator dynamics can be taken into account by designing controllers for the worst case actuator position.

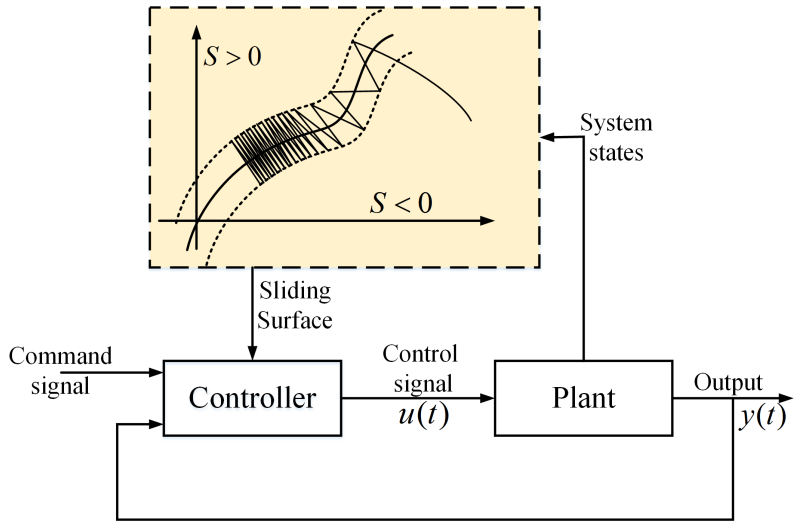

Figure 5.14: Schematic of the sliding mode control algorithm.

5.2 Control strategies for hydraulic systems

Against the background of the available accurate model knowledge at the one side, and available modern control design techniques at the other side, based on the application of the hydraulic shaking table and its hardware characteristics a number of control design issues will be briefly addressed here. Whereas a thorough discussion of the techniques and application of them falls beyond the scope of this thesis, the discussion is to be seen as an indication of possible directions for further research.

5.2.1 Sliding mode control

Sliding model control (SMC) first appeared in the context of variable structure systems. SMC has become an efficient tool in the control of complex systems with uncertainties due to its low sensitivity to disturbances and parameter variations [194, 161, 52, 194]. The basic concept is depicted schematically in figure 5.14. The main idea behind the SMC is to use a discontinuous control input to force the state trajectory to a certain well determined sliding surface ($S = 0$ in figure 5.14) and to remain on this surface over time, the so called "bang-bang control" concept.

The design of sliding mode control consists of two main steps: (1) develop a

realistic but stabilized sliding surface for the system states; (2) develop control laws to force the system dynamics to follow the desired sliding surface. The dynamic characteristics of the resulting closed-loop control system will be mainly determined by the design of the sliding surface. The most significant advantage of SMC is that once the states of the system reach the predefined sliding surface, the system behavior depends neither on the system parameters nor the disturbances. This property meets with the need of designing feedback control for dynamic systems under uncertainty conditions. In the following, the SMC control design procedure for a system is described.

Consider the system

$$\dot{x}(t) = F(x(t)) + \delta_1(x(t)) + G(x(t))[u(t) + \delta_2(x(t), u(t))] \tag{5.12}$$

where $x(t) \in R^n$ is the state, $u(t) \in R^p$ is the control input, and F, G, δ_1 and δ_2 are sufficiently smooth functions defined for $(x, u) \in D_0 \times R^p$ where D_0 is a domain that contains the origin. We assume that F and G are known, while δ_1 and δ_2 are uncertain terms. We consider both matched δ_2 and unmatched δ_1 uncertainties. Let $T : D_0 \to R^n$ be a diffeomorphism such that

$$\frac{\partial T}{\partial x} G(x) = \begin{bmatrix} 0 \\ G_2(x) \end{bmatrix} \tag{5.13}$$

where $G_2(x)$ is a $p \times p$ matrix that is nonsingular for all $x \in D_0$ The change of variables

$$\begin{bmatrix} \eta \\ \zeta \end{bmatrix} = T(x), \eta \in R^{n-p}, \zeta \in R^p \tag{5.14}$$

transforms the system into the form

$$\dot{\eta} = f(\eta, \zeta) + \delta_u(\eta, \zeta) \tag{5.15}$$

$$\dot{\zeta} = f_a(\eta, \zeta) + G_a(\eta, \zeta)[u + \delta_m(\eta, \zeta, u)] \tag{5.16}$$

where $G_a(\eta, \zeta) = G_2\left(T^{-1}\left(\begin{bmatrix} \eta \\ \zeta \end{bmatrix}\right)\right)$ is nonsingular for all $(\eta, \zeta) \in D = T(D_0)$. The form (5.15)-(5.16) is usually referred to as the regular form. We note that

the term δ_u, in (5.15) is due to the term δ_1 in (5.12), and $\delta_u = 0$ when $\delta_1 = 0$. Therefore, we shall refer to δ_u, as the unmatched uncertainty and to δ_m as the matched uncertainty. To introduce sliding mode control, let us consider the robust stabilization problem of designing a state feedback control to stabilize the origin ($\eta = 0$, $\zeta = 0$) in the presence of the uncertainties δ_u and δ_m. We assume that f, f_a, and δ_u, vanish at the origin, but we do not require to vanish at the origin. We approach the design via a backstepping approach. We start with the system in the equation (5.15) and view ζ as the control input. We seek a stabilizing state feedback control $\zeta = \phi(\eta)$ with $\phi(0) = 0$, so that the origin of

$$\dot{\eta} = f(\eta, \phi(\eta)) + \delta_u(\eta, \phi(\eta)) \tag{5.17}$$

is asymptotically stable. We will not dwell on this stabilization problem. We simply assume that we can find a stabilizing continuously differentiable function $\phi(\eta)$. The tools of linearization, exact feedback linearization, Lyapunov redesign, backstepping, or a combination of them could be used toward the design of $\phi(\eta)$. To proceed with the design of the sliding mode control, set

$$z = \zeta - \phi(\eta) \tag{5.18}$$

It is clear that if $z = 0$, we have $\zeta = \phi(\eta)$ and the variable η approaches the origin asymptotically. In sliding mode control, we design u to bring z to zero in finite time and then maintain the condition $z = 0$ for all future time; that is, we make $z = 0$ a positively invariant set of the closed-loop system. Toward that end, let us write the $\dot{z}$-equation

$$\dot{z} = f_a(\eta, \zeta) + G_a(\eta, \zeta)[u + \delta_m(\eta, \zeta, u)] - \frac{\partial \phi}{\partial \eta}[f(\eta, \zeta) + \delta_u(\eta, \zeta)] \tag{5.19}$$

Take the control u as

$$u = u_{eq} + G_a^{-1}(\eta, \zeta)v \tag{5.20}$$

where v will be determined shortly and u_{eq} is chosen to cancel the known terms on

the right-hand side of (5.19) ;that is,

$$u_{eq} = G_a^{-1}[-f_a(\eta,\zeta) + \frac{\partial\phi}{\partial\eta} f(\eta,\zeta)] \tag{5.21}$$

The control component u_{eq},, is called the equivalent control. In the absence of uncertainty, taking $u = u_{eq}$ results in $\dot{z} = 0$, which ensures that the condition $z = 0$ can be maintained for all future time. Substitution of (5.20) into (5.19) yields

$$\dot{z} = v + \Delta(\eta,\zeta,v) \tag{5.22}$$

where

$$\Delta(\eta,\zeta,v) = G_a(\eta,\zeta)\delta_m(\eta,\zeta,u_{eq} + G_a^{-1}(\eta,\zeta)v) - \frac{\partial\phi}{\partial\eta}\delta_u(\eta,\zeta) \tag{5.23}$$

We assume that Δ satisfies the inequality

$$\|\Delta(\eta,\zeta,v)\| \leq \rho(\eta,\zeta) + k\|v\|, \qquad \forall(\eta,\zeta,v) \in D \times R^p \tag{5.24}$$

where $\rho(\eta,\zeta) \geq 0$ (a continuous function) and $k \in [0,1)$ are known. Using the estimate (5.24), we proceed to design v to force z toward the manifold $z = 0$. Using $V = \frac{1}{2}z^T z$ as a Lyapunov function candidate for (5.25), we obtain

$$\dot{V} = z^T\dot{z} = z^T v + z^T\Delta(\eta,\zeta,v) \leq z^T v + \left\|z^T\right\|(\rho(\eta,\zeta) + k\|v\|) \tag{5.25}$$

Take

$$v = -\frac{\beta(\eta,\zeta)}{1-k} sgn(z) \tag{5.26}$$

where

$$\beta(\eta,\zeta) \geq \rho(\eta,\zeta) + b, \qquad \forall(\eta,\zeta) \in D \tag{5.27}$$

for some $b > 0$, and $sgn(.)$ is the signum nonlinearity. Then,

$$\begin{aligned} \dot{V} &\leq -\tfrac{\beta(\eta,\zeta)}{1-k}|z| + \rho(\eta,\zeta)|z| + k\tfrac{\beta(\eta,\zeta)}{1-k}|z| \\ &= -\beta(\eta,\zeta)|z| + \rho(\eta,\zeta)|z| \leq -b|z| \end{aligned} \tag{5.28}$$

The inequality $\dot{V} \leq -b|z|$ ensures that if the trajectory happens to be on the manifold $z = 0$ at some time, it will be confined to that manifold for all future time

because leaving the manifold requires to be positive, which is impossible in view of the inequality. The inequality ensures also that if $z(0) \neq 0$, then

$$|z(t)| \leq |z(0)| - bt, \forall t \geq 0 \tag{5.29}$$

which shows that trajectories starting off the manifold $z = 0$ must reach it in finite time. Thus, a typical motion under sliding mode control consists of a reaching phase during which trajectories starting off the manifold $z = 0$ move toward it and reach it in finite time, followed by a sliding phase during which the motion will be confined to the manifold $z = 0$ and the dynamics of the system will be represented by the reduced-order model (5.27). A sketch of this typical motion is shown in figure 5.14. The manifold $z = \zeta - \phi(\eta) = 0$ is called the sliding manifold.

The procedure for designing a sliding mode controller can be summarized by the following steps:

- Design the sliding manifold $\zeta = \phi(\eta)$ to control the motion of the reduced-order system (5.17).
- Estimate $\rho(\eta, \zeta)$ and k in (5.24).
- Take the control u as $u = u_{eq} + {G_a}^{-1}(\eta, \zeta)v$ where u_{eq} is the equivalent control given by (5.21) and v is the switching (discontinuous) control given by (5.26) .

This procedure exhibits model order reduction because the main design task is performed on the reduced-order system (5.17).

An important feature of sliding mode control is its robustness to uncertainties. To understand this feature, it is important to distinguish between the matched uncertainty δ_m and the unmatched uncertainty δ_u. We should also distinguish between the reaching and sliding phases. During the reaching phase, the tasks of forcing trajectories toward the sliding manifold and maintaining them on the manifold, once they are there, are achieved by the switching control (5.26) . This task is affected by both the matched and unmatched uncertainties, and robustness is achieved by choosing $\beta(\eta, \zeta) \geq \rho(\eta, \zeta) + b$ is a measure of the size of uncertainty as determined by inequality (5.24). Since we do not require $\rho(\eta, \zeta)$ to be small, the switching

controller can handle fairly large uncertainties, limited only by practical constraints on the amplitude of control signals. During the sliding phase, the motion of the system, as determined by (5.17), is affected only by the unmatched uncertainty δ_u. Robustness to δ_u will have to be achieved through the design of $\phi(\eta)$. In general, robust stabilization at the reduced-order level will require restricting the size or structure of δ_u. In the special case when there is only matched uncertainty, that is, $\delta_u = 0$, sliding mode control will guarantee robustness for any nominal manifold design $\zeta = \phi(\eta)$ that achieves the control objectives on the sliding manifold.

The sliding mode controller contains the discontinuous nonlinearity $sign(z)$. Discontinuous feedback control raises theoretical and practical issues. Theoretical issues like existence and uniqueness of solutions and validity of Lyapunov analysis will have to be examined in a framework that does not require the state equation to have locally Lipschitz right-hand side functions. There is also the practical issue of chattering due to imperfections in switching devices and delays. The sketch of figure 5.14 shows how delays can cause chattering. It depicts a trajectory in the region $z > 0$ heading toward the sliding manifold $z = 0$. It first hits the manifold at point a. In ideal sliding mode control, the trajectory should start sliding on the manifold from point a. In reality, there will be a delay between the time the sign of z changes and the time the control switches. During this delay period, the trajectory crosses the manifold into the region $z < 0$. When the control switches, the trajectory reverses its direction and heads again toward the manifold. Once again, it crosses the manifold, and repetition of this process creates the "zig-zag" motion (oscillation) shown in the sketch, which is known as chattering. Chattering results in low control accuracy, high heat losses in electrical power circuits, and high wear of moving mechanical parts. It may also excite unmodeled high-frequency dynamics, which degrades the performance of the system and may even lead to instability.

One approach to eliminate chattering is to use a continuous approximation of the discontinuous sliding mode controller. By using continuous approximation, we also avoid the theoretical difficulties associated with discontinuous controllers. In the literature, the most common nonlinear functions for approximating the signum function are as follows:

1. Saturation function which is shown in figure 5.15(a) defined by:

$$sat(Cy) = \begin{cases} y & if \quad |y| \leq C \\ sign(y) & if \quad |y| > C \end{cases} \tag{5.30}$$

2. Hyperbolic tangent function which is shown in figure 5.15(b) defined by:

$$\tanh(\frac{y}{C}) = \frac{e^{\frac{y}{C}} - e^{-\frac{y}{C}}}{e^{\frac{y}{C}} + e^{-\frac{y}{C}}} = \frac{e^{2\frac{y}{C}} + 1}{e^{2\frac{y}{C}} - 1} \tag{5.31}$$

In this thesis, for avoiding the chartering phenomena in chapter 6, the hyperbolic tangent function has been used.

5.2.2 Super twisting sliding mode control

As stated in the previous section, the sliding mode control systems become vulnerable when the output tracking signals present small oscillations of finite frequency known as chattering. The chattering problem is harmful because it leads to low control accuracy; high wear of moving mechanical parts and high heat losses in

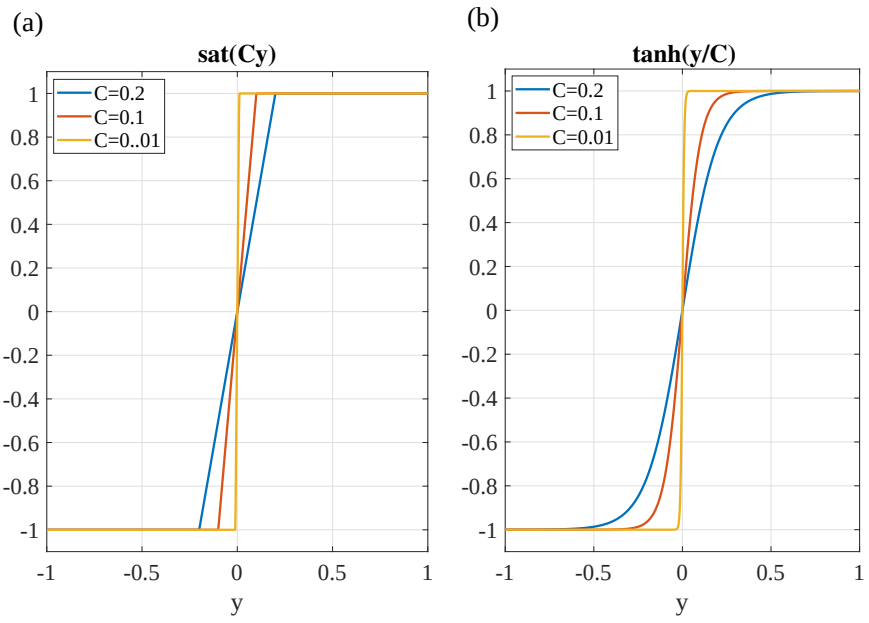

Figure 5.15: The approximation of signum function: (a) Saturation function, (b) Hyperbolic tangent function.

power circuits. The chattering phenomenon can be caused by the deliberate use of classical sliding mode control technique. This control technique is characterized by a discontinuous control action with an ideal infinite frequency. When fast dynamics are neglected in the mathematical model such phenomenon can appear. Another situation responsible for chattering is due to implementation issues of the sliding mode control signal in digital devices operating with a finite sampling frequency, where the switching frequency of the control signal cannot be fully implemented. Despite of the disadvantage presented by the sliding mode control, this is a popular technique among control engineer practitioners due to the fact that introduces robustness to unknown bounded perturbations that belong to the control subspace; moreover, the residual dynamic under the sliding regime, i.e., the sliding mode dynamic, can easily be stabilized with a proper choice of the sliding surface. A proof of their good performance in motion control systems can be found in the book by Utkin et al. (2009) [194]. A solution to this problem is the high order sliding mode (HOSM) technique [120, 121]. This control technique maintains the same sliding mode properties (in this sense, first-order sliding mode) with the advantage of eliminating the chattering problem due to the continuous-time nature of the control action. The actual disadvantage of this control technique is that the stability proofs are based on geometrical methods since the Lyapunov function proposing results in a difficult task [119]. The work presented in [144] proposes quadratic like Lyapunov functions for a special case of second-order sliding mode controller, the super-twisting sliding mode controller (STSMC), making possible to obtain an explicit relation for the controller design parameters. In the following lines this analysis will be revisited [175].

Consider a single-input uncertain nonlinear system

$$\dot{x} = f(x,t) + h(x,t)u \tag{5.32}$$

with $x \in R^n$ the state vector, $u \in R$ the control input, $f(x,t) \in R^n$ is a differentiable, partially known vector field. Assume that

(A1) A sliding variable $\sigma = \sigma(x,t) \in R$ is designed so that the systems (5.32) desirable compensated dynamics are achieved in the sliding mode $\sigma = \sigma(x,t) = 0$.

(A2) The systems (5.32) input-output ($u \to \sigma$) dynamics are of a relative degree one, and the internal dynamics are stable.
Therefore, the input-output dynamics can be presented

$$\dot{\sigma} = \underbrace{\frac{\partial \sigma}{\partial t} + \frac{\partial \sigma}{\partial x} f(x,t)}_{\varphi(x,t)} + \underbrace{\frac{\partial \sigma}{\partial x} h(x) u}_{b(x,t)} = \varphi(x,t) + b(x,t)u \tag{5.33}$$

(A3) The function $b(x,t) \in R$ is assumed to be uncertain and be presented as

$$b(x,t) = b_0(x,t) + \Delta b(x,t) \tag{5.34}$$

where $b_0(x,t) > 0$ is a known function and $\Delta b(x,t)$ is a bounded perturbation so that

$$\frac{|\Delta b(x,t)|}{b_0(x,t)} = \gamma(x,t) \leq \bar{\gamma} < 1 \tag{5.35}$$

$\forall x \in R^n$ and $t \in [0, \infty)$, with $\bar{g}amma$ unknown.

(A4) The function $\varphi(x,t) \in R$ is presented as

$$\varphi(x,t) = \varphi_1(x,t) + \varphi_2(x,t) \tag{5.36}$$

with the bounded terms

$$|\varphi_1(x,t)| \leq \delta_1 |\sigma|^{1/2}, \qquad |\dot{\varphi}_2(x,t)| \leq \delta_2 \tag{5.37}$$

where $\infty > \delta_1, \quad \delta_2 > 0$ exist but are not known.

Finally, one gets

$$\dot{\sigma} = \varphi(x,t) + \underbrace{\left(1 + \frac{\Delta b(x,t)}{b_0(x,t)}\right)}_{g(x,t)} w \tag{5.38}$$

where $w = b_0(x,t)u$ and

$$1 - \bar{\gamma} \leq g(x,t) \leq 1 + \bar{\gamma} \tag{5.39}$$

The problem is to drive the sliding variable σ and its derivative $\dot{\sigma}$ to zero in finite time in the presence of the bounded additive (5.37) and multiplicative (5.34) pertur-

bations with the unknown boundaries $\delta_1, \delta_2, \bar{\gamma} > 0$ by means of continuous control without the control gain overestimation. In this thesis, we are looking for an super twisting algorithm that is able to address this problem via generating continuous control function (chattering attenuation) so that based on the experimental setup in chapter 6, its gains are calculated.
The following super twisting control is considered [119]

$$w = -k_1|\sigma|^{1/2} sign(\sigma) + v, \qquad \dot{v} = -\frac{k_2}{2} sign(\sigma) \tag{5.40}$$

where the gains $k_1, k_2 > 0$ have to defined such that the system (5.32) in finite time converge to zero. In [144], based on the Lyapunov approach and the perturbation bounds of the system in equation (5.37), these gains are selected as:

$$k_1 > 2\delta_1, \qquad k_2 > k_1 \frac{5\delta_1 k_1 + 6\delta_2 + 4(\delta_1 + \delta_2/k_1)^2}{2(k_1 - 2\delta_1)} \tag{5.41}$$

. In this equation the gains k_1, k_2 are selected sufficiently high to assure the robustness of the globally asymptotic stability of the system. In chapter 6, by using of nonlinear least square method of the tracking errors, the optimal parameters of the controller are found.

5.3 observer

In control theory, a state observer is a system that provides an estimate of the internal state of a given real system, from measurements of the input and output of the real system. It is typically computer-implemented, and provides the basis of many practical applications.

Knowing the system state is necessary to solve many control theory problems; for example, stabilizing a system using state feedback. In most practical cases, the physical state of the system cannot be determined by direct observation. Instead, indirect effects of the internal state are observed by way of the system outputs. With this background of the state observer, in the case of hydraulic servo shaking table, for reducing the cost of the test and the limitation of the system hardware, an observer can estimate the states of the system by using of the position sensor.

In this section a second order sliding mode observer is described which is used to reconstruct the velocity and acceleration of the hydraulic servo-system from the position measurements.

5.3.1 Sliding mode observer design for triangular input form

The sliding mode observers are widely used due to the finite-time convergence, robustness with respect to uncertainties and the possibility of uncertainty estimation (see, for example, the bibliography in the recent tutorials [17, 53, 164, 214, 47]). This kind of observers for the mechanical systems with uncertainties is important for the following reasons:

- linear observers do not achieve adequate performance for complex systems;
- for a finite time convergence for all the observables states;
- robustness under parameter variations is possible, if the condition (dual of the well-known matching condition) is verified;
- model-based observers are usually restricted to the cases when the model is exactly known;
- high-gain differentiators [11] are not exact with any fixed finite gain and feature the peaking effect with high gains: The maximal output value during the transient grows infinitely as the gains tend to infinity (see, for example, [17, 53, 164, 214]).

First of all, we recall the definition of observability indices.
Definition [161] Let the system

$$\begin{aligned} \dot{x} &= f(x) \\ y &= h(x) \end{aligned} \tag{5.42}$$

which is observable at x_0 if there exists a neighborhood U of x_0 and p-tuple of integers $(\mu_1, ..., \mu_p)$ such that

1. $\mu_1 \geq \mu_2 \geq \cdots \geq \mu_p \geq 0$ and $\sum_{i=1}^{p} \mu_i = n$.

2. After suitable reordering of the h_i at each $x \in U$, the n row vectors $\left\{L_f^{j-1}(dh_i) : \quad i = 1, \ldots, p_i;\right.$ are linearly independent

3. If $l_1, ..., l_p$ satisfies (i) and after suitable reordering the n row vectors $\left\{L_f^{j-1}(dh_i) : i = 1, \ldots, p_i; j\right.$ are linearly independent at some $x \in U$

then $(l_1, \ldots, l_p) \geq (\mu_1, \ldots, \mu_p)$ in the lexicographic ordering $\{(l_1 > \mu_1)$ or $(l_1 = \mu_1)$ and $(l_2 > \mu_2)$ *or...or* $(l_1 = \mu_1, ..., l_p = \mu_p)\}$. The integers $\mu_1, ..., \mu_p$ are called observability indices at x_0.

After observability evaluation of the model, it has been considered the following SISO analytic system Σ for designing observer:

$$\begin{aligned} \dot{x} &= f(x) + g(x, u) \\ y &= h(x) \end{aligned} \tag{5.43}$$

where $x \in R^n$ is the state, $u \in R$ is the input, $y \in R$ is the output and f, g and h are analytical function vectors of appropriate dimensions. Moreover for any $x \in R^n$ the function $g(x, 0)$ is equal to zero and the system (5.43) is assumed bounded input bounded state in finite time. In order to transform (5.43) in a triangular input observer form, we define the observation rank condition as:

1. $$rank \begin{pmatrix} dh \\ dL_f h \\ \vdots \\ dL_f^{n-1} h \end{pmatrix} = n \tag{5.44}$$

   where L_f denotes the classical Lie derivative in f and dh is the classical one form. From this condition, it is known than the codistribution

   $$\Omega^i = span\left\{dh, ..., dL_f^i h\right\} \qquad 0 \leq i \leq n-1 \tag{5.45}$$

2. The vector field g verifies for any $u \in R$

   $$dL_g L_f^i h \in \Omega^i \qquad \forall i \in \{0, ..., n-1\} \tag{5.46}$$

Now based on these conditions, we can set the following Theorem:

Theorem 5.1 *System (5.43) may be transformed, by diffeomorphism, in the neighborhood of x in a triangular input observer form*

$$\begin{array}{l} \begin{pmatrix} \dot{\zeta}_1 \\ \dot{\zeta}_2 \\ \vdots \\ \dot{\zeta}_{n-1} \\ \dot{\zeta}_n \end{pmatrix} = \begin{pmatrix} \xi_2 + \bar{g}_1(\zeta_1, u) \\ \xi_3 + \bar{g}_2(\zeta_1, \zeta_2, u) \\ \vdots \\ \xi_n + \bar{g}_{n-1}(\zeta_1, ..., \zeta_{n-1}, u) \\ \bar{f}_n(\zeta) + \bar{g}_n(\zeta, u) \end{pmatrix} \\ y = \zeta_1 \end{array} \tag{5.47}$$

with $\bar{g}_i(., u = 0) = 0$ for any $i \in 1, ..., n$, if and only if conditions 1 and 2 hold in the neighborhood of x. (Proof of this theorem in more detail is given in [161] page 123).

Based on the the work in [47, 194, 161], we consider the sliding observer for triangular input form as:

$$\begin{pmatrix} \dot{\hat{\zeta}}_1 \\ \dot{\hat{\zeta}}_2 \\ \vdots \\ \dot{\hat{\zeta}}_{n-1} \\ \dot{\hat{\zeta}}_n \end{pmatrix} = \begin{pmatrix} \hat{\xi}_2 + \bar{g}_1(\zeta_1, u) + \lambda_1 sign(\zeta_1 - \hat{\zeta}_1) \\ \hat{\xi}_3 + \bar{g}_2(\zeta_1, \hat{\zeta}_2, u) + \lambda_2 sign(\tilde{\zeta}_2 - \hat{\zeta}_2) \\ \vdots \\ \hat{\xi}_n + \bar{g}_{n-1}(\zeta_1, \tilde{\zeta}_2, ..., \tilde{\zeta}_{n-1}, u) + \lambda_{n-1} sign(\tilde{\zeta}_{n-1} - \hat{\zeta}_{n-1}) \\ \bar{f}_n(\zeta_1, \tilde{\zeta}_2, ..., \tilde{\zeta}_n) + \bar{g}_n(\zeta_1, \tilde{\zeta}_2, ..., \tilde{\zeta}_n, u) + \lambda_n sign(\tilde{\zeta}_{n-1} - \hat{\zeta}_n) \end{pmatrix} \tag{5.48}$$

where

$$\begin{array}{c} \tilde{\zeta}_2 = \hat{\xi}_2 + \lambda_1 sign(\zeta_1 - \hat{\zeta}_1) \\ \tilde{\zeta}_3 = \hat{\xi}_3 + \lambda_2 sign(\tilde{\zeta}_2 - \hat{\zeta}_2) \\ \vdots = \vdots \\ \tilde{\zeta}_n = \hat{\xi}_n + \lambda_n sign(\tilde{\zeta}_{n-1} - \hat{\zeta}_{n-1}) \end{array} \tag{5.49}$$

and the $sign(\zeta)$ function denotes the usual signum function but with an an anti-peaking structure. This anti-peaking structure follows the idea that we do not inject the observation error information before reaching the sliding manifold linked with this information (i.e., $sign_i = E_i sign$, with $E_i = 1$ if $E_1 = ... = E_{i-1} = 1$ and

$\zeta_1 - \hat{\zeta}_1 = 0$ else $E_i = 0$). Moreover we reach the manifold one by one. Doing this we obtain a "high gain" dynamic of dimension one and consequently we do not have a peaking phenomena. More precisely $sign_i(.)$ is equal to zero if their exists $0 < j < i-1$ such that $\tilde{\zeta}_j - \hat{\zeta}_j \neq 0$ (by definition $\tilde{\zeta}_1 = \zeta_1$), else $sign_i(.)$ is equal to the usual $sign(.)$ function. In the observer structure, this particular $sign$ function allows that $\tilde{\zeta}_i - \hat{\zeta}_i$ converges to zero if all the $\tilde{\zeta}_i - \hat{\zeta}_i$ with $j < i$ have converged to zero before.

Theorem 5.2 *Considering a bounded input bounded state (BIBS) in finite time system (5.47) and observer (5.48), for any initial state $\zeta(0)$, $\hat{\zeta}(0)$ and any bounded input u, there exists a choice of λ_i such that the observer state $\hat{\zeta}$ converges in finite time to ζ.*

Proof From (5.47) and (5.48) and considering the initial state condition such that $\zeta_1(0) \neq \hat{\zeta}_1(0)$ (if this is not the case, we directly move on to the next step of the proof). Thus we are in the

- **First step** of our proof and we obtain the following observation error dynamics $e = \zeta - \hat{\zeta}$.

$$\begin{pmatrix} \dot{e}_1 \\ \dot{e}_2 \\ \vdots \\ \dot{e}_{n-1} \\ \dot{e}_n \end{pmatrix} = \begin{pmatrix} e_2 - \lambda_1 sign(\xi_1 - \hat{\xi}_1) \\ e_2 + \bar{g}_2(\xi_1, \xi_2, u) - \bar{g}_2(\xi_1, \hat{\xi}_2, u) \\ \vdots \\ e_2 + \bar{g}_{n-1}(\xi_1, \xi_2, \ldots, \xi_{n-1}, u) - \bar{g}_{n-1}(\xi_1, \hat{\xi}_2, \ldots, \hat{\xi}_{n-1}, u) \\ (\bar{f}_n(\xi) - \bar{f}_n(\xi_1, \hat{\xi}_2, \ldots, \hat{\xi}_n) + \bar{g}_n(\xi, u) - \bar{g}_n(\xi_1, \hat{\xi}_2, \ldots, \hat{\xi}_n) \end{pmatrix} \tag{5.50}$$

  Thus as the input u is bounded the state ζ does not go to infinity in finite time. Moreover if $\hat{\zeta}_1$ is bounded all the states of the observer are also bounded during step 1. Consequently the observation error state is also bounded. Now, setting $V_1 = \frac{e_1^2}{2}$, we have

$$\dot{V}_1 = e_1(e_2 - \lambda_1 sign(e_1)) \tag{5.51}$$

Thus choosing $\lambda_1 > |e_2|_{\max}$ the observation error e_1 goes to zero in finite time t_1. Moreover, if after t_1 the observation error stays equal to zero (i.e., $\lambda_1 > |e_2|_{\max}$) we have $e_2 = \lambda_1 sign(\zeta_1 - \hat{\zeta}_1)$ and consequently $\tilde{\zeta}_2 = \zeta_2$. Now we pass to the:

- **Second step.** Here, we ensure that the observation error e_2 is bounded in order to remain on the manifold $e_1 = 0$. Moreover, we want to reach the submanifold $e_1 = e_2 = 0$. Thus, at t_1, we have $e_1 = 0$, and the observation error is now equal to

$$\begin{pmatrix} \dot{e}_1 \\ \dot{e}_2 \\ \dot{e}_3 \\ \vdots \\ \dot{e}_{n-1} \\ \dot{e}_n \end{pmatrix} = \begin{pmatrix} e_2 - \lambda_1 sign(\xi_1 - \hat{\xi}_1) = 0 \\ e_3 - \lambda_2 sign(\xi_2 - \hat{\xi}_2) = 0 \\ e_4 + \bar{g}_3(\xi_1, \xi_2, \xi_3, u) - \bar{g}_3(\xi_1, \xi_2, \hat{\xi}_3, u) \\ \vdots \\ e_n + \bar{g}_{n-1}(\xi_1, \xi_2, \ldots, \xi_{n-1}, u) - \bar{g}_{n-1}(\xi_1, \hat{\xi}_2, \ldots, \hat{\xi}_{n-1}, u) \\ \bar{f}_n(\xi) - \bar{f}_n(\xi_1, \hat{\xi}_2, \ldots, \hat{\xi}_n) + \bar{g}_n(\xi, u) - \bar{g}_n(\xi_1, \hat{\xi}_2, \ldots, \hat{\xi}_n) \end{pmatrix} \tag{5.52}$$

Setting $V_2 = \frac{e_1^2}{2} + \frac{e_2^2}{2}$ we obtain

$$\dot{V}_2 = e_1(e_2 - \lambda_1 sign(e_1)) + e_2(e_3 - \lambda_2 sign(e_2)) \tag{5.53}$$

Moreover, if the condition $\lambda_1 > |e_2|_{\max}$ holds for $t > t_1$, we have $e_1 = 0$ and $e_2 - \lambda_1 sign(e_1) = 0$, thus we find

$$\dot{V}_2 = e_2(e_3 - \lambda_2 sign(e_2)) \tag{5.54}$$

Consequently e_2 goes to zero in finite time $t_2 > t_1$ if $\lambda_2 > |e_3|_{\max}$. Moreover, from $\dot{V}_2$ we obtain that the observation error is strictly decreasing during the period of time $[t_1, t_2]$. This implies that the condition on λ_1 is verified after t_1 if it is verified before t_1. Moreover as the input is bounded, the state ζ stays bounded during the period $[0, t_2]$ and from the structure of the observation error the dynamics e is also bounded and consequently $\hat{\zeta}$ is too.

Now let us assume that we are at the step $j < n$. This step starts at time t_{j-1}

and at t_{j-1}, all the $e_k = 0$ and all the conditions on λ_k are verified for $k < j$. Thus, we proceed to

- **Step j.** The observation error dynamic is equal to

$$\begin{pmatrix} \dot{e}_1 \\ \vdots \\ \dot{e}_{j-1} \\ \dot{e}_j \\ \dot{e}_{j+1} \\ \vdots \\ \dot{e}_{n-1} \\ \dot{e}_n \end{pmatrix} = \begin{pmatrix} e_2 - \lambda_1 sign(\xi_1 - \hat{\xi}_1) = 0 \\ \vdots \\ e_j - \lambda_{j-1} sign(\xi_{j-1} - \hat{\xi}_{j-1}) = 0 \\ e_{j+1} + \lambda_j sign(\xi_j - \hat{\xi}_j) \\ e_{j+2} + \bar{g}_{j+1}(\xi_1, \ldots, \xi_{j+1}, u) - \bar{g}_{j+1}(\xi_1, \ldots, \xi_j, \hat{\xi}_{j+1}, u) \\ \vdots \\ e_n + \bar{g}_{n-1}(\xi_1, \xi_2, \ldots, \xi_{n-1}, u) - \bar{g}_{n-1}(\xi_1, \hat{\xi}_2, \ldots, \hat{\xi}_{n-1}, u) \\ \bar{f}_n(\xi) - \bar{f}_n(\xi_1, \hat{\xi}_2, \ldots, \hat{\xi}_n) + \bar{g}_n(\xi, u) - \bar{g}_n(\xi_1, \hat{\xi}_2, \ldots, \hat{\xi}_n) \end{pmatrix} \tag{5.55}$$

Setting $V_j = \sum_{i=1}^{j} \frac{e_i^2}{2}$ we deduce from $e_k = 0 \ \ \forall i < j$ that

$$\dot{V}_j = e_j(e_{j+1} - \lambda_j sign(e_j)) \tag{5.56}$$

Consequently e_j goes to zero in finite time $t_j > t_{j-1}$ if $\lambda_j > |e_{j+1}|_{\max}$ and all λ_k conditions are verified for $k < j$. as the input is bounded and from the observer structure $\hat{\zeta}_j$ is also bounded during the period $[0, t_j]$. It follows that e_j is bounded and we can find λ_j such that $\lambda_j > |e_{i+1}|_{\max}$ is verified. Moreover, as e_j is decreasing during the period $[t_{j-1}, t_j]$, $\lambda_{j-1} > |e_j|_{\max}$ is verified during this period and therefore all the e_k remain equal to zero for any $k < j$. Now we go to:

- **Step n.** This step starts at the time t_{n-1} and at this time $e_k = 0$ for any

$k < n$. Thus we obtain the following observation error dynamics

$$\begin{pmatrix} \dot{e}_1 \\ \vdots \\ \dot{e}_{n-1} \\ \dot{e}_n \end{pmatrix} = \begin{pmatrix} e_2 + \lambda_1 sign(\xi_1 - \hat{\xi}_1) = 0 \\ \vdots \\ e_n + \lambda_{n-1} sign(\xi_{n-1} - \hat{\xi}_{n-1}) = 0 \\ \lambda_n sign(\xi_n - \hat{\xi}_n) \end{pmatrix} \tag{5.57}$$

Setting $V_n = \sum_{i=1}^{n} \frac{e_i^2}{2}$ we deduce from $e_k = 0 \ \ \forall i < n$ that

$$\dot{V}_n = e_n[-\lambda_n sign(e_n)] \tag{5.58}$$

So, e_n go to zero in finite time $t_n > t_{n-1}$ for any $\lambda_n > 0$ and if all the conditions on the λ_k for $k < n$ are verified after t_{n-1}. Condition on λ_{n-1} is always verified because e_n is decreasing after t_{n-1} and by induction all conditions follow.

Chapter 6

Data Analysis and Experimental Results

6.1 Introduction

In the previous chapters, the theoretical model, different identification and control strategies of the hydraulic servo-system have been introduced. In this chapter, these methods for modeling and control of hydraulic actuator are applied on a uni-axial servo-hydraulic shaking table to demonstrate the performance and different aspects of the methodologies presented in this thesis.

6.2 Experimental setup

The shaking table that has been used for the experiments, is located at the Department of Engineering and Applied Sciences of the University of Bergamo. A picture of the setup is given in figure 6.1.

As shown in this figure, for the setup, by means of removable loads, different load conditions can be created, such as to simulate different load conditions for the hydraulic actuator occurring in an earthquake shaking table simulator. In case all loads are removed, the mass of the table is about 450 $[kg]$. Placing the loads on the table, a maximum mass of the table 1200 $[kg]$ can be achieved.

Figure 6.1: Physical shaking table.

A 3D model of the setup is given in figure 6.2. This figure points out the elements composing a single degree-of-freedom (DOF) shaking table with operation range of $(0 - 15)$ $[Hz]$, driven by a servo hydraulic actuator: (A) moving platform for specimens housing (1200 $[mm]$ $\times$ 2000 $[mm]$) (the platform can be considered rigid because its first mode with components in the direction of the motion is the III, characterized by a frequency of 296 $[Hz]$, which is very far from the maximum working frequency of the system (15 $[Hz]$).); (B) rail guides for coupling with the fixed base (C) by using linear ball type guide-ways (D); (E) hydraulic actuator for moving the mobile base attached to it, by using the connection (F); (G) hydraulic system for the actuator supply; (H) mechanical end-stroke; (I) displacement potentiometer transducer; (K) accelerometer transducer.

A schematic drawing of the signal flow, including the measurement and control devices is given in figure 6.3. In this figure, A and D represent analog signal and digital signal, respectively. The signal conditioner is applied to condition the analog signals from the accelerometer and the displacement sensor, and the analog output signal to drive the servo valve. The conditioner is connected with the servo valve and sent the control input signal u from the target computer. The data acquisition board acquires the feedback displacement, and acceleration signal from the sensors. In the following, the specification of all these devices are described.

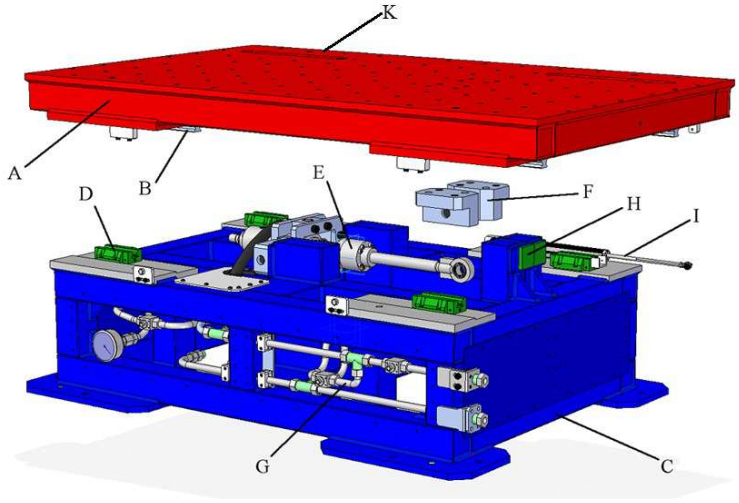

Figure 6.2: 3D model of the uni-axial servo hydraulic shaking table.

The shaking table is an electro-hydraulic system, meaning that electrical signals control and regulate hydraulic fluid with pressure to move the table. The electro-hydraulic actuator of the system, is a symmetric actuator of the double rode type, and has already been discussed as the actuator modeling example in chapter 3. This actuator is a Bosch-Rexroth CGH2 series with a 260 $[mm]$ stroke, 50 $[mm]$ bore diameter and a 36 $[mm]$ rod. The other part of the hydraulic actuator is the four-way three-position proportional directional valve (Bosch- Rexroth 4WS.2E series) which has an open center configuration with 0.5% underlap region and is characterized by a 20 $[l/min]$ nominal flow and by a bandwidth of about 150 $[Hz]$. In addition to the servo valve and the cylinder, there are a ball valve (R1) for the supply shut off, a ball valve (R2) for by-passing the actuator and a ball valve (R3) connected to a pressure gauge for the plant supply pressure display.

Due to the technical specification of the setup, the signals that could be measured are acceleration and position signals. The position and acceleration measurement of the system are carried out by Rectilinear Displacement Transducer (RDT) (PC-M-300) and accelerometer (ADXL05 EM-EM-3) separately. Although acceleration signal is available in the given setup, it should be noted here, that in the general case, only the position transducer will be available for control purposes.

The host computer in figure 6.3 is a common commercial PC, and is used as

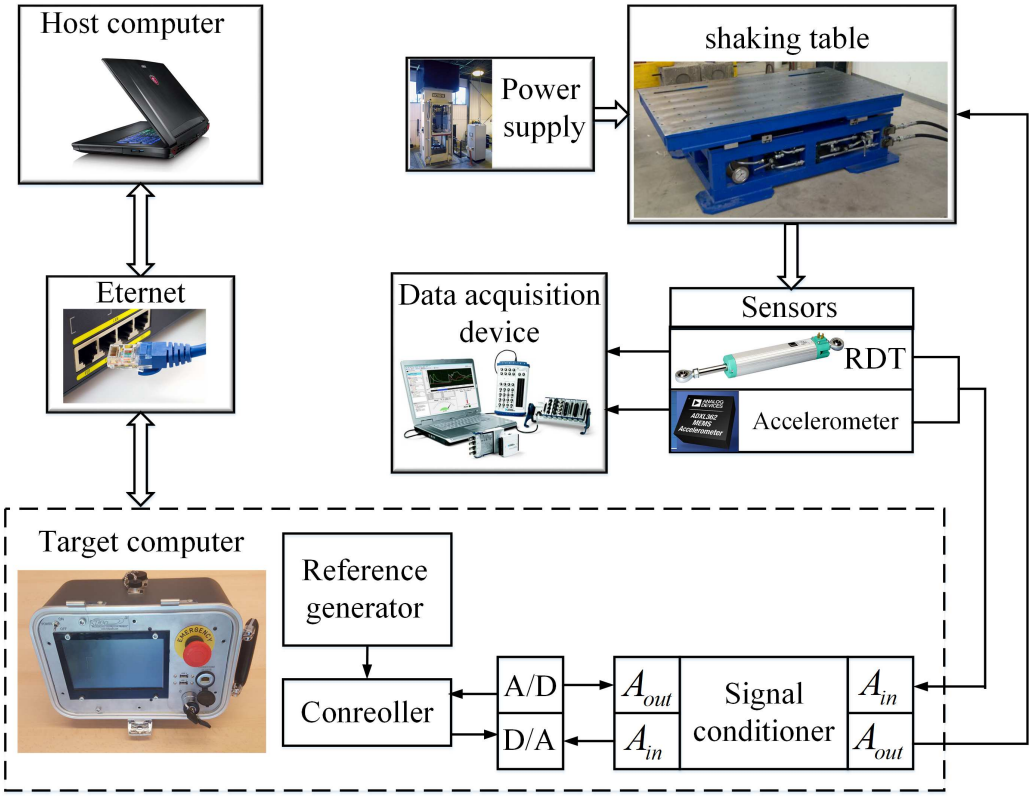

Figure 6.3: Schematic drawing of experimental setup including measurement and control devices.

a user interface to send commands and monitor the system states. The target computer is an industrial computer with an update rate of 1 $[kHz]$. This computer is equipped with a signal conditioner and a data acquisition board which is used as real-time controller for computing the total control algorithms. The signal conditioner contains analog-to-digital (AD), digital-to-analog (DA), and digital I/O conditioners for the analog transducer, servo valve control and digital I/O signals, respectively. The analog signal conditioning is used to subtract offsets and amplify, attenuate or filter signals if necessary. For instance, the position signal is filtered to avoid aliasing effects in digital control. Furthermore, the analog devices are used to make the desired connections between measurement devices, the actuator hardware and the digital control system. Acquired data that needs to be displayed or saved on the host computer is sent by the Ethernet. Ethernet, which is a family of frame-based

computer networking technologies for local area networks, supplies communication between the two computers.

With the measurement and control devices described here, the experimental setup allows extensive experimentation for modeling and control purposes. Many measurements in time domain have been performed. How these experiments are used for the identification and validation of the developed models, is discussed in the remaining sections of this Chapter.

6.3 Identification and validation

The aim of the identification and validation is to use experimental data from the system to identify the parameters of the model. In this thesis, the chosen approach to identification and validation of hydraulic servo-system, have been characterized as the identification of a gray-box(state space) model in the time domain, based on measured sinusoidal input, and subsequent validation by means of model simulation. As discussed in chapter 4, the identification and validation procedure of the hydraulic servo-system model, using experimental data of the real system, consists of four steps. First, some information about the acceleration output of the real system and impact of different excitation signal will be collected. Second, a typical nonlinear structure for simulating the behavior of the system is presented. Third, the nonlinear features of the system and their parameters based on the identification algorithms in chapter 4 are identified. Fourth, the identified parameters and the model of the system is analyzed and validated. Then, based on these results, two new nonlinear model for simulating the behavior of the hydraulic servo-system are proposed which increase the precision of the simulation results. Finally, this nonlinear model is simplified with a new method for design control in the next section.

6.3.1 Collect information about the system

In order to model a system, we should gather some information about the real behavior of the system. In the hydraulic servo-system, the type of the excitation signal during the experiments plays an important role in the modeling of the system. In this thesis, for identification purpose the sinusoidal input signal is used. From

the shaking table results, harmonic distortion exists in the acceleration response. Sinusoidal vibration tests indicate that the excitation signal has a great impact on harmonic distribution of the acceleration response of an electro-hydraulic shaking table. So, analyzing the impact of excitation sinusoidal signal upon the acceleration of the system is important.

For analyzing the results, total harmonic distortion (THD) criterion is always used to evaluate harmonic distortion. The THD criterion can be computed from [219]:

$$THD = \frac{\sqrt{A_2^2 + A_3^2 + A_4^2 + ...}}{A_1} \times 100\% \tag{6.1}$$

where A_1 is the fundamental amplitude, A_2 is the amplitude of second harmonic, A_3 is the amplitude of the third harmonic, and so on. First, we test the system with three sinusoidal inputs $u_1 = 0.3sin(2\pi \times 2t)$, $u_2 = 0.7sin(2\pi \times 2t)$ and $u_3 = 0.99sin(2\pi \times 2t)$ which have the same frequency and different amplitudes. The response to the acceleration input of $u_1 = 0.3sin(2\pi \times 2t)$ is shown in figure 6.4. It can be seen clearly that the acceleration response is seriously distorted and there are

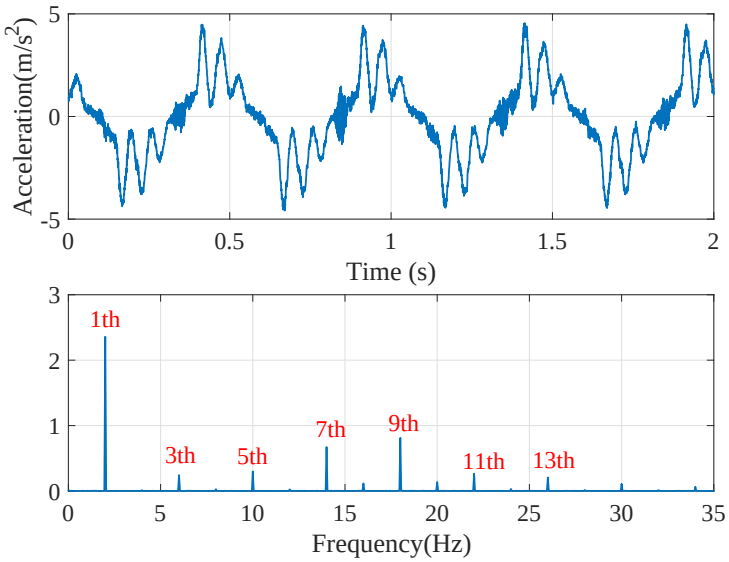

Figure 6.4: Acceleration response to the input $u_1 = 0.3sin(2\pi \times 2t)$. top: time domain response, bottom: frequency domain response.

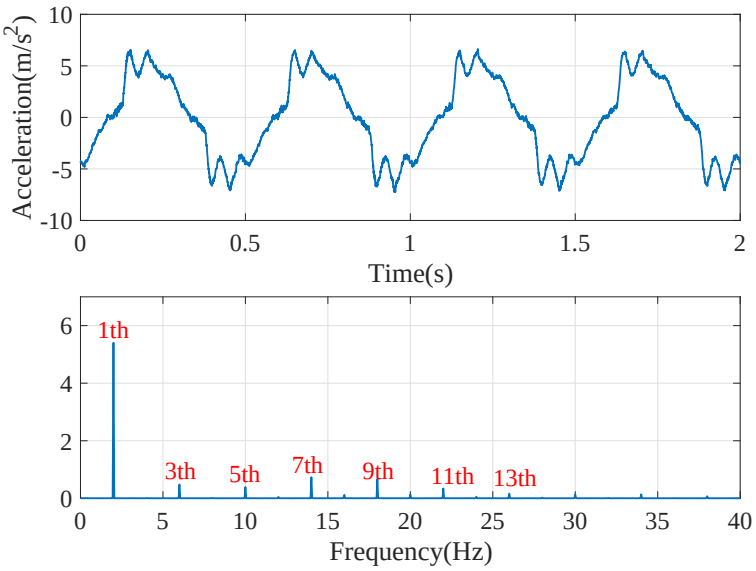

Figure 6.5: Acceleration response to the input $u_2 = 0.7sin(2\pi \times 2t)$. top: time domain response, bottom: frequency domain response.

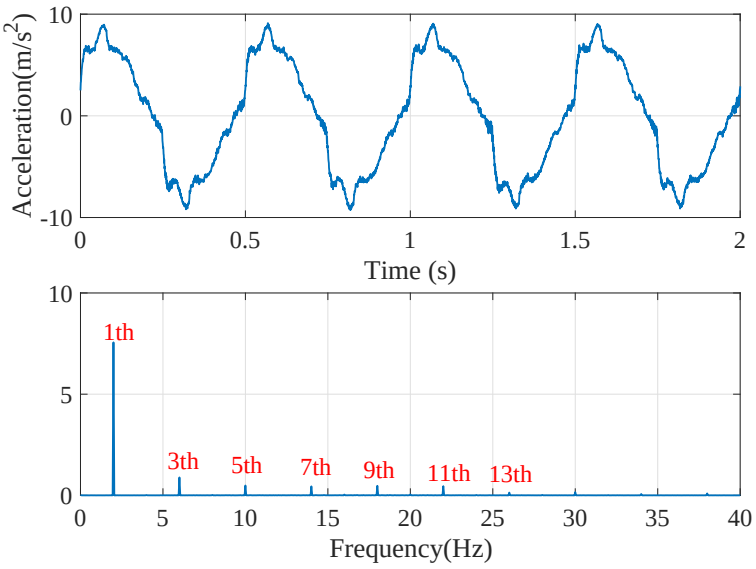

Figure 6.6: Acceleration response to the input $u_3 = 0.99sin(2\pi \times 2t)$. top: time domain response, bottom: frequency domain response.

serious harmonics in its response. The corresponding THD computed by equation (6.1) is shown in table 6.1. The ninth harmonic is dominant, because its amplitude is the largest. The seventh harmonic is larger than the fifth and the third harmonic. The even harmonics are the smallest. The value of THD is 49%.

The response of the acceleration to the input $u_2 = 0.7sin(2\pi \times 2t)$ is plotted in figure 6.5. There are serious harmonics. Its THD is shown in table 6.1. Also for this input, the ninth harmonic is the largest. the THD value is 22%.

Figure 6.6 shows the acceleration response corresponding to the input, $u_2 = 0.99sin(2\pi \times 2t)$. Serious harmonic distortion still exists in the acceleration response. Its THD analysis result is shown in table 6.1.

Table 6.1: THD analysis results

	u_1	u_2	u_3
Fundamental	2.35	5.4	7.5
3th harmonic	0.24	0.48	0.88
5th harmonic	0.29	0.39	0.48
7th harmonic	0.67	0.73	0.44
9th harmonic	0.81	0.66	0.47
11th harmonic	0.26	0.34	0.45
13th harmonic	0.2	0.16	0.14
THD	49%	22%	17%

It can be seen from table that for the input signal with the same frequency, by increasing the amplitude of the input, the harmonic distortion is decreased, ninth harmonic, is dominant in all harmonics and all even harmonics are the smallest.

In the second tests, in order to study the affect of the amplitude change on the acceleration signal, the system is tested with the sinusoidal input $u_1 = 0.2sin(2\pi \times 2t)$, $u_4 = 0.2sin(2\pi \times 5t)$ and $u_5 = 0.2sin(2\pi \times 10t)$ which have the same amplitude and different frequencies. The acceleration response for input u_1 is shown in figure 6.4.

The response of the acceleration to the input u_4 is plotted in figure 6.7. The curve is improved compared with the acceleration in figure 6.4. The THD of the acceleration signal is computed and the results are shown in table 6.2. They indicate that the amplitude of the second harmonic is the largest, so it accounts for the largest proportion of THD.

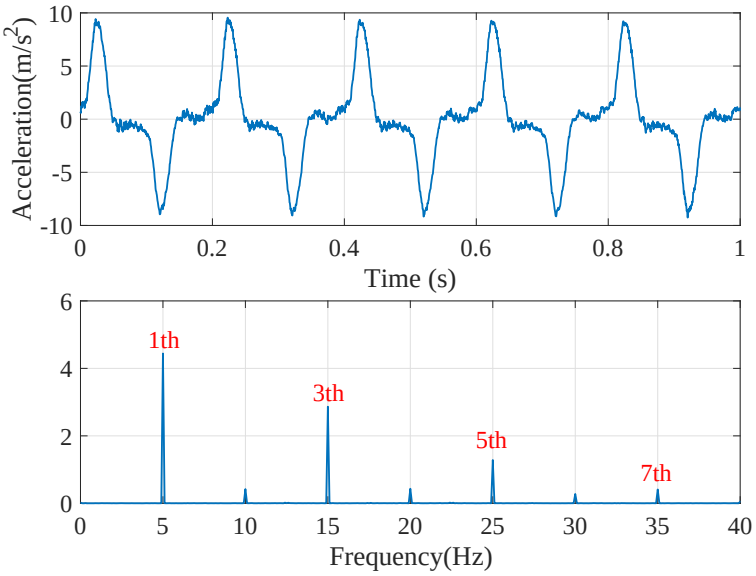

Figure 6.7: Acceleration response to the input $u_4 = 0.2sin(2\pi \times 5t)$. top: time domain response, bottom: frequency domain response.

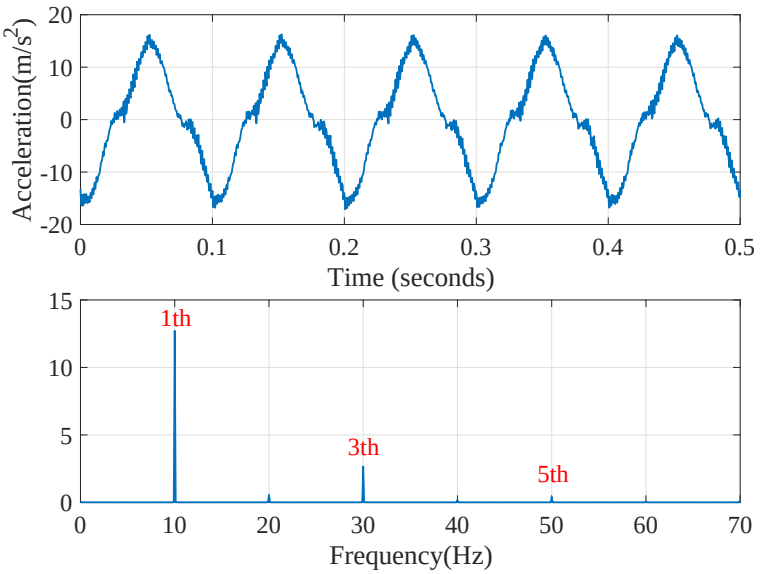

Figure 6.8: Acceleration response to the input $u_5 = 0.2sin(2\pi \times 10t)$. top: time domain response, bottom: frequency domain response.

Table 6.2: THD analysis results

	u_4	u_5
Fundamental	4.44	12.7
3th harmonic	2.86	2.66
5th harmonic	1.28	0.4
7th harmonic	0.41	–
THD	71%	0.21%

Figure 6.8 plot the acceleration signal to input u_5. The curve is smooth and is similar to a sinusoidal wave. The THD results are listed in Table 6.2, from which it can be seen that the THD is very small.

The time domain and the frequency of the acceleration response in figures 6.4-6.8 show the acceleration output of the system to sinusoidal inputs is seriously distorted. THD values of the signal in tables 6.1 and 6.2 express that with increasing the amplitude and frequency of the input, the harmonic distortion value is decreased. In addition, these results show that for all kinds of sinusoidal inputs with different frequencies and amplitudes, the even harmonics of the acceleration response are almost zero.

6.3.2 Nonlinear state space models of hydraulic servo-system

Based on the model of different components of hydraulic actuator which are presented in the chapter 3, the complete nonlinear state space model of the hydraulic servo-system are discussed in this section.

If the state variables and the input variables are defined as:

$$\begin{aligned} &x_1 = x_p, \quad x_2 = \dot{x}_p, \quad x_3 = P_A, \quad x_4 = P_B, \\ &x_5 = x_s^*, \quad x_6 = \dot{x}_s^*, \quad u = valve\ input \end{aligned} \tag{6.2}$$

then based on the equations (3.17), (3.18), (3.19), (3.23) and (3.26) in chapter 3, the model of the system which consists of a two-stage open center servo valve and

a symmetric double-rode cylinder can be written as:

$$\dot{x}_1 = x_2 \tag{6.3}$$

$$\dot{x}_2 = \frac{1}{M_p}\left[A_p(x_3 - x_4) - F_{fric}\right] \tag{6.4}$$

$$\dot{x}_3 = \frac{E_A}{V_A}\left[Q_A - Q_{el,A} - Q_{il} - A_p x_2\right] \tag{6.5}$$

$$\dot{x}_4 = \frac{E_B}{V_B}\left[-Q_B + Q_{el,B} - Q_{il} + A_p x_2\right] \tag{6.6}$$

$$\dot{x}_5 = x_6 \tag{6.7}$$

$$\dot{x}_6 = w_v^2\left[k_v u - \frac{2D_v}{w_v}x_6 - x_5 - f_{hs}sign(x_6)\right] \tag{6.8}$$

The total mass moved by the actuator (mobile base mass M_b pluse the specimen mass M_l) is given by:

$$M_p = M_b + M_l \tag{6.9}$$

The friction force based on the equation (3.34) is given by the equation:

$$F_{fric} = \left(F_C + (F_s - F_C)e^{-\frac{|x_2|}{x_{st}}}\right) sign(x_2) + F_v x_2 \tag{6.10}$$

The cylinder chamber volumes are given by

$$\begin{aligned} V_A &= \tfrac{V_t}{2} + A_p x_1 \\ V_B &= \tfrac{V_t}{2} - A_p x_1 \end{aligned} \tag{6.11}$$

where V_t is the total volume of the cylinder. The flow equations in equation (3.17) and (3.18), with considering $c_{rs} = 0$ and $d_{s1} = d_{s2} = d_{s3} = d_{s4} = d_s$ are characterized by

$$\begin{aligned} Q_A = {} & C_v sgt(x_5) sign(P_s - x_3)\sqrt{|P_s - x_3|} \\ & - C_v sgt(-x_5) sign(x_3 - P_T)\sqrt{|x_3 - P_T|} \\ Q_B = {} & C_v sgt(x_5) sign(x_4 - P_T)\sqrt{|x_4 - P_T|} \\ & - C_v sgt(-x_5) sign(P_s - x_4)\sqrt{|P_s - x_4|} \end{aligned} \tag{6.12}$$

where

$$sgt(x_5) = \begin{cases} 0 & x_5 \leq -d_s \\ x_5 + d_s & -d_s < x_5 < 1 \\ 1 & x_5 \geq 1 \end{cases} \tag{6.13}$$

The internal and external leakage can be calculated by:

$$\begin{aligned} Q_{il} &= C_{il}(x_4 - x_3) \\ Q_{el,A} &= C_{el}x_3 \\ Q_{el,B} &= C_{el}x_4 \end{aligned} \tag{6.14}$$

Note that a number of standard assumptions that are typically satisfied in practice have been made for the derivation of this nonlinear model:

- The hydraulic pump delivers a constant supply pressure, irrespective of the oil flow.
- The pressure in the tank is constant.
- A symmetrical open-center 4-way valve is modeled.
- The flow through the valve is turbulent.
- The leakage flow is laminar.
- The inefficient volumes of e.g. the pipelines between valve and actuator can be modeled as additive inefficient strokes.
- Coulomb, static and viscous friction are acting upon the actuator.
- The surroundings of the actuator and the load are rigid.
- There are not any external actions on the piston.
- The ball type guide-ways which use in the system are considered linear.
- Possible dynamic behavior of the pressure in the pipelines between valve and actuator is assumed to be negligible (i.e., the valve is placed directly upon the actuator).

In the next section, with the measurement and control devices described in previous section, many measurements have been performed on the shaking table which are used for the identification and validation of the developed models.

6.3.3 Matched the selected model structure to the measurements

As stated before, the parameters of the hydraulic systems are two types. First, the parameters which are known from equipment specifications. These parameters are calculated with mathematical formulation or by identification comprises the fit of the system time response with a fixed order state space model parameters. Second, the parameters which are unknown (such as friction parameters) or the measurement of them are very hard or expensive and time consuming (such as leakage, Effective bulk modulus, ...). These parameters are gain by minimizing the error between the real and the simulate output of the system in the sense of a mean square criterion, as explained in chapter 4. In table 6.3, the parameters of the system which are calculated from the catalog of the system, are listed. In addition, based on the the measurements have been done on the supply unit, supply pressure has almost a constant value except in high frequency. In high frequencies, it has low fluctuations over experiments, which could be ignored here. Figure 6.9 shows the fluctuation and the almost constant behavior of the supply unit. Therefore, based on the experiments the supply pressure in this thesis is considered a constant value.

Table 6.3: Values of the shaking table parameters.

Parameters	Values	SI unit
A_p	9.4562×10^{-4}	$[m^2]$
V_t	2.4586×10^{-4}	$[m^3]$
M_b	450	$[kg]$
P_s	206×10^5	$[Pa]$
U	0.005	$[m]$
C_v	1.28×10^{-7}	$[\frac{m}{\sqrt{kg/m^3}}]$

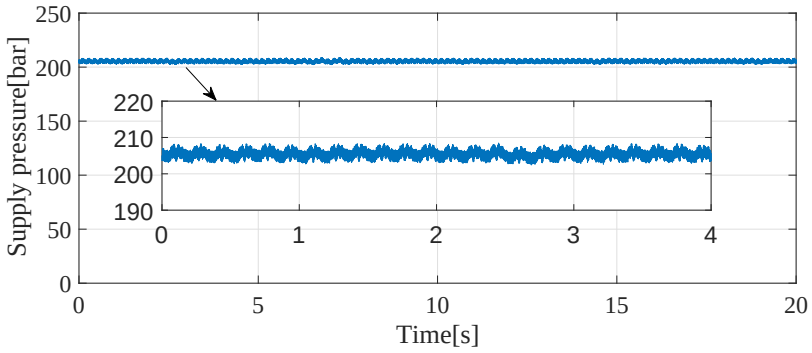

Figure 6.9: Supply pressure of the supply unit.

6.3.3.1 Servo-valve identification

Originally, one two-stage valve has been installed on the system for testing purposes. The dynamic nonlinear behavior of this valve, with flow capacity mentioned above, has been investigated in chapter 3. To obtain a model for simulation of valve behavior, the second order differential equation (6.7)-(6.8) have been implemented in MATLAB. As discussed in the chapter 3, for simplicity, the leakage flows and the valve friction were neglected. The parameters of the model (w_v, k_v, D_v and f_{hs}) will be identified, by fitting the step response of this model to the real system. Figure 6.10 shows a step response of the servo-valve (Bosch-Rexroth 4WS.2E series) without flow for a change in reference position from 0 to 1 which has been given in the data sheet of the valve. Here, only a small deviation is visible. The identified values of the parameters are listed in table 6.4. Figure 6.11 shows the corresponding step response of the servo-valve model by considering the identified parameters in table 6.4, which is simulated in MATLAB.

Table 6.4: Values of identified parameters of the servo-valve.

Parameters	Values	SI unit
w_v	1600	$[\frac{rad}{s}]$
k_v	1	$[-]$
D_v	0.736	$[-]$
f_{hs}	0.001	$[-]$

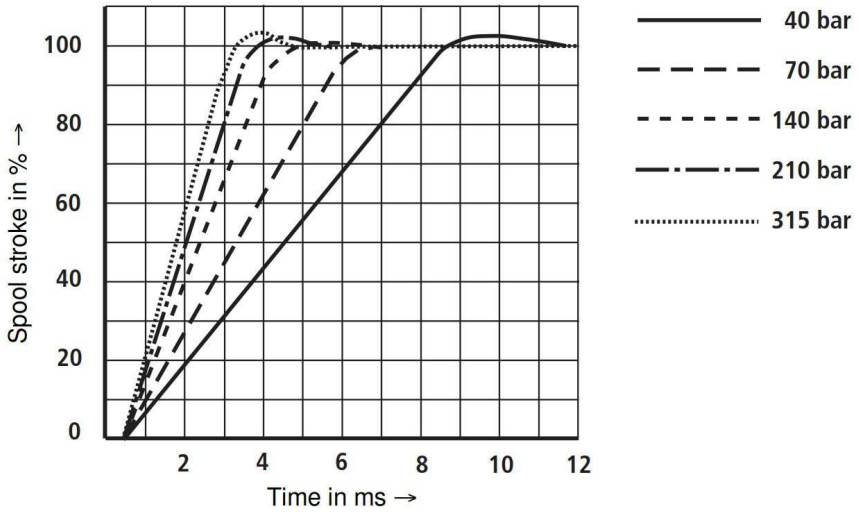

Figure 6.10: Step response of the Bosch-Rexroth 4WS.2E series servo-valve without flow.

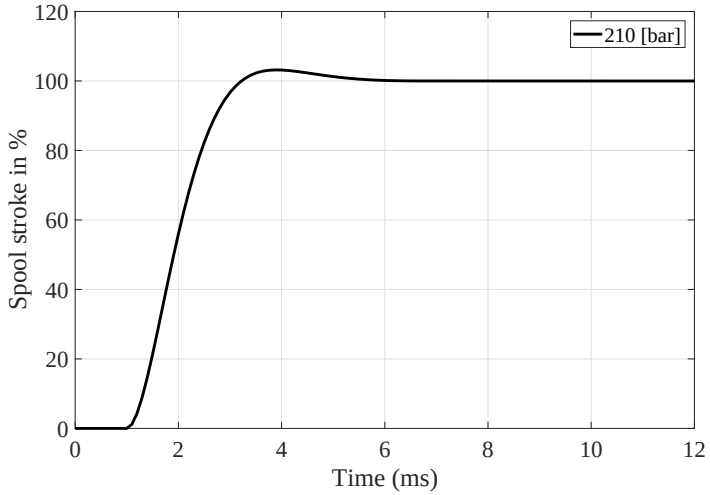

Figure 6.11: Step response of the servo-valve with considering equations (6.7)-(6.8) and the identified parameters in the table 6.4.

Besides this feature of the servo-valve which are set by the manufacture, a 400 $[Hz]$ oscillator is implemented in the analog built in electronics of the valve, which generates a dither signal. The application of a dither signal may modify the

nonlinear behavior of a system in a desirable way. In practice, when applied to the two-stage valve, this dither signal appears to be necessary and sufficient to eliminate hysteresis effects due to friction of the pilot-valve spool. In fact, the pilot-valve dynamics are continuously excited at the dither frequency, resulting in a sustained oscillation of the spool. Because 400 $[Hz]$ is well beyond the bandwidth of the two-stage valve, the amplitude of the dither is significantly attenuated, so that it does not excite the system dynamics too much.

The amplitude of the dither signal is to be adjusted by the user, and depends among others on the supply pressure. In practice, the dither adjustment was found to be rather sensitive. If the amplitude was chosen too small, the pilot-valve spool sticked, resulting in very bad low-frequency behavior of the two-stage valve. On the other hand, if the dither amplitude was chosen too large, the system dynamics were audibly excited. After some fine-tuning, a good adjustment could be found.

6.3.3.2 Hydraulic actuator identification

In the first stage of the identification and validation of the actuator dynamics, the dynamic model of effective bulk modulus of hydraulic oil are left out of consideration. Therefor, based on the common assumption in the literature, it is considered as a constant parameter. Taking the basic nonlinearities of the actuator into account, namely the valve flow nonlinearity (6.12) and leakage flow (6.14), the nonlinear actuator dynamics to be identified are described by the model that was presented in the equations (6.3)-(6.6). In this model, u the normalized input voltage of the valve is considered as input of the system and the x_1 and $\dot{x}_2$ where are position and acceleration of the system are considered as outputs of the experiment.

Because, in the first instance, the identification of the actuator dynamics is used to validate the derived model structure, and to obtain quantitative insight in the dynamics and nonlinearities of the actuator, the identification is performed in open loop configuration by measuring position and acceleration signals. Here, due to the open loop data gathering procedure, all the acquired position data of the system have drift which are not suitable for identification process. Therefore, velocity x_2 of the system was calculated by an approximate differentiation of the measured system

position. The noise in the calculated velocity signal is filtered by a butter-worth low-pass filter with order 8 and a bandwidth of 40 $[Hz]$.

The procedure described here, is well applicable to the nonlinear actuator model to identify the parameters of the system. In the following first, the parameters of three different kinds of friction model which have been discussed in chapter 3, are identified. Then, in order to model the system in a wide band width of frequency, the sensitivity of the model to variation of different parameters of the model, are described.

friction model

In this subsection, based on the paper [167], we have experimentally validated and identified the parameters of a robust numerical model that simulates the behavior of the system with considering different friction models. About the friction and its different kinds of modeling in the literature are discussed in more details, in chapter 3. Here, the parameters of the system are identified in presence of three different kinds of the friction model: the LuGre model the modified LuGre model and the new modified LuGre model. The main work here, is to estimate unknown parameters precisely with data from acceleration and position sensors without using pressure sensor. In the previous works, the parameter estimation is done with the data gathered from pressure and position/velocity sensors, in which case, the estimated model is not suitable for precise acceleration model. Our main advantage with respect to the precious work is using the acceleration sensor so it is suitable for constructed old shaking tables in which we cannot insert pressure sensor inside them without changing the structure of the table.

The parameter estimation of the three friction models have been perform on acceleration and velocity output data of the input $u = 0.1sin(2\pi t)$ by nonlinear least squares method based on the Trust-Region-Reflective algorithm which described in chapter 4, in MATLAB. The solver for these simulated results has been chosen ode23tb from Simulink toolbox, which is very robust for parameter estimation procedure with the minimum step of 10^{-4}. In order to excite all the relevant frequencies of the systems and to construct a good model, the results of the open loop test and corresponding simulation model is presented for the sinusoidal inputs with frequen-

Table 6.5: Values of the LuGre friction parameters

Parameters	Velocity of the system		SI unit
	$\dot{x}_p < 0$	$\dot{x}_p > 0$	
F_s	2344.9	-2115.4	$[N]$
F_c	2025.4	-102.8	$[N]$
v_s	0.0016	-0.0074	$[\frac{m}{s}]$
n	0.904	0.882	$[-]$
σ_2	1668.8	3858.15	$[\frac{Ns}{m}]$
σ_1	0.1		$[\frac{Ns}{m}]$
σ_0	1.14×10^8		$[\frac{N}{m}]$
E	6.0912×10^{12}		$[\frac{Pa}{m^3}]$
C_{il}	1×10^{-12}		$[\frac{m^3/s}{Pa}]$
C_{el}	1×10^{-12}		$[\frac{m^3/s}{Pa}]$
$I(CostFunction)$	106.14		

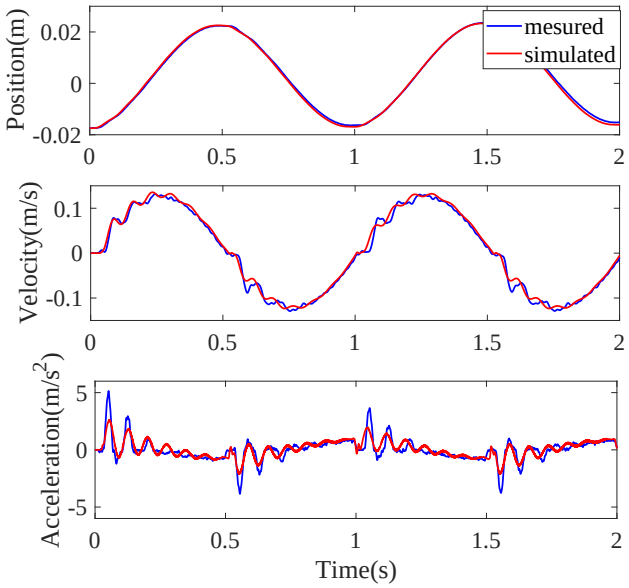

Figure 6.12: simulated and experimental system behavior with considering LuGre friction model for input of $u = 0.1sin(2\pi t)$.

cies $0.5[Hz]$ and $1[Hz]$. The parameters and the value of the cost function are shown in tables 6.5, 6.6 and 6.7.

The comparison between the simulation and experimental results are shown in figures 6.12-6.15. Figure 6.12 shows the comparisons between the dynamic behaviors

Table 6.6: Values of the Modified LuGre friction parameters

Parameters	Velocity of the system		SI unit
	$\dot{x}_p < 0$	$\dot{x}_p > 0$	
F_s	3889.9	-348.0091	$[N]$
F_c	3784.2	-159.8779	$[N]$
v_s	0.0024	-0.0124	$[\frac{m}{s}]$
n	2	2	$[-]$
σ_2	1254.1	5775.1	$[\frac{Ns}{m}]$
σ_1	0.1		$[\frac{Ns}{m}]$
σ_0	1.14×10^8		$[\frac{N}{m}]$
v_b	0.2492		$[\frac{m}{s}]$
τ_{hp}	0.0152		$[s]$
τ_{hn}	5.0529		$[s]$
τ_{h0}	31.0163		$[s]$
E	6.0912×10^{12}		$[\frac{Pa}{m^3}]$
C_{il}	1×10^{-12}		$[\frac{m^3/s}{Pa}]$
C_{el}	1×10^{-12}		$[\frac{m^3/s}{Pa}]$
$I(CostFunction)$	42.07		

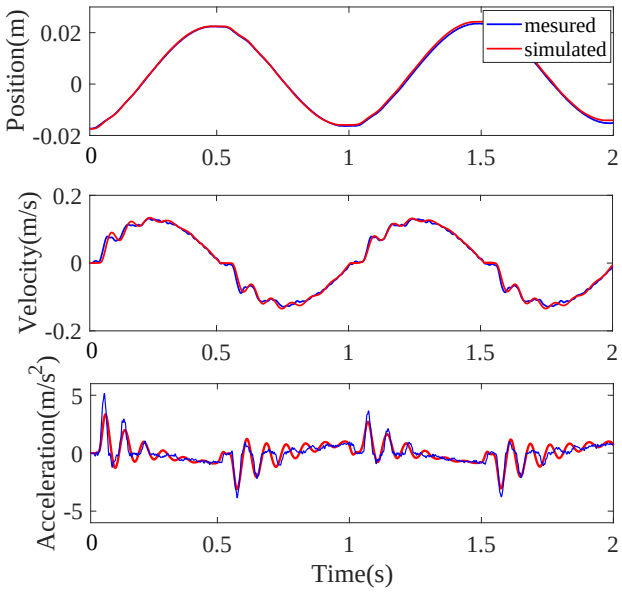

Figure 6.13: simulated and experimental system behavior with considering modified LuGre friction model for input of $u = 0.1sin(2\pi t)$.

of the system experimentally and the ones simulated with the LuGre friction model and a sinusoidal input $u = 0.1sin(\pi t)$. It is shown that the friction force cannot be simulated precisely by the LuGre model.

Figure 6.13 shows the simulation results of the system model with modified LuGre friction and the experimental results for input $u = 0.1sin(\pi t)$. As we can see from the figure modified LuGre friction has oscillation in acceleration and it can not track the acceleration of the system precisely.

Figures 6.14 and 6.15 shows the results obtained by the new modified LuGre model for sinusoidal inputs $u = 0.1sin(\pi t)$ and $u = 0.1sin(2\pi t)$, respectively. As can be seen from figure 6.14 and 6.15, the simulated results of the position, velocity and acceleration match well with the corresponding measurements. Also, the value of the cost function for this model has the minimum value between the other models. The comparison shows that the dynamic model of the hydraulic system with the new modified LuGre friction can simulate the dynamic behaviors of friction accurately under different frequencies of velocity variation.

Table 6.7: Values of the New Modified LuGre friction parameters

Parameters	Velocity of the system		SI unit
	$\dot{x}_p < 0$	$\dot{x}_p > 0$	
F_s	3889.9	-348.0091	$[N]$
F_c	3784.2	-159.8779	$[N]$
v_s	0.0024	-0.0124	$[\frac{m}{s}]$
n	2	2	$[-]$
σ_2	1254.1	5775.1	$[\frac{Ns}{m}]$
σ_1	0.1		$[\frac{Ns}{m}]$
σ_0	1.14×10^8		$[\frac{N}{m}]$
v_b	0.2492		$[\frac{m}{s}]$
τ_{hp}	0.0152		$[s]$
τ_{hn}	5.0529		$[s]$
τ_{h0}	31.0163		$[s]$
T	0.85		$[s]$
E	6.0912×10^{12}		$[\frac{Pa}{m^3}]$
C_{il}	1×10^{-12}		$[\frac{m^3/s}{Pa}]$
C_{el}	1×10^{-12}		$[\frac{m^3/s}{Pa}]$
$I(CostFunction)$	26.63		

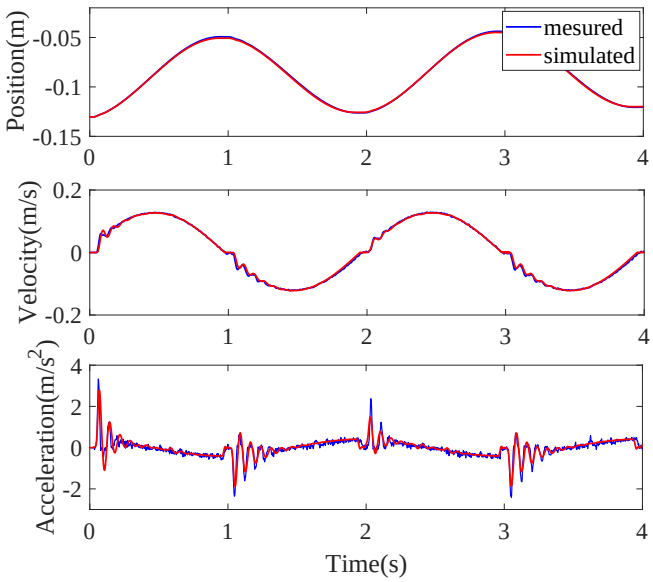

Figure 6.14: simulated and experimental system behavior with considering new modified LuGre friction model for input of $u = 0.1sin(\pi t)$.

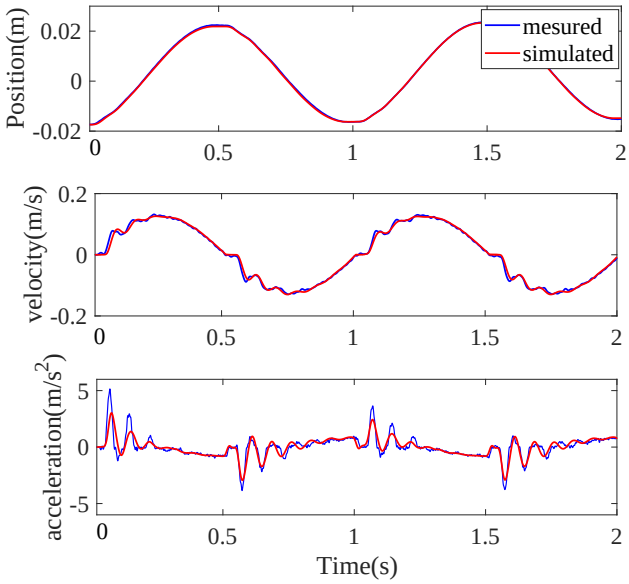

Figure 6.15: simulated and experimental system behavior with considering new modified LuGre friction model for input of $u = 0.1sin(2\pi t)$.

In this subsection, we consider the assumption of the frequency up to $2[Hz]$ and the velocity under $0.15[m/s^2]$, that is limiting in real practical shaking tables. So in the next section, in order to extend the model of the system in a wide range of frequency and velocity, the effect of the different parameters of the model on the system behavior are discussed.

6.3.4 Validation and analysis of the parameters variation

The dynamic features of the hydraulic servo-systems are highly nonlinear and relatively difficult to model and control. In the literature, several researches have been done on modeling the nonlinear behavior of these systems which arises from the compressibility of the hydraulic fluid [195], the complex flow characteristics of the servo-valve [34], internal and external leakage [68] and the friction in the hydraulic cylinder [227, 191, 136, 49, 215, 192, 190]. These features significantly affect system performance. However, including all these nonlinear features in the system structure makes the identification and control of the system very difficult.

In the previous subsection, the effect of different friction models are analyzed. However, it has been shown that in spite of the good results of the hydraulic model with considering different LuGre models, there are some restrictions on the frequency and velocity of the identified system. So, they are not suitable for our shaking table which has operating frequency range $(0-15)[Hz]$. In addition of this nonlinearities, as stated in the section 6.2, the shaking table which is used for the experiments has only the acceleration and position sensors and inserting pressure sensor inside it without changing the structure of the table was almost impossible. We don't have access to the pressure measurement inside the chambers of the system. This pressure is needed for studying the affect of each nonlinear features on the behavior of the system acceleration signal. Therefore, in order to discriminating the effect of each nonlinear feature on the acceleration behavior, we parametrize the model of the system. In this model, some constant parameters are defined. Then, the sensitivity of the model to variation of these parameters are analyzed.

The presented model in subsection 6.3.2 with considering the steady state model

in equation (6.10) is parametrized as:

$$\begin{cases} \dot{x}_1 = x_2 \\ \dot{x}_2 = \frac{A_p}{M_p}(x_3 - x_4) - \frac{1}{M_p}((\theta_1 + \theta_2 e^{-\theta_3|x_2|})sign(x_2) + \theta_4 x_2) \\ \dot{x}_3 = \frac{\theta_5}{V_A}(\theta_7 Q_A - A_p x_2 - \theta_6 x_3) \\ \dot{x}_4 = \frac{\theta_5}{V_B}(-\theta_7 Q_B + A_p x_2 - \theta_6 x_4) \\ \dot{x}_5 = x_6 \\ \dot{x}_6 = -w_v^2 x_5 - 2\frac{D_v}{w_v} x_6 + w_v^2 k_v u - w_v^2 f_{hs} sign(x_6) \end{cases} \tag{6.15}$$

The parameters of the system which are known from specifications, are listed in the table 6.3 and 6.4. The unknown parameters $[\theta_1, \theta_2, \theta_3, \theta_4, \theta_5, \theta_6, \theta_7]$ have to be experimentally studied and estimated.

The estimation of the system is carried out by nonlinear least squares method in MATLAB. The identified parameters of the system for the sinusoidal input with different frequency and amplitude $u_6 = 0.5sin(2\pi \times 3t)$, $u_7 = 0.8sin(2\pi \times 5t)$ and $u_8 = 0.9sin(2\pi \times 11t)$, are listed in table 6.8. With considering the equations (6.15) and the identified parameters in table 6.8, the system is simulated in MATLAB.

The comparison results between the simulated and real position, velocity and acceleration of the system are shown in figures 6.16 - 6.18 These figures show that the estimated model can simulate the behavior of the real shaking table with a good performance. The estimated parameters in table 6.8 express a small change in the parameters of the friction, but the parameters θ_5, θ_6 and θ_7 varies vastly for different input signals. In the following, the variation effect of these parameters on time and

Table 6.8: The identified parameters of the system model in equation (6.15) for inputs u_6, u_7 and u_8

Parameters	Values for u_6	Values for u_7	Values for u_8
θ_1 $[N]$	80	80	80
θ_2 $[N]$	160	160	160
θ_3 $[s/m]$	2.5	2.5	2.5
θ_4 $[N]$	2	2	2
θ_5 $[\frac{Pa}{m^3}]$	9.4×10^{12}	8.5×10^{12}	8.5×10^{12}
θ_6 $[\frac{m^3/s}{pa}]$	4.5×10^{-12}	19.5×10^{-12}	9×10^{-12}
θ_7 $[-]$	1.1	1.12	1.23

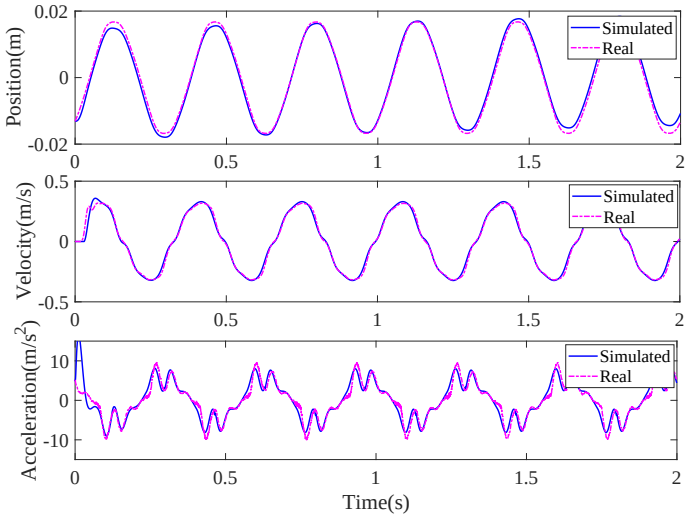

Figure 6.16: Experimental and simulated behavior of the system with considering the model in equation (6.15) and the parameters in table 6.8 to input $u_1 = 0.5sin(2\pi \times 3t)$.

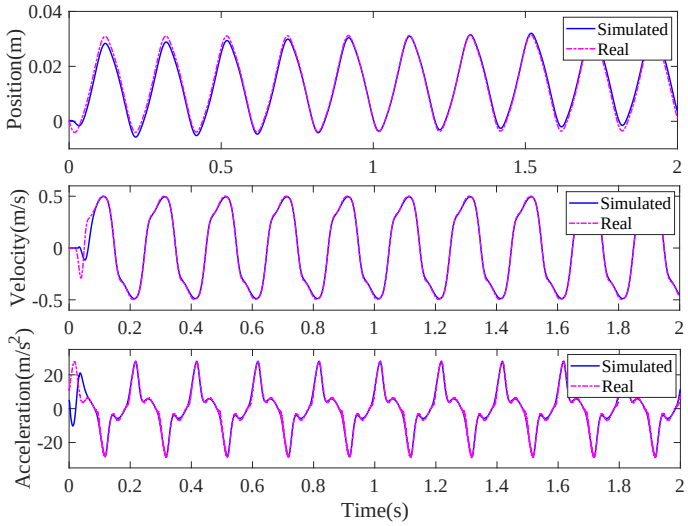

Figure 6.17: Experimental and simulated behavior of the system with considering the model in equation (6.15) and the parameters in table 6.8 to input $u_1 = 0.8sin(2\pi \times 5t)$.

frequency response of the system is analyzed.

In order to see the effect of the parameters first, for input signal $u_1 = 0.5sin(2\pi \times$

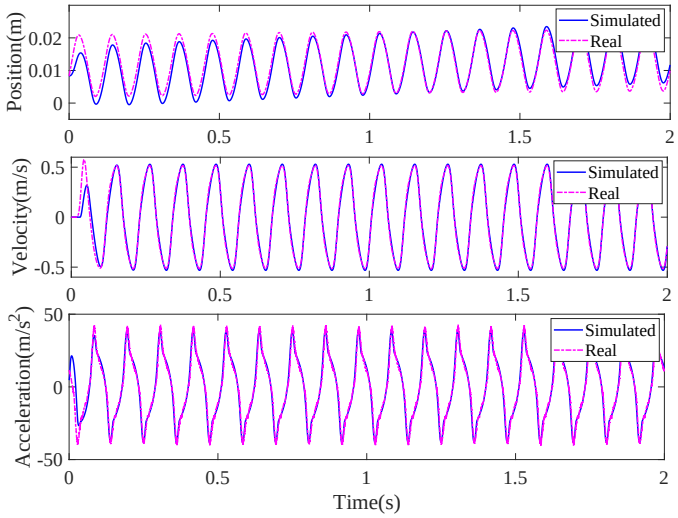

Figure 6.18: Experimental and simulated behavior of the system with considering the model in equation (6.15) and the parameters 6.8, to input $u_1 = 0.9sin(2\pi \times 11t)$.

$3t$), the parameters θ_6 and θ_7 are considered fixed and only the parameter θ_5 varies. Time response of the position, velocity and acceleration signals of the simulated and real system for different θ_5 are shown in figure 6.19. The different values of parameter θ_5 for simulating the model are $\theta_5 = 4.5 \times 10^{12}$, $\theta_5 = 12.5 \times 10^{12}$ and $\theta_5 = 9.4 \times 10^{12}$. The figure shows that the simulated model of the system in equation (6.15) have different performances for different values of parameter θ_5. As the figure shows, the variation of the parameter θ_5 has the most effect on the acceleration signal. So, for deep analysis of the system the frequency response of the acceleration is shown in the figure 6.20. This figure shows that the variation of this parameter can change the frequency of the dominant harmonic of the acceleration (For more detail see subsection 6.3.1). The value of the parameter θ_5 express the value of the effective bulk modulus of the hydraulic oil which is described in more detail in chapter 3. As discussed there, this parameter is depend on different conditions of the system (such as temperature, mechanical compliance, pressure, entertained air,...) and its value with considering only 1% of entertained air in the hydraulic oil, is decreased to 30% of its value without entertained air.

Next, in order to analyze the variation effect of parameter θ_6 on the model, the values of the parameters θ_5 and θ_7 are considered the same for different values

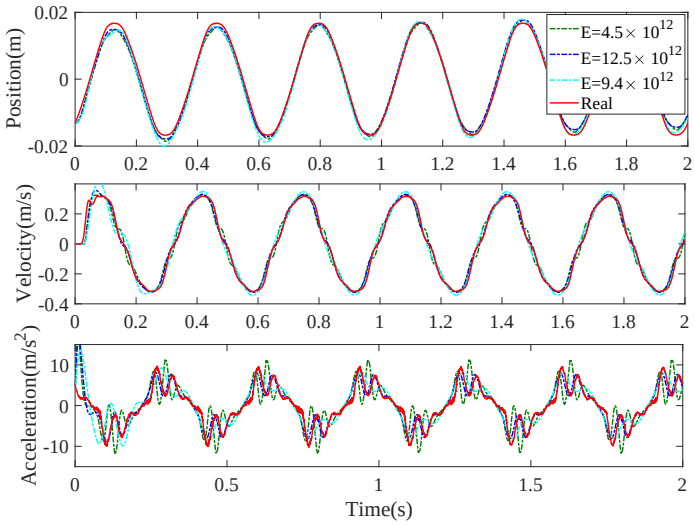

Figure 6.19: Response of the system with considering the model in equation (6.15) and different values for the parameter θ_5, to input $u_1 = 0.5sin(2\pi \times 3t)$.

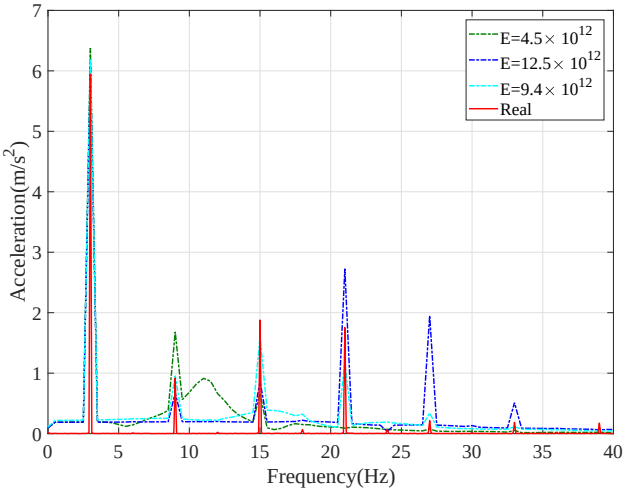

Figure 6.20: Frequency response of the acceleration signal with considering the model in equation (6.15) and different values for the parameter θ_5, to input $u_1 = 0.5sin(2\pi \times 3t)$.

of parameter θ_6. The comparison between the response of the real and simulated signals to the input $u_1 = 0.5sin(2\pi \times 3t)$ are shown in figure 6.21. As shown in this figure, the variation of the parameter θ_6 don't have so much effect on the response

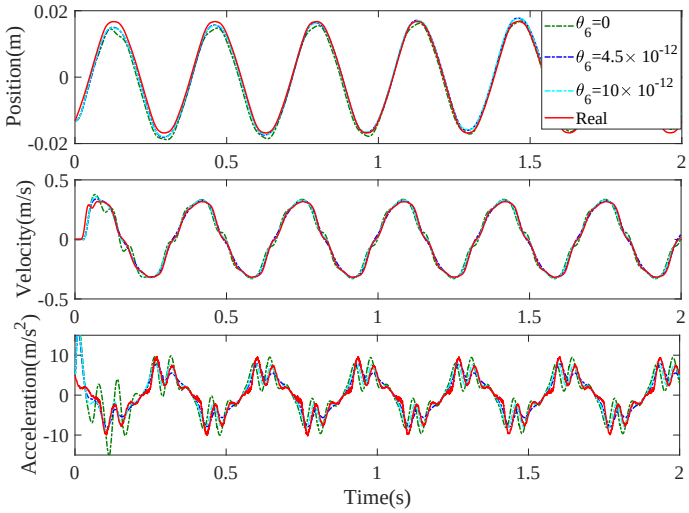

Figure 6.21: Response of the system with considering the model in equation (6.15) and different values for the parameter θ_6, to input $u_1 = 0.5sin(2\pi \times 3t)$.

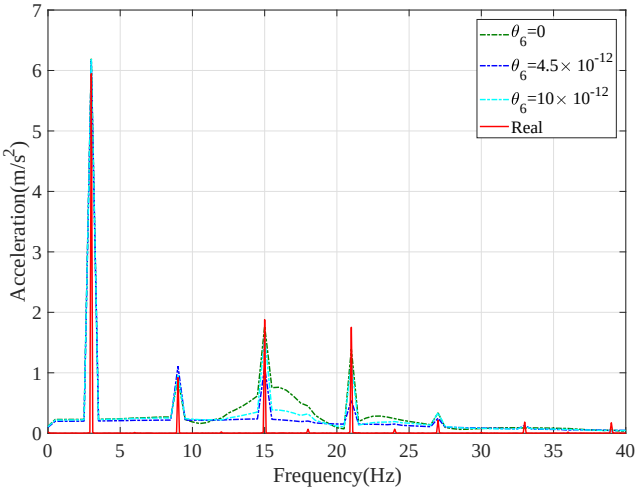

Figure 6.22: Frequency response of the acceleration signal with considering the model in equation (6.15) and different values for the parameter θ_6, to input $u_1 = 0.5sin(2\pi \times 3t)$.

of the system as θ_5. The frequency response of the system in figure 6.22 confirms this conclusion.

Finally, by considering a fixed value for the parameters θ_5 and θ_6, the variation effect of parameter θ_7 on the model are analyzed. Time and frequency domain

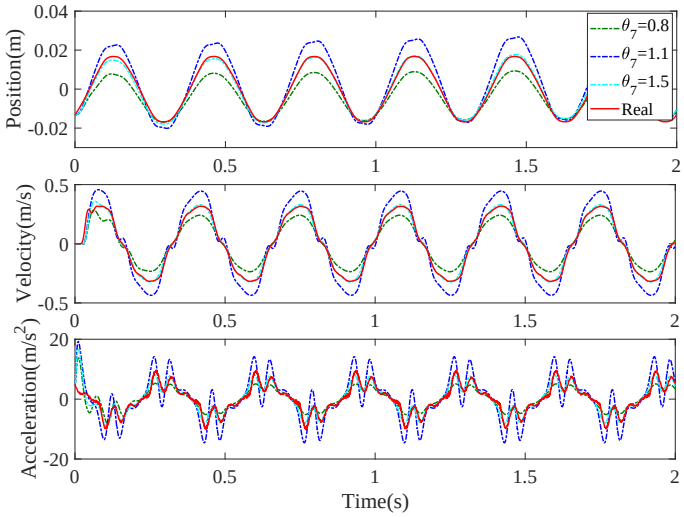

Figure 6.23: Response of the system with considering the model in equation (6.15) and different values for the parameter θ_7, to input $u_1 = 0.5sin(2\pi \times 3t)$.

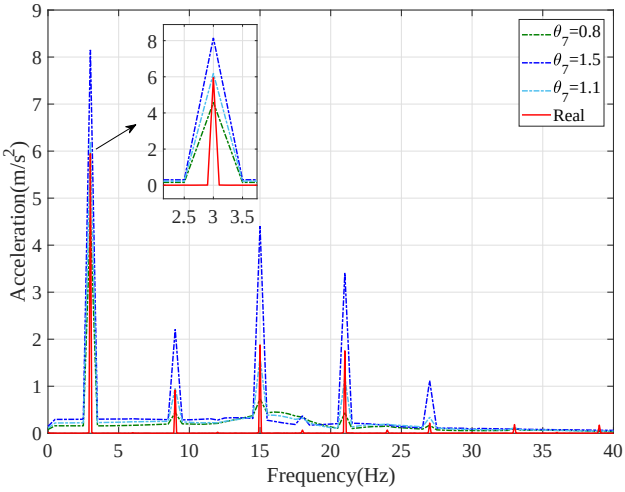

Figure 6.24: Frequency response of the acceleration signal with considering the model in equation (6.15) and different values for the parameter θ_7, to input $u_1 = 0.5sin(2\pi \times 3t)$.

response of the system to to input $u_1 = 0.5sin(2\pi \times 3t)$ are shown in figures 6.23 and 6.24. These figures show that, by increasing θ_7 the amplitude of the simulated response is increased and with decreasing it the amplitude is decreased. So, the parameter θ_7 have the most affect on the amplitude of the simulated response of the

system with equation (6.15).

In the following based on these results, two new nonlinear model for simulating the position, velocity and acceleration response of the system is proposed.

6.3.5 Gray-box modeling of the shaking table with Neural Network

This section is focused on identification of a gray-box position and acceleration response of the system with respect to sinusoidal input signal with different frequencies and amplitude [168]. For this purpose, the full parametrized model of the system which is defined in equation (6.15) is used for identification. For each input frequencies the unknown parameters of the model $[\theta_1, \theta_2, \theta_3, \theta_4, \theta_5, \theta_6, \theta_7]$, are identified based on nonlinear least square method. Then, the identified parameters are used to develop a dynamic feed forward neural network model. The gray-box model uses online short fast Fourier transform harmonic identification method to identify the harmonic and amplitude of input signal and the neural network model produces parameters of the system.

For train the feed forward Neural Network is used the Levenberg-Marquardt algorithm which is described in chapter 4. For comparison purposes, the back-propagation method with adaptive learning rate is used as the standard training method. The measure of comparison was based upon the following criteria:

1. Convergence: it is the most essential feature that a neural network must possess in order to solve a classification problem. In this context, convergence relates to the ability of a neural network to identify unknown function which can map input to output data.

2. Generalization: One of the major advantages of neural networks is their ability to generalize. This means that a trained network can predict the correct input/output relationship for the data that it has never seen before. This ability of neural networks are severely affected when the number of examples in the training set is significantly smaller than the possible number of examples in the application's input environment. To reach the best generalization, the data-set should be split into three parts: training set, validation set and test set.

3. Parameter selection: Each training algorithm has parameters that must be set properly to achieve an acceptable neural network performance. Some training/learning algorithms are highly sensitive to variations in these parameters. Different training algorithms have various numbers of parameters. The number and the sensitivity of parameters are the two major factors that define the complexity of the parameter selection problem.

4. Stop criteria: There are the rules that determine when to stop training multilayer networks;

   - The maximum number of epochs (repetitions) is reached.
   - The maximum amount of time is exceeded. Choose whether to specify a maximum number of minutes for the algorithm to run.
   - Performance is minimized to the goal. With this option, training will continue until the specified accuracy is attained. This may never happen, but you can interrupt training at any point and save the net with the best accuracy achieved so far.

A multi-layer feed forward neural network with two hidden layers which each layer has 100 neurons as shown in figure 6.25, is considered. Input of the neural network is amplitude and frequency of the normalized input voltage of the servo valve u which is acquired by online short time fast Fourier transform with $2[s]$ windows and 2^6 samples, and its output is the identified parameters with nonlinear least square method. These data are split into three sets;

- First 80% of the data are used for training
- Second 10% of the data are used for validating

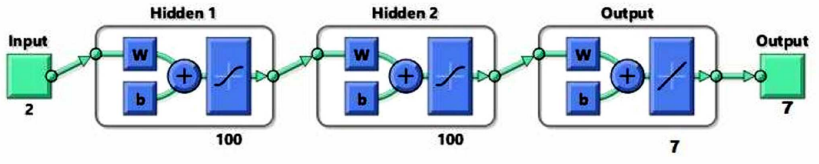

Figure 6.25: two-layer Feed-forward neural network.

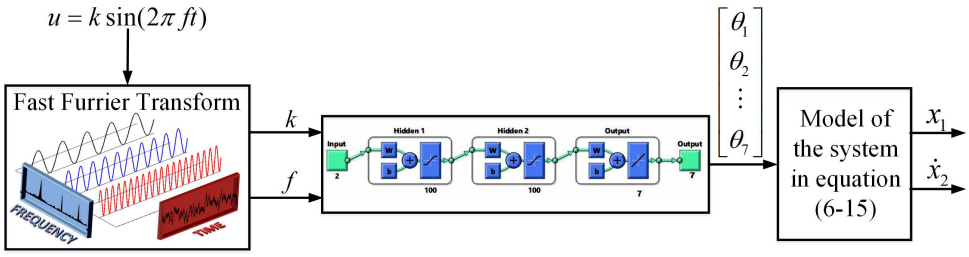

Figure 6.26: The block diagram of the identification procedure with Neural Network algorithm.

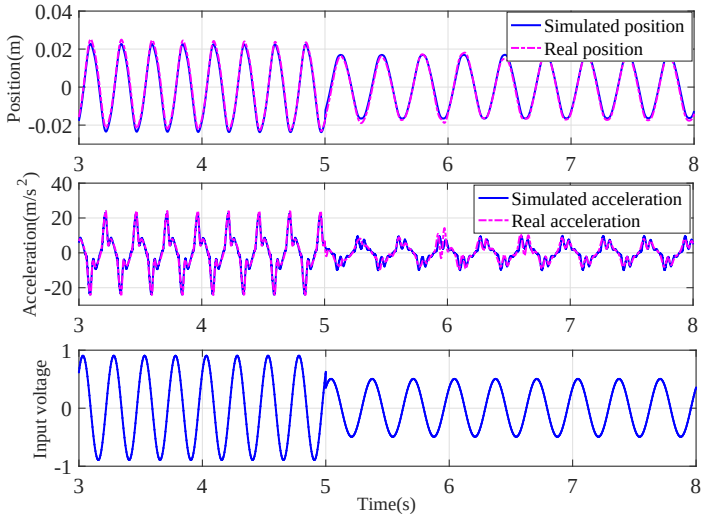

Figure 6.27: Simulated and experimental position and acceleration signal.

- One for testing, containing last 10% of the amount of data. This data set does not influence the training procedure.

The stop criterion of number of epochs for checking the increase of error on the validation data set is selected 1000 and the value of performance goal sets 10^{-6}.

The training algorithm and identification method described above was implemented using MATLAB. The comparison between the simulated position and acceleration signals of the model and the experimental ones are presented in figure 6.27. As shown in this figure, the simulated acceleration can track the experimental results with a good performance. In addition, the gray-box model could converge

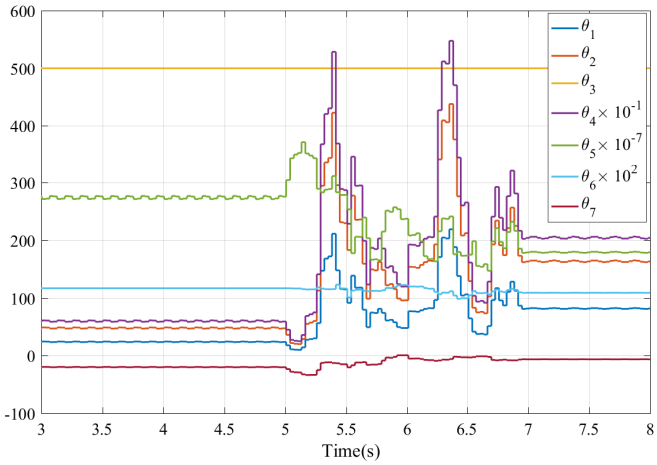

Figure 6.28: The online identified parameters of the gray-box from neural network.

to the experimental results while the input voltage changes abruptly. The identified unknown parameters from the neural network are shown in figure 6.28.

Despite the good performance of this method for simulating the behavior of the system, it needs high computation resources. In addition, it has $2[s]$ convergence window at the first run which in some cases it causes instability in control feedback loop. Thus, in order to model the behavior of hydraulic actuators with good performance to any kind of inputs, it is needed to model the effective bulk modulus of hydraulic oil which is the most effective nonlinear feature of the system as investigated before. In the following, a new mathematical model for simulating the behavior of the system is proposed.

6.3.6 Nonlinear model of the servo-hydraulic shaking table with considering a new dynamic model of Effective Bulk Modulus

In this section, based on the system model which is defined in section 6.3.2 built upon a modified IFAS model of the effective bulk modulus, a new empirical nonlinear model for simulating the position, velocity and acceleration output of the system is developed. As stated in the previous sections, the nonlinear model of a

hydraulic servo valve system in the literature, can simulate the position output of the system and somehow the velocity of the system. Additionally, in subsection 6.3.1 have been shown that the acceleration output of the system to the sinusoidal inputs, is distorted and it contains harmonics with the fundamental frequency and its integer multiplications. subsequently, the results in subsection 6.3.4 express that the variation of Effective bulk modulus of the hydraulic oil have the most effect on the acceleration response of the system. Thus, in order to model the acceleration behavior to any kind of inputs precisely, it is needed to model the main nonlinear features of the system such as effective bulk modulus and friction, as accurately as possible.

In the hydraulic systems the spring effect of a hydraulic oil is characterized by the value for the bulk modulus. It is a fundamental and inherent property of liquids which indicates the "stiffness" of the system and the speed of transmission of pressure waves. Therefore, system performances with respect to positioning, power loss, response time and stability of servo hydraulic systems is affected by the value of bulk modulus. As stated in the introduction chapter of the thesis, based on the experimental verification of different effective bulk modulus models in [104, 87], have been shown that the IFAS model in equation (2.32) can simulate most accurately the behavior of the E-Modulus. However, as shown in these papers, the minimum time for maximizing the input pressure are $2.5[s]$, which in our study is almost the steady state case.

In this thesis, in order to model the behavior of the system for a wide rage of frequency, the spring effect of the hydraulic oil is studied. In subsection 2.3.1, based on the fluid mechanical expressions, it has been proof that the minimum stiffness condition for the hydraulic oil in a double acting cylinder with symmetrical condition, occurs when the piston is in the center of its travel [3]. Therefore, based on this result and experimental acceleration signal, in the following by modifying the IFAS model of the effective bulk modulus a new empirical nonlinear model is proposed. In this model, the compressibility of the hydraulic oil in each two chambers is considered as a kind of nonlinear springs which are connected serially and affect each other. While the difference of the pressure in two chambers (load pressure) is lower than a threshold pressure, the energy which comes from the load pressure is stored in the chambers oil as a spring and it causes the velocity of the

system to be constant in this region. Then, with increasing the load pressure, this energy releases and causes the system to move with higher acceleration. In the modified IFAS model, these effects are simulated with a function based on the load pressure which multiplies the IFAS model in equation (2.32). This model is defined as:

$$E_{ai} = \frac{(1-\alpha)\Big(1+\frac{m(P_A-P_0)}{E_0}\Big)^{-\frac{1}{m}} + \alpha\Big(\frac{P_0}{P_A}\Big)^{\frac{1}{\kappa}}}{\frac{1}{E_0}(1-\alpha)\Big(1+\frac{m(P_A-P_0)}{E_0}\Big)^{-\frac{m+1}{m}} + \frac{\alpha}{\kappa P_0}\Big(\frac{P_0}{P_A}\Big)^{\frac{\kappa+1}{\kappa}}} \tag{6.16}$$

$$E_{bi} = \frac{(1-\alpha)\Big(1+\frac{m(P_B-P_0)}{E_0}\Big)^{-\frac{1}{m}} + \alpha\Big(\frac{P_0}{P_B}\Big)^{\frac{1}{\kappa}}}{\frac{1}{E_0}(1-\alpha)\Big(1+\frac{m(P_B-P_0)}{E_0}\Big)^{-\frac{m+1}{m}} + \frac{\alpha}{\kappa P_0}\Big(\frac{P_0}{P_B}\Big)^{\frac{\kappa+1}{\kappa}}} \tag{6.17}$$

$$E_A = E_{ai} h(P_A, P_B) \tag{6.18}$$

$$E_B = E_{bi} h(P_A, P_B) \tag{6.19}$$

$$h(P_A, P_B) = \lambda_1 - \lambda_2\Big(\tanh(\mu(P_A - P_B + P_{Lt})) - \tanh(\mu(P_A - P_B - P_{Lt}))\Big) \tag{6.20}$$

where λ_1, λ_2 and μ are constant coefficients and P_{Lt} is a threshold load pressure which at that load pressure value, the compressibility of the hydraulic oil inside two chambers can effect each other such as double nonlinear springs system with the load in between and so on effect the value of effective bulk modulus. This effect is modeled with equation (6.20).

The whole model of the system is modeled with the equations (6.3), (6.9), (6.11), (6.12) steady state friction model in (6.10) and the effective bulk modulus with equations (6.18) and (6.19). Here, for simplicity and the limitation of the LuGre model, the simple friction model is used for simulating the friction in the hydraulic cylinder. The unknown parameters of the model are estimated based on nonlinear least square method. These parameters are estimated and listed in table 6.9.

The comparison between the experimental results and the simulation one are shown in figures 6.29-6.36. First, with considering the specimen mass $M_l = 200[Kg]$, the comparison between simulation and experimental results are done for different

Table 6.9: Estimated parameters of the system with considering the modified IFAS and the IFAS E-Modulus model

Parameters	Value (Modified IFAS)	Value (IFAS)
C_i	4.343×10^{-13}	4.343×10^{-13}
C_e	4.05×10^{-14}	4.05×10^{-14}
F_c	573.72	531.85
F_s	1254.16	952.6
F_v	429.4	153.4
v_s	0.014	0.08
β	7.33	5.8
E_0	4.73×10^{8}	4.7×10^{8}
P_0	36.85	8.7
m	9.02	7.88
α	7.9×10^{-7}	6.8×10^{-7}
κ	0.49	0.7224
λ_1	1.2868	
λ_2	0.5401	
μ	8.80×10^{-6}	
P_{Lt}	9.177×10^{5}	

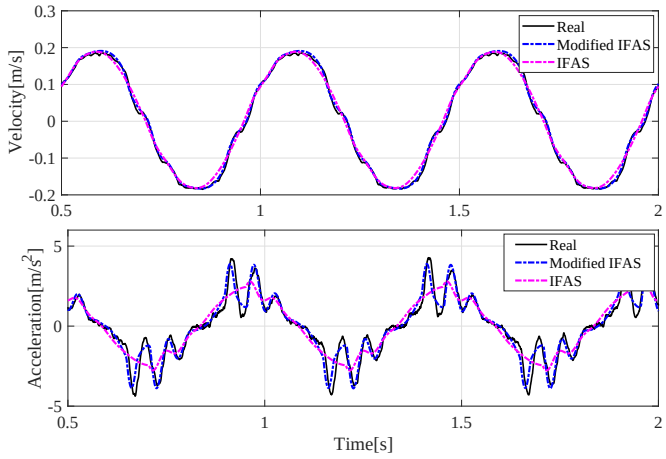

Figure 6.29: Simulated and experimental velocity and acceleration signals with considering the modified IFAS and the IFAS E-Modulus model, the specimen mass $M_l = 200[Kg]$, and the input voltage of the valve $u = 0.3\sin(2\pi \times 2t)$.

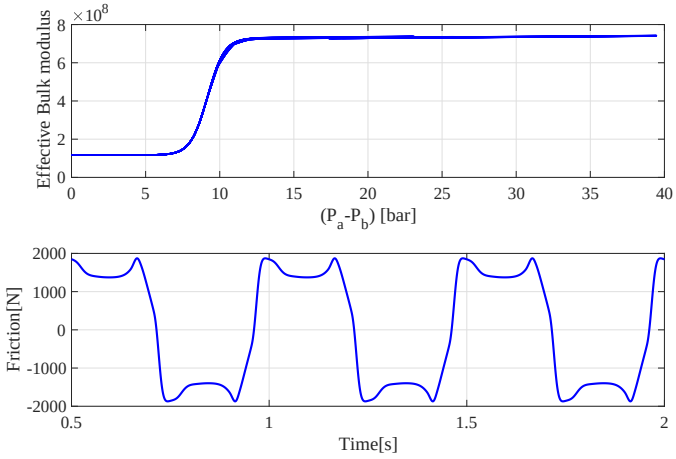

Figure 6.30: Top: the modified IFAS E-Modulus in chamber A in equation (6.18). Bottom: the steady state friction model correspond to the figure (6.29).

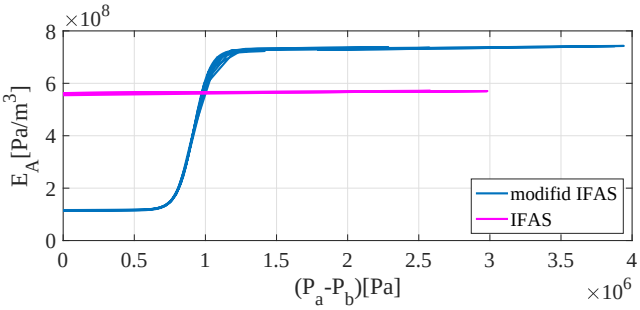

Figure 6.31: The modified IFAS E-modulus and IFAS bulk modulus.

sinusoidal frequencies 2, 8, 14 $[Hz]$. In figure 6.29, the experimental and the simulated velocity and acceleration signals by considering the modified IFAS model in equations (6.18), (6.19) and the IFAS E-Modulus in response to the input voltage $u = 0.3\sin(2\pi \times 2t)$, are shown. As it is shown in this figure, the new model can accurately simulate the experimental acceleration and velocity. However, the simulated model with IFAS model cannot simulate the acceleration behavior of the system. The modified IFAS E-Modulus and the friction model is shown in figure 6.30. In addition, for comparison the value of the E-Modulus based on the IFAS and modified IFAS model has been presented in figure 6.31.

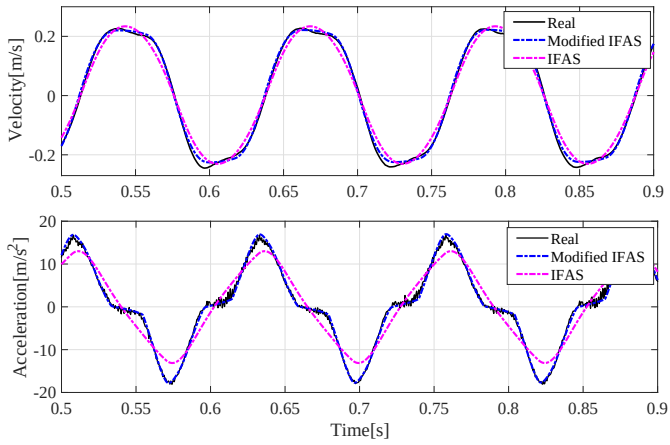

Figure 6.32: Simulated and experimental velocity and acceleration signals with considering the modified IFAS and the IFAS E-Modulus model, the specimen mass $M_l = 200[Kg]$ and the input voltage of the valve $u = 0.3\sin(2\pi \times 8t)$.

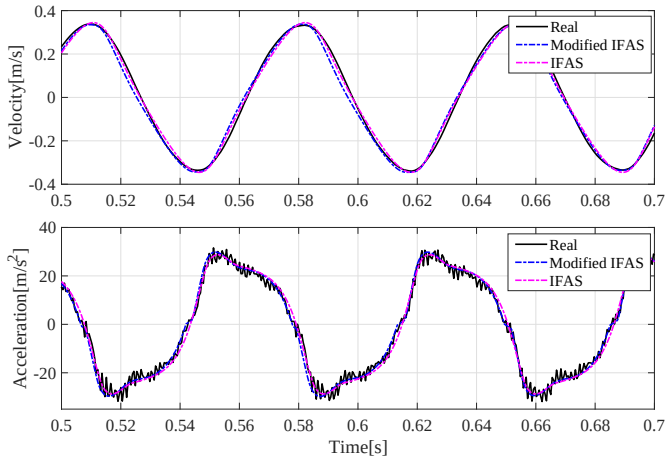

Figure 6.33: Simulated and experimental velocity and acceleration signals with considering the modified IFAS and the IFAS E-Modulus model, the specimen mass $M_l = 200[Kg]$ and the input voltage of the valve $u = 0.9\sin(2\pi \times 14t)$.

In order to verify the model at frequencies 8, 14 $[Hz]$, the simulation and experimental results are shown for the input voltage $u = 0.3\sin(2\pi \times 8t)$ and $u = 0.9\sin(2\pi \times 14t)$ in figure 6.32 and 6.33, respectively. As shown in these figures,

also in high frequencies the simulation velocity and acceleration with considering the new model can precisely simulate the experimental ones. Whereas, the simulation results with the IFAS model has so much errors with respect to experimental results in frequency $8[Hz]$. In frequency $14[Hz]$, as indicated in figure 6.33, the results for the modified IFAS model and the IFAS E-Modulus are almost the same and both models can simulate the experimental velocity and acceleration signals.

Next, with changing the specimen mass of the table to $M_l = 650[kg]$, the experimental and simulation results are shown in figures 6.34 and 6.35. In figure 6.34, the simulation and experimental results with considering the input voltage as:

$$u = \begin{cases} \sin(4\pi t), & 0 < t < 4.35s \\ 2\sin(4\pi t), & 4.35 < t < 6s \end{cases} \tag{6.21}$$

are shown. This figure displays that, even when the input voltage is in transition between two sinusoidal signals with different amplitudes, the new model can simulate the transient time behavior precisely. In contrary, the system model with considering the IFAS E-Modulus model cannot simulate the acceleration of the system. In figure 6.33, the acceleration and velocity of the system in response to the input voltage $u = 0.2sin(2\pi \times 5t)$ is displayed. As shown in this figure, the performance of the new model for simulating the experimental results with asymmetric acceleration response is better than the IFAS E-Modulus model.

Then, in order to verify the model with respect to other kinds of input signals, the experiment has been done with a pulse signal as input voltage. The comparison results between the experimental velocity and acceleration and the simulated ones with the specimen mass $M_l = 250[Kg]$ based on the modified IFAS model and IFAS E-Modulus, are shown in figure 6.36. This figure illustrates that, with different kinds of input signals the new model can reproduce the experimental velocity and acceleration results accurately. While, the model of the system with considering the IFAS E-Modulus cannot simulate the behavior of the system, as correctly as the new model.

Finally, the values of the cost function I in equation (4.1), for aforementioned different inputs and weights of specimen have been depicted in table 6.10. As indicated in this table and conforming the figures, the values of the cost function for

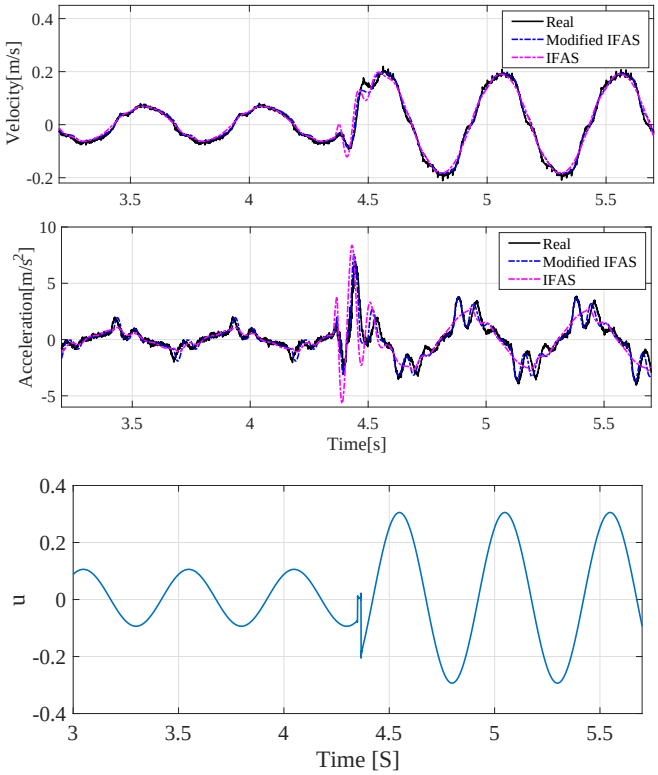

Figure 6.34: Top: Simulated and experimental velocity and acceleration signals with considering the modified IFAS and the IFAS E-Modulus model, the specimen mass $M_l = 650[Kg]$ and bottom: the input voltage in equation (6.21).

Table 6.10: The values of the cost function I in equation (4.1) for the parameters estimation of the modified IFAS and the IFAS E-Modulus model

Input	Mass	Value of I (Modified IFAS)	Value of I (IFAS)
$u = 3sin(4\pi t)$	$200[kg]$	31.4	119.1
$u = 3sin(16\pi t)$	$200[kg]$	53.88	310.92
$u = 9sin(28\pi t)$	$200[kg]$	132.71	141.51
u in equation (6.21)	$650[kg]$	17.6	50.57
$u = 2sin(10\pi t)$	$650[kg]$	54.49	188.1
u in figure 6.36	$200[kg]$	41.69	125.8

the parameters estimation of the system model based on the modified IFAS model is less than the IFAS E-Modulus.

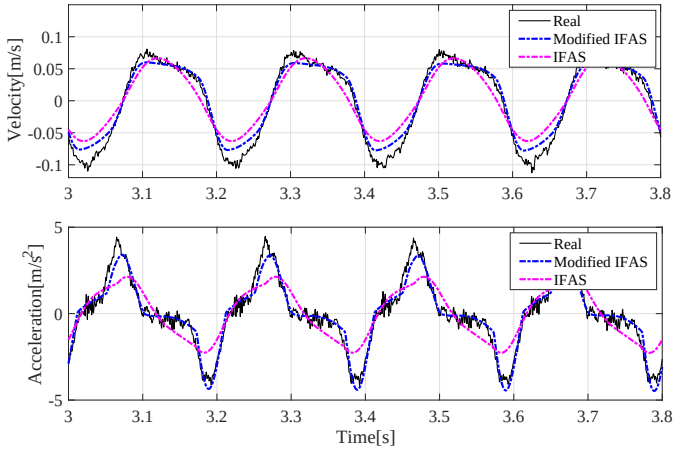

Figure 6.35: Simulated and experimental velocity and acceleration signals with considering The modified IFAS and the IFAS E-Modulus model, the specimen mass $M_l = 650[Kg]$ and the input voltage $u = 0.2sin(2\pi \times 5t)$.

The experimental and simulated comparison between the simulated model with the new model and IFAS effective bulk modulus and the real velocity and acceleration signals show the accuracy of the new model. These results express that the new model can simulate accurately the acceleration and velocity of the system with respect to different kinds of inputs such as pulse and sinusoidal signals and different weights of the specimen. Whereas, based on the figures and the values of the cost function in table 6.10, the model of the system with considering the IFAS E-Modulus model cannot reproduce the behavior of the acceleration signal as accurate as the new model.

This nonlinear model of the shaking table can use for Software-in-the-Loop simulation. This method represents the integration of compiled production source code into a mathematical model simulation, providing engineers with a practical, virtual simulation environment for the development and testing of detailed control strategies for large and complex systems. With this method, we can use a PC to directly and iteratively test and modify the controller structure and parameters to fined the optimal parameters. Software-in-the-Loop simulation makes it possible to test software prior to the initialization of the hardware prototyping phase, significantly acceler-

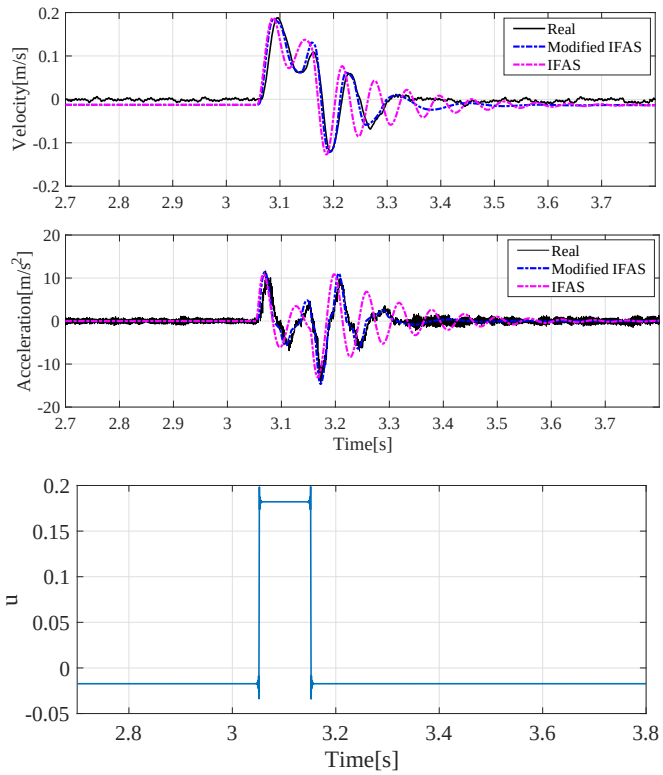

Figure 6.36: Top: Simulated and experimental velocity and acceleration signals with considering the modified IFAS and the IFAS E-Modulus model, the specimen mass $M_l = 200[Kg]$ and bottom: a pulse signal as input voltage.

ating the development cycle and reducing the costs of later stage troubleshooting, when the number and complexity of component interactions is greater. In the next section, all the parameters of the designed controller are optimize by using of this model instead of real shaking table.

6.3.7 Reduced-order and simplified model of hydraulic servo-system

In the previous subsection the full order model of hydraulic cylinder controlled by a servo-valve is formulated and used for identification purpose. This subsection described a new reduced-order and simplified model of an actuated hydraulic servo

system suitable for system dynamics analysis and motion control design.

The full-order model presented in previous subsection 6.3.6, incorporates the valve spool dynamics with combined dead-zone and saturation nonlinearities–inherent for the orifice flow. It includes the continuity equations of hydraulic circuits coupled with the dynamics of mechanical part of cylinder drive. The resulted model is the sixth-order and nonlinear in states. The reduced model which will presented in the following, neglects the fast servo-valve dynamics, simplifies both the orifice and continuity equations through an aggregation, and considers the cylinder rod position, velocity and acceleration as output states of the system. The reduced model is third-order that facilitates designing different model based controller.

The reduced model takes advantages of the fast servo-valve spool dynamics which presented in subsection 6.3.3.1, so that the second-order closed-loop behavior of the servo-valve can be neglected. Alternatively, this can be approximated by some constant time delay, if the corresponding phase lag is still to be taken into account when designing a feedback control of the hydraulic cylinder. Consequently, the input of the reduced model can be assumed as $x_5 = u$ that means the input current applied to the spool valve is directly proportional to the percentage of the spool position opening.

Introducing the load related pressure $P_L = P_A - P_B = x_3 - x_4$ and assuming a closed hydraulic circuit i.e. $|Q_A| = |Q_B|$ and the relation (provided leakage flows are negligible)

$$P_s + P_T = x_3 + x_4 \tag{6.22}$$

yields

$$x_3 = \frac{P_s + P_T + P_L}{2} \tag{6.23}$$

$$x_4 = \frac{P_s + P_T - P_L}{2} \tag{6.24}$$

and the orifice equations can be aggregated into one:

$$\begin{aligned} Q_L = Q_A + Q_B = C_v sgt(u)[sign(P_s - x_3)\sqrt{|P_s - x_3|} + sign(x_4 - P_T)\sqrt{|x_4 - P_T|}] \\ -C_v sgt(-u)[sign(x_3 - P_T)\sqrt{|x_3 - P_T|} - sign(P_s - x_4)\sqrt{|P_s - x_4|}] \end{aligned} \tag{6.25}$$

In this equation, the input signal of the system has a nonlinear relation with respect to the states of the system or it is not affine. However, the affine condition of the input controller is necessary for designing sliding mode control in equation (5.12). Therefore, we use the approximation of the square root function in equation (6.25), based on the Taylor series expansion.

The Taylor series of a real or complex-valued function $g(x)$ that is infinitely differentiable at a real or complex number a is the power series

$$g(a) + \frac{\dot{g}(a)}{1!}(x-a) + \frac{\ddot{g}(a)}{2!}(x-a)^2 + \frac{\dddot{g}(a)}{3!}(x-a)^3 + ... \tag{6.26}$$

where $n!$ denotes the factorial of n.
By approximating the square root function in equation (6.25) based on the Taylor expansion at pressure $P_1 = P_T$ and $P_2 = P_s$ when $x_V > 0$ and at pressure $P_1 = P_s$ and $P_2 = P_T$ when $x_V < 0$ ([69]), the Q_L can be express as

$$\begin{aligned} Q_L = &\frac{C_d w}{\sqrt{\rho}} sgt(u) \left[\sqrt{P_s - P_T} - \frac{x_3 - P_T}{2\sqrt{P_s - P_T}} + \sqrt{P_s - P_T} + \frac{x_4 - P_s}{2\sqrt{P_s - P_T}} \right] \\ &- \frac{C_d w}{\sqrt{\rho}} sgt(-u) \left[\sqrt{P_s - P_T} + \frac{x_3 - P_s}{2\sqrt{P_s - P_T}} + \sqrt{P_s - P_T} - \frac{x_4 - P_T}{2\sqrt{P_s - P_T}} \right] \end{aligned} \tag{6.27}$$

by using (6.23) and (6.24) and neglecting the spool underlap region $U \cong 0$, the equation (6.27) becomes:

$$\begin{aligned} Q_L &= \frac{C_d w}{\sqrt{\rho}} (sgt(u) - sgt(-u)) \left[\frac{1}{2} \sqrt{P_s - P_T} \right] \\ &\quad - \frac{C_d w}{\sqrt{\rho}} (sgt(u) + sgt(-u)) P_L \left[\frac{1}{2\sqrt{P_s - P_T}} \right] \\ &= \frac{C_d w}{\sqrt{\rho}} u \left[\frac{1}{2} \sqrt{P_s - P_T} \right] - \frac{C_d w}{\sqrt{\rho}} usign(u) P_L \left[\frac{1}{2\sqrt{P_s - P_T}} \right] \end{aligned} \tag{6.28}$$

Following the above way of aggregation, the hydraulic continuity equations (6.5)

and (6.6) can be transformed into one related to the load pressure gradient

$$\begin{aligned}\dot{P}_L = \dot{x}_3 - \dot{x}_4 &= \frac{2E}{V_t}\left[Q_L - (Q_{el,A} + Q_{el,B}) - 2A_p x_2\right] \\ &= \frac{2E}{V_t}\left[Q_L - C_{el}P_L - 2A_p x_2\right]\end{aligned} \tag{6.29}$$

Thereby, it has been assumed that

$$\begin{aligned}E_A &= E_B = E \\ V_A &= V_B = V_t.\end{aligned} \tag{6.30}$$

Correspondingly, the dynamics (6.4) of mechanical part transform into:

$$\dot{x}_2 = \frac{1}{M_p}\left[A_p P_L - F(x_2) - f_v x_2\right] \tag{6.31}$$

where friction equation in (6.10) is remodeled as:

$$F_{fric} = F(x_2) + f_v x_2 \tag{6.32}$$

The state variables of this hydraulic system dynamic model include ($x_p, \dot{x}_p$, P_A, P_B) but it is necessary to control variables ($x_p, \dot{x}_p, P_L$). Therefore, from (6.31), it is known that it is sufficient to control states ($x_p, \dot{x}_p, \ddot{x}_p$) so for control purpose, states ($x_p, \dot{x}_p, \ddot{x}_p$) are used to replace ($x_p, \dot{x}_p, P_L$). In addition, in a practical hydraulic system under normal working condition, P_A and P_B are both bounded, in fact, $0 < P_T < P_A < P_s$, $0 < P_T < P_B < P_s$ so it is feasible to use a third-order model of using the states ($x_p, \dot{x}_p, \ddot{x}_p$) to represent a dynamic model in the variables ($x_p, \dot{x}_p, P_L$).

Define the new state variables as:

$$z_1 = x_p = x_1, \quad z_2 = \dot{x}_p = x_2, \quad z_3 = \ddot{x}_p = \dot{x}_2. \tag{6.33}$$

The entire system including equations 6.28, 6.29 and 6.31 can be expressed in a new

state space form as follows:

$$\begin{aligned}
\dot{z}_1 &= z_2 \\
\dot{z}_2 &= z_3 \\
\dot{z}_3 &= \frac{1}{M_p}\left[A\dot{P}_L - \dot{F}(z_2) - f_v z_3\right] \\
&= \frac{2EA}{V_t M_p}\left[Q_L - C_{el}P_L - 2Az_2\right] - \frac{1}{M_p}\left[\dot{F}(z_2) + f_v z_3\right] \\
&= -\frac{(2EC_e f_v + 4EA^2)}{V_t M_p} z_2 - \left[\frac{2EC_{el}}{V_t} + \frac{f_v}{M_p}\right] z_3 + \left[\frac{EAC_d w}{V_t M_p \sqrt{\rho}}\sqrt{P_s - P_T}\right] u \\
&- \left[\frac{EC_d w}{V_t M_p \sqrt{\rho}\sqrt{P_s - P_T}}\right] |u| \left(M_p z_3 + f_v z_2 + F(z_2)\right) - \frac{\dot{F}(z_2)}{M_p} - \frac{2EC_{el}}{V_t M_p} F(z_2)
\end{aligned} \tag{6.34}$$

In order to simplify the state-space equation, first, define the parameters set

$$\begin{aligned}
\beta_1 &= -\frac{(2EC_e f_v + 4EA^2)}{V_t M_p} \\
\beta_2 &= -\frac{2EC_e}{V_t} - \frac{f_v}{M_p} \\
\beta_3 &= \frac{EAC_d w}{V_t M_p \sqrt{\rho}}\sqrt{P_s - P_T} \\
\beta_4 &= -\frac{EC_d w}{V_t \sqrt{\rho}\sqrt{P_s - P_T}} \\
\beta_5 &= -\frac{EC_d w f_v}{V_t M_p \sqrt{\rho}\sqrt{P_s - P_T}} \\
\beta_6 &= -\frac{EC_d w}{V_t M_p \sqrt{\rho}\sqrt{P_s - P_T}} - \frac{2EC_e}{V_t M_p}.
\end{aligned} \tag{6.35}$$

Thus the state space in equation (6.34) is transformed to

$$\begin{cases}
\dot{z}_1 = z_2 \\
\dot{z}_2 = z_3 \\
\dot{z}_3 = \beta_1 z_2 + \beta_2 z_3 + \beta_3 u + \delta_2(z, u)
\end{cases} \tag{6.36}$$

where

$$\begin{aligned} \delta_2(z,u) &= |u|\left(\beta_4 z_3 + \beta_5 z_2\right) + d(t) \\ d(t) &= \beta_6 F(z_2) - \frac{1}{M_p}\dot{F}(z_2) \end{aligned} \tag{6.37}$$

and the function $d(t)$ is lumped uncertain nonlinearity due to external disturbances, the unmodeled friction forces, damping viscous friction forces on the load, and the cylinder rod and other hard-to-model terms. The parameters of the system in (6.35), with considering $F(z_2) = 0$ are identified by nonlinear least squares method based on the Trust-Region-Reflective algorithm which described in chapter 4, in MATLAB. In this procedure, the input signals are $u_1 - u_7$ which are defined in section 6.3.4 and the outputs are the velocity and acceleration signals. The value of the parameters are listed in table 6.11.

Table 6.11: Identified parameters of equation (6.36).

Parameters	Values
β_1	-1.091×10^4
β_2	-3.062
β_3	6991
β_4	-0.3291
β_5	-141.3

Simulation results of the model with considering the new simplified model and the identified parameters in table 6.11 are shown in figures 6.37 and 6.38. Figure 6.37 shows the performance of the simplified model for a sinusoidal input with frequency $3[Hz]$. Although the acceleration response of the model cannot track the real one, the simulated velocity and position performance are adequate for designing a controller. Figure 6.38 shows the performance of the simplified model for a sinusoidal input with high frequency $9[Hz]$. Because of the low distortion of the acceleration output in high frequency, the simplified model can simulate the behavior of the system accurately. Therefore, based on these figures the performance of the model is adequate for designing controller and observer in the next section.

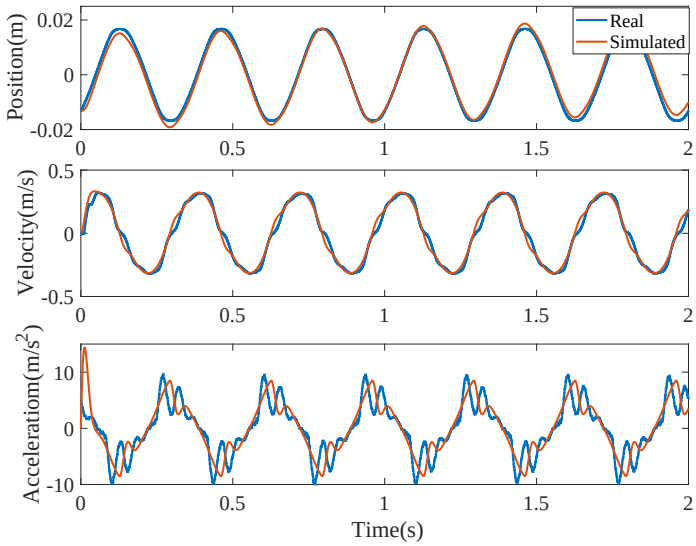

Figure 6.37: The real and simulated position, velocity and acceleration signal with equation (6.36) and parameters in table 6.11 to input $u = 0.5sin(2\pi \times 3t)$.

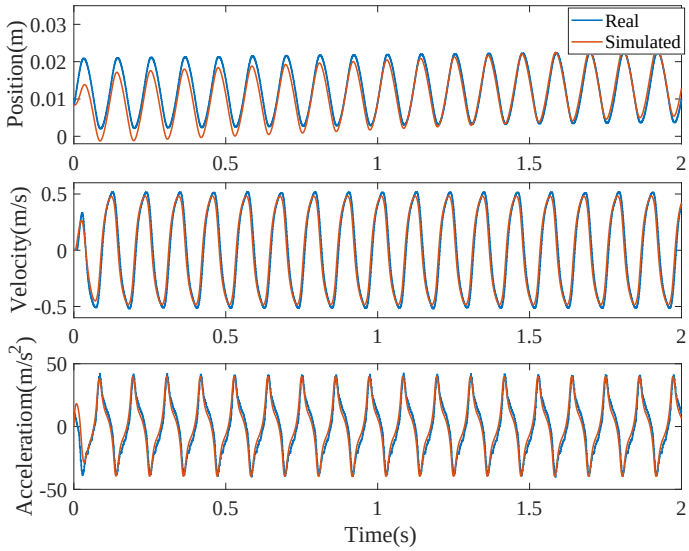

Figure 6.38: The real and simulated position, velocity and acceleration signal with equation (6.36) and parameters in table 6.11 to input $u = 0.9sin(2\pi \times 9t)$.

6.4 Design and application of hydraulic actuator control

In this section, the linear and nonlinear control algorithms that presented in chapter 5 are experimentally verified to provide an experimental evaluation of the different proposed control strategies for hydraulic servo-systems. Thereby, the evaluation takes place with respect to the task specification given in subsection 5.1.1. This basically comprises the tracking of a desired trajectory from the reference generator, with robust performance and respect to varying load conditions.

In this thesis, for designing all different kinds of controllers, the reduced order and simplified nonlinear model which is presented in previous section 6.3.6 is used. As stated before in the experimental setup description, only the position sensor is available for control purposes. Therefore, in subsection 6.4.2, for estimating the velocity and acceleration of the real system a nonlinear sliding mode observer is designed based on the simplified nonlinear model. This observer uses the position sensor measurements and estimates the velocity and acceleration of the system. Finally, three different kinds of controllers are designed and the comparison between the response of the simulated model and real system to these controllers are shown.

6.4.1 Sliding mode observer

In the hydraulic actuator nonlinear control strategies, discussed in chapter 5, velocity and acceleration feedback is applied. However, due to the hardware limitation in the experimental rig only the position sensor is available. In addition, based on the goal of this shaking table case study which is tracking the position signal with different weights of the specimen, only the position sensor would be enough and more sensors are extra costs. Therefore, in order to apply the proposed control strategies to the experimental setup, described in chapter 5, a velocity and acceleration estimation has to be performed.

The use of a state estimator in state feedback control applications of hydraulic actuators, is common. In the literature, the most attention is given to velocity estimator from the basic dynamics of the hydraulic servo-system, while the pressure difference and the position are assumed to be measured. However in this thesis, on

the experimental shaking table described in section 6.2, only the position transducer is available for control purpose. Therefore, based on the nonlinear sliding mode observer which is described in chapter 5, an acceleration and velocity estimator design will be worked out below.

With considering the 3^{rd} order model of the hydraulic actuator in equation (6.36), the nonlinear sliding mode observer structure is: (see equation (5.48)):

$$\begin{pmatrix} \dot{\hat{z}}_1 \\ \dot{\hat{z}}_2 \\ \dot{\hat{z}}_3 \end{pmatrix} = \begin{pmatrix} \hat{z}_2 + \tilde{z}_1 \\ \hat{z}_3 + \tilde{z}_2 \\ \beta_1 \hat{z}_2 + \beta_2 \hat{z}_3 + \beta_3 u + (\beta_4 z_3 + \beta_5 z_2)\,|u| + \tilde{z}_3 \end{pmatrix} \tag{6.38}$$

where

$$\begin{aligned} \tilde{z}_1 &= \lambda_1 sign(z_1 - \hat{z}_1) \\ \tilde{z}_2 &= \lambda_2 sign(\tilde{z}_1) \\ \tilde{z}_3 &= \lambda_3 sign(\tilde{z}_2). \end{aligned} \tag{6.39}$$

The identified parameters are listed in table 6.12. The estimation is performed by nonlinear least squares method based on the Trust-Region-Reflective algorithm which described in chapter 4, in MATLAB. In this procedure, the input signals are $u_1 - u_7$ which are defined in section 6.3.4 and the outputs are the velocity and acceleration signals.

Table 6.12: Identified parameters of the observer

Parameters	Values
λ_1	0.03
λ_2	2.5
λ_3	5

Figure 6.40 shows the comparison of the full-order simulated model in subsection 6.3.6 and estimated velocity and acceleration states with respect to input which has been shown in figure 6.39. This figure shows the performance of the designed observer for estimating the velocity and acceleration states. Then, in order to see the performance of the designed observer on the actual shaking table, the above observer was implemented under a closed loop condition in the target computer with a sample rate $1[kHz]$.

Figure 6.41 shows the real velocity and acceleration of the system and the observed ones which computed in the target computer with respect to the input in figure 6.39. As this figure shows both the estimated states converge to the correct values. The high noise in the initial phase of the acceleration can be observed. Due to the position limitation of the hydraulic stroke when the shaking table starts to run servo valve mechanical feedback (according to the datasheet) tries to put the position of the piston in the center of the shaking table to prevent from collision to the boundary and allow maximum possible displacement. This high noise is happened because of the mechanical controller which was applied before our proposed controllers. As the figure shows after applying the proposed controllers this high noise behavior disappears. Furthermore, the first phase behavior of the acceleration shows the robustness of the observer which can estimate the acceleration with high accuracy. Application results of the discussed designs will be given in sliding mode control subsection.

6.4.2 Feedforward PI controller

PID-controller is the most common in many industrial applications and it has been stated in chapter 5 that many researchers have used a PID-controller in position control of hydraulic servo-systems. Figure 6.42 illustrates the complete simulink block of the system with a feedforward PI controller as:

$$u_{PI}(t) = K_p e_p + K_I \int_0^t e_p dt + K_{ff} \dot{x}_{p,ref} \tag{6.40}$$

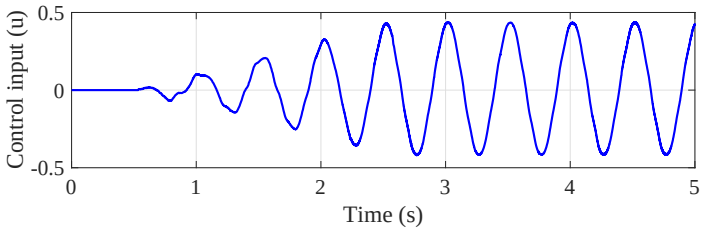

Figure 6.39: Input signal of the system.

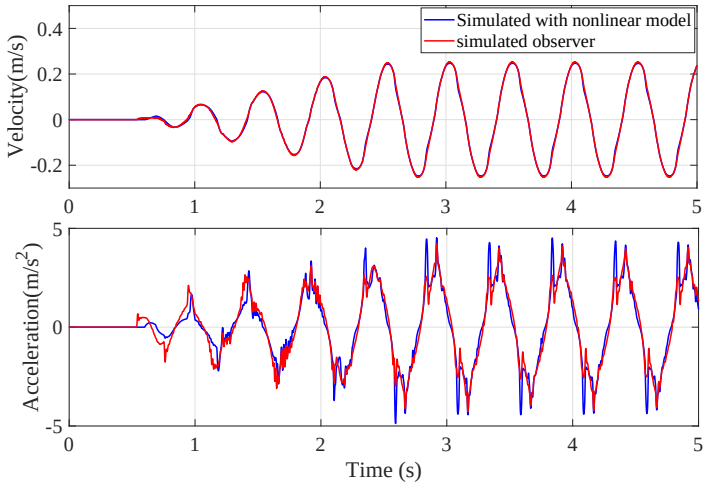

Figure 6.40: Velocity and acceleration of the simulated model and estimated states with respect to input in figure 6.39.

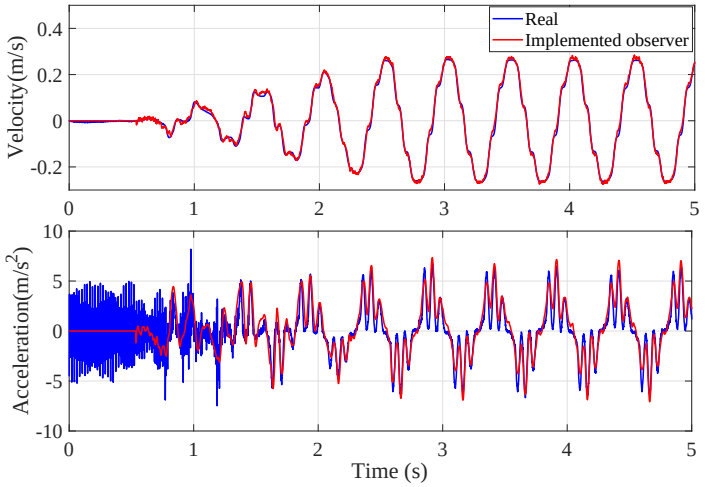

Figure 6.41: Velocity and acceleration of the real shaking table and estimated states in the target computer with respect to input in figure 6.39.

where

$$e_p = \hat{x}_p - x_{p,ref} \tag{6.41}$$

The output signal of reference generator is the sinusoidal and earthquake signals which will be position and velocity reference (i.e. $x_{p,ref}$ and $\dot{x}_{p,ref}$) for the controller. The feedback loop will loop back and compensate the error signal and PI controller will be compensated so that system will produce the best performance.

In the literature the parameters of the PID controller with respect to the linearized servo hydraulic model are usually designed using either one or two measurement points of the system frequency response as Ziegler-Nichols method. The control performance design with this method may not satisfy the desired time-response requirements. Therefore in this thesis, the optimal feedforward PI controller for the system with considering the time response of the system is design. In order to have a good closed-loop time response, the following performance function based on the nonlinear least square method needs to be minimize to find the optimal parameters of the controller:

$$J = \int_0^t \left[(x_p - x_{p,ref})^2 + (\dot{x}_p - \dot{x}_{ref})^2 \right] dt \tag{6.42}$$

where $J(K_p, K_I, K_{ff})$ is the integral time of square errors of position and velocity of the system. Using the MATLAB optimization toolbox, the optimal parameters of the controller are listed in table 6.13.

Table 6.13: Parameters of the feedforward PI controller

Parameters	Values
K_p	-25.005
K_I	-0.453
K_{ff}	1.52

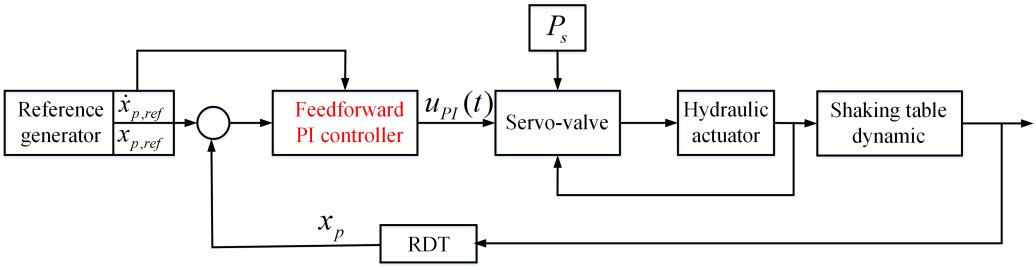

Figure 6.42: Block diagram of feedforward PI controller of the hydraulic servo-shaking table.

After implementation of the designed controller, under specified experimental conditions with a sample rate of $1[kHz]$ and the specimen mass of $M_s = 200[kg]$, the performance of the real system has to be evaluated. Figures 6.43 and 6.45 show the performance of the optimal feedforward PI controller with respect to sinusoidal and real earthquake reference signals, respectively. In these figures, the comparison results between the real and simulated closed-loop response with respect to given desired trajectory show the good performance of the controller. The corresponding controller signal for each case are shown in figures 6.44 and 6.46. Based on both experiments for different reference signals, it clearly shows that the output of the system has successfully tracked the desired references. Besides, the experiment results also show that the tracking output of real system is following the performance of the simulation result. Thus, the proposed controller has been fine tuned in simulation study before implementation with real system.

6.4.3 Sliding model controller

In this section, we would like to derive a sliding controller for the hydraulic servo-system using presented approach in chapter 5. As stated before, the goal of the

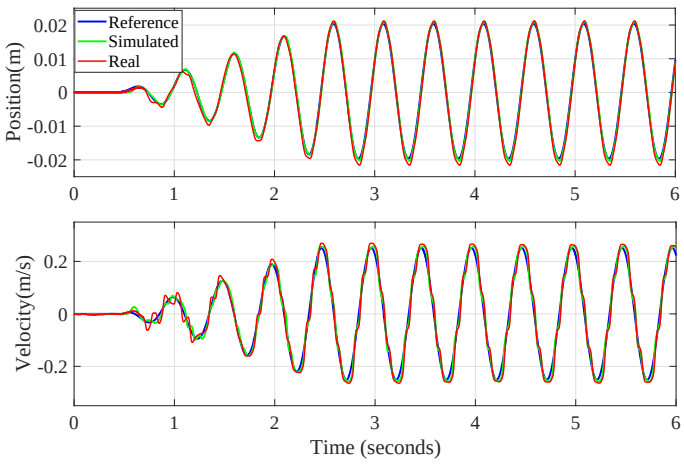

Figure 6.43: Real and simulated responses of the close loop system with respect to feedforward PI controller to a sinusoidal position and velocity reference signals.

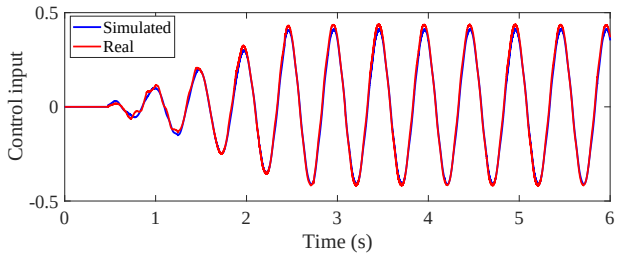

Figure 6.44: Real and simulated control inputs of feedforward PI controller to a sinusoidal reference signal in figure 6.43.

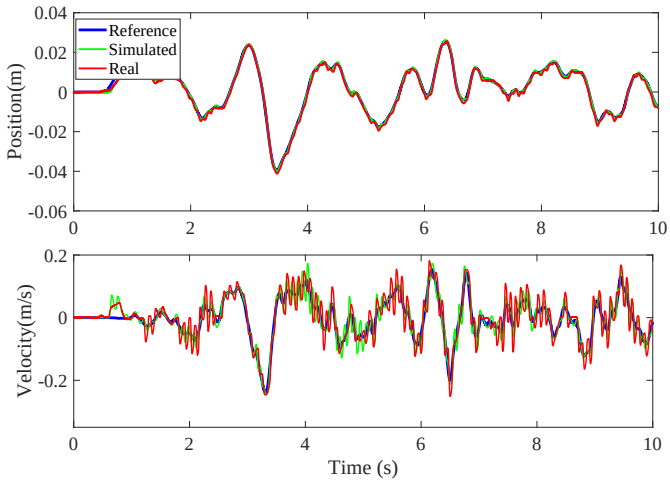

Figure 6.45: Real and simulated responses of the close loop system with respect to feedforward PI controller to an earthquake position and velocity reference signals.

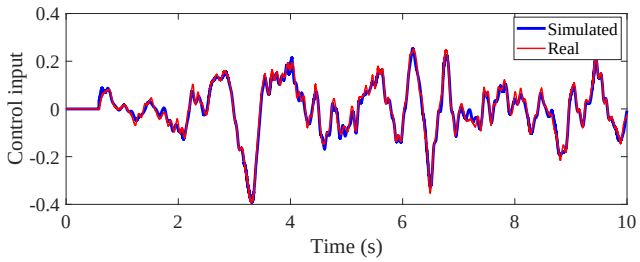

Figure 6.46: Real and simulated control input of feedforward PI controller to an earthquake reference signal in figure 6.45.

hydraulic servo-shaking table is to track the desired position and velocity trajectory with robust performance to different load conditions. Apart from the uncertain load condition, hydraulic servo-systems are highly nonlinear and also have the large extent of model uncertainties due to parametric uncertainties and uncertain nonlinearities which presented in chapter 3, explain the necessity of designing a robust controller for such systems. Therefore in this thesis, in order to obtain a robust behavior for the system, a sliding mode controller is designed.

With the assumption that position, velocity and acceleration of the simplified state space of the system in equation (6.36) are estimated by the observer and the boundedness of the lumped uncertain nonlinearity of the system $d(t)$, a controller is designed to give asymptotic convergence performance of the output error. Figure 6.47 illustrates the complete simulink block of the system with a sliding mode controller. For designing the controller based on the simplified model in equation (6.36), trajectory tracking error dynamic can be obtain as:

$$\begin{pmatrix} \dot{e}_1 \\ \dot{e}_2 \\ \dot{e}_3 \end{pmatrix} = \begin{pmatrix} e_2 \\ e_3 \\ \beta_1 e_2 + \beta_2 e_3 + \beta_3 u + h(e,u,t) \end{pmatrix} \tag{6.43}$$

where

$$\begin{aligned} e_1 &= x_p - x_{p,ref} \\ e_2 &= \dot{x}_p - \dot{x}_{p,ref} \\ e_3 &= \ddot{x}_p - \ddot{x}_{p,ref} \end{aligned} \tag{6.44}$$

and

$$h(e,u,t) = \beta_1 \dot{x}_{p,ref} + \beta_2 \ddot{x}_{p,ref} - \dddot{x}_{p,ref} + |u| \left(\beta_4 z_3 + \beta_5 z_5\right) + d(t) \tag{6.45}$$

the lumped uncertainty is bounded as $|d(t)| \leqslant \gamma$.

Let us define an integral sliding surface as:

$$S = K_{s1} \int_0^t e_1 + K_{s2} e_1 + K_{s3} e_2 + K_{s4} e_3 \tag{6.46}$$

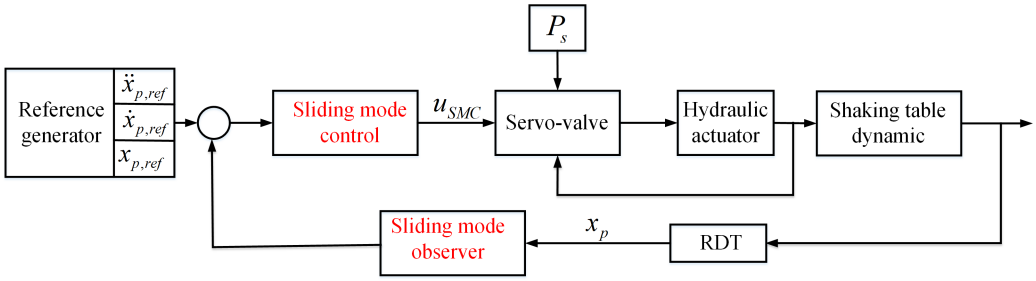

Figure 6.47: Block diagram of sliding mode controller of the hydraulic servo-shaking table.

Thus

$$\dot{S} = K_{s1}e_1 + K_{s2}e_2 + K_{s3}e_3 + K_{s4}\dot{e}_3 \tag{6.47}$$

Using the control law

$$\begin{aligned} u_{SMC} = \frac{1}{K_{s4}\beta_3}[&-K_{s1}e_1 - (K_{s4}\beta_1 + K_{s2})e_2 - (K_{s4}\beta_2 + K_{s3})e_3 \\ &- F(e) - K_s \tanh(\alpha_1 S)] \end{aligned} \tag{6.48}$$

where

$$F(e) = \beta_1 \dot{x}_{p,ref} + \beta_2 \ddot{x}_{p,ref} + \alpha_2(\beta_4 z_3 + \beta_5 z_5) \tag{6.49}$$

since $K_s \geqslant \gamma$ and $[K_{s1}, K_{s2}, K_{s3}, K_{s4}] > 0$ the reachability condition is satisfied. So, based on the lyapunov function $V = \frac{1}{2}S^2$ the boundedness of the output error can be concluded.

The optimal parameters of the controller are calculated based on the nonlinear

Table 6.14: Parameters of the sliding mode controller.

Parameters	Values
K_{s1}	1.31
K_{s2}	1.58×10^4
K_{s3}	279.7
K_{s4}	0.84
K_s	150
α_1	0.11
α_2	4.7

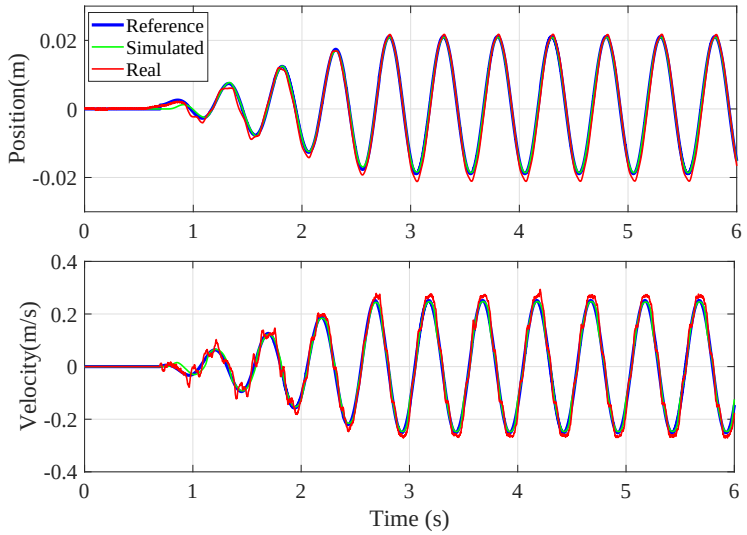

Figure 6.48: Real and simulated responses of the close loop system with respect to sliding mode controller to a sinusoidal position and velocity reference signals with $M_l = 0$.

least square method with considering the performance function in equation 6.42 in MATLAB optimization toolbox. The identified parameters are listed in table 6.14.

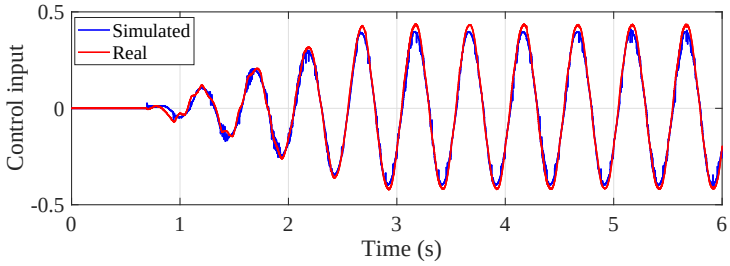

Figure 6.49: Real and simulated control input of sliding mode controller to a sinusoidal reference signal in figure 6.48.

The simulated and real experimental response of the system with respect to the sliding mode controller are shown in figures 6.48 - 6.53. Figure 6.48 displays desired position and velocity signals and the response of the simulated and real system to the designed controller. It shows that the controller has a good performance for

tracking desired position and velocity. Figure 6.49 displays the simulated and real control input. As this figure shows, by using the function *tanh* instead of *signum* function, the chattering phenomena is eliminated in the simulated and real control input. Despite of this function reduce the tracking performance of the controller, it produces a smooth control input signal which as discussed before. It eliminates the disadvantages of the chattering phenomena but reduces the performance of the controller.

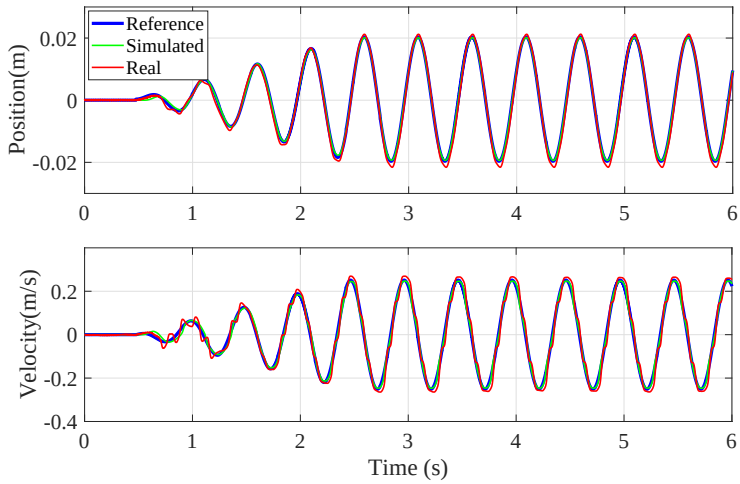

Figure 6.50: Real and simulated responses of the close loop system with respect to sliding mode controller to a sinusoidal position and velocity reference signals with $M_l = 500[kg]$.

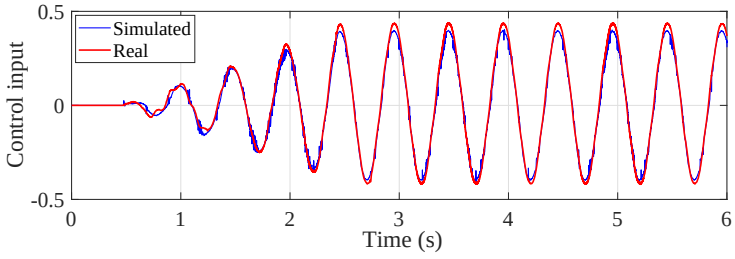

Figure 6.51: Real and simulated control input of sliding mode controller to a sinusoidal reference signal in figure 6.50.

Afterward, in order to test the robustness of the controller to different load conditions, a specimen with $M_l = 500[kg]$ is put on the table during the experiment which is shown in figure 6.50. As can be observed from this figure, the performance of the controller for tracking the desired position and velocity with $M_l = 500[kg]$ is the same as the figure 6.48 without any load. Therefore, the controller can robustly track the desired position and velocity signals. The corresponding real and simulated control input signal is shown in figure 6.51.

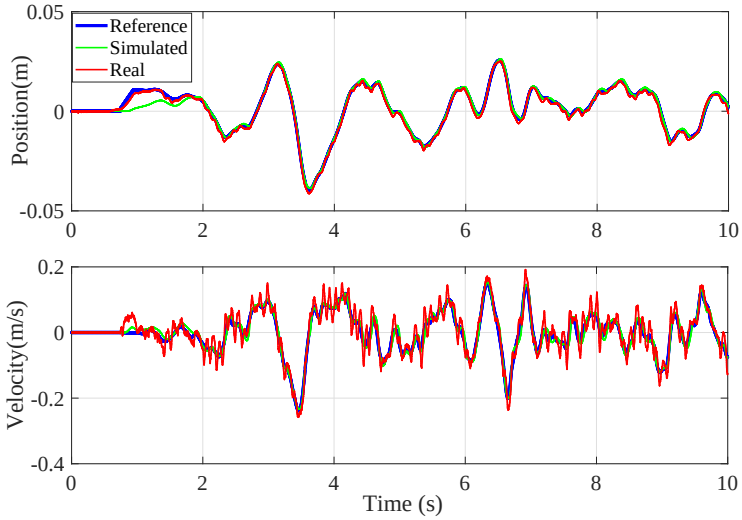

Figure 6.52: Real and simulated responses of the close loop system with respect to sliding mode controller to an earthquake position and velocity reference signals with $M_l = 200[kg]$.

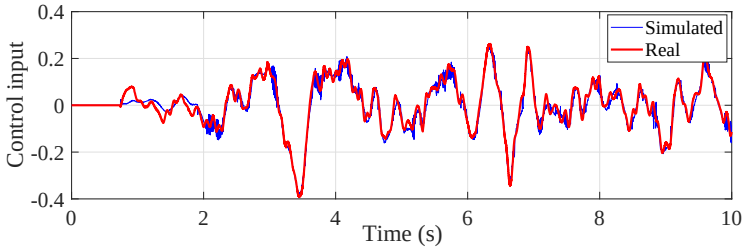

Figure 6.53: Real and simulated control input of sliding mode controller to an earthquake reference signal in figure 6.52.

Finally, in order to show the performance of the controller with respect to other reference signals, an earthquake reference signals have been given to the system. Performance of the simulated and real position and velocity of the system with $M_l = 200[kg]$ have been shown in figure 6.52. This figure shows that the closed loop system with considering the controller and observer has a good performance for track the desire position and velocity of an earthquake reference signal which includes different frequencies and amplitudes. Figure 6.53 shows the real and simulated control input of the system with respect to the reference signals in figure 6.53. Based on the experiments with different mass and reference signals, it clearly shows that the output of the system has successfully tracked the desired references. In addition, the simulated response of the system shows the same performance as the real one which demonstrate the accuracy of the simulated model and the values of the controller optimal parameters.

6.4.4 Super twisting second order sliding mode controller

In this section, in order to design a high performance controller, a super twisting sliding mode controller which has been discussed in chapter 5, is designed. The block diagram of the system with super twisting sliding mode controller is shown in figure 6.54. Compared to the first order sliding mode algorithms, well known in the literature for possessing such properties and designed in the previous subsection, this controller trajectories are smoother, avoiding the strong chattering effect of the classical sliding modes. The structure of this controller based on equation (5.40) in

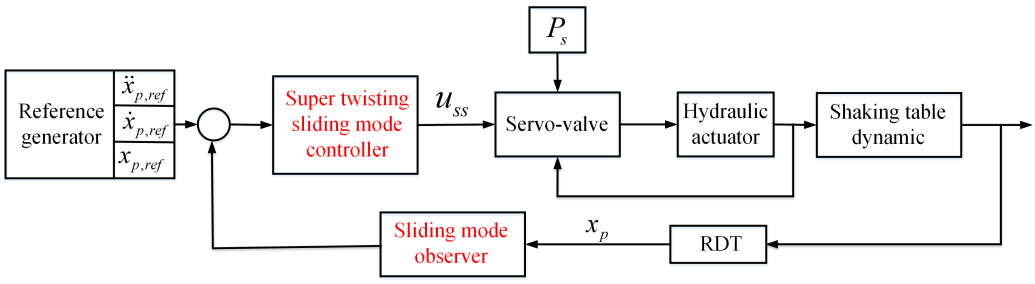

Figure 6.54: Block diagram of super twisting second order sliding mode controller of the hydraulic servo-shaking table.

Table 6.15: Parameters of the super twisting controller.

Parameters	Values	Parameters	Values
K_{ss1}	133.37	α_{ss1}	199.48
K_{ss2}	4891.1	α_{ss2}	1.84
K_{ss3}	149	$\alpha ss3$	5.1
K_{ss4}	1.24	α_{ss4}	-1.3

chapter 5 is defined as:

$$u_{ss} = -\alpha_{ss1}\sqrt{|S_{ss}|}\tanh(\alpha_{ss2}S_{ss}) - \alpha_{ss3}\int_0^t sign(S_{ss}) - \alpha_{ss4}\dot{x}_{p,ref} \tag{6.50}$$

where

$$S_{ss} = K_{ss1}\int_0^t e_1 + K_{ss2}e_1 + K_{ss3}e_2 + K_{ss4}e_3 \tag{6.51}$$

The optimal parameters of the controller are calculated based on the nonlinear least square method with considering the performance function in equation 6.42. The identified parameters are listed in table 6.15. The simulation and real

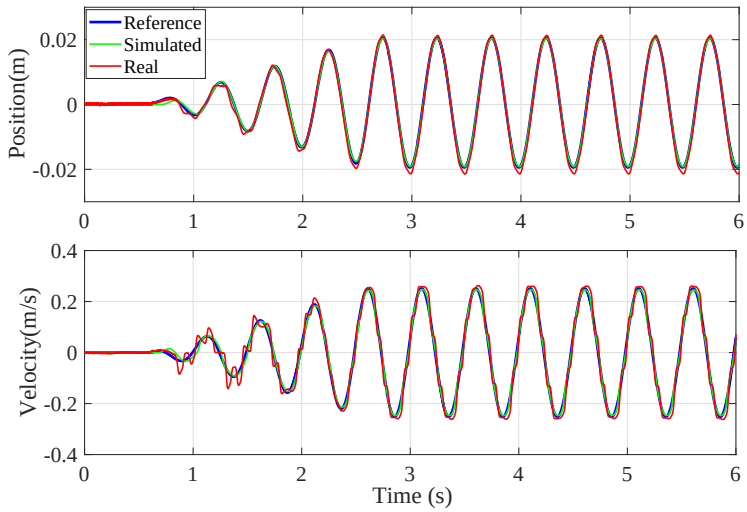

Figure 6.55: Real and simulated responses of the close loop system with respect to super twisting sliding mode controller to a sinusoidal position and velocity reference signals with $M_l = 0$.

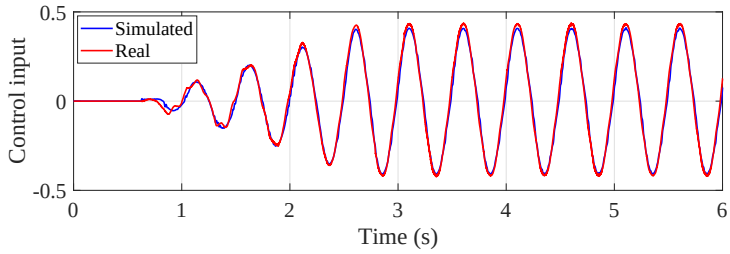

Figure 6.56: Real and simulated control input of super twisting sliding mode controller to a sinusoidal reference signal in figure 6.55.

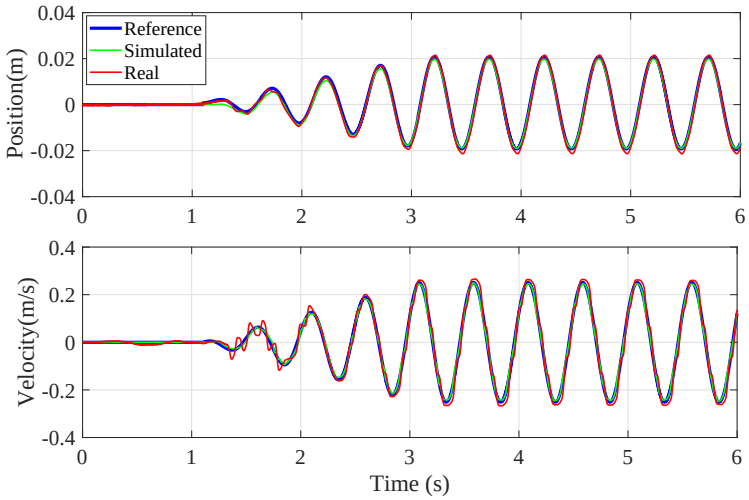

Figure 6.57: Real and simulated responses of the close loop system with respect to super twisting sliding mode controller to a sinusoidal position and velocity reference signals with $M_l = 500[kg]$.

response of the system, with considering this controller is shown in figures 6.55-6.60. In figure 6.55, the real and simulation response of the system to a sinusoidal input with considering $M_l = 0$, is shown. In this figure, tracking of desired position and velocity are quite satisfactory and the simulation results show the accuracy of the simulated system in predicting the response of the proposed controller, given that the physical key components of the hydraulic servo-system are accurately modeled through intensive experimental procedure. The corresponding control input of the system is shown in figure 6.56.

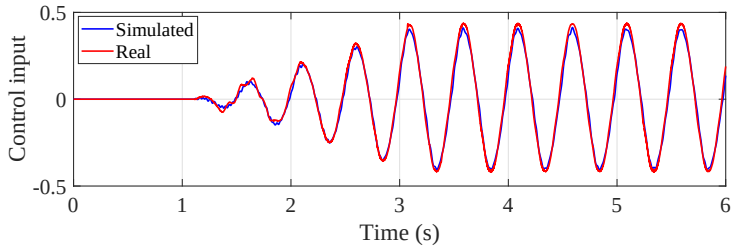

Figure 6.58: Real and simulated control input of super twisting sliding mode controller to a sinusoidal reference signal in figure 6.57.

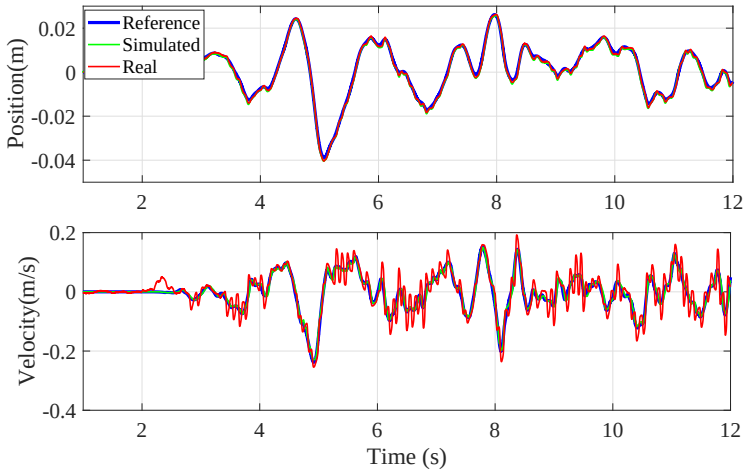

Figure 6.59: Real and simulated responses of the close loop system with respect to super twisting sliding mode controller to an earthquake position and velocity reference signals with $M_l = 200[kg]$.

Then, in order to test the robustness of the controller to different load conditions, a load with $M_l = 500[kg]$ is put on the table during the experiments which is shown in figure 6.57 and 6.58. The figure 6.57 displays that the performance of the proposed controller is satisfactory regardless of the different load conditions. The response of the hydraulic system is similar to the one expected theoretically, i.e. it results in a response of the full-order hydraulic servo-system model in subsection 6.3.6 for the same position and velocity error input. The corresponding simulated and real control inputs are shown in figure 6.58.

Finally, the performance of the controller with respect to other reference signals

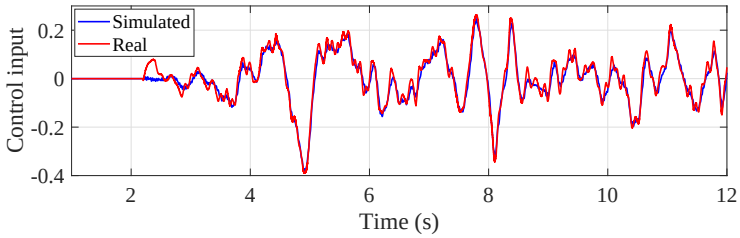

Figure 6.60: Real and simulated control input of sliding mode controller to an earthquake reference signal in figure 6.59.

are tested. So, an earthquake reference signal has been given to the system and the performance of the simulated and real position and velocity of the system have been shown in figure 6.59. Figure 6.60 shows the real and simulated control input of the system with respect to the reference signals in figure 6.59. This figure and figures 6.57 - 6.55, display the effectiveness of the super twisting sliding mode controller that the trajectory tracking of desired position and velocity signal is accurate in spite of different reference signals and load conditions.

6.4.5 Comparison of three designed controllers

The closed loop system performance for trajectory tracking with considering the proposed three different kinds of controller are compared in figure 6.61 and 6.62. Errors between the position and velocity of real system and desired reference with considering three controllers feedforward PI controller, sliding mode and super twisting sliding mode controller are plotted in this figure. As the figure 6.61 shows, the position error with respect to super twisting controller is lees than the other methods which shows the satisfactory performance of the controller and the velocity error of the super twisting controller shows smaller and smother behavior regarding to the other controllers.

In figure 6.62, the spectrum of the position and velocity of the super twisting controller shows better performance regarding to the other controllers. Therefore, besides the robustness of the designed super twisting algorithm, it also has better performance tracking accuracy in the presence of both parametric uncertainties

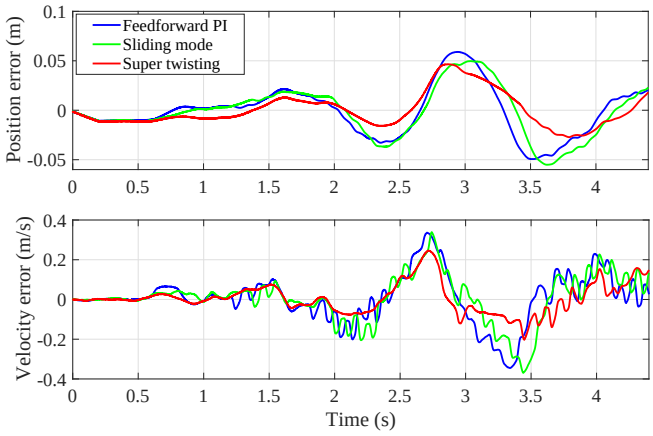

Figure 6.61: Real position and velocity error of the close loop system with respect to three different kind of controllers with respect to an earthquake position and velocity reference signals with $M_l = 200[kg]$.

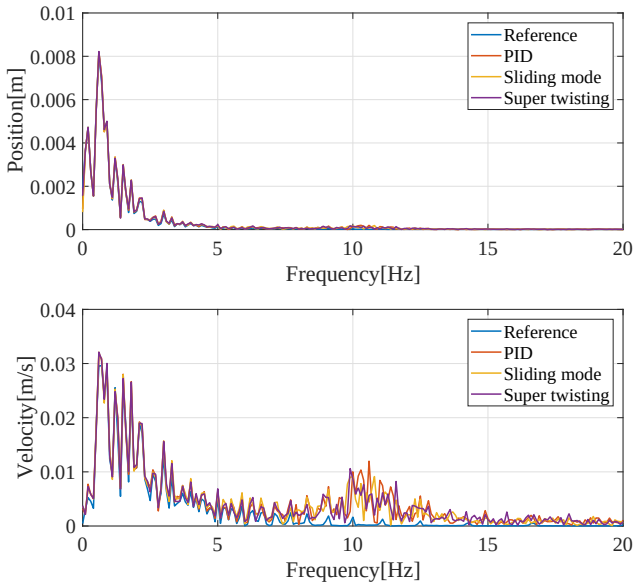

Figure 6.62: Real position and velocity spectrum of the close loop system with respect to three different kind of controllers with respect to an earthquake position and velocity reference signals with $M_l = 200[kg]$.

and uncertain nonlinearities of the hydraulic servo-system than the other two controllers. The presented experimental results verify the good performance nature of the proposed control strategy and the improvement of tracking accuracy.

Chapter 7

Conclusion

In the past decades, the hydraulic servo technique has developed to a high level of technology, among others due to the hydrostatic bearing technique for hydraulic actuators. Furthermore, recent developments in computer technology have created new possibilities in the digital control of this kind of servo-systems. Therewith, recent advances in the area of control theory, involving nonlinear, multi-variable and robust control techniques, can now be utilized and applied to real systems. Especially where an improved performance of motion is required, such as shaking table system for simulating an earthquake signal.

In the scope of the developments sketched here, the nonlinear modeling and control of hydraulic servo-systems are the main contributions of this thesis. The nonlinear model of the system based on the physical laws has provided much insight in the behavior of these systems, as well with respect to their dynamics as to their nonlinearities. The developed models are shown to be quite useful, with experimental evidence, both for control design and for system design. Then, the experimental results of designed model-based robust controllers for the system based on only position sensor can demonstrate the robustness and accuracy of these controllers.

Related to the two main research topics of this thesis, the contribution of this thesis can be worked out in a number of conclusions, which is done in chapter 6. Topics that fell beyond the scope of this thesis, but deserve further research, are discussed as recommendations for future work in Section 7.3.

7.1 Modeling and identification of a hydraulic servo-system

The dynamic features of hydraulic servo-systems are highly nonlinear and designing a high accuracy tracking control for them is a difficult problem. The experimental results of the application shaking table shows the dynamics and nonlinearities of the servo-valve and the compressibility of hydraulic oil, which constitute the limits of the controlled servo-system performance. Especially, in case of acceleration simulation of the system. In this thesis, in order to identify the hydraulic servo-system parameters, in contrary of the previous works, which in them position and pressure sensors are used, only the position and acceleration sensor are available.

In order to obtain structural insight in the way that the performance is limited by the properties of (the subsystems of) the hydraulic servo-system, the modeling of this system has been treated thoroughly in this thesis. At the one hand, this has opened the way to model-based control design, so that unavoidable limits of performance can be narrowly approached. At the other hand, the obtained insight appears to be useful in the system design stage, such that potential control problems may be avoided by proper system design.

Because of the twofold purpose of the modeling, with control design requiring quantitatively accurate models and simulating the behavior of the system precisely which requiring qualitative insight in the system behavior, the so-called white box and grey-box modeling approach has been applied. These approaches comprise physical modeling including model analysis by means of simulation, and subsequent identification and validation of the obtained physical models, using experimental data.

In the physical modeling stage, a consistent integration of the nonlinear dynamic modeling of the different subsystems of the hydraulic servo-system, namely servo-valve and actuator are presented. In this model, the most nonlinearities of the system which arise from compressibility of the hydraulic fluid, the complex flow properties of the servo-valve, valve overlap and friction in the hydraulic cylinder are simulated. Four different kinds of friction model are considered and the accuracy of these models for simulating the behavior of the system are compared experimentally.

However, due to the limitation of these models in high velocity and bandwidth, it has been shown that for simulating the behavior of the system, nonlinear modeling of the friction is not enough. Then, by gathering some position and acceleration information of the real system, the sensitivity of the model to different nonlinearity of the system are investigated. This led to the insight, that only some of the modeled nonlinear effects are relevant, such as the nonlinear flow characteristic of the servo-valve spool due to non-ideal port geometries and the compressibility of hydraulic oil, and the position dependence of the actuator dynamics.

Based on the experimental results, two new nonlinear dynamic models for simulating the behavior of the servo-hydraulic shaking table are proposed. First in the grey-box model, with defining six main parameters of the model and their identification for different sinusoidal inputs, a neural network model is proposed. The experimental performance of this model has been shown in chapter 6. Despite the good performance of the method for simulating the behavior of the system, it needs high computation resources. In addition, it has $2[s]$ convergence window at the first run which in some cases it causes instability in control feedback loop. Thus, this model is not suitable for control designing. Therefore, in order to model the behavior of hydraulic actuators with good performance to any kind of inputs, the nonlinear features of the system have been modeled based on the physical laws. This white- box model is based on a new empirical nonlinear model for effective bulk modulus of hydraulic oil, which built upon IFAS model. The proposed model increases the accuracy of the model to predict the behavior of the position, velocity and acceleration outputs of the system. The experimental and simulated comparison between the velocity and acceleration of the model based on the new effective bulk modulus and IFAS effective bulk modulus show the accuracy of the new model. These results express that in contrary of IFAS model, the new model can simulate accurately the acceleration and velocity of the system with respect to different kinds of inputs such as pulse and sinusoidal signals and different weights of the specimen. The achievements of this model would be helpful for following reasons:

1. Since the proposed model can predict precisely the behavior of the system, the designed controller based on this model can enhance the performances of the

model based force controller which is the goal of the shaking table for tracking acceleration reference signal.

2. It reduces the cost of the hydraulic servo-systems with eliminating the acceleration and internal pressure sensors. In all the previous works, using the pressure or force sensors for controlling the force or acceleration of the servo-hydraulic actuators are necessary. While, with considering this new model the pressure and force output of the system can be estimated with high accuracy.

3. It is not always possible to measure the full state of the servo-hydraulic system due to the hardware limitations. Therefore, it is suitable for constructed old industrial systems (such as the shaking table) which inserting pressure sensor inside them without changing the structure of the system is impossible.

4. The computational simulation developed by model could serve as a powerful result-interpretation tool and parameter optimization of the designed controller with respect to any parameter identification.

In this thesis, the link between the physical and the system theoretic interpretation of the properties of the hydraulic servo system are strongly emphasized. This makes, that the presented models are not only useful for shaking table design, but also for the design of the hydraulic servo-system.

7.2 Control methods for hydraulic servo-system

Based on the task specification of the shaking table, which is tracking the position and velocity reference signals with considering different load conditions, different kinds of robust controller design are presented. The theoretical procedure of designing these controllers are described in chapter 5. In this chapter, due to uncertain load condition of the system, a sliding mode and a super twisting controller are designed. For this purpose, the full order dynamic model of the system is simplified in a new approach and then due to the availability of only the position sensor on the experimental setup, a robust sliding mode observer has been designed which can estimate robustly the velocity and acceleration states of the system from the

position sensor with high accuracy. Experiments with a hydraulic actuator in a single degree-of-freedom setup have shown the validity of the approach for control design. The experimental results of the closed loop system by considering three different designed controllers, feed forward PI controller, sliding mode and super twisting controller for uncertain load condition have been presented. An analysis of the control strategies for this setup shows that the position and velocity output of the system with considering the sliding mode and super twisting controller and different load conditions can robustly and accurately track the reference signals. In addition, the comparison between the responses of these three controllers demonstrates that the super twisting sliding mode controller has smaller error and smother input controller and response than the sliding mode and feedforward PI controller.

7.3 Future works

With the main emphasis of this thesis on the modeling and control of hydraulic servo-systems, the modeling of system components have been elaborated less thoroughly. Actually, the proposed model for simulating the effective bulk modulus of hydraulic oil is derived empirically. In addition, all the existed models in the literature are structured based on a single side hydraulic actuator. This proposed model can tested experimentally and expanded to different kinds of hydraulic actuator. Furthermore, a high accuracy with high bandwidth dynamic friction model can be investigated and model with more experiments and different actuator packages.

Bibliography

[1] Ahmed Abo-Ismail and FM Wassef. Dynamics of a speed control servo system with some non linearities. *The Journal of fluid control*, 19(3):23–43, 1988.

[2] MS Ahmed and IA Tasadduq. Neural-net controller for nonlinear plants: design approach through linearisation. *IEE Proceedings-Control Theory and Applications*, 141(5):315–322, 1994.

[3] Arthur Akers, Max Gassman, and Richard Smith. *Hydraulic power system analysis*. CRC press, 2006.

[4] Farid Al-Bender. Fundamentals of friction modeling. In *Proceedings, ASPE Spring Topical Meeting on Control of Precision Systems, MIT, April 11-13, 2010*, pages 117–122. ASPE-The American Society of precision Engineering, 2010.

[5] Farid Al-Bender, Vincent Lampaert, and Jan Swevers. The generalized maxwell-slip model: a novel model for friction simulation and compensation. *IEEE Transactions on automatic control*, 50(11):1883–1887, 2005.

[6] Andrew Alleyne. Nonlinear force control of an electro-hydraulic actuator. In *Proceedings of the 1996 Japan-USA Symposium on Flexible Automation. Part 2 (of 2)*, 1996.

[7] Liang An and Nariman Sepehri. Hydraulic actuator leakage fault detection using extended kalman filter. *International Journal of Fluid Power*, 6(1):41–51, 2005.

[8] HA Arafa and M Rizk. Spool hydraulic stiffness and flow force effects in electrohydraulic servo-valves. *Proceedings of the Institution of Mechanical Engineers, Part C: Journal of Mechanical Engineering Science*, 201(3):193–199, 1987.

[9] Brian Armstrong-Helouvry. *Control of machines with friction*, volume 128. Springer Science & Business Media, 2012.

[10] Brian Armstrong-Hélouvry, Pierre Dupont, and Carlos Canudas De Wit. A survey of models, analysis tools and compensation methods for the control of machines with friction. *Automatica*, 30(7):1083–1138, 1994.

[11] AN Atassi and HK Khalil. Separation results for the stabilization of nonlinear systems using different high-gain observer designs. *Systems & Control Letters*, 39(3):183–191, 2000.

[12] Derek P Atherton. Early developments in nonlinear control. *IEEE Control Systems*, 16(3):34–43, 1996.

[13] Nay Zar Aung and Songjing Li. A numerical study of cavitation phenomenon in a flapper-nozzle pilot stage of an electrohydraulic servo-valve with an innovative flapper shape. *Energy conversion and management*, 77:31–39, 2014.

[14] Nay Zar Aung, Qingjun Yang, Meng Chen, and Songjing Li. Cfd analysis of flow forces and energy loss characteristics in a flapper–nozzle pilot valve with different null clearances. *Energy conversion and management*, 83:284–295, 2014.

[15] Wolfgang Backé. *Grundlagen der Ölhydraulik: Umdruck zur Vorlesung*. Institut für hydraulische und pneumatische Antriebe und Steuerungen der RWTH, 1972.

[16] Bruno HG Barbosa, Luis A Aguirre, Carlos B Martinez, and Antônio P Braga. Black and gray-box identification of a hydraulic pumping system. *IEEE Transactions on control systems technology*, 19(2):398–406, 2011.

[17] J Barbot, M Djemai, and T Boukhobza. Sliding mode observers. *Sliding Mode Control in Engineering*, 11, 2002.

[18] William B Bean. History of hydraulics. *AMA Archives of Internal Medicine*, 101(6):1174–1175, 1958.

[19] Damiano Belloli, Fabio Previdi, SM Savaresi, Alberto Cologni, and Mauro Zappella. Modeling and identification of an electro-hydrostatic actuator. *IFAC Proceedings Volumes*, 43(18):620–625, 2010.

[20] Wallace M Bessa, Max S Dutra, and Edwin Kreuzer. Sliding mode control with adaptive fuzzy dead-zone compensation of an electro-hydraulic servo-system. *Journal of Intelligent & Robotic Systems*, 58(1):3–16, 2010.

[21] SA Billings and S Chen. The determination of multivariable nonlinear models for dynamic systems using neural networks. 1996.

[22] SA Billings, S Chen, and MJ Korenberg. Identification of mimo non-linear systems using a forward-regression orthogonal estimator. *International journal of control*, 49(6):2157–2189, 1989.

[23] SA Billings and QM Zhu. Model validation tests for multivariable non-linear models including neural networks. *International Journal of Control*, 62(4):749–766, 1995.

[24] Stephen A Billings. *Nonlinear system identification: NARMAX methods in the time, frequency, and spatio-temporal domains*. John Wiley & Sons, 2013.

[25] Stephen A Billings and SY Fakhouri. Identification of systems containing linear dynamic and static nonlinear elements. *Automatica*, 18(1):15–26, 1982.

[26] John Francis Blackburn. *Fluid power control*. Mit Press, 1969.

[27] SA BlLLINGS and WSF Voon. Correlation based model validity tests for non-linear models. *International journal of Control*, 44(1):235–244, 1986.

[28] Li Chun Bo and D Pavelescu. The friction-speed relation and its influence on the critical velocity of stick-slip motion. *Wear*, 82(3):277–289, 1982.

[29] JE Bobrow and K Lum. Adaptive, high bandwidth control of a hydraulic actuator. *Journal of dynamic systems, measurement, and control*, 118(4):714–720, 1996.

[30] Adrian Bonchis, Peter I Corke, David C Rye, and Quang Phuc Ha. Variable structure methods in hydraulic servo systems control. *Automatica*, 37(4):589–595, 2001.

[31] Wolfgang Borutzky, B Barnard, and J Thoma. An orifice flow model for laminar and turbulent conditions. *Simulation Modelling Practice and Theory*, 10(3):141–152, 2002.

[32] Hydraulics Research Station (Great Britain). *Charts for the hydraulic design of channels and pipes*. Thomas Telford, 1990.

[33] CR Burrows, C Mu, and J Darling. A dynamic analysis of a nozzle-flapper valve with integral squeeze film damper. *Journal of dynamic systems, measurement, and control*, 113(4):702–708, 1991.

[34] Massimo Cardone and Salvatore Strano. Fluid-dynamic analysis of earthquake shaking table hydraulic circuit. In *ESDA2012-82422), in Proc. of the ASME 11th Biennial Conference on Engineering Systems Design and Analysis (ESDA2012)*, volume 2, pages 343–350, 2012.

[35] Yunus A Cengel. *Fluid mechanics*. Tata McGraw-Hill Education, 2010.

[36] Otto Cerman and Petr Hušek. Adaptive fuzzy sliding mode control for electro-hydraulic servo mechanism. *Expert Systems with Applications*, 39(11):10269–10277, 2012.

[37] Peter Chapple. *Principles of Hydraulic Systems Design*. Momentum Press, 2014.

[38] Hong-Ming Chen, Jyh-Chyang Renn, and Juhng-Perng Su. Sliding mode control with varying boundary layers for an electro-hydraulic position servo system. *The International Journal of Advanced Manufacturing Technology*, 26(1):117–123, 2005.

[39] Sheng Chen, SA Billings, and PM Grant. Non-linear system identification using neural networks. *International journal of control*, 51(6):1191–1214, 1990.

[40] Yuvin Chinniah, Richard Burton, and Saeid Habibi. Viscous damping coefficient and effective bulk modulus estimation in a high performance hydrostatic actuation system using extended kalman filter. *International Journal of Fluid Power*, 4(3):27–34, 2003.

[41] Martin Choux, Ilya Tyapin, and Geir Hovland. Extended friction model of a hydraulic actuated system. In *Reliability and Maintainability Symposium (RAMS), 2012 Proceedings-Annual*, pages 1–6. IEEE, 2012.

[42] Alberto L Cologni, Mirko Mazzoleni, and Fabio Previdi. Modeling and identification of an electro-hydraulic actuator. In *Control and Automation (ICCA), 2016 12th IEEE International Conference on*, pages 335–340. IEEE, 2016.

[43] JP Conte and TL Trombetti. Linear dynamic modeling of a uni-axial servo-hydraulic shaking table system. *Earthquake engineering & Structural dynamics*, 29(9):1375–1404, 2000.

[44] Devi D Putra. *Control of limit cycling in frictional mechanical systems*. PhD thesis, Technische Universiteit Eindhoven, 2004.

[45] K Dasgupta and R Karmakar. Modelling and dynamics of single-stage pressure relief valve with directional damping. *Simulation Modelling Practice and Theory*, 10(1):51–67, 2002.

[46] K Dasgupta and H Murrenhoff. Modelling and dynamics of a servo-valve controlled hydraulic motor by bondgraph. *Mechanism and Machine Theory*, 46(7):1016–1035, 2011.

[47] Jorge Davila, Leonid Fridman, and Arie Levant. Second-order sliding-mode observer for mechanical systems. *IEEE transactions on automatic control*, 50(11):1785–1789, 2005.

[48] Douwe Klaas de Vries. *Identification of model uncertainty for control design*. Delft University of Technology, Faculty of Mechanical Engineering and Marine Technology, 1994.

[49] C Canudas De Wit, Hans Olsson, Karl Johan Astrom, and Pablo Lischinsky. A new model for control of systems with friction. *IEEE Transactions on automatic control*, 40(3):419–425, 1995.

[50] Duncan Dowson. *History of Tribology*. Professional Engineering Publishing, Wiley, 1998.

[51] Pierre Dupont, Vincent Hayward, Brian Armstrong, and Friedhelm Altpeter. Single state elastoplastic friction models. *IEEE Transactions on automatic control*, 47(5):787–792, 2002.

[52] Christopher Edwards and Sarah Spurgeon. *Sliding mode control: theory and applications*. Crc Press, 1998.

[53] Christopher Edwards, Sarah K Spurgeon, and Chee Pin Tan. On the development and application of sliding mode observers. *LECTURE NOTES IN CONTROL AND INFORMATION SCIENCES*, pages 253–282, 2002.

[54] Siegrid Eggerth. *Beitrag zur Messung von Volumenströmen viskoser Flüssigkeiten in Druckleitungen*. PhD thesis, 1980.

[55] Karam M Elbayomy, Jiao Zongxia, and Zhang Huaqing. Pid controller optimization by ga and its performances on the electro-hydraulic servo control system. *Chinese Journal of Aeronautics*, 21(4):378–384, 2008.

[56] Donald F Elger and John A Roberson. *Engineering fluid mechanics*. Wiley Hoboken (NJ), 2013.

[57] FD Ezekiel and HM Paynter. Computer representation of engineering systems involving fluid transients. *Trans. ASME*, 79(8):1840–1850, 1957.

[58] TS Ferreira and J Lainor. Analysis of the influence of valve geometric parameters on the effective flow and force areas. 1986.

[59] A Von Feuser. Design of state controllers in the time and frequency domain for position control of a valve-controlled servo-hydraulic linear drive. *Regelungstechnik*, 32(9):309–316, 1984.

[60] Dudley D Fuller. Theory and pratice of lubrication for engineers. 1956.

[61] CF Fung, SA Billings, and H Zhang. Generalised transfer functions of neural networks. *Mechanical systems and signal processing*, 11(6):843–868, 1997.

[62] Shen Gang, Zhu Zhen-Cai, Zhang Lei, Tang Yu, Yang Chi-fu, Zhao Jin-song, Liu Guang-da, and Han Jun-Wei. Adaptive feed-forward compensation for hybrid control with acceleration time waveform replication on electro-hydraulic shaking table. *Control engineering practice*, 21(8):1128–1142, 2013.

[63] JM Gasiorek and WG Caster. Mechanics of fluids for mechanical engineering, 1967.

[64] R Ghazali, YM Sam, MF Rahmat, WIM Hashim, and Zulfatman Zulfatman. Sliding mode control with pid sliding surface of an electro-hydraulic servo system for position tracking control. 2010.

[65] Hossein Gholizadeh, Doug Bitner, Richard Burton, and Greg Schoenau. Modeling and experimental validation of the effective bulk modulus of a mixture of hydraulic oil and air. *Journal of Dynamic Systems, Measurement, and Control*, 136(5):051013, 2014.

[66] Fouad Giri and Er-Wei Bai. *Block-oriented nonlinear system identification*, volume 1. Springer, 2010.

[67] AO Gizatullin and KA Edge. Adaptive control for a multi-axis hydraulic test rig. *Proceedings of the Institution of Mechanical Engineers, Part I: Journal of Systems and Control Engineering*, 221(2):183–198, 2007.

[68] Amin Yazdanpanah Goharrizi and Nariman Sepehri. A wavelet-based approach for external leakage detection and isolation from internal leakage in valve-controlled hydraulic actuators. *IEEE Transactions on Industrial Electronics*, 58(9):4374–4384, 2011.

[69] Michael D Greenberg. *Advanced engineering mathematics*. Prentice-Hall, 1988.

[70] Cheng Guan and Shuangxia Pan. Adaptive sliding mode control of electro-hydraulic system with nonlinear unknown parameters. *Control Engineering Practice*, 16(11):1275–1284, 2008.

[71] Cheng Guan and Shuangxia Pan. Nonlinear adaptive robust control of single-rod electro-hydraulic actuator with unknown nonlinear parameters. *IEEE Transactions on Control Systems Technology*, 16(3):434–445, 2008.

[72] Cheng Guan and Shan-An Zhu. Derivative and integral sliding mode adaptive control for a class of nonlinear system and its application to an electro-hydraulic servo system. In *Zhongguo Dianji Gongcheng Xuebao(Proc. Chin. Soc. Electr. Eng.)*, volume 25, pages 103–108, 2005.

[73] Beitao Guo, Hongyi Liu, Zhong Luo, and Fei Wang. Study of pid neural network for hydraulic system. In *Automation and Logistics, 2009. ICAL'09. IEEE International Conference on*, pages 228–232. IEEE, 2009.

[74] Martin T Hagan and Mohammad B Menhaj. Training feedforward networks with the marquardt algorithm. *IEEE transactions on Neural Networks*, 5(6):989–993, 1994.

[75] H Hahn, A Piepenbrink, and KD Leimbach. Input/output linearization control of an electro servo-hydraulic actuator. In *Proceedings of the 1994 Conference on Control Applications*, pages 995–1000, 1994.

[76] Leslie Hamill. *Understanding hydraulics*. Palgrave Macmillan, 2011.

[77] HM Handroos and MJ Vilenius. Flexible semi-empirical models for hydraulic flow control valves. *Journal of Mechanical Design*, 113(3):232–238, 1991.

[78] Simon Haykin. *Neural networks: a comprehensive foundation*. Prentice Hall PTR, 1994.

[79] ATJ Hayward. Compressibility measurements on hydraulic fluids. *Hydraulic pneumatic power*, 11:643–646, 1965.

[80] ATJ Hayward. How to estimate the bulk modulus of hydraulic fluids. *Hydraulic Pneumatic Power*, 16(181):28–40, 1970.

[81] J Heintze and AJJ Van Der Weiden. Inner-loop design and analysis for hydraulic actuators, with an application to impedance control. *Control Engineering Practice*, 3(9):1323–1330, 1995.

[82] DP Hess and A Soom. Friction at a lubricated line contact operating at oscillating sliding velocities. *Journal of tribology*, 112(1):147–152, 1990.

[83] Akira Hibi and Tsuneo Ichikawa. Mathematical model of the torque characteristics for hydraulic motors. *Bulletin of JSME*, 20(143):616–621, 1977.

[84] Werner Hoffmann. *Dynamisches Verhalten hydraulischer Systeme, automatischer Modellaufbau und digitale Simulation*. PhD thesis, Rheinisch-Westfälische Technische Hochschule Aachen, 1981.

[85] Colter L Hollingshead, Michael C Johnson, Steven L Barfuss, and RE Spall. Discharge coefficient performance of venturi, standard concentric orifice plate, v-cone and wedge flow meters at low reynolds numbers. *Journal of Petroleum Science and Engineering*, 78(3):559–566, 2011.

[86] T Horiuchi, Y Dozono, and T Konno. 'improvement of accuracy of seismic-acceleration waveforms of shaking tables by compensating for the reaction force in real-time. In *Trans. 16th International Conference on Structural Mechanics in Reactor Technology*, 2001.

[87] Adam M Hurst and Joe VanDeWeert. A study of bulk modulus, entrained air, and dynamic pressure measurements in liquids. *Journal of Engineering for Gas Turbines and Power*, 138(10):101601, 2016.

[88] Y Ikebe, S Yokota, T Nakada, and K Yokoyama. Load insensitive electro-hydraulic servo system. *Fluidics Quarterly*, 13:41–55, 1981.

[89] Norlela Ishak, Mazidah Tajjudin, Hashimah Ismail, Mohd Hezri Fazalul Rahiman, Yahaya Md Sam, and Ramli Adnan. Pid studies on position tracking

control of an electro-hydraulic actuator. *International Journal of Control Science and Engineering*, 2(5):120–126, 2012.

[90] Mohieddine Jelali and Andreas Kroll. *Hydraulic servo-systems: modelling, identification and control*. Springer Science & Business Media, 2012.

[91] Yao Jianjun. Research on acceleration harmonic cancellation of electro-hydraulic servo shaking table. *Harbin Institute of Technology, PhD Thesis*, 2007.

[92] Yao Jianjun, Jiang Guilin, Di Duotao, and Liu Sheng. Acceleration harmonic identification for an electro-hydraulic servo shaking table based on the normalized least-mean-square adaptive algorithm. *Journal of Vibration and Control*, 19(1):47–55, 2013.

[93] Zong-Xia Jiao, Jun-Xia Gao, Hua Qing, and Shao-Ping Wang. The velocity synchronizing control on the electro-hydraulic load simulator. *Chinese journal of aeronautics*, 17(1):39–46, 2004.

[94] Yu Jinghong, Chen Zhaoneng, and Lu Yuanzhang. The variation of oil effective bulk modulus with pressure in hydraulic systems. *Journal of dynamic systems, measurement, and control*, 116(1):146–150, 1994.

[95] DN Johnston, KA Edge, and ND Vaughan. Experimental investigation of flow and force characteristics of hydraulic poppet and disc valves. *Proceedings of the institution of mechanical engineers, part a: journal of power and energy*, 205(3):161–171, 1991.

[96] Claude Kaddissi, Jean-Pierre Kenne, and Maarouf Saad. Identification and real-time control of an electrohydraulic servo system based on nonlinear backstepping. *IEEE/ASME Transactions on Mechatronics*, 12(1):12–22, 2007.

[97] J Kajaste, H Kauranne, A Ellman, and M Pietola. Experimental validation of different models for effective bulk modulus of hydraulic fluid. In *The Ninth Scandinavian Conference on Fluid Power, SICFP´ 05, June 1-3, 2005, Linköping, Sweden*, 2005.

[98] Tolgay Kara and I Eker. Experimental nonlinear identification of a two mass system. In *Control Applications, 2003. CCA 2003. Proceedings of 2003 IEEE Conference on*, volume 1, pages 66–71. IEEE, 2003.

[99] Zulfiqar A Khan, Vivek Chacko, and Hammad Nazir. A review of friction models in interacting joints for durability design. *Friction*, 5(1):1–22, 2017.

[100] Zohreh Khodaee, Mohammad Zareinejad, and Saeed Shiry Ghidary. Modeling of a two-stage flapper-nozzle electrohydraulic servo valve exposed to acceleration. In *Robotics and Mechatronics (ICRoM), 2014 Second RSI/ISM International Conference on*, pages 268–273. IEEE, 2014.

[101] Dean H Kim and Tsu-Chin Tsao. A linearized electrohydraulic servovalve model for valve dynamics sensitivity analysis and control system design. *Journal of Dynamic Systems, Measurement, and Control*, 122(1):179–187, 2000.

[102] Gi-Woo Kim and KW Wang. On-line monitoring of fluid effective bulk modulus using piezoelectric transducer impedance. In *Proceedings of IMECE*, volume 7, 2007.

[103] JW Kim, DJ Xuan, and Y-B Kim. Design of a forced control system for a dynamic road simulator using qft. *International Journal of Automotive Technology*, 9(1):37–43, 2008.

[104] Sunghun Kim and Hubertus Murrenhoff. Measurement of effective bulk modulus for hydraulic oil at low pressure. *Journal of Fluids Engineering*, 134(2):021201, 2012.

[105] Wonhee Kim, Daehee Won, Donghoon Shin, and Chung Choo Chung. Output feedback nonlinear control for electro-hydraulic systems. *Mechatronics*, 22(6):766–777, 2012.

[106] Horace Williams King and Ernest Fredrick Brater. Handbook of hydraulics for the solution of hydrostatic and fluid-flow problems. Technical report, 1963.

[107] EE Klaus and JA O'brien. Precise measurement and prediction of bulk-modulus values for fluids and lubricants. *Journal of Basic Engineering*, 86(3):469–473, 1964.

[108] J Kuehn, D Epp, and WN Patten. High-fidelity control of a seismic shake table. *Earthquake engineering & structural dynamics*, 28(11):1235–1254, 1999.

[109] E Kuss. Pvt-daten bei hohen drücken. *DGMK-Forschungsbericht*, 4510(1975):69, 1976.

[110] Byung-Jae Kwak, Andrew E Yagle, and Joel A Levitt. Nonlinear system identification of hydraulic actuator. friction dynamics using a hammerstein model. In *Acoustics, Speech and Signal Processing, 1998. Proceedings of the 1998 IEEE International Conference on*, volume 4, pages 1933–1936. IEEE, 1998.

[111] Jung-ho Kwon, Tae-hyeong Kim, Ji-Seong Jang, and Ill-yeong Lee. Feedback linearization control of a hydraulic servo system. In *SICE-ICASE, 2006. International Joint Conference*, pages 455–460. IEEE, 2006.

[112] Seth L Lacy and Dennis S Bernstein. Identification of an electromagnetic actuator. In *IEEE CONFERENCE ON DECISION AND CONTROL*, volume 4, pages 4521–4526. IEEE; 1998, 2002.

[113] Vincent Lampaert, Jan Swevers, and Farid Al-Bender. Experimental comparison of different friction models for accurate low-velocity tracking. In *Proceedings of the 10th Mediterranean Conference on Control and Automation (MED'02)*, 2002.

[114] Vincent Lampaert, Jan Swevers, and Farid Al-Bender. Modification of the leuven integrated friction model structure. *IEEE transactions on Automatic Control*, 47(4):683–687, 2002.

[115] Yoan D Landau. Adaptive control: The model reference approach. *IEEE Transactions on Systems, Man, and Cybernetics*, (1):169–170, 1984.

[116] Kyo-Il Lee. *Dynamisches Verhalten der Steuerkette Servoventil-Motor-Last*. PhD thesis, 1978.

[117] Pedro J Lee, John P Vítkovskỳ, Martin F Lambert, and Angus R Simpson. Valve design for extracting response functions from hydraulic systems using pseudorandom binary signals. *Journal of Hydraulic Engineering*, 134(6):858–864, 2008.

[118] IJ Leontaritis and SA Billings. Experimental design and identifiability for non-linear systems. *International Journal of Systems Science*, 18(1):189–202, 1987.

[119] Arie Levant. Sliding order and sliding accuracy in sliding mode control. *International journal of control*, 58(6):1247–1263, 1993.

[120] Arie Levant. Quasi-continuous high-order sliding-mode controllers. In *Decision and Control, 2003. Proceedings. 42nd IEEE Conference on*, volume 5, pages 4605–4610. IEEE, 2003.

[121] Arie Levant and Lela Alelishvili. Integral high-order sliding modes. *IEEE Transactions on Automatic control*, 52(7):1278–1282, 2007.

[122] Hong-Nan Li, Ying Jia, and Su-Yan Wang. Theoretical and experimental studies on reduction for multi-modal seismic responses of high-rise structures by tuned liquid dampers. *Modal Analysis*, 10(7):1041–1056, 2004.

[123] Songjing Li, Nay Zar Aung, Shengzhuo Zhang, Junzhang Cao, and Xinzhi Xue. Experimental and numerical investigation of cavitation phenomenon in flapper–nozzle pilot stage of an electrohydraulic servo-valve. *Computers & Fluids*, 88:590–598, 2013.

[124] Chong-Jer Liaw and FT Brown. Nonlinear dynamics of an electrohydraulic flapper nozzle valve. *Journal of Dynamic Systems, Measurement, and Control*, 112(2):298–304, 1990.

[125] A Lichtarowicz. Flow and force characteristics of flapper valves. In *3 rd International Fluid Power Symposium, pp. B1-1-B1-11*, pages 9–11, 1973.

[126] SJ Lin and A Akers. A dynamic model of the flapper-nozzle component of an electrohydraulic servovalve. *Journal of dynamic systems, measurement, and control*, 111(1):105–109, 1989.

[127] SJ Lin and A Akers. Dynamic analysis of a flapper-nozzle valve. *Journal of dynamic systems, measurement, and control*, 113(1):163–167, 1991.

[128] TG Ling, MF Rahmat, AR Husain, and R Ghazali. System identification of electro-hydraulic actuator servo system. In *Mechatronics (ICOM), 2011 4th International Conference On*, pages 1–7. IEEE, 2011.

[129] Y Liu and H Handroos. Technical note sliding mode control for a class of hydraulic position servo. *Mechatronics*, 9(1):111–123, 1999.

[130] Lennart Ljung. System identification. In *Signal analysis and prediction*, pages 163–173. Springer, 1998.

[131] Alexander G Loukianov, Edgar Sanchez, and Carlos Lizalde. Force tracking neural block control for an electro-hydraulic actuator via second-order sliding mode. *International Journal of Robust and Nonlinear Control*, 18(3):319–332, 2008.

[132] Vincent G Magorien. How hydraulic fluids generate air. *Hydraulics & Pneumatics*, 21(6):104, 1968.

[133] Vincent G Magorien. Dissolved gas-the hidden saboteur. Technical report, SAE Technical Paper, 1993.

[134] Dechrit Maneetham and Nitin Afzulpurkar. Modeling, simulation and control of high speed nonlinear hydraulic servo system. *Journal of Automation Mobile Robotics and Intelligent Systems*, 4:94–103, 2010.

[135] ND Manring. The effective fluid bulk-modulus within a hydrostatic transmission. *Journal of dynamic systems, measurement, and control*, 119(3):462–466, 1997.

[136] Lőrinc Márton, Szabolcs Fodor, and Nariman Sepehri. A practical method for friction identification in hydraulic actuators. *Mechatronics*, 21(1):350–356, 2011.

[137] Lrinc Marton and Bla Lantos. Modeling, identification, and compensation of stick-slip friction. *IEEE Transactions on Industrial Electronics*, 54(1):511–521, 2007.

[138] RH Maskrey and WJ Thayer. A brief history of electrohydraulic servomechanisms. *Moog Technical Bulletin*, 141, 1978.

[139] D McCloy. Discharge characteristics of servo valve orifices. In *Fluid International Conference*, pages 43–50, 1968.

[140] Donaldson McCloy and Hugh Robert Martin. Control of fluid power: analysis and design. *Chichester, Sussex, England, Ellis Horwood, Ltd.; New York, Halsted Press, 1980. 505 p.*, 1980.

[141] Herbert E Merritt. *Hydraulic control systems*. John Wiley & Sons, 1967.

[142] Vladimir Milić, Željko Šitum, and Mario Essert. Robust h_∞ position control synthesis of an electro-hydraulic servo system. *ISA transactions*, 49(4):535–542, 2010.

[143] Amit Mohanty and Bin Yao. Indirect adaptive robust control of hydraulic manipulators with accurate parameter estimates. *IEEE Transactions on Control Systems Technology*, 19(3):567–575, 2011.

[144] Jaime A Moreno and Marisol Osorio. A lyapunov approach to second-order sliding mode controllers and observers. In *Decision and Control, 2008. CDC 2008. 47th IEEE Conference on*, pages 2856–2861. IEEE, 2008.

[145] Bruce R Munson, Donald F Young, and Theodore H Okiishi. Fundamentals of fluid mechanics. *New York*, 3(4), 1990.

[146] H Murrenhoff. Grundlagen der fluidtechnik, teil 1: Hydraulik umdruck zur vorlesung, institut für fluidtechnische antriebe und steuerungen, steinbachstr. 53, d-52074 aachen, 1, 1997.

[147] Hubertus Murrenhoff and D Linden. Grundlagen der fluidtechnik, teil 1: Hydraulik. *Shaker-Verlag, Herzogenrath, Germany, Chap. 3*, 2011.

[148] Narutoshi Nakata. Acceleration trajectory tracking control for earthquake simulators. *Engineering Structures*, 32(8):2229–2236, 2010.

[149] Oliver Nelles. *Nonlinear system identification: from classical approaches to neural networks and fuzzy models*. Springer Science & Business Media, 2013.

[150] Rüdiger Neumann, Andreas Engeike, and Woifgang Moritz. Robuster simultaner regler-beobachterentwurf durch parameteroptimierung für einen hydraulischen portalroboter/robust simultaneous controller/observer design by parameter optimization for a hydraulic portal robot. *at-Automatisierungstechnik*, 39(1-12):151–157, 1991.

[151] Devin P Newell, Hongliang Dai, Michael K Sain, Peter Quast, and BF Spencer. Nonlinear modeling and control of a hydraulic seismic simulator. In *American Control Conference, Proceedings of the 1995*, volume 1, pages 801–805. IEEE, 1995.

[152] N Niksefat and N Sepehri. Design and experimental evaluation of a robust force controller for an electro-hydraulic actuator via quantitative feedback theory. *Control Engineering Practice*, 8(12):1335–1345, 2000.

[153] Richard F Nowak, David A Kusner, Rodney L Larson, and Bradford K Thoen. Utilizing modern digital signal processing for improvement of large scale shaking table performance. In *Proceedings of 12th World Conference on Earthquake Engineering*, volume 2035, pages 1–8, 2000.

[154] THA Nykanen, S Esque, and AU Ellman. Comparison of different fluid models. In *Bath Workshop on Power Transmission and Motion Control (PTMC 2000), Bath, UK*, pages 101–110, 2000.

[155] Henrik Olsson, Karl Johan Åström, C Canudas De Wit, Magnus Gäfvert, and Pablo Lischinsky. Friction models and friction compensation. *European journal of control*, 4(3):176–195, 1998.

[156] Stefano Pagano, Riccardo Russo, Salvatore Strano, and Mario Terzo. Modelling and control of a hydraulically actuated shaking table employed for vibration absorber testing. In *ESDA2012-82118), in Proc. of the ASME 11th Biennial Conference on Engineering Systems Design and Analysis (ESDA2012)*, volume 1, pages 651–660, 2012.

[157] Xudong Pan, Guanglin Wang, and Zesheng Lu. Flow field simulation and a flow model of servo-valve spool valve orifice. *Energy conversion and management*, 52(10):3249–3256, 2011.

[158] Richard F Pannett, PK Chawdhry, and Clifford R Burrows. Alternative robust control strategies for disturbance rejection in fluid power systems. In *American Control Conference, 1999. Proceedings of the 1999*, volume 2, pages 739–743. IEEE, 1999.

[159] Virendra C Patel, Wolfgang Rodi, and Georg Scheuerer. Turbulence models for near-wall and low reynolds number flows- a review. *AIAA journal*, 23(9):1308–1319, 1985.

[160] Jimoh Pedro and Olurotimi Dahunsi. Neural network based feedback linearization control of a servo-hydraulic vehicle suspension system. *International Journal of Applied Mathematics and Computer Science*, 21(1):137–147, 2011.

[161] Wilfrid Perruquetti and Jean-Pierre Barbot. *Sliding mode control in engineering*. CRC Press, 2002.

[162] JC Peyton Jones and SA Billings. Interpretation of non-linear frequency response functions. *International Journal of Control*, 52(2):319–346, 1990.

[163] Brian M Phillips, Nicholas E Wierschem, and BF Spencer. Model-based multimetric control of uniaxial shake tables. *Earthquake Engineering & Structural Dynamics*, 43(5):681–699, 2014.

[164] AS Poznyak. Stochastic output noise effects in sliding mode state estimation. *International Journal of Control*, 76(9-10):986–999, 2003.

[165] Mohd Fua'ad Rahmat, Zulfatman Has, Abdul Rashid Husain, Yahya Md Sam, Kashif Ishaque, Rozaimi Ghazaly, and Sahazati Md Rozali. Modeling and controller design of an industrial hydraulic actuator system in the presence of friction and internal leakage. *International Journal of the Physical Sciences*, 6(14):3502–3517, 2011.

[166] Paolo Righettini, Roberto Strada, Vittorio Lorenzi, Alberto Oldani, and Mattia Rossetti. Modeling, control and experimental validation of a device for seismic events simulation. *International Journal of Structural Analysis Design*, 2(1):83–88, 2015.

[167] Paolo Righettini, Roberto Strada, Shirin Valilou, and Ehsan Khademolama. Nonlinear modeling and experimental validation of uni-axial servo-hydraulic shaking table. In *BATH/ASME 2016 Symposium on Fluid Power and Motion Control*, pages V001T01A037–V001T01A037. American Society of Mechanical Engineers, 2016.

[168] Paolo Righettini, Roberto Strada, Shirin Valilou, and Ehsan Khademolama. Gray-box acceleration modeling of an electro hydraulic servo shaking table with neural network. In *Proceedings of the 2017 IEEE International Conference on Advanced Intelligent Mechatronics, Munich, Geermany*, pages 335–340. IEEE, 2017.

[169] Hunter Rouse and Simon Ince. History of hydraulics. Technical report, 1980.

[170] Sayako SAKAMA, Yutaka TANAKA, and Hiroyuki GOTO. Mathematical model for bulk modulus of hydraulic oil containing air bubbles. *Mechanical Engineering Journal*, 2(6):15–00347, 2015.

[171] Kenta Seki, Makoto Iwasaki, Motohiro Kawafuku, Hiromu Hirai, and Kazuki Yasuda. Improvement of control performance in shaking-tables by feedback compensation for reaction force. In *Industrial Electronics, 2008. IECON 2008. 34th Annual Conference of IEEE*, pages 2551–2556. IEEE, 2008.

[172] Nariman Sepehri, GAM Dumont, Peter D Lawrence, and Farrokh Sassani. Cascade control of hydraulically actuated manipulators. *Robotica*, 8(3):207–216, 1990.

[173] Junpeng Shao, Lihua Chen, Yajuan Ji, and Zhibin Sun. The application of fuzzy control strategy in electro-hydraulic servo system. In *Communications and Information Technology, 2005. ISCIT 2005. IEEE International Symposium on*, volume 1, pages 165–170. IEEE, 2005.

[174] Zhanqun Shi, Fengshou Gu, Barry Lennox, and AD Ball. The development of an adaptive threshold for model-based fault detection of a nonlinear electro-hydraulic system. *Control Engineering Practice*, 13(11):1357–1367, 2005.

[175] Y Shtessel, Franck Plestan, and Mohammed Taleb. Lyapunov design of adaptive super-twisting controller applied to a pneumatic actuator. *IFAC Proceedings Volumes*, 44(1):3051–3056, 2011.

[176] JC Slattery and Energy Momentum. Mass transfer in continua. *McGrawf Hill, New York*, page 191, 1972.

[177] AC Smith. Some notes on the data on hydraulic oil properties required by systems designers. *Industrial Lubrication and Tribology*, 17(2):63–69, 1965.

[178] Steve C Southward, Clark J Radcliffe, and CR MacCluer. Robust nonlinear stick-slip friction compensation. *Journal of Dynamic Systems, Measurement, and Control*, 113(4):639–645, 1991.

[179] Manfred Spilker. *Druck-und temperaturabhängige Eigenschaften von Schmierstoffen und Hydraulikflüssigkeiten*. PhD thesis, Rheinisch-Westfälische Technische Hochschule Aachen, 1981.

[180] Joseph Spurk. *Strömungslehre: Einführung in die Theorie der Strömungen*. Springer-Verlag, 2013.

[181] JS Stecki and DC Davis. Hydraulic system analysis—prediction and measurement of effective bulk modulus. *Basic Fluid Power Research Journal*, 14(4):333–335, 1981.

[182] Matthew Stehman and Narutoshi Nakata. Direct acceleration feedback control of shake tables with force stabilization. *Journal of Earthquake Engineering*, 17(5):736–749, 2013.

[183] David P Stoten and Eduardo G Gómez. Adaptive control of shaking tables using the minimal control synthesis algorithm. *Philosophical Transactions of the Royal Society of London A: Mathematical, Physical and Engineering Sciences*, 359(1786):1697–1723, 2001.

[184] DP Stoten and N Shimizu. The feedforward minimal control synthesis algorithm and its application to the control of shaking-tables. *Proceedings of the institution of mechanical engineers, Part I: Journal of Systems and Control Engineering*, 221(3):423–444, 2007.

[185] Jan Swevers, Farid Al-Bender, Chris G Ganseman, and Tutuko Projogo. An integrated friction model structure with improved presliding behavior for accurate friction compensation. *IEEE Transactions on automatic control*, 45(4):675–686, 2000.

[186] Y Tagawa and K Kajiwara. Controller development for the e-defense shaking table. *Proceedings of the institution of mechanical engineers, Part I: Journal of Systems and Control Engineering*, 221(2):171–181, 2007.

[187] Ai Hui Tan and Keith R Godfrey. The generation of binary and near-binary pseudorandom signals: an overview. *IEEE Transactions on Instrumentation and Measurement*, 51(4):583–588, 2002.

[188] Harold Neville Vazeille Temperley and DH u Trevena. *Liquids and Their Properties: A Molecular and Microscopic Treatise*. Halsted Press, 1978.

[189] George E Totten. *Handbook of hydraulic fluid technology*. CRC Press, 2011.

[190] Xuan Bo Tran, Nur Hafizah, and Hideki Yanada. Modeling of dynamic friction behaviors of hydraulic cylinders. *Mechatronics*, 22(1):65–75, 2012.

[191] Xuan Bo Tran, War Htun Khaing, H Endo, and Hideki Yanada. Effect of friction model on simulation of hydraulic actuator. *Proceedings of the Institution of Mechanical Engineers, Part I: Journal of Systems and Control Engineering*, 228(9):690–698, 2014.

[192] Xuan Bo Tran, Akinori Matsui, and Hideki Yanada. Effects of viscosity and type of oil on dynamic behaviors of friction of hydraulic cylinder. *Transactions of the Japan Fluid Power System Society*, 41(2):28–35, 2010.

[193] Tsu-Chin Tsao and Masayoshi Tomizuka. Robust adaptive and repetitive digital tracking control and application to a hydraulic servo for noncircular machining. *Journal of dynamic systems, measurement, and control*, 116(1):24–32, 1994.

[194] Vadim Utkin, Jürgen Guldner, and Jingxin Shi. *Sliding mode control in electromechanical systems*, volume 34. CRC press, 2009.

[195] James D Van de Ven. On fluid compressibility in switch-mode hydraulic circuits—part ii: Experimental results. *Journal of Dynamic Systems, Measurement, and Control*, 135(2):021014, 2013.

[196] Gerard Van Schothorst. Modelling of long-stroke hydraulic servo-systems for flight simulator motion control and system design. 1997.

[197] Taco J Viersma. Analysis, synthesis, and design of hydraulic servosystems and pipelines(book). *Amsterdam, Elsevier Scientific Publishing Co.(Studies in Mechanical Engineering.*, 1, 1980.

[198] Matti Vilenius and Tapio Virvalo. *The Effect of Nonlinearities on the Dynamic Characteristics of an Elctrohydraulic Servovalve*. Tampereen teknillinen korkeakoulu, 1975.

[199] Gholamreza Vossoughi and Max Donath. Dynamic feedback linearization for electrohydraulically actuated control systems. *Transactions-American of Mechanical Engineering Journal of Dynamic Systems Measurement and Control*, 117:468–477, 1995.

[200] Ronald B Walters. *Hydraulic and electric-hydraulic control systems*. Springer, 2000.

[201] D Wang, R Dolid, M Donath, and J Albright. Development and verification of a two-stage flow control servovalve model. *Proceedings of the ASME-IMECE FPST-Fluid Power Systems Tech*, 2:121–129, 1995.

[202] Tao Wang, Maolin Cai, Kenji Kawashima, and Toshiharu Kagawa. Modelling of a nozzle-flapper type pneumatic servo valve including the influence of flow force. *International Journal of Fluid Power*, 6(3):33–43, 2005.

[203] Xianbin Wang, Yiyan Wu, and Bernard Caron. Transmitter identification using embedded pseudo random sequences. *IEEE Transactions on Broadcasting*, 50(3):244–252, 2004.

[204] J Watton. The dynamic performance of an electrohydraulic servovalve/motor system with transmission line effects. *Journal of dynamic systems, measurement, and control*, 109(1):14–18, 1987.

[205] J Watton. On linearized coefficients for an underlapped servo-valve coupled to a single-rod cylinder. *Journal of dynamic systems, measurement, and control*, 112(4):794–796, 1990.

[206] J Watton and MJ Tadmori. Damping characteristics of transmission lines with sudden closure of underlapped electrohydraulic servovalves. *Dynamic Systems: Modelling and Control*, 1:135–140, 1985.

[207] WR White. Charts for the hydraulic design of channels and pipes. 1983.

[208] Dieter Will and Norbert Gebhardt. *Hydraulik: Grundlagen, Komponenten, Systeme*. Springer-Verlag, 2015.

[209] Klaus Witt. *Druckflüssigkeiten und thermodynamisches Messen*. Ingenieur Digest Verlag-Ges., 1974.

[210] WA Wright. Prediction of bulk moduli and pressure-volume-temperature data for petroleum oils. *ASLE TRANSACTIONS*, 10(4):349–356, 1967.

[211] Ruh-Hua Wu and Pi-Cheng Tung. Studies of stick-slip friction, presliding displacement, and hunting. *Journal of dynamic systems, measurement, and control*, 124(1):111–117, 2002.

[212] Zhen-shun Wu, Jian-jun Yao, and Dong-hai Yue. A self-tuning fuzy pid controller and its application [j]. *Journal of Harbin institute of technology*, 11:157–159´, 2004.

[213] E Benjamin Wylie, Victor Lyle Streeter, and Lisheng Suo. *Fluid transients in systems*, volume 1. Prentice Hall Englewood Cliffs, NJ, 1993.

[214] Bin Xian, Marcio S de Queiroz, Darren M Dawson, and Michael L McIntyre. A discontinuous output feedback controller and velocity observer for nonlinear mechanical systems. *Automatica*, 40(4):695–700, 2004.

[215] Hideki Yanada and Yuta Sekikawa. Modeling of dynamic behaviors of friction. *Mechatronics*, 18(7):330–339, 2008.

[216] Hideki Yanada, Kazuya Takahashi, and Akinori Matsui. Identification of dynamic parameters of modified lugre model and application to hydraulic actuator. *Transactions of the Japan Fluid Power System Society*, 40(4):57–64, 2009.

[217] TY Yang and A Schellenberg. Using nonlinear control algorithms to improve the quality of shaking table tests. In *Proceedings of the 14th World Conference on Earthquake Engineering*, pages 12–17, 2008.

[218] Bin Yao, Fanping Bu, John Reedy, and GT-C Chiu. Adaptive robust motion control of single-rod hydraulic actuators: theory and experiments. *IEEE/ASME transactions on mechatronics*, 5(1):79–91, 2000.

[219] Jian-Jun Yao, Sheng-Hai Hu, Wei Fu, and Jun-Wei Han. Impact of excitation signal upon the acceleration harmonic distortion of an electro-hydraulic shaking table. *Journal of Vibration and Control*, 17(7):1106–1111, 2011.

[220] Jianjun Yao, Duotao Di, Guilin Jiang, Shuang Gao, and Han Yan. Identification of acceleration harmonic for an electro-hydraulic servo shaking table based on kalman filter. *Transactions of the Institute of Measurement and Control*, 35(8):986–996, 2013.

[221] Jianjun Yao, Duotao Di, Guilin Jiang, Shuang Gao, and Han Yan. Real-time acceleration harmonics estimation for an electro-hydraulic servo shaking table using kalman filter with a linear model. *IEEE Transactions on Control Systems Technology*, 22(2):794–800, 2014.

[222] Jianjun Yao, Matt Dietz, Rui Xiao, Han Yu, Tao Wang, and Donghai Yue. An overview of control schemes for hydraulic shaking tables. *Journal of Vibration and Control*, 22(12):2807–2823, 2016.

[223] Jianjun Yao and Chengjun Wang. Model reference adaptive control for a hydraulic underwater manipulator. *Journal of Vibration and Control*, 18(6):893–902, 2012.

[224] Jianjun Yao, Liquan Wang, Caidong Wang, Zhonglin Zhang, and Peng Jia. Ann-based pid controller for an electro-hydraulic servo system. In *Automation and Logistics, 2008. ICAL 2008. IEEE International Conference on*, pages 18–22. IEEE, 2008.

[225] Jianjun Yao, Rui Xiao, Shuo Chen, Duotao Di, Shuang Gao, and Han Yu. Acceleration harmonic identification algorithm based on the unscented kalman filter for shaking signals of an electro-hydraulic servo shaking table. *Journal of Vibration and Control*, 21(16):3205–3217, 2015.

[226] Jianyong Yao, Wenxiang Deng, and Zongxia Jiao. Adaptive control of hydraulic actuators with lugre model-based friction compensation. *IEEE Transactions on Industrial Electronics*, 62(10):6469–6477, 2015.

[227] Jianyong Yao, Zongxia Jiao, and Songshan Han. Friction compensation for low velocity control of hydraulic flight motion simulator: a simple adaptive robust approach. *Chinese Journal of Aeronautics*, 26(3):814–822, 2013.

[228] Jianyong Yao, Zongxia Jiao, and Dawei Ma. Extended-state-observer-based output feedback nonlinear robust control of hydraulic systems with backstepping. *IEEE Transactions on Industrial Electronics*, 61(11):6285–6293, 2014.

[229] JJ Yao. Research on acceleration harmonic cancellation of electro-hydraulic servo shaking table. *Harbin Institute of Technology, China*, 2007.

[230] Eunjong Yu, Daniel H Whang, Joel P Conte, Jonathan P Stewart, and John W Wallace. Forced vibration testing of buildings using the linear shaker seismic simulation (lsss) testing method. *Earthquake engineering & structural dynamics*, 34(7):737–761, 2005.

[231] Hong Yu, Zheng-jin Feng, and Xu-yong Wang. Nonlinear control for a class of hydraulic servo system. *Journal of Zhejiang University-Science A*, 5(11):1413–1417, 2004.

[232] Hairong Zeng and Nariman Sepehri. Tracking control of hydraulic actuators using a lugre friction model compensation. *Journal of Dynamic Systems, Measurement, and Control*, 130(1):014502, 2008.

[233] Tienan Zhao and Tapio Virvalo. Fuzzy control of a hydraulic position servo with unknown load. In *Fuzzy Systems, 1993., Second IEEE International Conference on*, pages 785–788. IEEE, 1993.

[234] Guang L Zheng and Steve A Billings. Radial basis function network configuration using mutual information and the orthogonal least squares algorithm. *Neural Networks*, 9(9):1619–1637, 1996.

[235] Wen-Hong Zhu and Jean-Claude Piedboeuf. Adaptive output force tracking control of hydraulic cylinders with applications to robot manipulators. *Journal of dynamic systems, measurement, and control*, 127(2):206–217, 2005.

[236] K Ziaei and N Sepehri. Modeling and identification of electrohydraulic servos. *Mechatronics*, 10(7):761–772, 2000.

[237] K Ziaei and N Sepehri. Design of a nonlinear adaptive controller for an electro-hydraulic actuator. *Journal of Dynamic Systems, Measurement, and Control*, 123(3):449–456, 2001.

Publications list

1) P. Righettini, R. Strada, S. Valilou, E. Khademolama, "Output feedback sliding mode controller with H2 performance for robot manipulator" IEEE International Conference on Automation and Computing (ICAC), 2015 21st, pp. 1-6, 11-12 September 2015.

2) P. Righettini, R. Strada, E. Khademolama, S. Valilou, "Symbolic kinematic and dynamic modelling toolbox for Multi-DOF robotic manipulators" IEEE International Conference on Automation and Computing (ICAC), pp. 1-7, 11-12 September 2015.

3) P. Righettini, R. Strada, S. Valilou, E. Khademolama, "Nonlinear modeling and experimental validation of uni-axial servo hydraulic shaking table" International Conference of Bath/ASME on Fluid Power and Motion Control, 2016, 7-9 September.

4) P. Righettini, R. Strada, S. Valilou, E. Khademolama, "Gray-box acceleration modeling of an electro hydraulic servo shaking table with Neural Network" IEEE International Conference on Advanced Intelligent Mechatronics, Munich, 2017, 3-7 July.

5) P. Righettini, S. Roberto Strada, E. KhademOlama, and S. Valilou. "Online Wavelet Complementary velocity Estimator." ISA transactions (2018).

Submitted papers

1) P. Righettini, R. Strada, S. Valilou, E. Khademolama, "Nonlinear Model of a Servo-Hydraulic Shaking Table with Dynamic Model of Effective Bulk Modulus" Mechanical Systems and Signal Processing, Elsevier.

2) P. Righettini, R. Strada, S. Valilou, E. Khademolama, "Output feedback sliding mode control of an Electro hydraulic servo shaking table" Mechanical Systems and Signal Processing, Elsevier.